2003-04-15

The Pseudo-Rigid-Body Model for Dynamic Predictions of Macro and Micro Compliant Mechanisms

Scott Marvin Lyon
Brigham Young University - Provo

THE PSEUDO-RIGID-BODY MODEL FOR DYNAMIC PREDICTIONS OF MACRO AND MICRO COMPLIANT MECHANISMS

by

Scott M. Lyon

A dissertation submitted to the faculty of

Brigham Young University

in partial fulfillment of the requirements for the degree of

Doctor of Philosophy

Department of Mechanical Engineering

Brigham Young University

August 2003

BRIGHAM YOUNG UNIVERSITY

GRADUATE COMMITTEE APPROVAL

of a dissertation submitted by

Scott M. Lyon

This dissertation has been read by each member of the following graduate committee and by majority vote has been found to be satisfactory.

Date	Larry L. Howell, Chair
Date	Jonathan D. Blotter
Date	Kenneth W. Chase
Date	Timothy W. McLain
Date	John N. Harb

BRIGHAM YOUNG UNIVERSITY

As chair of the candidate's graduate committee, I have read the dissertation of Scott M. Lyon in its final form and have found that (1) its format, citations, and bibliographical style are consistent and acceptable and fulfill university and department style requirements; (2) its illustrative materials including figures, tables, and charts are in place; and (3) the final manuscript is satisfactory to the graduate committee and is ready for submission to the university library.

Date

Larry L. Howell
Chair, Graduate Committee

Accepted for the Department

Brent L. Adams
Graduate Coordinator

Accepted for the College

Douglas M. Chabries
Dean, College of Engineering and Technology

ABSTRACT

THE PSEUDO-RIGID-BODY MODEL FOR DYNAMIC PREDICTIONS OF MACRO AND MICRO COMPLIANT MECHANISMS

Scott M. Lyon

Mechanical Engineering

Doctor of Philosophy

This work discusses the dynamic predictions of compliant mechanisms using the Pseudo-Rigid-Body model (PRBM). In order to improve the number of mechanisms that can be modeled, this research develops and identifies several key concepts in the behavior of beam segments where both ends are fixed to a rigid body (fixed-fixed flexible segments). A model is presented, and several examples are discussed. The dynamic behavior of several compliant segments is predicted using the PRBM and the results are compared to finite element analysis and experimental results. Details are presented as to the transient behavior of a typical uniform rectangular cross section beam. The results of this study are extended and applied to compliant planar mechanisms. It is shown by comparison with finite element analysis and experimental results that the PRBM is a good model of the physical system's dynamic behavior. The method is also demonstrated for use with compliant microelectromechanical (MEMS) systems.

ACKNOWLEDGMENTS

I would like to thank all those who have helped in various areas of this research, and given of the time to assist me. I quickly realized that it would not be possible to acknowledge all who have helped with this research by name, but I will always be grateful for the help and support. There are many who gave of their time and resources to help me. I would like to say thank you to each who has given of their time and talents.

Contents

Acknowledgments v

List of Figures xvi

1 Background Information 1

1.1 Introduction 1

1.2 Previous Work 5

1.2.1 The Pseudo-Rigid-Body 5

1.2.2 Modeling Fixed-Fixed Flexible Segments in Mechanisms . . . 8

1.2.3 Dynamics 9

1.2.4 Constant-Force Mechanisms 10

1.3 Summary 11

1.4 Contributions and Directions 12

2 Force-Moment End-Load Conditions 13

2.1 Introduction 13

2.2 Force-Moment End-Load Modeling Cases 14

2.3 Case I: Force and Moment in the Same Direction 14

2.4 Case II: Force and Moment in the Opposite Direction - No Inflection Point 17

2.5 Case III Force and Moment in the Opposite Direction - Inflection Point 19

2.6 Example 23

2.6.1 Decoupling Loads and Path 24

2.7 Summary 25

3 Simplified Model for Force and Moment End Loads **27**

3.1 Simplified PRBM for Fixed-Fixed Segments 27

3.2 Simplified Model 28

3.2.1 Chain Algorithm 29

3.3 Simplified Model Description 29

3.4 Results and Discussion of Results 34

3.4.1 Example Problem 48

3.5 Summary 53

4 Beam Dynamics **55**

4.1 Analytical Approach to Nonlinear Cantilever Beam Dynamics 55

4.2 Assuming a Point Mass End-Loading Condition 59

4.3 Applications to Mechanisms 60

4.3.1 Fixed-Pinned/Fixed-Guided Flexible Segments 60

4.3.2 Fixed-Fixed Flexible Segment 61

4.3.3 Small Length Flexural Pivot Dynamic Modeling Assumptions 62

4.4 The PRBM for a Dynamically Loaded Cantilever Beam 63

4.5 Finite Element Analysis 63

4.5.1 Analysis Method 66

4.5.2 Cantilever Beam FEA Results 66

4.5.3 Experimental Results 68

4.6 Investigation of Modal Frequencies 70

4.7 Summary 80

5 Modeling the Dynamics of Compliant Mechanisms using the Pseudo-Rigid-Body Model **81**

5.1 Model Development 83

5.2 Modeling Straight-Line Mechanisms with Heavy Shuttles 87

5.3 Modeling the Dynamics of Parallel Mechanisms 89

5.4 Summary 91

6 Model Comparisons **93**

6.1 Parallel Mechanisms 93

6.1.1 Dynamic Results 93

6.1.2 Experimental Results 98

6.2 Hoeken Straight-Line Mechanism 100

6.3 Young Mechanism 103

6.3.1 Experimental Setup 104

6.3.2 Results 105

6.3.3 Fixed-Fixed Flexible Segments 115

6.3.4 Modal Frequency of the Cross-Axis Flexural Pivot 118

6.4 Summary 119

7 Micro Mechanisms **123**

7.1 Important Effects of Scaling 123

7.2 Micro Cantilever Beams 126

7.3 Micro Compliant Parallel Mechanism Dynamic Response 127

7.3.1 Modal Frequency Behavior 131

7.4 Folded Beam Structure 131

7.5 Compliant Roberts Straight Line Mechanism 134

7.6 Summary 143

8 Conclusions and Recommendations **145**

8.1 Contributions of This Work 145

8.1.1 Force and Moment Loads (Fixed-Fixed Flexible Segments) . . 145

8.1.2 Dynamic Behavior of the PRBM 146

8.1.3 Micro Compliant Mechanisms 146

8.2 Future Directions of This Work 146

8.2.1 Dynamic-Based Design of Compliant Mechanisms 147

8.2.2 Model Prediction Based on the Dynamic Response 147

8.2.3 Mechanical Energy Harvesting 149

8.3 Summary 149

Bibliography **150**

Appendix **157**

A Supplementary Beam Models **159**

A.1 Modeling the Deflected Shape of a Compliant Segment 159

A.2 Modified Chain Algorithm 165

A.3 Application to curved Beams 169

B Matlab Files **173**

B.1 Micro Folded Beam PRBM 173

B.2 Generic Four-bar Dynamic Model Applied to the Young Mechanism . 175

B.3 Generic Four-bar Dynamic Model Applied to the Roberts Straight Line Mechanism 184

B.4 Generic Four-bar Dynamic Model Applied to the Cross-Axis Flexural Pivot 195

B.5 Young Mechanism Data Analysis File 205

C ANSYS Batch Files **213**

C.1 Micro Beam Models 213

C.2 Micro Roberts Straight Line Mechanism Model 216

C.3 Large Parallel Mechanism Model 220

C.4 Large Young Mechanism Model 224

C.5 Micro Parallel Mechanism Model 228

C.6 Micro Folded Beam Structure Model 232

C.7 Beam Model 238

List of Figures

1.1 A flexible segment subjected to force end loads. 6
1.2 An illustration of the PRBM of a cantilever beam subjected to force end-loads. 6
1.3 Small-length flexural pivot 7
1.4 Fixed-guided beam model. 8
1.5 General PRBM of a crank slider mechanism. 11
2.1 A cantilever beam with the Case I loading conditions and the corresponding bending moment diagram. 15
2.2 A curved flexible segment with the corresponding PRBM. This figure is a modified version of the figure presented by [13] 16
2.3 A cantilever beam with Case II loading conditions and the corresponding bending moment diagram. 18
2.4 A cantilever beam with moment created by the end-force and moment both in the same direction at the base. 18
2.5 The inversion of the Case I loading conditions to represent the Case II loading conditions. 19
2.6 A cantilever beam with the Case III loading conditions and the corresponding bending moment diagram. 20
2.7 The complete PRBM for the Case III loading conditions. 20
2.8 Plot of the deflection path of the endpoint of the beam for Case I and Case II loading conditions. 24
3.1 The simplified model for determining the path of a mechanism with both force and moment loads on an individual segment. 28

3.2 An example of how the relative error of the simplified model was compared to the chain algorithm. 30
3.3 A simplified model for determining the path of a mechanism with both force and moment loads on an individual segment, as compared to the chain algorithm. Note that the deflection and the rotation are in the upper right hand corner of the figure. In this case, the vertical deflection is 55% of the beam length, and the rotation of the end of the beam is 22° from the horizontal. 31
3.4 In this case, the vertical deflection is 54.6 percent of the beam length, and the rotation of the end of the beam is -9° from the horizontal. . 32
3.5 Free-Body-Diagram of the center section of the model shown in Figure 3.1. 32
3.6 The optimum values of $K_{\Theta E}$ and $K_{\Theta A}$ that can be used, based on the anticipated rotation of the end on the cantilever beam ($n = 0$). 34
3.7 The optimum values of $K_{\Theta E}$ and $K_{\Theta A}$ that can be used, based on the anticipated rotation of the end on the cantilever beam ($n = 3$). 35
3.8 The optimum values of $K_{\Theta E}$ and $K_{\Theta A}$ that can be used, based on the anticipated rotation of the end on the cantilever beam ($n = 9$). 35
3.9 The relative error between the proposed PRBM model and the predicted deflection of a chain algorithm (for $n = 0$). 37
3.10 The relative error between the proposed PRBM model and the predicted deflection of a chain algorithm (for $n = 1$). 38
3.11 The relative error between the proposed PRBM model and the predicted deflection of a chain algorithm ($n = 3$). 39
3.12 The relative error between the proposed PRBM model and the predicted deflection of a chain algorithm ($n = 9$). 40
3.13 The percent error between force predicted by the simplified PRBM, and the force predicted by the chain algorithm (for $n = 0$). 41
3.14 The percent error between the moment predicted by the PRBM, and the force predicted by the chain algorithm(for $n = 0$). 42

3.15 The percent error between force predicted by the simplified PRBM, and the force predicted by the chain algorithm (for $n = 3$). 43
3.16 The error associated with the prediction of moment from the PRBM (for $n = 3$). 44
3.17 The percent error between force predicted by the PRBM, and the force predicted by the chain algorithm (for $n = 9$). 45
3.18 The error associated with the prediction of the moment from the PRBM (for $n = 9$). 46
3.19 A representation of the mechanism that was analyzed with the PRBM and compared to the chain algorithm. 49
3.20 The paths of the tracking point, as predicted by the PRBM and the chain algorithm. 50
3.21 The paths of the tracking point, as predicted by the PRBM and the chain algorithm. Scales are adjusted to make the error in the model more visible. 51
3.22 The mechanism analyzed in the example. 51
3.23 PRBM of the mechanism. 52
4.1 Differential segment of a cantilever beam. 56
4.2 Fixed-pinned PRBM equivalent parallel mechanism. 60
4.3 The cantilever beam used in the FEA model. 64
4.4 Vertical and horizontal components of the end of the cantilever beam plotted over time. 67
4.5 End location of the cantilever beam over time. 68
4.6 FFT of the vertical position 69
4.10 Test setup for cantilever beams. 70
4.12 Showing the basic beam loads as applied to a PRBM of a cantilever beam under dynamic loads. 71
4.7 Resonance frequency of a cantilever beam 72
4.8 Predicted frequencies for the smaller beam masses 73
4.9 FEA and PRBM comparisons 74

4.11 FEA and PRBM compared with the measured frequencies 76
4.13 Modal frequency 78
4.14 Diagram of the various loads on a cantilever beam. 79
5.1 Pseudo-rigid-body of a four-bar mechanism. 83
5.2 Graphical depiction of the terms used to describe the links. 84
5.3 The generic model used in the development of the equations of motion for a linear mechanism. Note that the mass of the spring is assumed to be zero, and the shuttle mass will be the dominant mass in the system. 88
5.4 The PRBM for a parallel mechanism. 89
6.1 Parallel Guiding Mechanisms 94
6.2 PRBM for each of the mechanisms in Figure 6.1. 95
6.3 A description of the dimensions given in Table 6.1 96
6.4 Tested Parallel A (Steel) 98
6.5 Hoeken straight line mechanisms 101
6.6 PRBM for each of the Hoeken straight line mechanisms 102
6.7 A depiction the Hoeken straight line mechanisms tested. 103
6.8 Scanning Electron Microscope images of a Young mechanism in both stable positions. 104
6.9 Number 5 test specimen for testing the dynamics of macro compliant mechanisms. 105
6.10 Graphical description of the young mechanism dimensions. 107
6.11 The measured transient response of the Young mechanism around the manufactured stable position. 108
6.12 The measured transient response of the young mechanism around the second stable position. 109
6.13 Plot showing the resulting frequency plot from the FFT of set A of the measured data from the Young mechanisms. 110
6.14 Plot showing the resulting frequency plot from the FFT of set B of the measured data from the Young mechanisms. 110

6.15 Plot showing the resulting frequency plot from the FFT of set C of the measured data from the Young mechanisms. 111
6.16 Unmodified Potential Energy. 112
6.17 Modified Potential Energy 112
6.18 A comparison of the relative change in the rotational angles of the large inertia, and the input angles. The graphic shows why the mechanism exhibits nonlinear behavior. 114
6.19 Representation of a cross axis flexural pivot. The a) frontal, b) side, and c) isometric views are included. 116
6.20 Cross axis flexural pivot dimensions (PRBM) 117
6.21 Cross axis flexural pivot dimensions 117
6.22 PRBM prediction of the path 121
6.23 PRBM prediction of the rotations of the various links. θ_3 is the rotation of the coupler. 121
7.1 An isometric view of a folded beam structure which is a combination of several parallel mechanisms (Left), and a parallel mechanism (right). 124
7.2 A top view and front view of a parallel mechanism with basic size relationships. 125
7.3 Resulting plots (350 micron leg lengths, 80% deflection) for the time characteristics of the horizontal displacement, and the resulting frequency response. 128
7.4 Resulting plots (350 micron leg lengths, 50% deflection) for the time characteristics of the horizontal displacement, and the resulting frequency response (FFT). 129
7.5 Resulting plots (35,000 micron leg lengths, 80% deflection) for the time characteristics of the horizontal displacement, and the resulting frequency response. 130
7.6 An isometric view of a folded beam structure. 132
7.7 Mechanical dimensions of the folded beam structure. 133
7.8 Compliant Roberts Straight-Line mechanism with PRBM Model. . . 135

7.9 Resulting plots (900 micron equivalent leg lengths, 675 micron deflection) for the time characteristics of the horizontal displacement, and the resulting frequency response. 137
7.10 Approximate beam deflection of a cantilever beam in a compliant Roberts straight-line mechanism. 138
7.11 Coupler Rotation Roberts straight-line 139
7.12 FEA prediction of the y deflection. 139
7.13 PRBM dynamic response of the x direction. 140
7.14 PRBM dynamic response of the y direction 141
7.15 PRBM dynamic response 142
8.1 A system that has two perceived degrees of freedom, and one practical degree of freedom. 148
A.1 A deflected cantilever beam, showing the various properties of the beam and the loading conditions. 160
A.2 The Pseudo-Rigid-Body model of a cantilever beam with graphical representations of the various components. 161
A.3 A deflected cantilever beam cut at a center location in the beam. . . 162
A.4 A graphical depiction of combining two cantilever beams to find a central location on the beam. 163
A.5 The path of the beam as represented by the PRBM 164
A.6 Beam elements for the modified chain algorithm. 166
A.7 A beam element (i+1) with applied end-force and moment loads. . . 168
A.8 A comparison of an element based, PRBM, and a modified chain algorithm 170

Chapter 1

Background Information

The purpose of this research is to develop a method for modeling the dynamic response of compliant mechanisms using the Pseudo-Rigid-Body Model (PRBM). First, the PRBM is extended to include segments with fixed-fixed end conditions, and this model is later used in the dynamic analysis of compliant mechanisms with fixed-fixed flexible segments. The dynamic prediction of compliant segments is followed by modeling the dynamics of macro and micro compliant mechanisms. Before going into specific detail in these areas, an introduction to the PRBM and the current literature is presented.

1.1 Introduction

In the world around us we see branches moving and swaying in the wind, the grass blowing, and many other ways in which flexibility is used nature. However, engineering practice is often to avoids flexibility in design. For modeling and design purposes many systems are designed and assumed to be rigid [1, 2]. Mechanisms that gain some or all of their motion through the deflection of flexible members are classified as compliant mechanisms [3]. Compliant mechanisms are different, in that they depend on the motion of flexible segments in order for them to perform their function. Why then would so much effort be placed in avoiding flexibility in design, when a flexible system could work better? Traditional methods of design are based on simple cases and do not require significant calculations. However, with the growth of the computers, engineers are able to solve complex systems using numerical methods without much difficulty. One problem that is easier to solve, due to the

increased availability of numerical methods, is a force end-loaded beam with nonlinear deflections.

Interest in research of compliant mechanisms has expanded, largely due to the development advanced materials such as engineering polymers. Industry has encouraged expansion in compliant mechanism. Two of the most predominant reasons industry is interested in compliant mechanisms are the reduction in manufacturing cost and part count reduction. In many cases, a compliant mechanism can be molded with little or no secondary processing. Compliant mechanisms that have no sliding surfaces (referred to as fully-compliant mechanisms), will have a precise motion that is difficult to achieve with traditional joints. The growing need for compliant mechanisms, and the ever-present need of industry to move from a design concept to an actual product in the minimum amount of time, has helped to intensify the need for a modeling technique for the design of compliant mechanisms.

In recent years, two separate approaches have been developed that allow an engineer to design compliant mechanisms. One of these methods uses optimization to determine the topology for a device to have a specified force-displacement relationship. This approach allows the designer to specify the inputs of a mechanism and the desired outputs of the mechanism. The computer uses the desired input and output and varies the geometry between them, until the output motion moves or produces a force with the desired relationship to the input. There are several approaches as to how the material between the inputs and outputs is defined and what is allowed to change or vary with each iteration. Both the grid and the method of varying the material depend on the type of optimization that is being done, and the problem that is being analyzed. This type of approach is classified as topology optimization.

Topology optimization [4, 5, 6, 7] has the ability to develop non-traditional geometries, and is not limited by preconceived ideas of the designer. One form of topology optimization uses structural optimization to determine the topology for a device to have a specified force-displacement relationship [5]. Multi-criteria optimization with a penalty function has been used for topology optimization of compliant mechanisms with a large number of design variables [6]. Another method of topology

optimization of compliant mechanisms has also been presented by [8], where the optimization problem is solved using the method of moving asymptotes. Each of these methods is a powerful way of using computers to design a compliant mechanism.

The second approach to the design of compliant mechanisms uses the Pseudo-Rigid-Body Model (PRBM). Here the goal is to replace the flexible portions or beams (referred to as flexible segments) with an equivalent system of pin joints, rigid links, and torsional springs. With the replacement of a flexible segment with a rigid body equivalent linkage, traditional methods of kinematic analysis and design are available to the designer. The PRBM technique utilizes the many years of research and the knowledge that have been developed for kinematic analysis and design. Traditional mechanisms provide several examples for conversion to a compliant counterpart. In addition to providing examples, the PRBM technique is compatible with traditional kinematic synthesis techniques. An additional significant advantage of using the PRBM is the ability to visualize the systems, and the motion of that system. This allows the designer to bring intuition from the behavior of the kinematic systems. FEA analysis brings the ability to more accurately model systems, but it is difficult to model a system with FEA without first having a general structure of a the compliant mechanism. In this way the PRBM allows for the initial design of the complaint mechanism, and then FEA can be used for model refinement, and more accurate analysis of the system. Both methods being required for most completed designs.

Both topology optimization and the PRBM allow the designer to utilize different bodies of knowledge. The method of topology optimization has the ability to develop mechanisms that have never been conceived of previously. The PRBM technique applies the body of knowledge that has been developed for rigid-body techniques to compliant mechanisms. The work presented in this dissertation will focus on the Pseudo-Rigid-Body Model.

The PRBM has been shown to be a useful tool in design [9, 10, 11, 12, 13]. There is a need for a simple model for predicting the dynamic behavior of compliant mechanisms. The focus of the research will be on validating the PRBM modeling technique as a viable method for predicting the dynamics of compliant mechanisms.

Although the use of the PRBM has been demonstrated and more uses are being developed continually, there is still room for expanding the PRBM to cover a larger range of beam loading conditions. In the past few years, there has been a growing interest in developing a PRBM for a beam with both force and moment end-loads. Once developed this model will also be used to model the dynamics of compliant mechanisms with fixed-fixed flexible segments. A fixed-fixed flexible segment allows the rigid bodies to move with respect to each other, however the beam is required to maintain both the rotational and position characteristics of the rigid body at each end of the flexible segment.

Understanding the ability of the PRBM to predict the dynamic behavior of compliant mechanisms is vital to obtaining designs quickly. FEA is a powerful tool in analyzing compliant mechanisms, but the FEA package requires that the geometry of the mechanisms is specified. The PRBM is vital in the development of that geometry, which once defined can be analyzed in FEA. Many of these designs are required to have a specified transient response. With every PRBM configuration of a mechanism, there are a significant number of variations that can be developed. An example comes from a parallel mechanism. Research on the parallel mechanism has shown that there are twenty-eight possible configurations that can be developed [9]. Each of these mechanisms has a different geometry. Use of FEA at this point would require the designer analyze each of the twenty eight configurations in order to determine if they meet the transient behavior requirements. Each of those twenty eight configurations would require a specified geometry, and rebuilding of the FEA model. However, the same PRBM is used for each of the configurations. As mechanisms become more complex, the number of configurations continues to increase. Showing that the PRBM can predict the dynamic behavior of compliant mechanisms speeds up the design process, by allowing the geometry of the mechanisms to be determined. Once the geometry is determined, then other methods (FEA, Chain Algorithm, etc.) can be used to complete a detailed analysis of the mechanisms.

1.2 Previous Work

The work that has already been completed on the PRBM is vital to this work, and is reviewed in this section. Because this information is readily available from multiple sources [3, 9, 10, 11, 12, 13, 14, 15, 16], the material will not be presented in great detail.

1.2.1 The Pseudo-Rigid-Body

The Pseudo-Rigid-Body Model (PRBM) asserts that the deflection of flexible segments that are undergoing large deflections can be approximated with rigid-body equivalent systems. An example of a flexible segment is given in Figure 1.1. The flexible segment is subjected to a force load at one end of the segment, and is fixed at the other end of the segment. If the correct geometry is used, the flexible system of Figure 1.1 can be replaced with the system shown in Figure 1.2. Note that the path of the end of the beam is easily determined without knowing the magnitude of the applied forces. The rigid-body model and the flexible segment will have essentially the same path. The model shown in Figure 1.2 is easily implemented in a kinematic system, whereas the model in Figure 1.1 is difficult to implement, because the forces need to be known in order to determine the location of the end of the flexible segment. The specific details behind the force end-loaded cantilever beam are discussed by Howell et al. [15]. Without the PRBM, the system would require the solution of closed-form equations involving elliptic integrals [17, 18, 19, 15]. Other methods of solving the system include FEA techniques and the use of a chain algorithm [20, 21, 22, 23].

The small-length flexural pivot [3] is used to model a flexible segment where the moment is much larger than the forces that are applied to that segment. In addition, the small-length flexural pivot requires the length of the flexible segment to be short in comparison to the rigid segment to which it is attached. Figure 1.3 shows a small-length flexural pivot attached to a long rigid segment. If a vertical force is applied to the rigid segment then the moment in the flexible segment will be significantly larger than the force for a large range of motion. The behavior of the

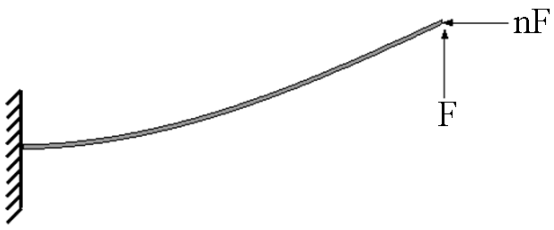

Figure 1.1: A flexible segment subjected to force end loads.

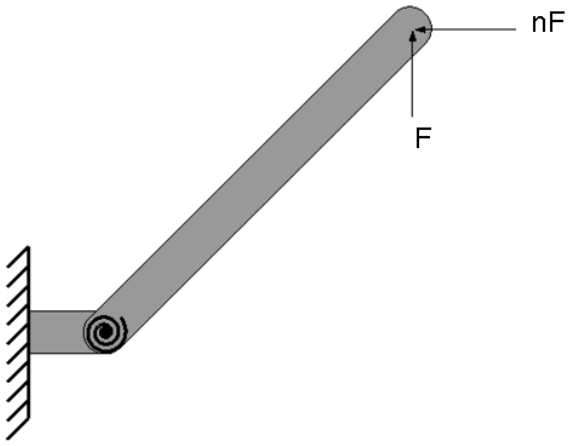

Figure 1.2: An illustration of the PRBM of a cantilever beam subjected to force end-loads.

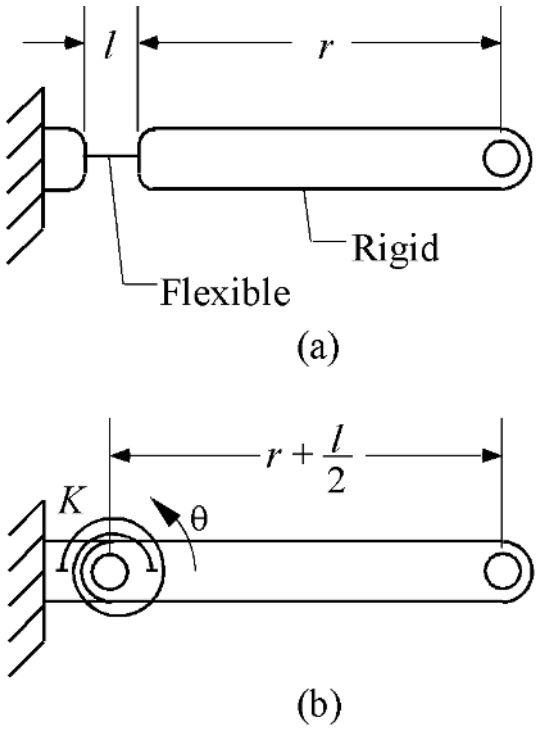

Figure 1.3: An example location for the use of a small-length flexural pivot.

flexible segment can easily be modelled if the assumption is made that the flexible segment is only subjected to a moment load. The deflection can be approximated by placing a pin joint at half of the length, and using a torsional spring to represent the resistance to motion.

The initially-curved segment provides a slightly new challenge to overcome in the development of a PRBM that will adequately model the system. The initially-curved segment [16] has the same basic model as was presented in Figure 1.2, with different parameters to account for the initial curvature of the beam. This model will be discussed in more detail in Section 2.3.

In the case of a fixed-guided flexible segment, the moments in the center of the beam will be zero. From the Bernoulli-Euler equation it is known that where the moment is zero, the curvature is also zero. The fact that there is no moment, or curvature, at the center of the beam suggests that the fixed-guided segment can be

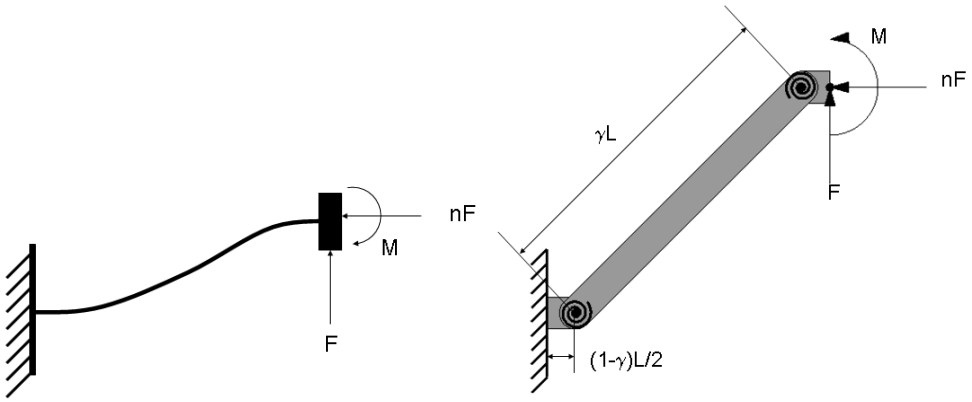

Figure 1.4: The basic model for the fixed-guided beam.

modeled as two cantilever beams with force end-loads only. Each of the models has a length of one-half of the length of the fixed-guided segment. The two cantilever segments are then joined in the center as shown in Figure 1.4.

The functionally binary pinned-pinned segments are defined as having a pin joint at each end of a flexible segment [24]. Due to the nature of the pin joint, no moment can be transferred through the ends. Thus, the reaction force is in the line between the two pin joints. For the special case of a curved member between the two pin joints, a model has been developed for determining the reaction force [24].

1.2.2 Modeling Fixed-Fixed Flexible Segments in Mechanisms

Other researchers have discussed development of a PRBM for force and moment end-loaded beams. Saxena and Kramer [25] use a model that consists of two torsional springs and a slider. The slider is required because the path of the cantilever beam changes with the change in the relationship of the force and moment end-loads. The variation of the length of the internal link allows the model to adjust and change based on the curvature of the beam, due to the changing relationship between the force and the moment. This method is effective in determining the path, but requires iteration for every step during the motion of a mechanism, since the force and moment are not decoupled from the path.

Tsai et al. [26] discuss both the elliptic integrals and the PRBM. The work analyzes the elliptic integrals and essentially re-parameterizes for the cases where both force and moment end-loads are applied. The methods developed allow a PRBM to be developed for the case where an inflection point exists in the cantilever beam. The work completed did not examine loading conditions without an inflection point in the beam.

Being able to model a flexible segment with force and moment end loads will increase the usefulness of the PRBM technique. The method will allow for a greater number of mechanisms to be modeled.

1.2.3 Dynamics

The topic of the dynamics of linkages has been studied for many years [27, 28, 29]. However, the same mechanisms that have a well-established method for analysis cannot be analyzed using kinematic analysis if a single link is replaced with a flexible segment. The problem of how to approach the analysis has been considered by many authors using a variety of methods. A brief review of some techniques that have been used for determining the dynamic behavior of flexible kinematic systems are discussed below.

One common approach for modeling flexible segments is called a lumped parameter model [30, 31, 32, 33, 34], which splits the beam into rigid segments with point masses, pin joints, and torsional springs. The accuracy of the lumped parameter model increases as the number of lumps increases. A single flexible segment could have as many springs and masses in the system as the modeler chooses. The more parameters, the more accurate the model would become; however, the computation time would also increase with an increase in the number of parameters. The benefits of this modeling technique include the ability to accurately model the motion of a flexible segment to the first three to four modal frequencies [35].

In recent years, with the increase in speed and decreasing cost of computers, finite element analysis (FEA) has become more common. FEA methods are well

understood, and many FEA codes are available for research. In FEA, the compliant segment is broken up into a series of small pieces or segments. Each of these small segments is then analyzed using small-deflection analysis. The solution is then determined by combining the individual segment results. It is important to note that for nonlinear deflections, the results need to be obtained iteratively, and the forces cannot be separated from the deflection path. The nonlinear aspect of the FEA process requires a more sophisticated FEA code. Several researchers have published in the area of FEA methods for the determination of the dynamics of flexible segments [36, 37, 38, 39].

1.2.4 Constant-Force Mechanisms

The crank-slider mechanism represents a great number of mechanisms that have linear and rotary motion in the same system. The crank-slider mechanism is used in a variety of systems, including constant-force compression springs. A great deal of work has already been completed in the modeling of constant-force compression springs [10, 40, 41, 42]. A brief summary of the work completed by Boyle [40, 43] is presented here.

Boyle et al. [40] discuss the application of the PRBM to constant force mechanisms. The mechanisms were tested under both static and dynamic loading conditions. The general model of the mechanisms that were tested is a crank slider mechanism with torsional springs at each of the three pin joint locations, as illustrated in Figure 1.5. Depending on the configuration that was selected, some of the torsional springs are eliminated, and replaced with traditional pin joints. The work [43] also used a Lagrangian approach to develop the equations of motion. Although these general equations are not repeated here, they can be found on pages 17-32, and 56-59 of [43]. The dynamic model included two terms that were required to compensate for friction characteristics. The two terms were coulomb friction (τ_C) and unmodeled torque (τ_{um}). Coulomb friction is not unusual to dynamic systems, and it is not surprising that the term was used for the dynamic model. The unmodeled

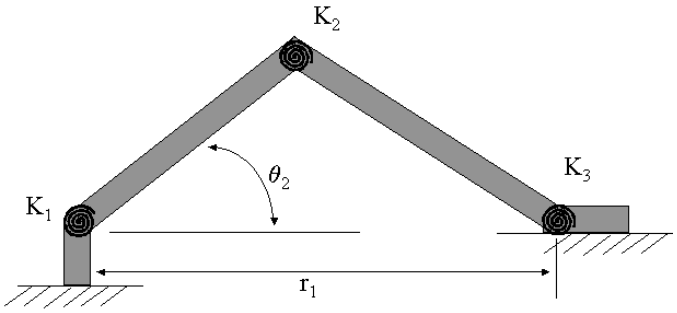

Figure 1.5: General PRBM of a crank slider mechanism.

torque is a different problem, and some explanation is valuable. The compliant mechanisms that were tested typically required at least one of the joints to be a traditional revolute joint. This joint typically consists of two surfaces that slide with respect to one another. The two surfaces will naturally require an additional torque, which is defined by the coefficient of friction between the two surfaces. For the work that was presented by [43, 40], the choice of pin joints created a significant amount of friction in the system. This friction created the need for the additional term (τ_{um}), which is intended to compensate for the friction that is created in the pin joints.

The constant-force mechanisms were then driven by a near sinusoidal input. The force response was measured, and compared with the response that was predicted by the model. The author concludes that the PRBM made was a good representation of the physical system.

1.3 Summary

A significant amount of research has attempted to move from a design problem to a compliant solution. The PRBM produces a result that is compatible with the kinematic analysis and design techniques, since the PRBM technique decouples the forces from the deflection path. The decoupling of the forces from the deflection path is the key to allowing the research that has already been completed for rigid-body mechanisms to be used with compliant mechanisms.

Significant research has also been completed in the development of a PRBM for force and moment loads on flexible segments. However, the models have been unable to decouple the forces from the deflection path. Because the path and the forces have not been decoupled for this loading condition, kinematic analysis techniques are not as easily implemented.

A brief review of the dynamics of flexible segments has been provided. The most common techniques are lumped parameters models and FEA. Neither of these methods are compatible with traditional kinematics.

1.4 Contributions and Directions

The major contribution of this work is a method for modeling the dynamic behavior of compliant mechanisms using the PRBM. This dynamic evaluation of the PRBM examines the individual beams that are used in compliant mechanisms, and then expands into compliant mechanisms on both the macro and micro scale. In order to increase the number of systems that are able to be modeled, a contribution will also be made in the development of a PRBM technique that allows for the design of mechanisms that have individual compliant segments that are fixed rigidly to links at both ends.

The research presented is divided up into three sections. The first section, Chapters 2 and 3, contain the development of a PRBM for flexible segments that have force and moment end-loads (or fixed-fixed boundary conditions). The second section, Chapters 4 to 6, discusses the dynamic behavior of flexible segments, and application to compliant mechanisms. The third section, Chapter 7, applies the modeling techniques on the micro scale to microelectromechanical systems, and compares the result with FEA.

Chapter 2

Force-Moment End-Load Conditions

2.1 Introduction

The physical phenomenon that occurs with force and moment loading of a beam can be determined using the Bernoulli-Euler equation. The Bernoulli-Euler equation states that the bending moment is proportional to curvature, or

$$M = EI\frac{d\theta}{ds} = EI\frac{\frac{d^2y}{dx^2}}{(1+(\frac{dy}{dx})^{\frac{3}{2}})}. \tag{2.1}$$

The solution of this equation yields the deflection path of the beam. For large, nonlinear deflections, Equation (2.1) can be solved using elliptic integrals [17, 18, 19, 15]. Nonlinear finite element analysis (FEA) may also be used to determine the deflection path. Both methods are useful for analysis once a configuration has been chosen, but are difficult to use in design since neither method decouples the force and moment from the path of the beam. For compliant mechanism design, which is the motivation for this research, a beam used in a mechanism would need to have the path decoupled from the forces and moments in order to use kinematic analysis and synthesis methods. Chapter 1 covered the basic ideas behind two models that have already been presented [25, 26]. However, due to the limitations in these models an efforts has been made to improve upon the ideas that were presented. This chapter will focus on developing an understanding of the loading conditions, that can occur in a segment with force and moment load conditions, in addition several models will be discussed that have the ability to model the flexible segment with each set of loading conditions.

2.2 Force-Moment End-Load Modeling Cases

This section presents a model that can be used to predict the deflections of a cantilever beam with force and moment end-load conditions. The direction of the force will remain constant (i.e. the value of n (as seen in Figure 1.2) remains constant.) All of the cases investigated treat a flexible segment with different end-loading conditions. In Case I, the applied end force creates a moment at the base of the beam that is in the same direction as the applied moment. Case II occurs when an applied end force creates a moment at the base of the beam that is in the opposite direction of the applied moment, where the magnitude of the moment created by the force load is smaller than the applied moment. Finally, Case III has the same loading conditions as Case II; however, for Case III loading the magnitude of the moment created by the force load is larger than the applied moment. Case III loading will have an inflection point where the magnitude of the sum of the moments is zero.

2.3 Case I: Force and Moment in the Same Direction

Case I may be represented by a cantilever beam with an applied force and moment. The force and moment are applied at the endpoint of the beam and act to create moments in the same direction. The beam with end-loading conditions and the bending moment diagram are shown in Figure 2.1, where the moment in the cantilever beam is given by the sum of the moment due to the applied moment (M) and the moment due to the force (M_f). Developing a PRBM for this loading condition is accomplished by realizing that the moment creates a curvature in the beam that is continuous throughout the entire beam. The continuous curvature due to the moment is the same as a beam that is initially curved, where the non-dimensional representation of the curvature is defined by [16] as

$$\kappa_o = \frac{M_o l}{EI}, \tag{2.2}$$

(where M_o is the applied moment, l is the length of the beam, E is the modulus of elasticity, and I is the area moment of inertia)

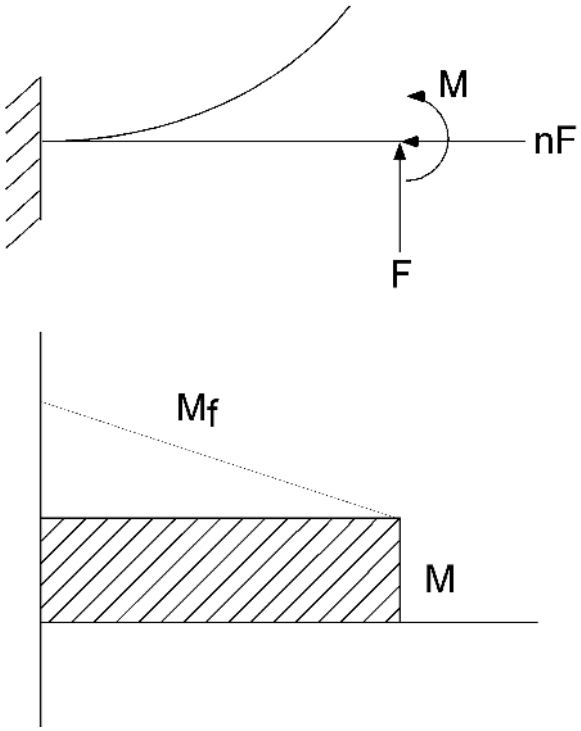

Figure 2.1: A cantilever beam with the Case I loading conditions and the corresponding bending moment diagram.

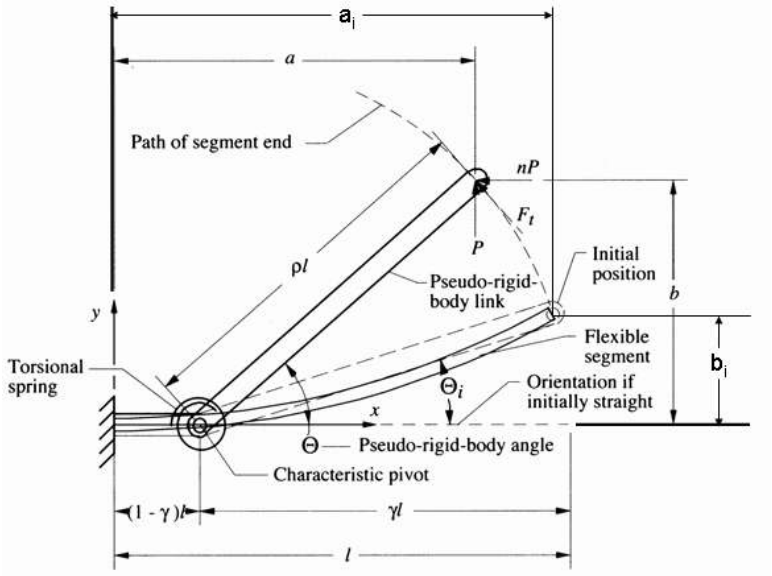

Figure 2.2: A curved flexible segment with the corresponding PRBM. This figure is a modified version of the figure presented by [13]

Using the model developed for initially-curved beams consisting of two rigid links, and a torsional spring [16], and Equation (2.2) the deflection can be easily evaluated. Figure 2.2 shows a segment with the applied end-load and moment corresponding to the PRBM, where the initial curvature is the curvature due to the moment load on the beam. The application of the end-force and moment produce an additional curvature in the segment such that the pseudo-rigid-body angle has a non-zero value, Θ_i, given as

$$\Theta_i = atan(\frac{b_i}{a_i - l(1-\gamma)}). \tag{2.3}$$

The length of the pseudo-rigid-body link, ρl is found from

$$\rho = [(\frac{a_i}{l} - (1-\gamma))^2 + (\frac{b_i}{l})^2]^{\frac{1}{2}}, \tag{2.4}$$

where ρ is the characteristic radius, and a_i and b_i are the initial x and y coordinates of the end-point of the segment. The values of a_i and b_i can be found using Equations (2.5) and (2.6):

$$\frac{a_i}{l} = \frac{R_i}{l} sin(\frac{l}{R_i}) \tag{2.5}$$

$$\frac{b_i}{l} = \frac{R_i}{l}(1 - cos(\frac{l}{R_i})), \tag{2.6}$$

where R_i is the initial radius of the beam, which is inversely proportional to the moment applied to the beam

$$\frac{1}{R_i} = \frac{M_o l}{EI}. \tag{2.7}$$

M_o is the moment applied to the end of the beam, l is the length of the beam, E is the Young's Modulus of the beam, and I is the area moment of inertia of the beam. Finally, the deflection path of the segment may be approximated by

$$\frac{a}{l} = 1 - \gamma + \rho cos(\Theta) \tag{2.8}$$

and

$$\frac{b}{l} = \rho sin(\Theta). \tag{2.9}$$

2.4 Case II: Force and Moment in the Opposite Direction - No Inflection Point

Case II occurs when an applied end-force creates a moment at the base of the beam that is in the opposite direction as the applied moment, where the magnitude of the force is small enough that no inflection point is created in the beam. Figure 2.3 shows the Case II loading conditions and a possible bending moment diagram. A model for these loading conditions comes from examining a beam with a moment and force in the same direction. If the reaction forces are examined, it is apparent that the reaction force acts in the opposite direction of the applied force, as shown in Figure 2.4. This suggests that the model for a force and moment in opposite directions is given by the same model as Case I, with one minor exception: the ground is switched to the opposite side of the beam, as shown in Figure 2.5. In mechanism analysis and design, switching the ground link is called an inversion. Though not exactly the same, this term will be used to describe the case where a different beam end is fixed. The same equations that were used in Case I may also be applied to Case II, by taking into account the inversion described above, and shown in Figure 2.5.

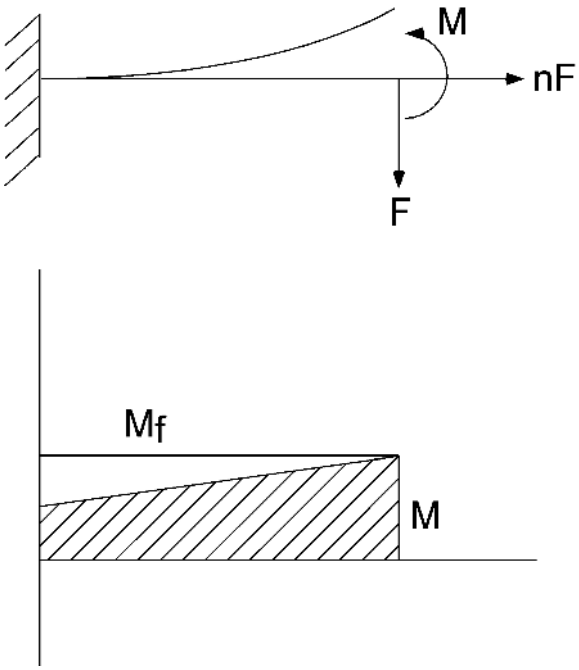

Figure 2.3: A cantilever beam with Case II loading conditions and the corresponding bending moment diagram.

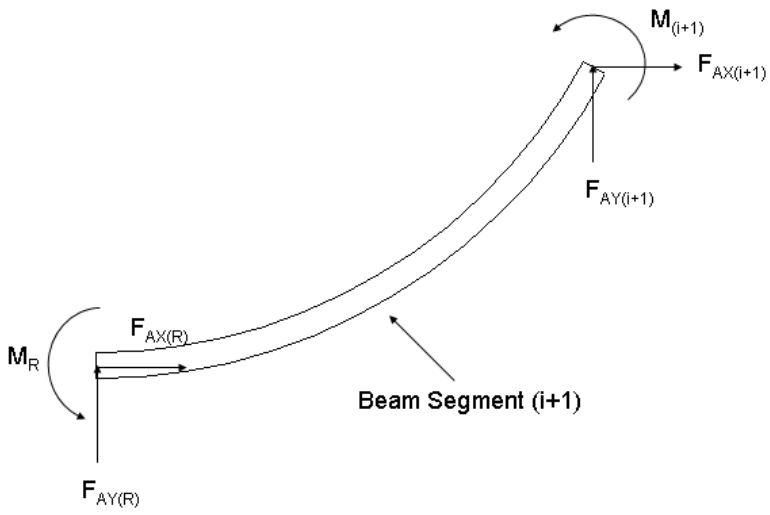

Figure 2.4: A cantilever beam with moment created by the end-force and moment both in the same direction at the base.

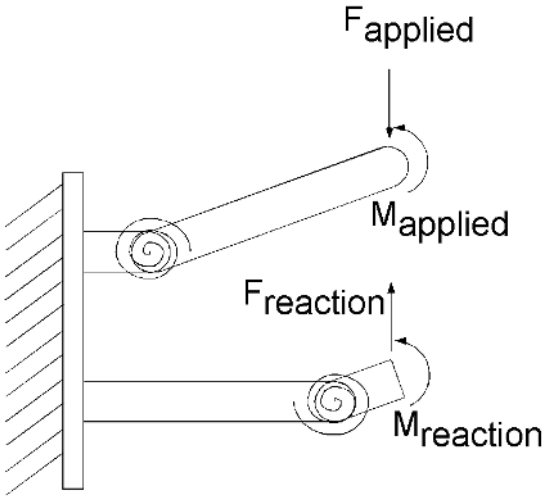

Figure 2.5: The inversion of the Case I loading conditions to represent the Case II loading conditions.

2.5 Case III Force and Moment in the Opposite Direction - Inflection Point

Case III is a cantilever beam with the applied end-force and moment acting in opposite directions. For this case, the applied moment is such that there exists an inflection point in the deflected beam. Figure 2.6 shows the cantilever beam with the Case III loading conditions and a bending moment diagram. The Bernoulli-Euler equation states that the bending moment is proportional to the curvature. At the inflection point there is zero moment, and therefore zero curvature. Modeling of this case requires knowledge of the location of the inflection point in the segment. The model of Case III uses the combination of two separate PRBM's. Figure 2.7 shows the model for the Case III loading conditions. Examination of the model gives

$$\theta_E = \theta_A + \beta - \theta_B = C_A\theta_A - C_B\theta_B. \tag{2.10}$$

In order to satisfy the requirement of continuous curvature throughout the beam,

$$\beta = (C_A - 1)\theta_A - (C_B - 1)\theta_B, \tag{2.11}$$

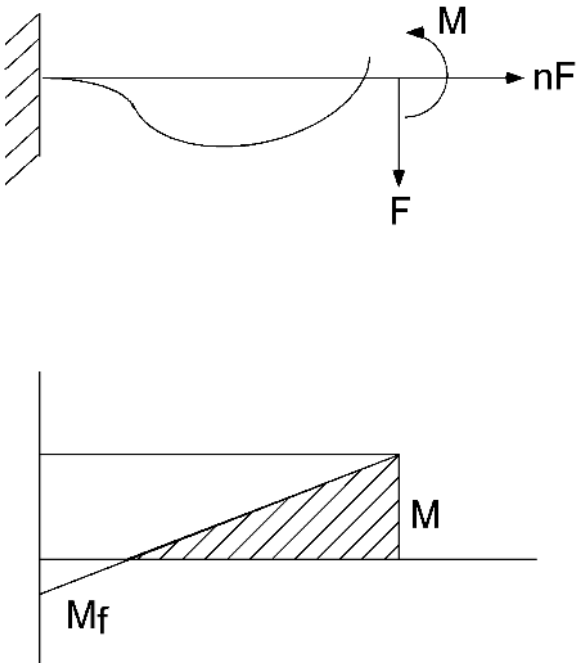

Figure 2.6: A cantilever beam with the Case III loading conditions and the corresponding bending moment diagram.

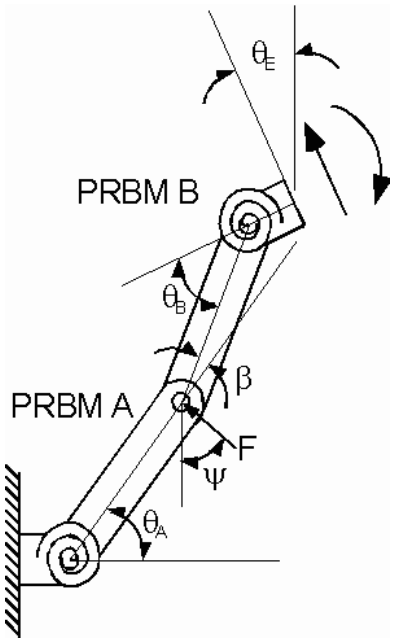

Figure 2.7: The complete PRBM for the Case III loading conditions.

where C_A and C_B are the parametric angle coefficients [15]. Using the PRBM developed for a cantilever beam with an applied end-force for PRBM A and PRBM B (Figure 2.7) yields

$$F\cos(\psi)(\gamma_A l_A)\cos(\theta_A) + F\sin(\psi)(\gamma_A l_A)\sin(\theta_A) = k\theta_A \tag{2.12}$$

and

$$F\cos(\psi+\theta_E)(\gamma_B l_B)\cos(\theta_B) + F\sin(\psi+\theta_E)(\gamma_B l_B)\sin(\theta_B) = k\theta_B \tag{2.13}$$

with the value of k equal to:

$$k = \frac{\gamma K_\Theta EI}{l}. \tag{2.14}$$

γ is the characteristic radius factor, K_Θ is the spring constant for the torsional spring, E is the Young modulus, I is the area moment of inertia, and l is the length of the beam. Substituting Equation (2.14) for k, dividing Equation (2.12) by Equation (2.13), and simplifying the result yields:

$$\frac{\theta_A}{\theta_B} = \frac{K_{\Theta B} l_A^2(\cos(\psi)\cos(\theta_A) + \sin(\psi)\sin(\theta_A)}{K_{\Theta A} l_B^2(\cos(\psi-\theta_E)\cos(\theta_B) + \sin(\psi-\theta_E)\sin(\theta_B)}. \tag{2.15}$$

Also note that

$$l_B = l_A - l_{total}. \tag{2.16}$$

However, this will not provide enough equations to solve for all of the independent variables. The last required equation comes from the total energy that is stored in the beam. The energy that is stored in the beam is approximated by

$$Energy = \frac{1}{2}k_A\theta_A^2 + \frac{1}{2}k_B\theta_B^2. \tag{2.17}$$

The energy in the system will tend to stay at a minimum value, due to the natural tendency of all physical systems to remain in a minimum energy state. The minimum energy state will occur when the derivative of the energy is zero. The derivative of Equation (2.17) with respect to θ_A is

$$\frac{dEnergy}{d\theta_A} = -\frac{\gamma_A K_{\Theta_A}\theta_A^2 EI}{2{l_A}^2}\frac{dl_A}{d\theta_A} - \frac{\gamma_B K_{\Theta_B}\theta_B^2 EI}{2{l_B}^2}\frac{dl_B}{d\theta_A} + \frac{\gamma_A K_{\Theta_A} EI\theta_A}{l_A} + \frac{\gamma_B K_{\Theta_B} EI\theta_B}{l_B}\frac{d\theta_B}{d\theta_A} \tag{2.18}$$

The only real solution to this equation is found if each of the following quadratic formulas are zero:

$$-\frac{\gamma_A K_{\Theta_A} \theta_A^2 EI}{2{l_A}^2}\frac{dl_A}{d\theta_A} + \frac{\gamma_A K_{\Theta_A} EI\theta_A}{l_A} = 0 \tag{2.19}$$

$$-\frac{\gamma_B K_{\Theta_B} \theta_B^2 EI}{2{l_B}^2}\frac{dl_B}{d\theta_A} + \frac{\gamma_B K_{\Theta_B} EI\theta_B}{l_B}\frac{d\theta_B}{d\theta_A} = 0 \tag{2.20}$$

resulting in:

$$\theta_A = \frac{2l_A}{\frac{dl_A}{d\theta_A}}, 0 \tag{2.21}$$

$$\theta_B = \frac{2l_B\frac{d\theta_B}{d\theta_A}}{\frac{dl_B}{d\theta_A}}, 0. \tag{2.22}$$

Using the two nontrivial solutions and dividing one by the other, it can be shown that the ratio of θ_A to θ_B is

$$\frac{\theta_A}{\theta_B} = \frac{2l_A\frac{dl_B}{d\theta_A}}{2l_B\frac{dl_A}{d\theta_A}\frac{d\theta_B}{d\theta_A}}, \tag{2.23}$$

where

$$\frac{dl_A}{dl_B} = 1. \tag{2.24}$$

Taking the derivative of Equation (2.10) and simplifying, results in

$$\frac{d\theta_A}{d\theta_B} = \frac{(C_B)}{(C_A)}. \tag{2.25}$$

Substitution of Equation 2.25 into of Equation (2.23) and simplifying yields

$$\frac{\theta_A}{\theta_B} = \frac{l_A(C_B)}{l_B(C_A)}. \tag{2.26}$$

With Equation (2.26) there are sufficient equations to determine all of the states in the system.

An approach that decouples the path, the applied forces, and moments is needed. Although these models can be used in the development of the deflection path of a segment with force and moment end-loads, they do not decouple the path from the loads. They are of more value as a tool to understand the behavior of each of the segments.

There are times when these models provided valuable insight into the problems that can occur in beam loading. Two example problems have been provided to show how the methods can be applied.

Table 2.1: Coefficients for PRBM for Initially-curved Cantilever Beams [16]

κ_o	n	Θ_i	γ	ρ	K_Θ
1.50	0	52.28	0.8141	0.7832	2.8234
1.50	0.25	52.70	0.8069	0.7788	2.7816
1.50	0.5	53.10	0.8002	0.7747	2.7575
1.50	1.0	53.55	0.7926	0.7702	2.7663
1.50	2.0	53.95	0.7859	0.7662	2.7786
1.50	10.0	54.47	0.7773	0.7612	2.7786

2.6 Example

Problem: Part a) Find the PRBM of a steel (E =206 GPa) beam 0.6096 m in length, with a cross-sectional area of 0.000794 m by 0.0254 m. The beam is fixed at one end, and has an applied moment of 0.538 N-m and an applied vertical force with a variable magnitude at the other end.

Solution: Using Equation 2.27 solve for the value of κ_o:

$$\kappa_o = \frac{M_o l}{EI} = \frac{(0.538)(0.6906)}{(206 \times 10^9)(1.06 \times 10^{-12})}. \tag{2.27}$$

With the value of n, the horizontal load component, equal to zero, and the value of κ_o, the other PRBM variables are given in Table 2.1. Parameters for other types of loding conditions may be obtained from Howell and Midha [16]. The values for the model are: $n = 0$, $\Theta_i = 52.28$, $\gamma = 0.8141$, $\rho = 0.7832$, and $K_\Theta = 2.8234$ for this problem, where K_Θ is the stiffness coefficient for the torsional spring, and the other variables have been described above. The resulting deflections are $a = 0.405$ and $b = 0.378$. The deflection path of the endpoint of the beam is presented in Figure 2.8 as the force is increased in the positive y direction.

Part b) On the same plot show the Case II loading conditions by plotting the path of the beam as the force is increased in the negative direction. The same value of κ_o applies in this direction as in the previous case so each of the parameters $n = 0$, $\Theta_i = 52.28$, $\gamma = 0.8141$, $\rho = 0.7832$, and $K_\Theta = 2.8234$ remain the same. In this case the model used is inverted, as is demonstrated in Figure 2.5. Figure 2.8 shows the

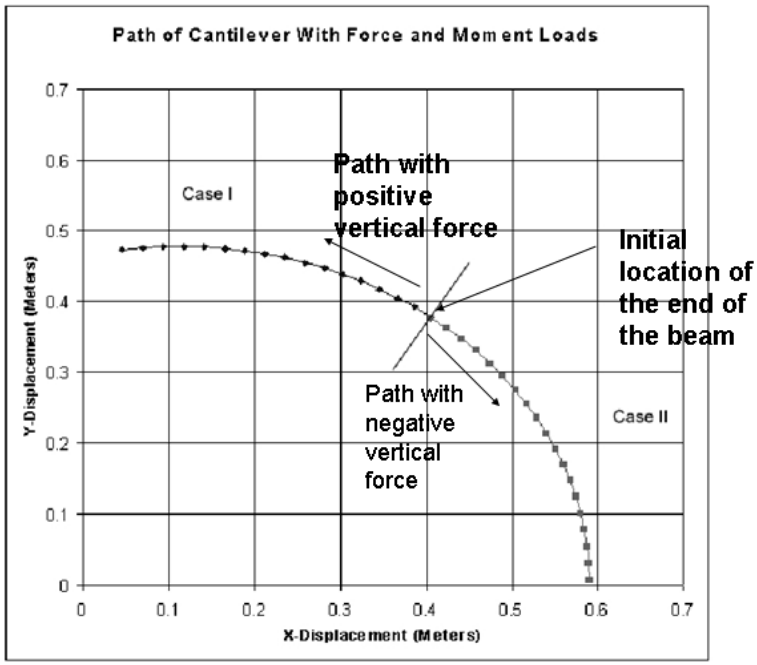

Figure 2.8: Plot of the deflection path of the endpoint of the beam for Case I and Case II loading conditions.

resulting behavior of the beam. As can be seen from Figure 2.8, the beam begins at the undeflected location and, depending on the direction of the force, moves in two different paths.

2.6.1 Decoupling Loads and Path

Although several models have been discussed for the development of a PRBM for a cantilever beam with force and moment loads, the transition to kinematic modeling of mechanisms has not been made. Each of the above methods depends on forces and/or moments in order to create the geometry that would be used with the PRBM. It is thus necessary to change the model every time the input of the mechanism is changed. Because the model is changing with the motion of the input link, an iterative technique is required. With the improvements in the speed of computers and optimization, the iteration is a simple task.

The challenge comes when traditional kinematic methods of design and analysis are applied to a mechanism with a link length that is varying with the input. In addition to this variation, the applied forces and moments must also be known. The coupling between the forces and the path requires the design and analysis to be kinetic instead of kinematic, and is a primary justification for researching a model that is decoupled from the applied forces and moments. So the question is: Is it possible to decouple the forces and the moments from the geometry of the modelled links[1]? If it is possible, then what error is caused by the approximation? The following chapter investigates each of these questions.

2.7 Summary

Several models have been presented to approximate the deflection path of a cantilever beam with applied force and moment loads. The problem was divided into three classifications for end loading conditions. Each of these three techniques were examined and PRBM's were developed for each individual case. The model proves to be useful in the case where the moment is constant and the forces vary; however, when both the force and the moment vary, the model is not as useful. Since methods for mechanism design and kinematic synthesis have all been developed around traditional rigid-body systems, the coupled behavior of the models presented make them difficult to use with these traditional methods. A method that decouples the applied forces and moments from the path is required. The significant contribution of this chapter was the development of several compliant models that represent the basic motion of compliant segments that have both a position and rotation defined on each end. The next chapter builds on this idea with a simplified model that decouples the loads from the path.

[1]In this case, decoupling load and path means that the overall path of the beam end can be determined without knowledge of the loads. The load is required only for the force deflection behavior of the system.

Chapter 3

Simplified Model for Force and Moment End Loads

The research presented in this chapter focuses on the development of a simplified Pseudo-Rigid-Body Model (PRBM) for fixed-fixed flexible segments. The model predicts the path within ten percent of the results obtained from a chain algorithm. This error is larger than PRBM's of other types of flexible segments, but is still useful in preliminary design of compliant mechanisms. The model's major advantage is that the force and moment are decoupled from the link length in the model, allowing the model to be used with traditional kinematic mechanism design and synthesis techniques.

3.1 Simplified PRBM for Fixed-Fixed Segments

For the compliant mechanisms designer it is important to be able to predict the path of a mechanism before finalizing the actual cross sectional dimensions and material of the mechanism. This is because the compliant mechanism designer is typically interested in creating a mechanism that follows a given path. With traditional kinematic methods, the path is determined before the forces are calculated. The cases presented in the previous chapter are difficult in mechanism design because an equivalent link length of the flexible segment is not known, so the path is also unknown. Since this equivalent link length is not known, the model requires successive iterations in order to determine the actual path of the mechanism.

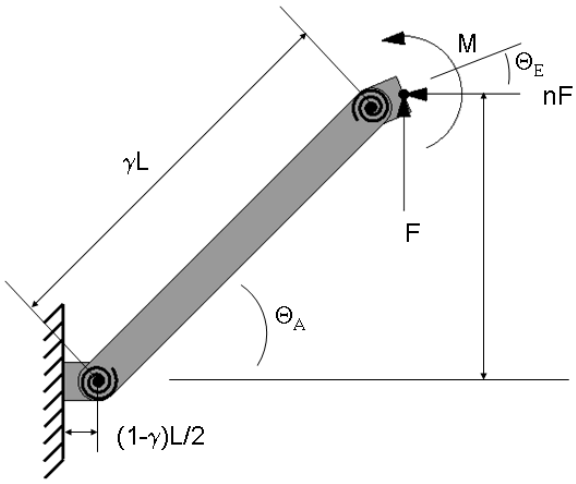

Figure 3.1: The simplified model for determining the path of a mechanism with both force and moment loads on an individual segment.

3.2 Simplified Model

The proposed simplified model is presented in Figure 3.1. The model is similar to that used by a fixed-guided [13] segment. In this case, however, the two end segments are not constrained to remain at zero rotation, but rather to have the same rotation as the link to which they are attached. This gives the designer the specific advantage that no link lengths will change during the motion of the mechanism. Since no link length changes, the model can be more easily analyzed using traditional rigid-link methods without iteration. This assumption introduces error into the model, making it less valuable for analysis purposes. However, the primary purposes of the model are design and visualization.

It can be shown that the model in Figure 3.1 will have two degrees of freedom for any given value of n. Although the two torsional spring values will vary with the motion of the beam, the link lengths will not change. Traditional kinematic path design techniques can therefore be used, allowing the designer the versatility of synthesis techniques that have been used for kinematics.

3.2.1 Chain Algorithm

A brief introduction of the chain algorithm is valuable at this point because it will be used to evaluate the error of the proposed PRBM. There are several reasons for choosing the chain algorithm over elliptic integrals. The main reason is that the chain algorithm is flexible when working with inflection points. (Elliptic integrals will also work with inflection points, but they require separate solutions for different cases of loading.) Nonlinear finite element analysis (FEA) would produce the same results as the chain algorithm, but the chain algorithm was chosen over FEA because of ease in obtaining output for many solution cases quickly.

The chain algorithm is discussed and applied in several publications [13, 20, 21, 22, 23]. The method is very similar to FEA, in that a long flexible segment is broken up into multiple short flexible segments. Each of the shorter segments is then iteratively analyzed, using small deflection approximations. The difference is that the chain algorithm will solve for the deflection of the first segment and then use the deflection and orientation of the end of that segment as the starting point for the next segment. The number of elements and the number of iterations determine the accuracy of the model and the time required to obtain a solution.

3.3 Simplified Model Description

In order to examine the error in the proposed PRBM, the results of the model were compared to the chain algorithm. Both the chain algorithm and the PRBM require two inputs. The rotation of the end of the flexible segment and the vertical deflection were selected as the inputs. The deflections of the flexible segments all originated at a location of zero degrees rotation and zero deflection. The angle of rotation was then set to vary linearly with the vertical deflection, allowing the flexible segment to reach a maximum rotation at the maximum deflection. The maximum rotation was varied between $-50\,^\circ$ and $50\,^\circ$. The error is determined by dividing the distance of the vector labeled "**Delta x**" in Figure 3.2 by the magnitude of the deflection calculated by the chain algorithm (labeled "chain algorithm" in Figure 3.2).

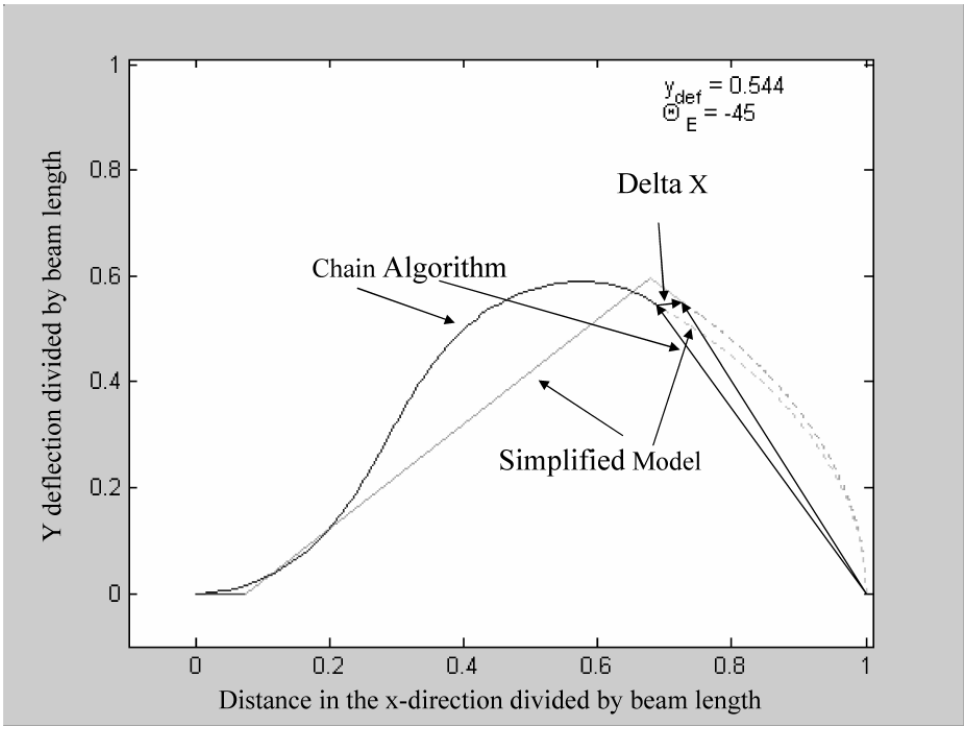

Figure 3.2: An example of how the relative error of the simplified model was compared to the chain algorithm.

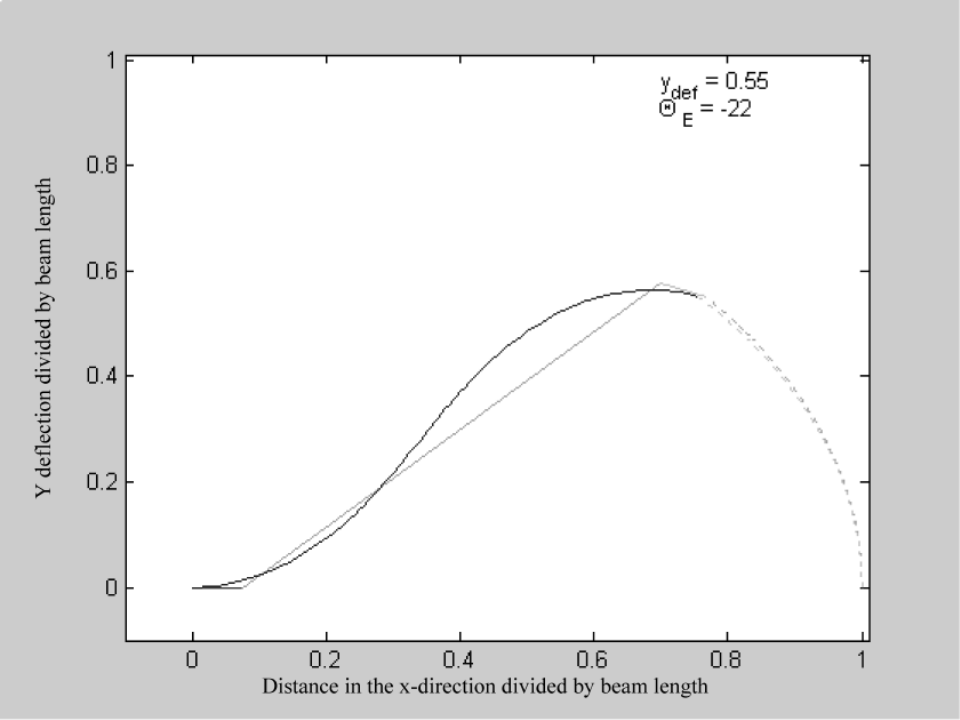

Figure 3.3: A simplified model for determining the path of a mechanism with both force and moment loads on an individual segment, as compared to the chain algorithm. Note that the deflection and the rotation are in the upper right hand corner of the figure. In this case, the vertical deflection is 55% of the beam length, and the rotation of the end of the beam is 22 ° from the horizontal.

Several output plots are shown to demonstrate the method used to determine the relative error. Figures 3.3 to 3.4 show both the path of the chain algorithm and the path of the PRBM. Each figure has different values of rotation and deflection. All of the models show that there is a good correlation between the two methods.

Although the path is easily determined from the model, the predicted force and moments from a linear torsional spring (comparable to the torsional spring developed by [13]) do not produce results within the same accuracy. Applying some simple techniques can improve the accuracy of the model. Figure 3.5 shows a free-body-diagram of the center portion of the model presented in Figure 3.1.

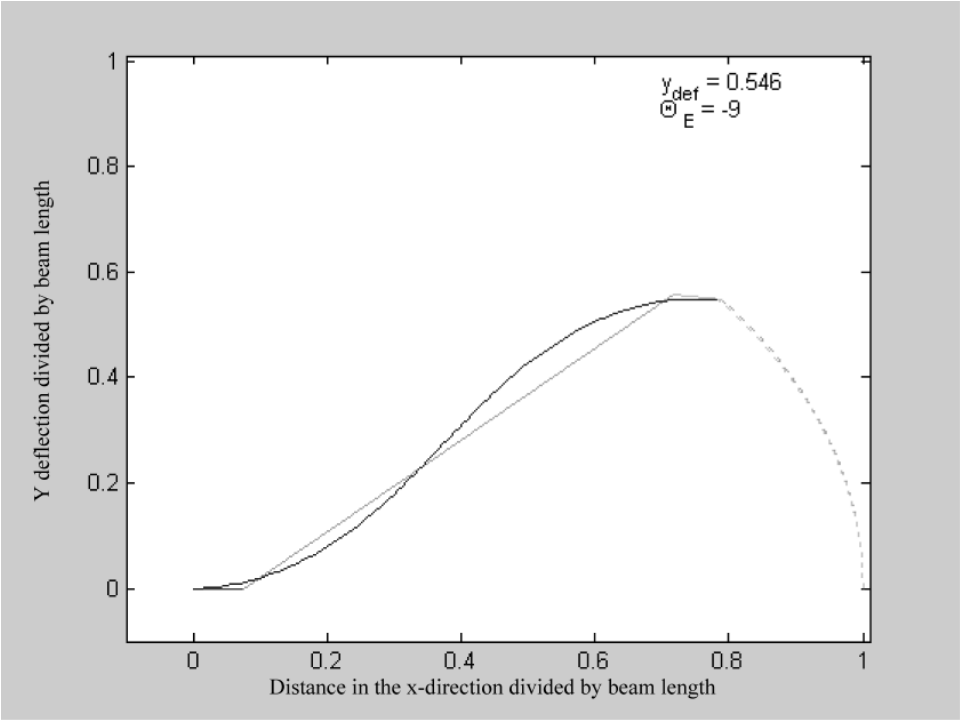

Figure 3.4: In this case, the vertical deflection is 54.6 percent of the beam length, and the rotation of the end of the beam is $-9\,^\circ$ from the horizontal.

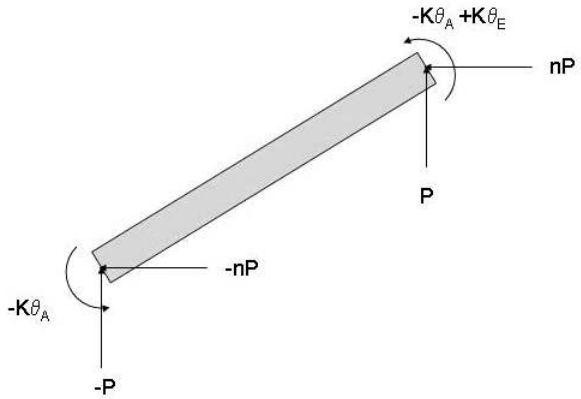

Figure 3.5: Free-Body-Diagram of the center section of the model shown in Figure 3.1.

Setting the moments equal to zero about the lower left center of the beam results in the following equation:

$$-K\theta_A - K(\theta_A - \theta_E) + \gamma PL(\cos(\theta_A) + n\sin(\theta_A)) = 0. \tag{3.1}$$

where $K = 2\gamma K_\Theta EI/L$ is the torsional spring constant [13], γ is the characteristic radius factor, E is young Modulus, I is the area moment of inertia, L is the length of the beam, and K_Θ is the stiffness coefficient. After rearranging, it can be shown that the value of the applied force, P, is predicted by

$$P = \frac{2K\theta_A - K\theta_E}{\gamma L(\cos(\theta_A) + n\sin(\theta_A))}. \tag{3.2}$$

The value of the predicted applied moment was found in a similar fashion. The upper portion of the linkage in Figure 3.1 was analyzed, and the moments were again summed about the pin joint. The following equation results:

$$M_{end} = K\theta_E - K\theta_A - \frac{(1-\gamma)PL}{2}(\cos(\theta_E) + n\sin(\theta_E)). \tag{3.3}$$

The result of using the same torsional spring constant for both of the members produces a high level of error when predicting the applied force and moment. To reduce the error, the spring constants were modified so that the torsional spring constant of the end angle rotation was independent of the torsional spring constant on the base angle. This resulted in a model that was adaptable for varying forces and moments associated with the changing end angle. The model is represented by the following two equations:

$$P = \frac{2K_A\theta_A - K_E\theta_E}{\gamma L(\cos(\theta_A) + n\sin(\theta_A))} \tag{3.4}$$

$$M_{end} = -K_E\theta_E + K_A\theta_A - \frac{(1-\gamma)PL}{2}(\cos(\theta_E) + n\sin(\theta_E)), \tag{3.5}$$

where K_E and K_A are equal to

$$K_E = \frac{2\gamma K_{\Theta E} EI}{L} \tag{3.6}$$

and

$$K_A = \frac{2\gamma K_{\Theta A} EI}{L}. \tag{3.7}$$

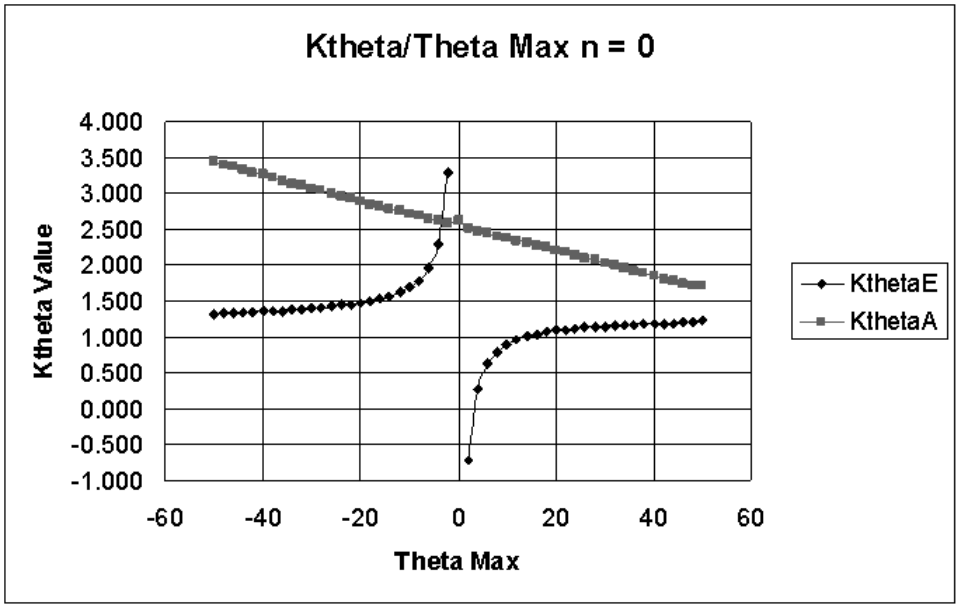

Figure 3.6: The optimum values of $K_{\Theta E}$ and $K_{\Theta A}$ that can be used, based on the anticipated rotation of the end on the cantilever beam ($n = 0$).

The values of $K_{\Theta A}$ and $K_{\Theta E}$ will vary, depending on the loading condition and the value of n for any given maximum rotation of the end of the beam. The values of each of these two variables are shown for three different values of n in Figures 3.6 to 3.8. Note that the value for the cases where the rotation of the end of the beam is zero are roughly the same as the values that were presented for fixed-guided segments [13].

3.4 Results and Discussion of Results

Figure 3.9 shows the relative error for the case where the value of n is set to zero (a vertical force). Results were obtained by varying the maximum rotation of the beam from $-50\,^\circ$ to $50\,^\circ$ at the maximum deflection. The maximum vertical component of deflection is 60% of the beam length. Even with the relatively large deflection of 60% of the beam length and rotations of the end of the beam at fifty degrees, the error stays within 5% of the results predicted by the chain algorithm for the case of $n = 0$. Note that the plot presents only flexible segments with applied

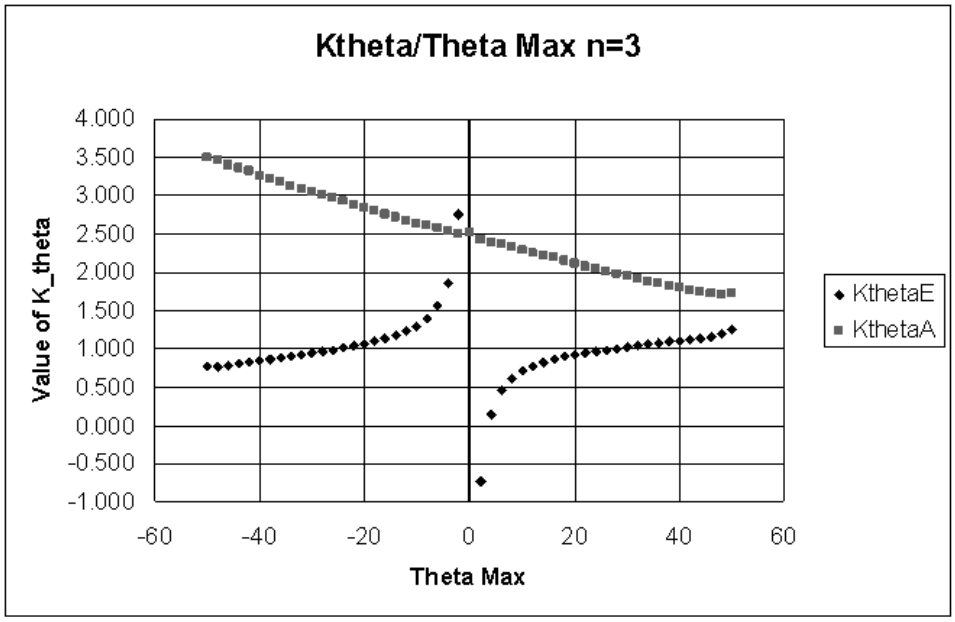

Figure 3.7: The optimum values of $K_{\Theta E}$ and $K_{\Theta A}$ that can be used, based on the anticipated rotation of the end on the cantilever beam ($n = 3$).

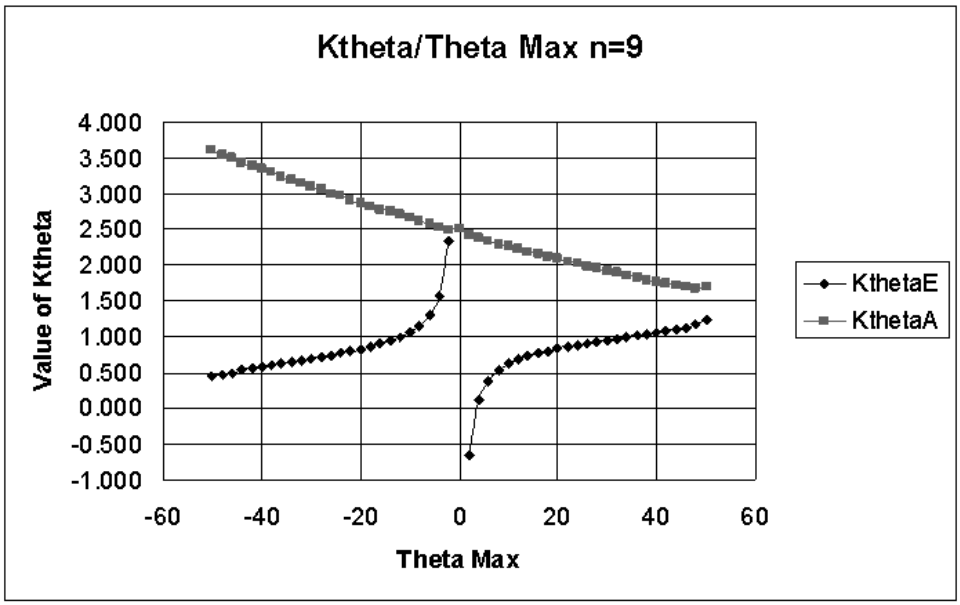

Figure 3.8: The optimum values of $K_{\Theta E}$ and $K_{\Theta A}$ that can be used, based on the anticipated rotation of the end on the cantilever beam ($n = 9$).

vertical forces. Although this is a special case, similar results were found for more general cases. Figure 3.10 shows the results for the case when the vertical and horizontal forces are equal ($n = 1$). Figure 3.11 shows the results when the horizontal load is three times that of the vertical load ($n = 3$). Figure 3.12 shows the result when the horizontal load is nine times that of the vertical load ($n = 9$). Note that for every set of load conditions the value of the characteristic radius (γ) was changed in accordance with [13]:

$$\gamma = \begin{pmatrix} 0.841655 - 0.0067807n + 0.000438n^2 \\ \text{for } (0.5 < n < 10.0) \\ \\ 0.852144 - 0.0182867n \\ \text{for } (-1.8316 < n < 0.5) \\ \\ 0.912364 + 0.0145928n \\ \text{for } (-5 < n < -1.8316). \end{pmatrix} \tag{3.8}$$

As shown in each of the figures, there are large regions where the error is less than 5%. The error increases steadily as the value of n increases at the high angles of rotations and vertical displacements. Figure 3.12 shows that the majority of the deflections and rotations result in a modeling error of less than 5%. The portion of the graph that has higher error comes from a large negative rotation of the beam and a large deflection of the beam. The model is encouraging and can be used to model the path of most mechanisms that fit within the areas that were studied, without more than a 5% deviation from the numerical solution.

The errors in the forces and moments are presented in Figures 3.13 to 3.18. Note that for high values of n and large deflections, that the deviations of the force and moment are larger than the error in the deflection prediction. The figures show that for a large range of the motion modelled by the simplified PRBM, the force can also be predicted. The force prediction is not as accurate as the predictions for the deflection of the system. This is expected since other PRBM's show the same trend.

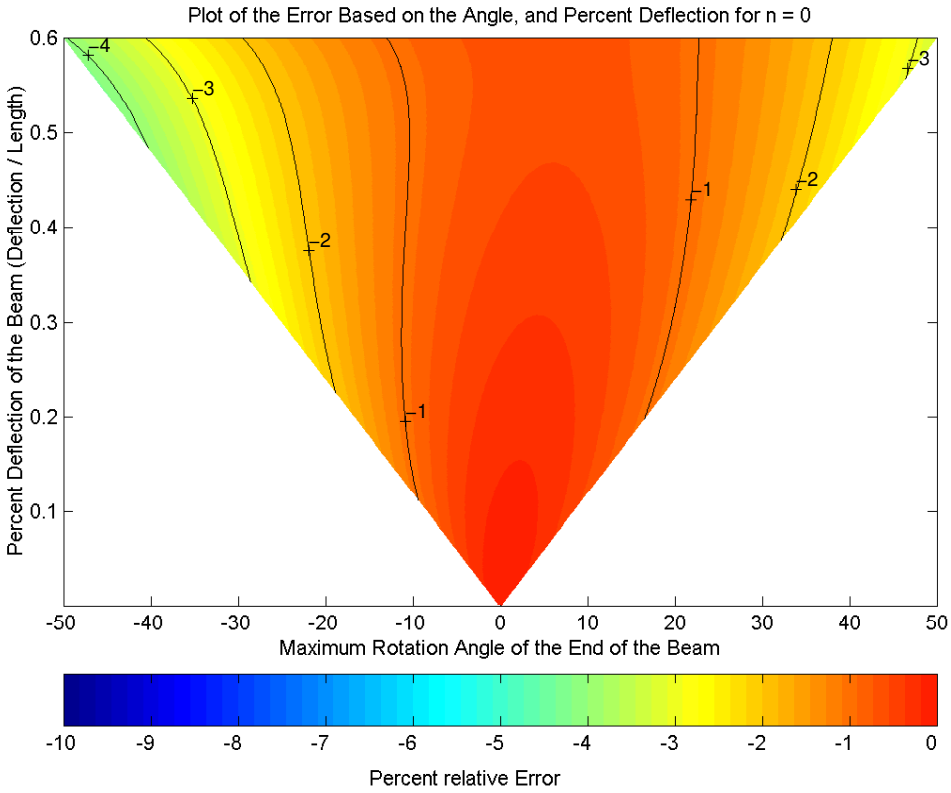

Figure 3.9: The relative error between the proposed PRBM model and the predicted deflection of a chain algorithm (for $n = 0$).

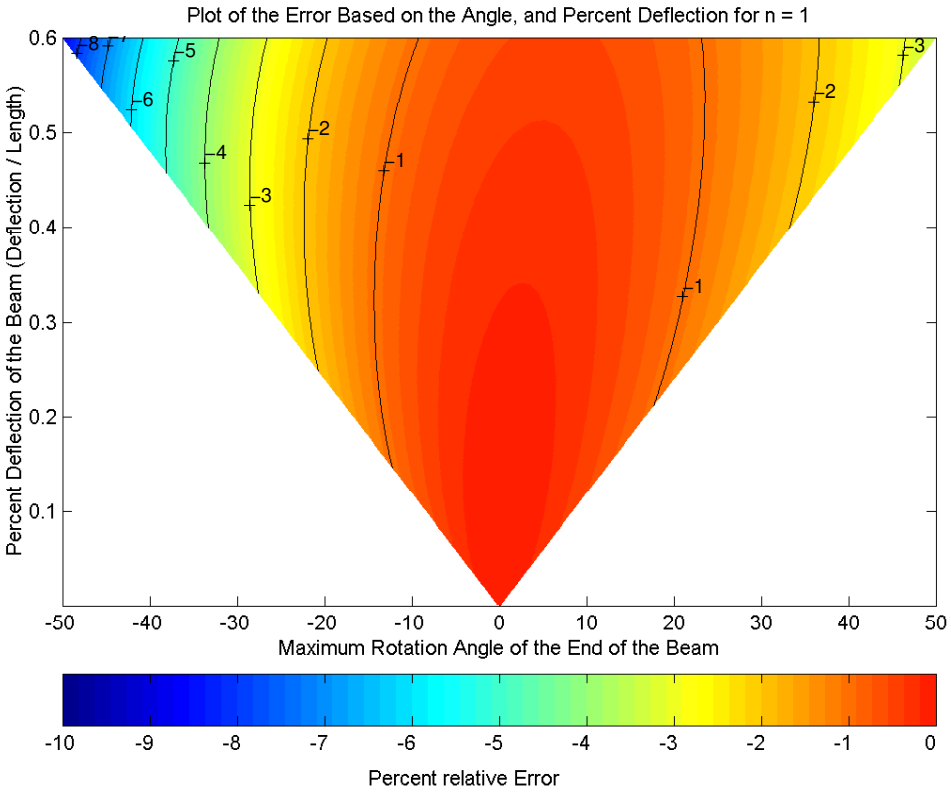

Figure 3.10: The relative error between the proposed PRBM model and the predicted deflection of a chain algorithm (for $n = 1$).

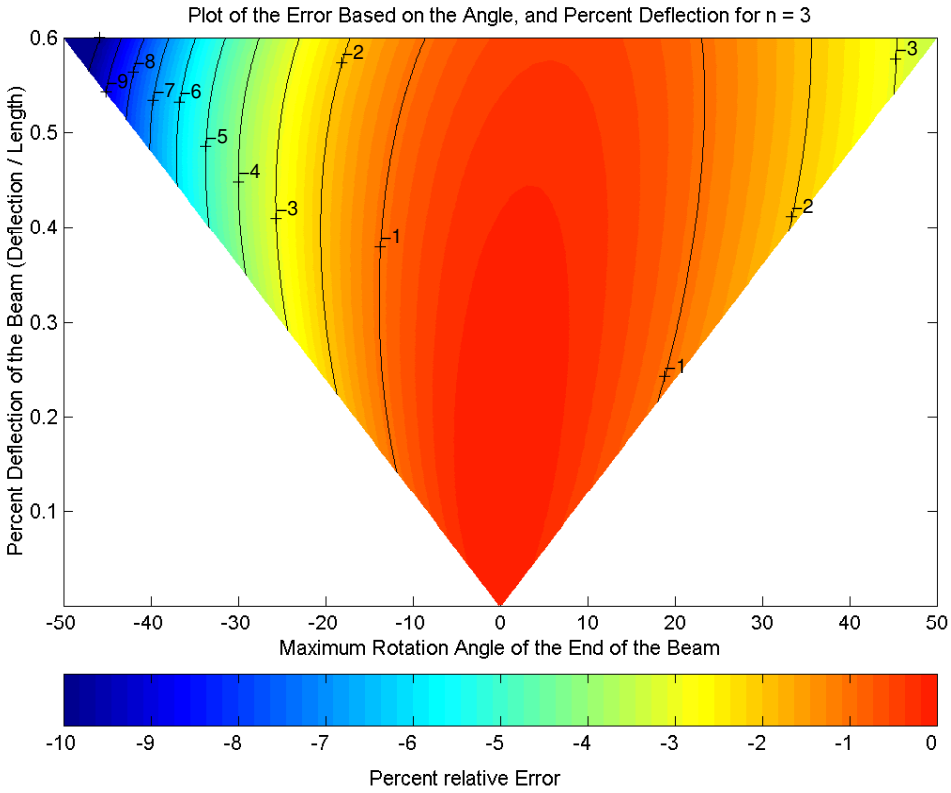

Figure 3.11: The relative error between the proposed PRBM model and the predicted deflection of a chain algorithm ($n = 3$).

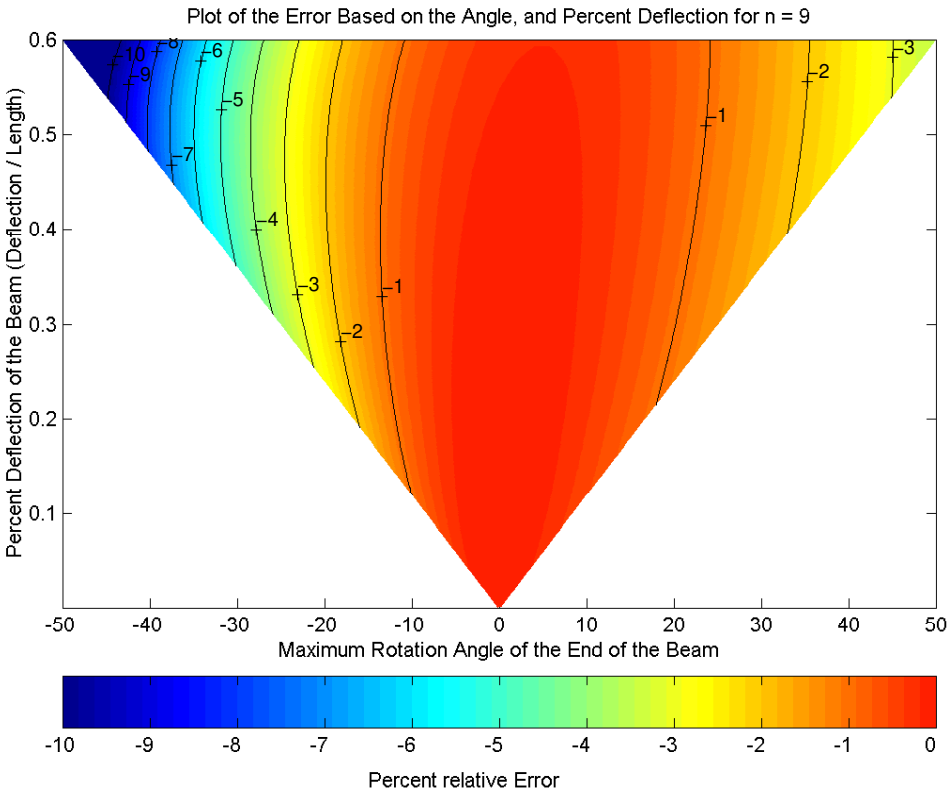

Figure 3.12: The relative error between the proposed PRBM model and the predicted deflection of a chain algorithm ($n = 9$).

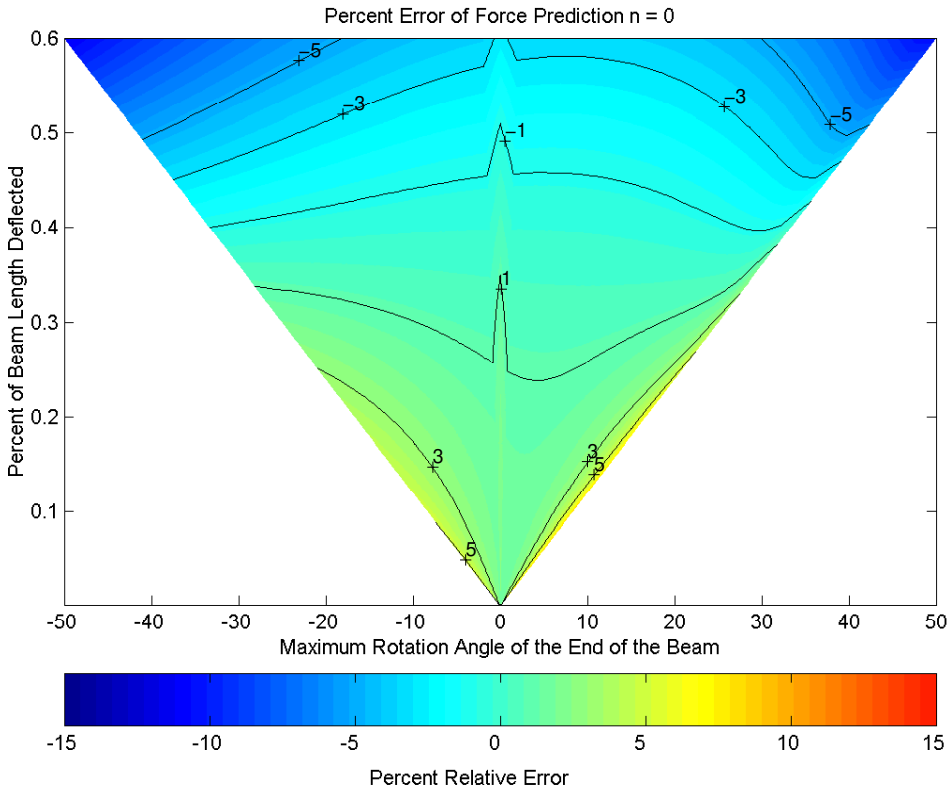

Figure 3.13: The percent error between force predicted by the simplified PRBM, and the force predicted by the chain algorithm (for $n = 0$).

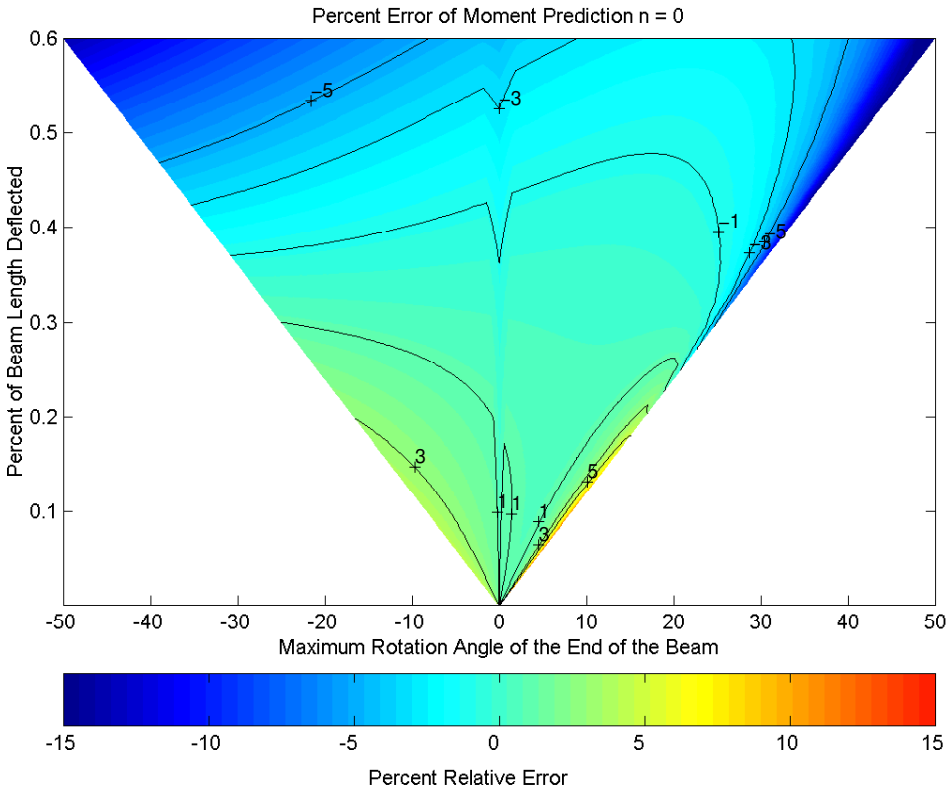

Figure 3.14: The percent error between the moment predicted by the PRBM, and the force predicted by the chain algorithm(for $n = 0$).

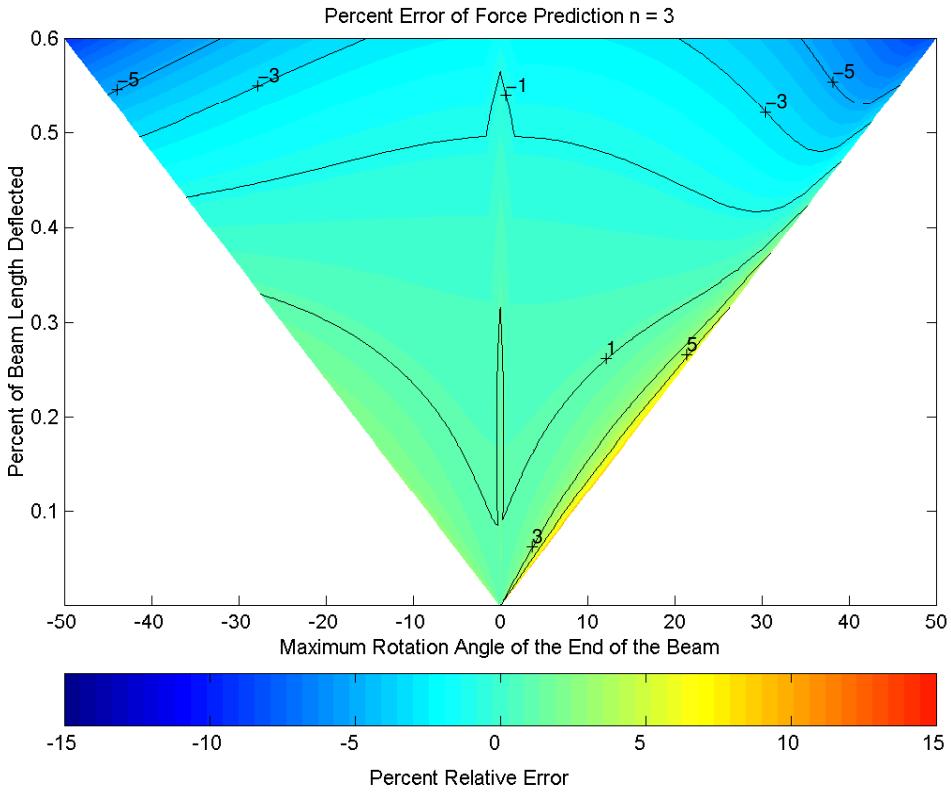

Figure 3.15: The percent error between force predicted by the simplified PRBM, and the force predicted by the chain algorithm (for $n = 3$).

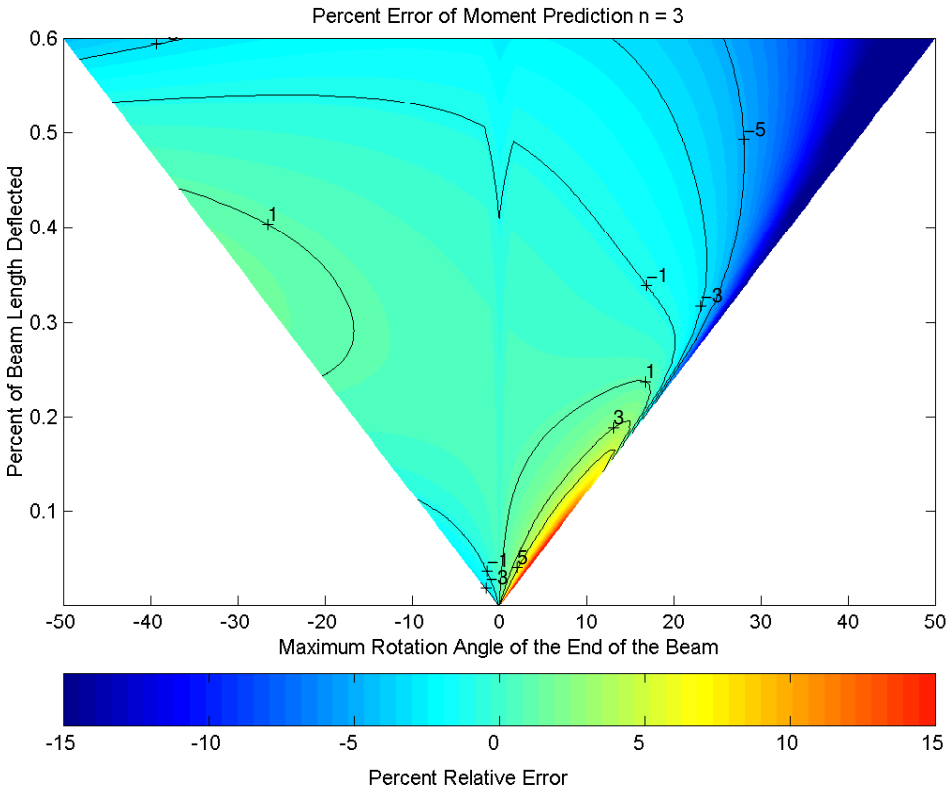

Figure 3.16: The error associated with the prediction of moment from the PRBM (for $n = 3$).

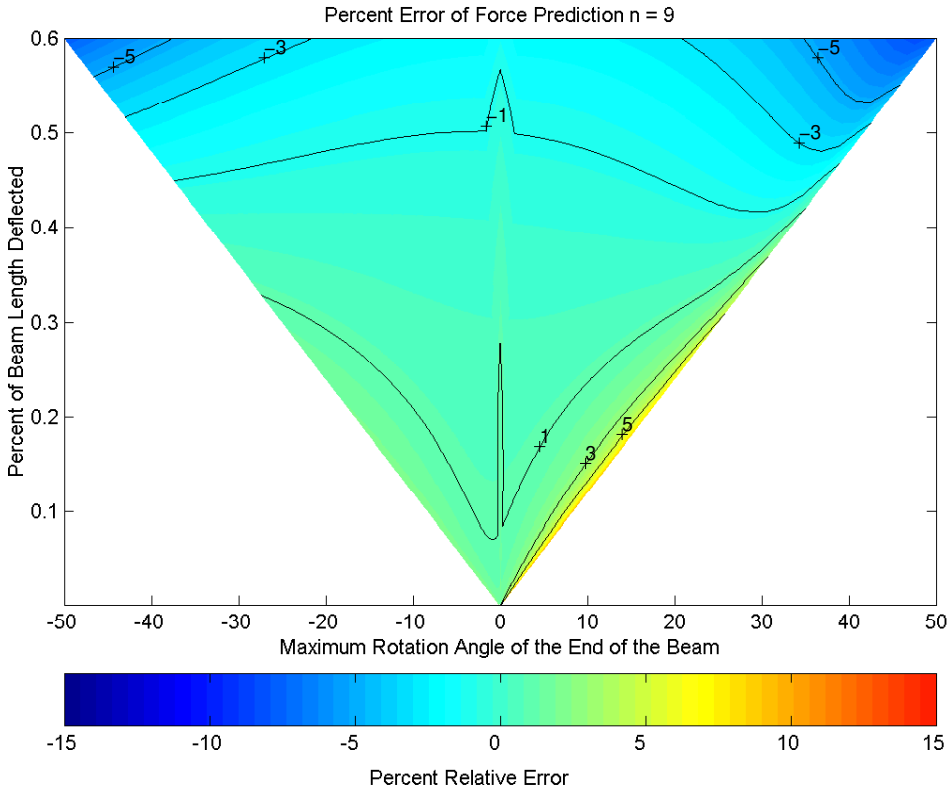

Figure 3.17: The percent error between force predicted by the PRBM, and the force predicted by the chain algorithm (for $n = 9$).

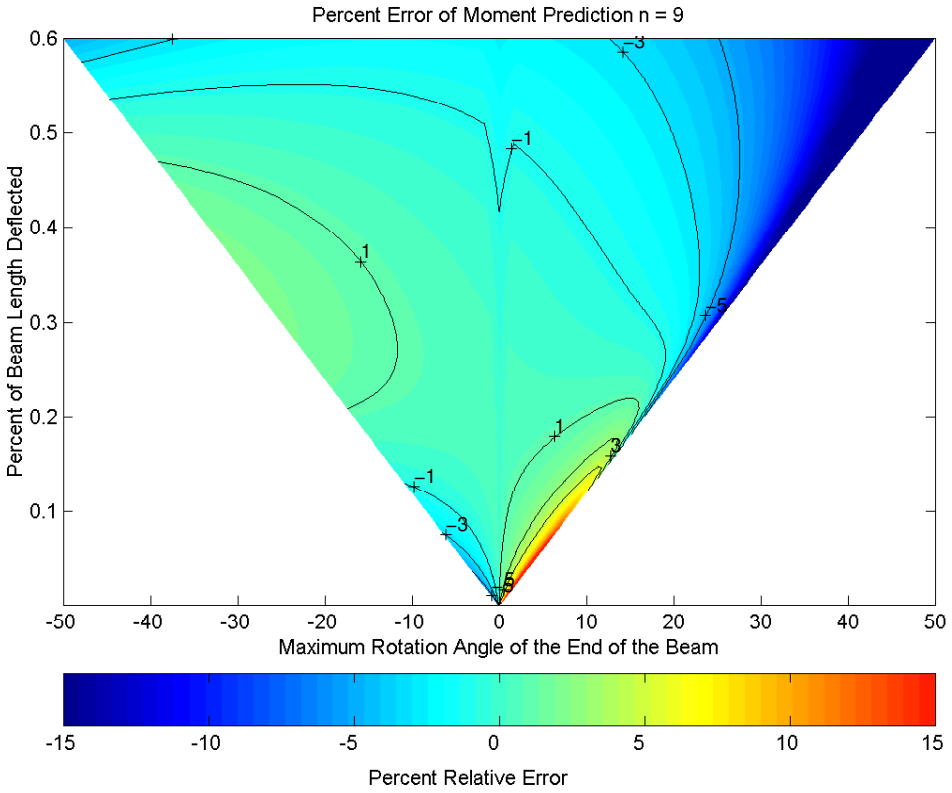

Figure 3.18: The error associated with the prediction of the moment from the PRBM (for $n = 9$).

The value of the $K_{\Theta E}$ term has a singularity as the value of the term approaches zero. That is also expected, since the value of the rotation of the end angle approaches zero. The relatively large increase in the value of the $K_{\Theta E}$ term as the rotation of the end angle approaches zero is due to this same effect. The values of $K_{\Theta E}$ and $K_{\Theta A}$ were tabulated for various values of n and the maximum rotation. The equations below may also be used to determine approximations of these values. The values for A, B, C, D, K and L are in Table 3.1.

$$\Theta_{Max} = \frac{0.6\ \theta_E\ L}{y_{def}} \tag{3.9}$$

A simpler, and quicker way of determining the stiffness coefficients is through the figures presented (Figure 3.6-3.8). After calculating the value of Θ_{max}[1] the values can be determined from the charts. However The following equations are easily implemented in a computer program.

$$K_{\Theta E} = \frac{A}{\tan(\Theta_{Max})} + Bn^2 + Cn + D + F\ \Theta_{Max} \tag{3.10}$$

$$K_{\Theta A} = K\ {\Theta_{Max}}^2 + L\ \Theta_{Max} + Mn^2 + Rn + S \tag{3.11}$$

The results shown in the figures are based on the calculated optimum values of $K_{\Theta E}$ and $K_{\Theta A}$. The curve fit produces similar results to that of the optimum values.

The model produces reasonable results, however, in an actual mechanism the direction of the force will tend to change with the rotation of the coupler, and the path can only be varied based on a previously determined γ. This should make the results for an actual mechanism slightly less accurate than the results presented in Section 3.4. To demonstrate the model's usefulness for predicting the path of mechanisms with fixed-fixed elements, two mechanisms were simulated and compared to numerical methods. The main objective is predicting the path of the mechanisms. Therefore this example looked at the various paths, but not on the actual forces that are produced.

Figure 3.19 represents a mechanism that was analyzed. Figure 3.20 shows a plot of the path of the tracking point (the end of the fixed-fixed segment as labeled

[1] Θ_{Max} is in radians

Table 3.1: Parameters for the determination of the torsional spring constants. They can be used with Equations (3.10) and (3.11).

Constant	Negative Rotation	Positive Rotation
A =	-0.0599	-0.0582
B =	0.0097	0.0024
C =	-0.1604	-0.0383
D =	1.4419	1.0623
F =	0.3344	0.3344
K =	0.1577	0.1577
L =	-1.0589	-1.0589
M =	0.00153	0.00153
R =	-0.0164	-0.0164
S =	2.4983	2.4983

Table 3.2: Dimensions of Modelled Mechanism

Segment/Link	Length	Unit
Segment 1	2.54	cm
Segment 3	5.842	cm
Link 2	0.762	cm
Fixed-Fixed	5.08	cm

in Figure 3.19) and dimensions of the mechanism are given in Table 3.2. Figure 3.21 again shows the path with a change in the vertical scale. The path of the PRBM modeling technique presented in this chapter, and the mechanisms that is presented in this chapter are very similar. Showing the the technique is a viable method for capturing the behavior.

3.4.1 Example Problem

The mechanism illustrated in Figure 3.22 is subject to an input rotation of $-30\,^{\circ}$ from the horizontal. Ignoring friction, calculate the deflection of the slider and the required input torque. Compare these results with those obtained from the chain algorithm. The flexible part of the mechanism has a width (b) of 0.01 meters (b is

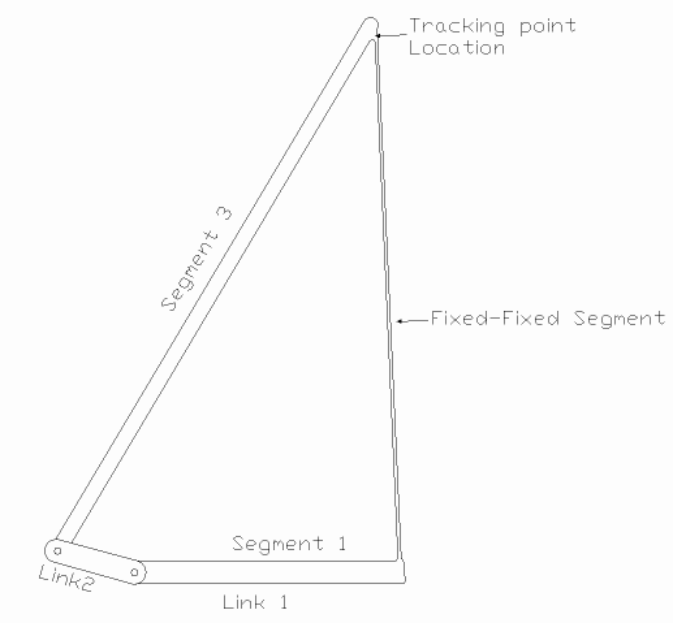

Figure 3.19: A representation of the mechanism that was analyzed with the PRBM and compared to the chain algorithm.

the width into the page in Figure 3.22), a height (h) of 0.001 meters, and a length (L) of 1 meter. The material is steel with a modulus of elasticity of (E) 206.8 GPa. The other members may be assumed to be rigid. The length between the pin joint and the flexible segment is (r) 0.8 meters.

Figure 3.23 shows the PRBM of the mechanism in the deflected position. Based on the geometry created by the PRBM and using a value of $\gamma = 0.85$, the model becomes a crank-slider mechanism. Table 3.3 can be constructed using traditional analysis techniques.

Table 3.3 shows the geometry of the mechanism in the deflected position. The value of θ_A is the angle closest to the slider. Θ_{Max} for this problem can be found from y_{def}, calculated in Table 3.3, and the rotation of the end of the beam. Each of these variables is defined in Figure 3.1.

$$\Theta_{Max} = \frac{0.6\ \theta_E\ L}{y_{def}} = -0.785(or - 45\,^\circ) \tag{3.12}$$

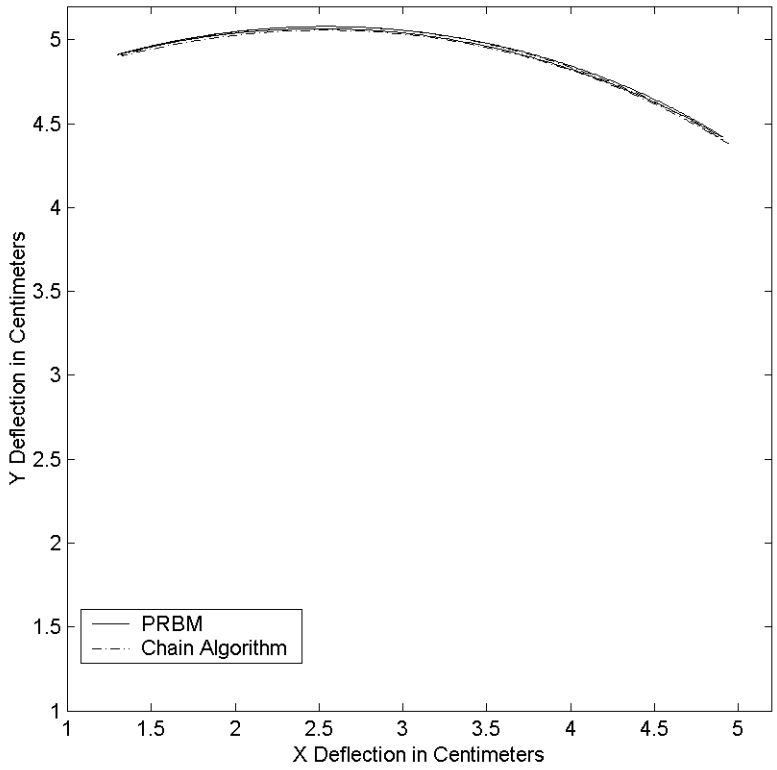

Figure 3.20: The paths of the tracking point, as predicted by the PRBM and the chain algorithm.

Table 3.3: Geometry Values

Variable	Equation	Value
$r_2 =$	$0.8 + \frac{(1-\gamma)L}{2}$	0.875 (meters)
$r_3 =$	$\gamma \times L$	0.85 (meters)
$\theta_2 =$	Given	$-30\,^\circ$
$\theta_3 =$	$\sin^{-1}(\frac{-r_2 \sin(\theta_2)}{r_3})$	$30.978\,^\circ$
$r_1 =$	$r_2 \cos(\theta_2) + r_3 \cos(\theta_3)$	1.062 (meters)
$y_{def} =$	$r_2 \sin(\theta_2)$	-0.4 (meters)
$\delta_x =$	$0.8 + 1.0 - r_1$	0.239 (meters)

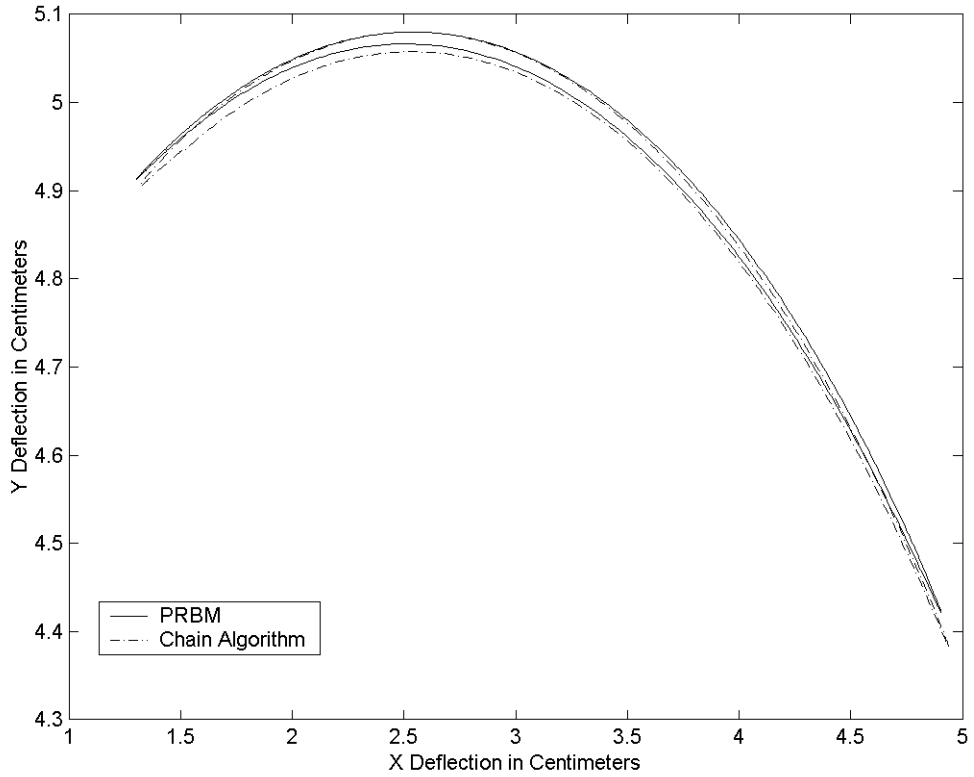

Figure 3.21: The paths of the tracking point, as predicted by the PRBM and the chain algorithm. Scales are adjusted to make the error in the model more visible.

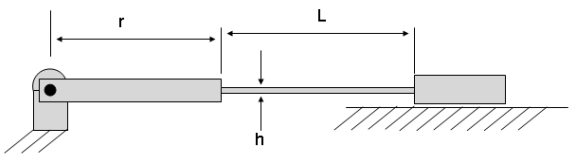

Figure 3.22: The mechanism analyzed in the example.

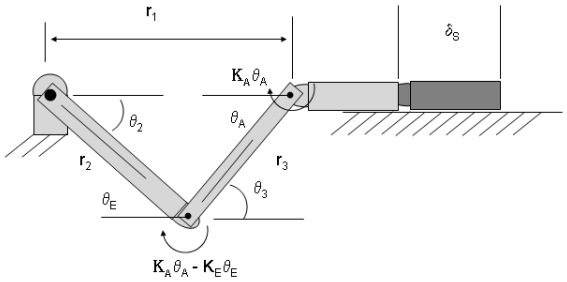

Figure 3.23: PRBM of the mechanism.

After finding the value of Θ_{Max}, and recognizing that, with no slider friction, the value of n is zero, the values of the torsional spring constants can be calculated from Equations (3.10) and (3.11) as $K_{\theta_E} = 1.2391$ and $K_{\theta_A} = 3.427$. The value of the torque produced at the torsional springs can now be determined.

$$\begin{aligned} K_A\theta_A &= \frac{2\gamma K_{\theta_A} EI\theta_A}{L} \\ &= -\frac{2 \times 0.85 \times 3.427 \times 0.172 \times 0.541}{1.0} \\ &= -0.543 \end{aligned} \tag{3.13}$$

$$\begin{aligned} K_A\theta_A - K_E\theta_E &= \frac{2\gamma EI}{L}(K_{\theta_A}\theta_A - K_{\theta_E}\theta_E) \\ &= -\frac{2 \times 0.85 \times 0.17 \times (3.42 \times 0.54 - 1.23 \times 0.52)}{1.0} \\ &= -0.73 \end{aligned}$$

The force that is exerted can be calculated by summing the moments on Link 3 of the PRBM. Using Equation (3.2) results in a reaction force, P, of

$$P = \frac{2K_A\theta_A - K_E\theta_E}{\gamma L \cos(-\theta_E - \pi)} = -1.751 \text{ N}. \tag{3.14}$$

Table 3.4: Comparison of Results

Property	Chain Algorithm	PRBM
δ_S	0.250	0.239 m
$Force$	-1.749	-1.751 N
$Moment$	-0.865	-0.846 Nm
$Input\ Torque$	-2.076	-2.06 Nm

The moment at the end of the beam can be calculated by examining the small section between the end of the PRBM Link 2 and the first PRBM pin joint. The moment is:

$$\begin{aligned} M_{end} &= K_E\theta_E - K_A\theta_A - \frac{F\ (1-\gamma)}{2} L\cos(-\theta_E - \pi) \\ &= -0.8468\ N \times m. \end{aligned} \tag{3.15}$$

Calculating the input torque that needs to be applied to deflect Link 2 comes from a summation of moments about the pin joint on the input arm (Link 2), as

$$T_{in} = M_{in} + Pr_2 cos(\theta 2) = -2.06 \text{ Nm} \tag{3.16}$$

Table 3.4 shows the comparison between the values given by the PRBM and the values produced by the chain algorithm.

3.5 Summary

This chapter described a simplified method for modeling fixed-fixed flexible segments that decoupled the path from the applied forces. Although the error in the model is greater than that of PRBM's for other types of flexible members, the model is shown to be within five percent of the physical system for most loading conditions. Since the path of the fixed-fixed flexible segment can be separated from the forces and moments that are applied to the flexible segment, all of the work and knowledge from previous kinematic analysis and design is available to a designer for preliminary design of compliant mechanisms. After a design is obtained, it can be analyzed and refined with more complex and more accurate models. The major contribution of

this chapter is the development of a modeling technique that will allow for additional compliant mechanisms to be developed, and their dynamic behavior predicted. The model will be evaluated as to its ability to predict the transient responses of compliant mechanisms in the next chapters.

Chapter 4

Beam Dynamics

There are several methods for calculating the dynamics of compliant segments. The two most common methods for small deflections are lumped mass models, and analytical solutions. In recent years, finite element analysis (FEA) techniques have become more popular due to increases in computational power, convenience, and accessibility. Most of these methods are discussed in common vibration texts. Usually FEA is not used for simple geometries with small deflections, since analytical solutions exist. However, in the case of nonlinear deflections or complex geometries, finite element methods (FEM) and lumped mass models prove useful, since closed-form analytical solutions do not typically exist. For this work, FEA was chosen as a comparison method for the Pseudo-Rigid-Body Model (PRBM).

The chapter proceeds with a discussion of an analytical approach to solving the dynamic equations. After this discussion, the analytical models are compared with the PRBM in order to draw conclusions about the validity of using the PRBM in this situation. The PRBM technique is then applied to a flexible cantilever beam with varying masses at the end of the cantilever beam. The results of the PRBM are compared to the results obtained from FEA of the same system.

4.1 Analytical Approach to Nonlinear Cantilever Beam Dynamics

The approach taken for developing the equation of motion of a cantilever beam with known boundary conditions is discussed in this section. Following this discussion, there is a brief summary of important topics that come from the development.

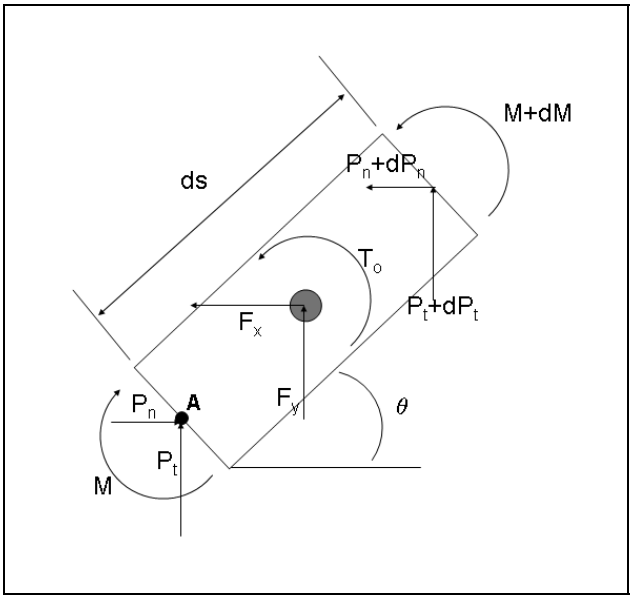

Figure 4.1: Differential segment of a cantilever beam.

Figure 4.1 shows a differential segment of a cantilever beam subjected to large deflections. The analytical model can be developed by starting with the equations from a summation of forces in the x and y directions, and by summing the moments about point A. For this model it is assumed that the dynamic load is applied as a distributed load across the element. The dynamic load is then concentrated into the terms F_x and F_y. Summing the forces in the x direction yields

$$-P_n + P_n + dP_n + F_x = 0, \tag{4.1}$$

where P_n is the load on the differential segment in the x-direction, and F_x is the inertial load (due to the acceleration of the differential segment in the x-direction). Summing the forces in the y direction yields

$$-P_t + F_y + P_t + dP_t = 0, \tag{4.2}$$

where P_t is the load on the differential segment in the y-direction, and F_y is the load due to the acceleration of the differential segment in the y-direction (also shown in Figure 4.1). Summing the moments about point A results in

$$\begin{aligned} - \quad & M + M + dM + T_o + (P_t + dP_t)ds\cos(\theta) - (P_n + dP_n)ds\sin(\theta) \\ + \quad & \frac{F_y ds\cos(\theta)}{2} - \frac{F_x ds\sin(\theta)}{2} = 0. \end{aligned} \tag{4.3}$$

From Equations (4.1) and (4.2) we find that

$$dP_n = -F_x \tag{4.4}$$

and

$$dP_t = -F_y. \tag{4.5}$$

Substituting these values into Equation (4.3) and simplifying the result yields

$$-\frac{dM}{ds} = \frac{T_o}{ds} + P_t\cos(\theta) - P_n\sin(\theta) - \frac{F_y\cos(\theta)}{2} + \frac{F_x\sin(\theta)}{2}. \tag{4.6}$$

Since $F_x = \rho A\ddot{x}ds$ and $F_y = \rho A\ddot{y}ds$, the value of these terms would be minimal in comparison to the values of P_n and P_t. As ds approaches zero, the terms F_x and F_y also approach zero. Here T_o is the torque due to the mass moment of inertia, $T_o = \frac{Mh^2}{12} = \frac{A\rho h^2\alpha ds}{12}$. Eliminating these terms from the equations, Equation (4.6) simplifies to

$$-\frac{dM}{ds} = \frac{A\rho h^2\alpha}{12} + P_t\cos(\theta) - P_n\sin(\theta). \tag{4.7}$$

From Equations (4.4) and (4.5) and $F_x = \rho A\ddot{x}ds$ and $F_y = \rho A\ddot{y}ds$ it can be shown that

$$\frac{dP_t}{ds} = -F_y = A\rho\ddot{y} = A\rho\frac{d\dot{y}}{dt} = A\rho\frac{d\left(\frac{dy}{ds}\frac{ds}{d\theta}\frac{d\theta}{dt}\right)}{dt} = A\rho\frac{d\frac{\omega}{\kappa}\sin(\theta)}{dt} \tag{4.8}$$

$$\frac{dP_n}{ds} = -F_x = A\rho\ddot{x} = A\rho\frac{d\dot{x}}{dt} = A\rho\frac{d\left(\frac{dx}{ds}\frac{ds}{d\theta}\frac{d\theta}{dt}\right)}{dt} = A\rho\frac{d\frac{\omega}{\kappa}\cos(\theta)}{dt}. \tag{4.9}$$

Using the equality of mixed partial derivaties[1]

$$\frac{d\kappa}{dt} = \frac{d\frac{d\theta}{ds}}{dt} = \frac{d\frac{d\theta}{dt}}{ds} = \frac{d\omega}{ds}, \tag{4.10}$$

the equations can be further expanded into

$$\frac{dP_t}{ds} = A\rho\left(\frac{\alpha}{\kappa}\sin(\theta) - \frac{\omega}{\kappa^2}\frac{d\omega}{ds}\sin(\theta) + \frac{\omega^2}{\kappa}\cos(\theta)\right) \tag{4.11}$$

and

$$\frac{dP_n}{ds} = A\rho\left(\frac{\alpha}{\kappa}\cos(\theta) - \frac{\omega}{\kappa^2}\frac{d\omega}{ds}\cos(\theta) - \frac{\omega^2}{\kappa}\sin(\theta)\right). \tag{4.12}$$

From these equations, the dynamic behavior of a cantilever beam can be predicted. It should be noted that if all of the dynamic loads are reduced to zero, then Equations (4.7), (4.11), and (4.12) all reduce to the elliptic integral equation that is presented by [13] except for the sign of the P_n term. The difference in sign values is due to a change in the direction of an assumed positive force.

The equations presented show some of the difficulties that can arise in determining the dynamics of a cantilever beam subjected to large deflections. First, the various forces depend on the values of $\frac{d\theta}{ds} = \kappa$, $\frac{d\omega}{ds} = \frac{d\kappa}{dt}$, θ, $\dot{\theta} = \omega = \frac{d\theta}{dt}$, and $\ddot{\theta} = \alpha = \frac{d^2\theta}{dt^2}$, which are all required in determining the change in the values of the forces across the beam. The values of θ and κ depend on the values of the forces P_n, P_t and the value of $\ddot{\theta}$. Since κ depends on $\ddot{\theta}$, the problem becomes inherently iterative in nature.

These equations account for the dynamic loading of the cantilever beam. Because the mass of the beam is uniformly distributed, each of the individual elements will have mass. The mass will affect the dynamic behavior of the beam. The beam modeled by these equations models the entire beam, with the distributed dynamic

[1]The assumption comes from the equality of mixed partial derivatives. This is stated by [44] as "If $u = f(x, y)$ has continuous second partial derivatives, then the mixed partial derivatives are equal."

effect of each individual segment. Since the PRBM models beams with end load conditions, it is important to consider a case that is closer to the loading conditions for which the PRBM is valid.

4.2 Assuming a Point Mass End-Loading Condition

The Equations (4.7), (4.11), and (4.12) are examined in the case of a cantilever beam where the beam mass is insignificant compared to a point mass on the tip of the beam. Examination of Equations (4.11) and (4.12) yields the following two equations:

$$\int dP_t = \int A\rho F_1(t)ds = C_1F_1(t) \tag{4.13}$$

$$\int dP_n = \int A\rho F_2(t)ds = C_2F_2(t), \tag{4.14}$$

where $F_1(t)$ and $F_2(t)$ contain all of the time dependent terms from Equations (4.11) and (4.12) respectively. The result above is due to the density (ρ) being similar to a Dirac Delta Function. The integral of the Dirac Delta Function becomes a step function, and, in this case, the result becomes a constant along the beam. Because both equations depend only on time and not on the location along the beam, the integration becomes possible. The resulting values of the functions become constants in location along the beam. Recall that Equation (4.7) is similar to the equation of a cantilever beam subjected to a static end load, or

$$\frac{dM}{ds} = -\frac{A\rho h^2\alpha}{12} - P_t\cos(\theta) + P_n\sin(\theta). \tag{4.15}$$

Since the beam has a point mass on the end of the beam, the relative value of the inertial term will diminish as the point mass increases. This results in the following equation:

$$\frac{dM}{ds} = -P_t\cos(\theta) + P_n\sin(\theta). \tag{4.16}$$

It is important to note that for each time step, the values of P_t and P_n are constant throughout the length of the beam. The resulting equation then becomes exactly the same equation as is presented for the PRBM of a fixed-pinned segment. The result suggests the PRBM will predict the dynamic behavior of the cantilever beam, with an

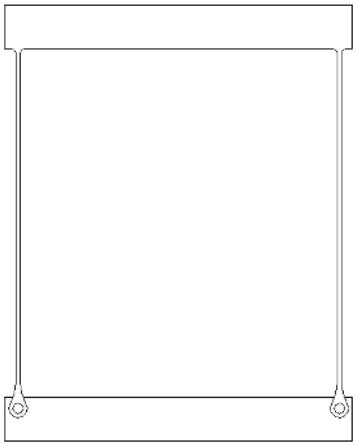

Figure 4.2: Fixed-pinned PRBM equivalent parallel mechanism.

end point mass significantly larger than the mass of the beam. This is an important condition in compliant mechanisms because flexible segments are usually attached to rigid segments that have a much higher mass.

4.3 Applications to Mechanisms

The evaluation of compliant beams is a first step to analyzing more complex mechanisms. Compliant mechanisms can usually be divided into discrete segments containing cantilever beams with varying end-load conditions. Examining several beam types, and comparing them to their respective pseudo-rigid-body assumptions, will provide insight into the variations and constraints that will come from each of the loading conditions. Each of these models will be examined with respect to the behavior that comes from use within a mechanism.

4.3.1 Fixed-Pinned/Fixed-Guided Flexible Segments

The mass of the coupler in the mechanism illustrated in Figure 4.2 is significantly larger than the masses of the flexible segments, assuming that both are made of the same material and have the same out-of-plane thickness. In addition, the coupler on this mechanism will not rotate, which eliminates the rotational inertia term.

If the mechanism were inverted, by switching the coupler and the ground, then the dynamics would also be the same. This mechanism is very similar to the model of a massless beam with a point load applied on the end, and in this way is similar to most compliant mechanisms. In general, the constraints that are required to use the dynamic modeling technique will be natural consequences of the static design, since rigid bodies will naturally tend to have more mass than flexible bodies. For these cases, the PRBM should be an adequate representation of the dynamic behavior.

The fixed-guided model is very similar in nature to the fixed-pinned model, and will have a similar behavior to the fixed-pinned segments for dynamic loadings. The mass of the rigid segments should be larger than the mass of the flexible segments in order for the mechanism to behave in a fashion similar to what is predicted by the PRBM.

4.3.2 Fixed-Fixed Flexible Segment

The fixed-fixed flexible segment presents a unique challenge to the dynamic equations of motion. The fixed-pinned segment can not transfer a moment. In the case of the fixed-fixed segment, a moment can be transferred, and thus the equation depends on the rotational inertia of the link adjoined to the the fixed-fixed segment, represented as

$$-\frac{dM}{ds} = P_t \cos(\theta) - P_n \sin(\theta), \tag{4.17}$$

With a boundary condition that requires the moment at the end of the beam to be $I_r \alpha_r$. Where I_r represents the mass moment of inertia of the rigid segment to which the beam is attached; α_r represents the angular acceleration of the rigid link; P_t, and P_n are the tangential and normal loads applied to the cantilever beam; θ is the rotation that the free end of the cantilever beam makes with the undeflected state; s is the distance along the beam and M is the moment for any given s; and M is equal to $EI\frac{d\theta}{ds}$. The $I_r \alpha_r$ term depends on the value of the inertia of the rigid segment and the resulting acceleration, so the magnitude of the applied moment will change as the dynamic loading increases. Because the moment can vary significantly for large masses or accelerations, the loading conditions in these situations are better suited to

a moment-based PRBM technique, since this will be the dominant effect. However, for most moderate cases, the predicted dynamic behavior of the mechanism from the PRBM and the actual behavior should be similar, again assuming that the rigid link masses are larger than the flexible beam masses. This particular case also suggests one additional constraint: the moment created by the mass moment of inertia and the angular acceleration must remain within the bounds which have been created for the fixed-fixed model. Also note that there will be a small change in the path through which the mechanism will travel under dynamic loading conditions, but the proposed model will not predict that change.

4.3.3 Small Length Flexural Pivot Dynamic Modeling Assumptions

The small-length flexural pivot is perhaps the simplest flexure to analyze. It is assumed that for a beam with a small-length flexural pivot, the value of the moment is significantly larger than the values of the forces that are applied. This suggests that the values of the two time dependent forces could be assumed to be small in comparison to the moment produced by these forces. Also, the value of the inertia term will approach zero if the mass of the flexible segments is small, in comparison to the mass of the rigid segments. This results in a very simple differential equation at each time step or:

$$M = \int dM = \int C \times F(t)\ ds = C \times F(t). \tag{4.18}$$

Once again, the resulting equation is that which was used for the development of the PRBM for small length flexural pivots; thus, if the rigid segment masses are large in comparison to the flexible segments, the PRBM will predict the dynamic response of the mechanism.

4.4 The PRBM for a Dynamically Loaded Cantilever Beam

The predicted resonance frequency of the PRBM for the dynamically loaded cantilever beam can be put into equation form as

$$\omega = \sqrt{\frac{K_t}{I_{pin}}} \quad (rad/sec)$$
$$f = \sqrt{\frac{K_t}{2\pi I_{pin}}} \quad (Hz), \tag{4.19}$$

where K_t is the torsional spring constant. (In the case of a cantilever beam the value is $\frac{\gamma K_\Theta EI}{l}$.) I_{pin} is the mass moment of inertia of the moving rigid link produced by the PRBM at the pin joint. (In the case of a cantilever beam I_{pin} is $\frac{\gamma l A \rho (\gamma l)^2}{3}$, which assumes a thin member with a constant rectangular cross section and a uniform density.) As shown by the equations, using the PRBM to calculate the resonance frequency of a cantilever beam is relatively simple.

4.5 Finite Element Analysis

Finite element methods are often applied to problems where the geometry or the type of deflection is difficult to model with other techniques. Finite element analysis (FEA) breaks up a complex geometry into several smaller sections. The sections are typically small elements of a geometry that can be solved analytically. Each of the small sections (or elements) are then solved, and the solutions are combined to create the solution for the complex geometry. In the case of nonlinear deflections, an additional iterative step is required in order to solve the system. For the work that is described here, each of the flexible segments was broken up into multiple beam sections. Beam elements were chosen for their simplicity, and also because they include the important characteristics of the flexible segments. Although FEA is not the only method that can be used to solve this type of problem, the versatility and availability of this method have made it the method of choice.

A discussion of the governing equations for the dynamics of a cantilever beam were presented in the previous section. The equations showed that for small and

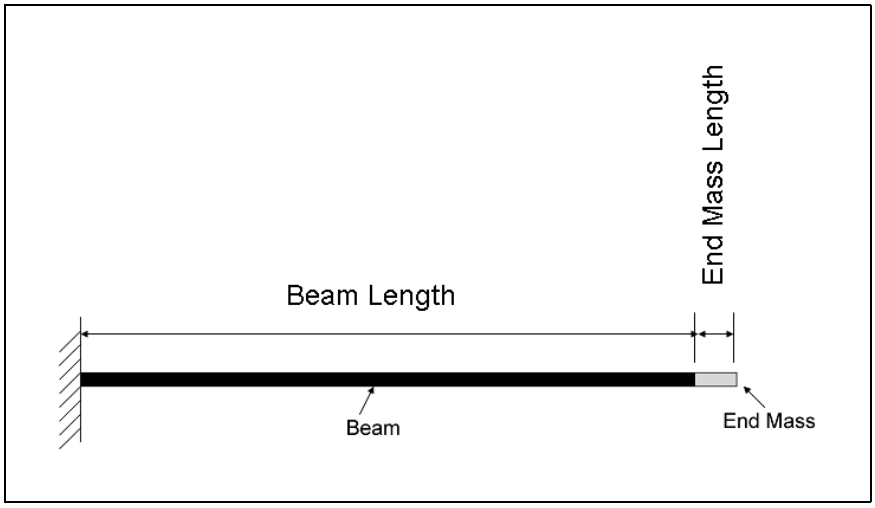

Figure 4.3: The cantilever beam used in the FEA model.

heavy point loads on the end of the beam, the equations should be similar to that of the PRBM.

In order to show these trends in the dynamics of a cantilever beam, a model was created of a cantilever beam with one end fixed and the other end attached to a small cantilever beam. The small beam was rigidly attached to the end of the long beam, as shown in Figure 4.3, and used as a local mass. The density of the small beam was changed, in order to increase the mass of the end of the beam with respect to the cantilever beam. The second beam was small in comparison to the overall length (roughly two percent of the overall length of the two beams). The beam was 23.5 inches long (0.5969 meters), with 30 elements. The end mass was one-half inch long (0.0127 meters) and consisted of two elements. Each element had three degrees of freedom: translation in the vertical and horizontal directions, as well as an in-plane rotation. The material properties that were used in each of the elements are shown in Table 4.1. The mass of the end of the cantilever beam was varied as

$$\rho_2 = \rho_1 \times (47 \times MassRatio + 1), \tag{4.20}$$

Table 4.1: Beam Properties

Property	Value	Unit	Value	Unit
Modulus of Elasticity	$30x10^6$	psi	206.8	GPa
Density-Beam	0.28	Lb/in^3	7800	Kg/m^3
Density-End mass	Equation (4.20)	$Slugs/in^3$	Equation (4.20)	Kg/m^3
Width	1.25	in	0.0318	m
Height	0.03125	in	0.000794	m
Area Moment of Inertia	$3.179x10^{-6}$	in^4	$1.3232x10^{-12}$	m^4
Area	0.039	in^2	$2.52x10^-5$	m^2
Poisons Ratio	0.3	-	0.3	-
Length Beam	23.5	in	0.5969	meters
Length-End Mass	.5	in	0.0127	meters

where the constant term (47) is the ratio of lengths of the end mass and the beam ($\frac{23\frac{1}{2}}{\frac{1}{2}}$), and the $MassRatio$ is the mass of the small segment, divided by the mass of the longer segment.

The beam was then deflected to 75 percent of the beam length (18.0 inches or 0.4572 meters), using a y-deflection constraint. Due to the nonlinear nature of the problem, the initial deflection had to take place through multiple small steps so that the FEA solution would converge. The boundary condition on the deflected end of the beam was then removed, and the motion of the beam was tracked through time. The time step for the results presented was 0.0005 seconds between evaluations. Only the fundamental frequency of the beam was of interest, since the PRBM is a single degree of freedom model. Because of the nonlinear nature of the deflection, the model would only converge with this very small time step. This time step proved to be sufficiently small to allow each of the models to converge. All of the models were run for at least a 20 second time period, with selected models being run for up to 100 seconds.

4.5.1 Analysis Method

An FEA modal analysis can be performed to represent the simplest FEA approximation of the beam. However, because of the large nonlinear deflections included in the motion, it was anticipated that a more complex analysis would be required to investigate the natural frequencies. In order to evaluate the information that was produced by FEA, the position of the end of the beam was tracked and stored at every analysis point. Figures 4.4 and 4.5 show a typical set of information. Figure 4.4 shows the values of the vertical and horizontal components of the position of the end of the beam. The figure suggests that the motion is regular and consistent. Figure 4.5 shows the end of the beam and the path. The path generally remains regular and consistent, however some variation in the path is shown. This is due, in part, to the approximations that are inherent to FEA. Another portion of this error comes from the higher modal frequencies that are inherent in a flexible system. The majority of the data is consistent with the figures that are shown, with the exception of the beams with an end mass greater than 20 times the mass of the beam. In those cases, the second resonance frequency began to increase in magnitude.

In order to convert the data from FEA results into a frequency, a Fast-Fourier-Transform (FFT) of the vertical position was taken. Figure 4.6 shows a typical result from the FFT of the vertical position data. Note that the vertical scale and the horizontal scale are not the same. The vertical scale shows a very large increase in the value of the peak. The peak is also very slender, which would be expected from a system that has little to no damping or noise. The small rippling effects around the peak are due to the rectangular windowing in the FFT. The peak frequency is easily determined from the results of the FFT.

4.5.2 Cantilever Beam FEA Results

Figures 4.8 and 4.9 show the results of the FEA and the PRBM for various end masses. The difference between the behavior predicted by the PRBM and the behavior predicted by the FEA is larger for small end-point masses, and the difference steadily decreases as the mass is increased. The difference then increases again for the

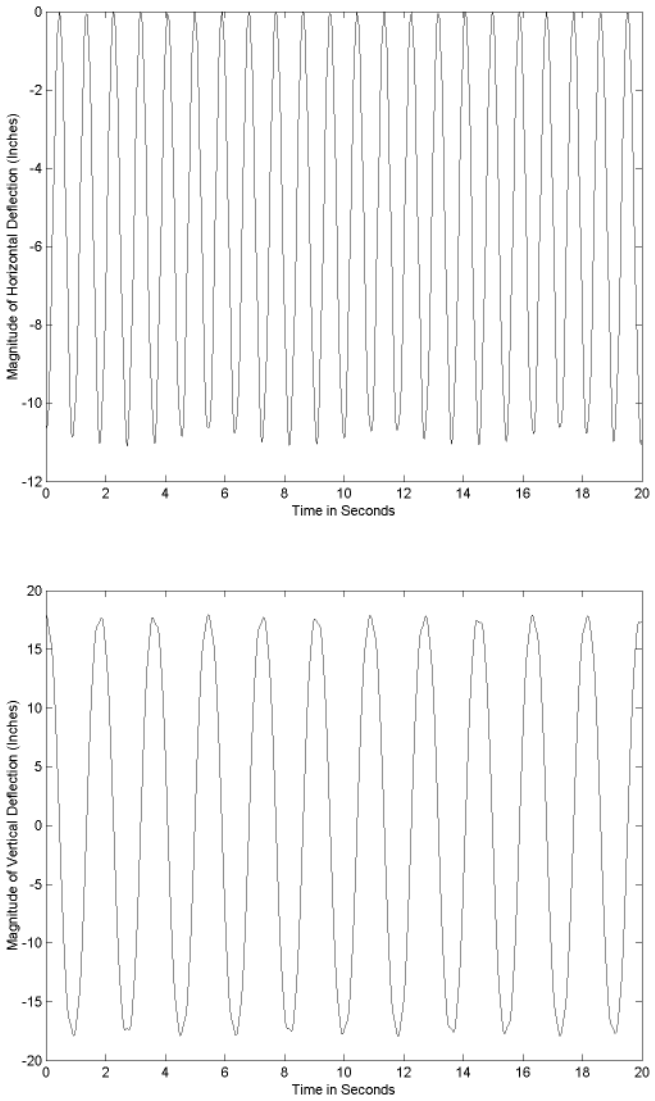

Figure 4.4: Vertical and horizontal components of the end of the cantilever beam plotted over time.

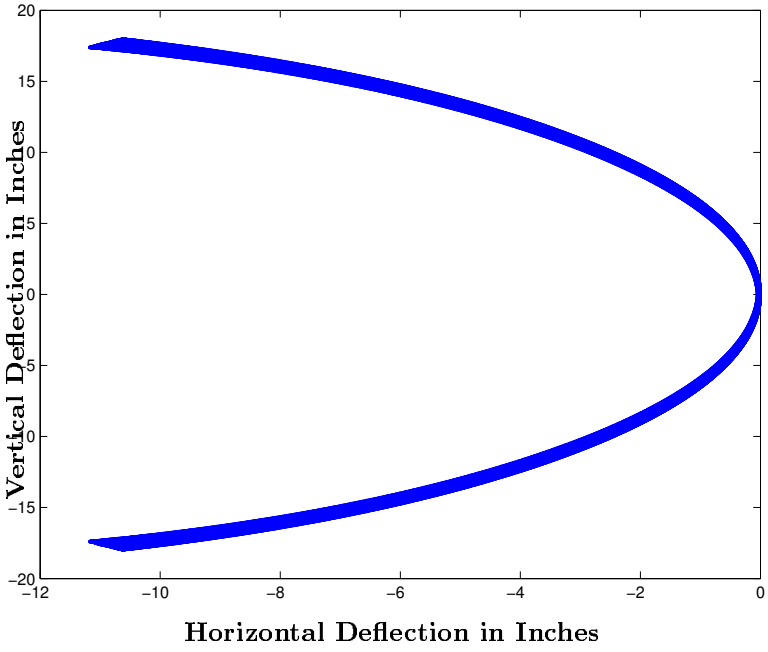

Figure 4.5: End location of the cantilever beam over time.

larger masses, due to the resolution of the FFT, which is proportional to the length of time the system was allowed to run. Longer time periods were used for several of the beams with large mass ratios in order to increase the resolution of the FFT. Several beams were chosen for longer run times and the results of the selected beams are displayed in Figure 4.7. The results were expected from the discussion earlier in this section. The percent difference plot in Figure 4.9 suggest that the PRBM provides comparable results.

4.5.3 Experimental Results

A cantilever beam was excited by mounting a clamp onto a linear bearing. The clamp could then be moved in a near sinusoidal manner by using a variable frequency motor driver and AC motor combination. Figure 4.10 shows a cantilever beam in the mount during excitation. The clamp holding the cantilever beam was moved one inch in total travel. The beam output was then visually inspected and the speed was

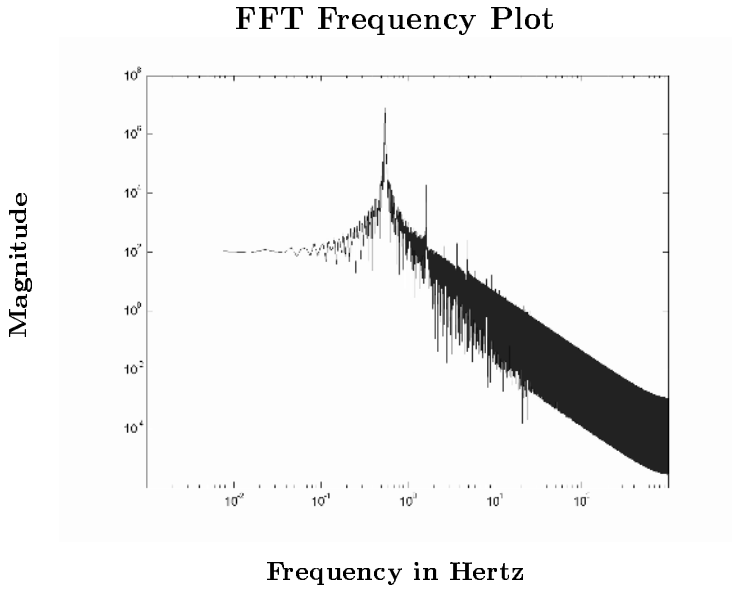

Figure 4.6: FFT of the vertical position data presented in Figure 4.4.

adjusted until the resonance frequency was reached. This approach helped isolate the first modal frequency and mitigated the effects of damping from the air, and ensured large nonlinear beam deflections. The mass of the end of the beam was then adjusted by adding small masses to the end of the beam. Table 4.2 shows the results of these measurements.

In order to obtain a loading condition similar to a point mass small weights were added to the end of the cantilever beam. The measured resonance frequency of the beam then became the damped resonance frequency. The results from the FEA represent a beam that is undamped. The two can be compared, since the damping coefficient for the measured beam is typically very low in steel. (The results of Section 6.1 show that the damping in steel beams is relatively low.) In this case, the higher mode damping that is apparent from a static release of the beam is not significantly excited, and the result is that the damped resonance frequency is a good measurement of the resonance frequency. The results shown were compared with the

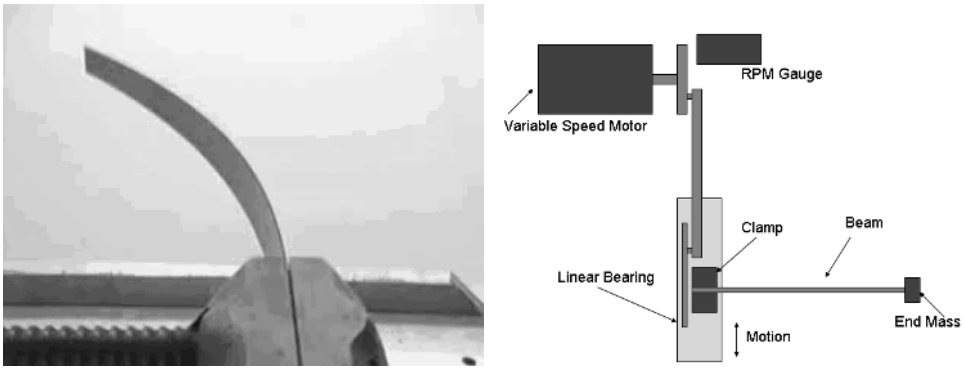

Figure 4.10: Test setup for cantilever beams.

results obtained from both the PRBM model and the FEA models. These results are presented in graphical form in Figure 4.11.

4.6 Investigation of Modal Frequencies

The equations that model large deflections of a cantilever beam are nonlinear. However, the predicted dynamic response of a cantilever beam under a deflection load using the PRBM, results in a linear model. Figure 4.12 shows the basic beam loads as applied to a PRBM of a cantilever beam under dynamic loads. The equation of motion is

$$I_{pin}\ddot{\Theta} + k\Theta = 0 \tag{4.21}$$

where I_{pin} is the mass moment of inertia about the pin joint, Θ is the PRBM angle, and k is the torsional stiffness. (In this case $k = \frac{\gamma K_\Theta EI}{L}$, where γ is the characteristic length, K_Θ is a Stiffness coefficient, E is the Young Modulus, I is the area moment of inertia, and L is the length of the cantilever beam.) The inertia can be handled in two ways, the first is shown in the equations above. The more common approach is to take the moment of inertia at the center of mass, and then include the force created due to the acceleration of the beam

$$I_{cm}\ddot{\Theta} + m\ddot{\Theta}{L_{cm}}^2 + k\Theta = 0, \tag{4.22}$$

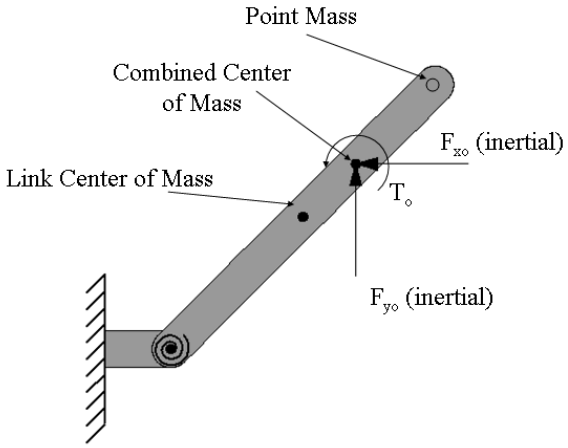

Figure 4.12: Showing the basic beam loads as applied to a PRBM of a cantilever beam under dynamic loads.

where I_{cm} is the mass moment of inertia about the center of mass, L_{cm} is the distance from the pin joint to the center of mass, and the other variables are as previously defined. Both equations yield linear differential equations for the response of the beam, and the response of the system will not depend on the initial deflection of the beam. From the equations presented earlier, and from the nonlinearities in a cantilever beam, this is a somewhat surprising result.

In order to study the problem in more detail, one of the beam models from was chosen as a test case (a relative point mass of 5 was chosen). Using the same properties as were defined previously (Table 4.1), and changing the initial conditions, the beams were simulated for a $20 - 40$ second time period. An FFT algorithm was then used to convert the resulting response into a frequency. Table 4.3 shows the resulting frequencies based on the FEA results. An FEA modal analysis was also performed (this is independent of any deflection) and resulted in a resonance frequency of 0.393 Hz. In addition, the other beam models were also examined, and compared with the results presented earlier in the chapter. The results are summarized in Figure 4.13 and 4.14.

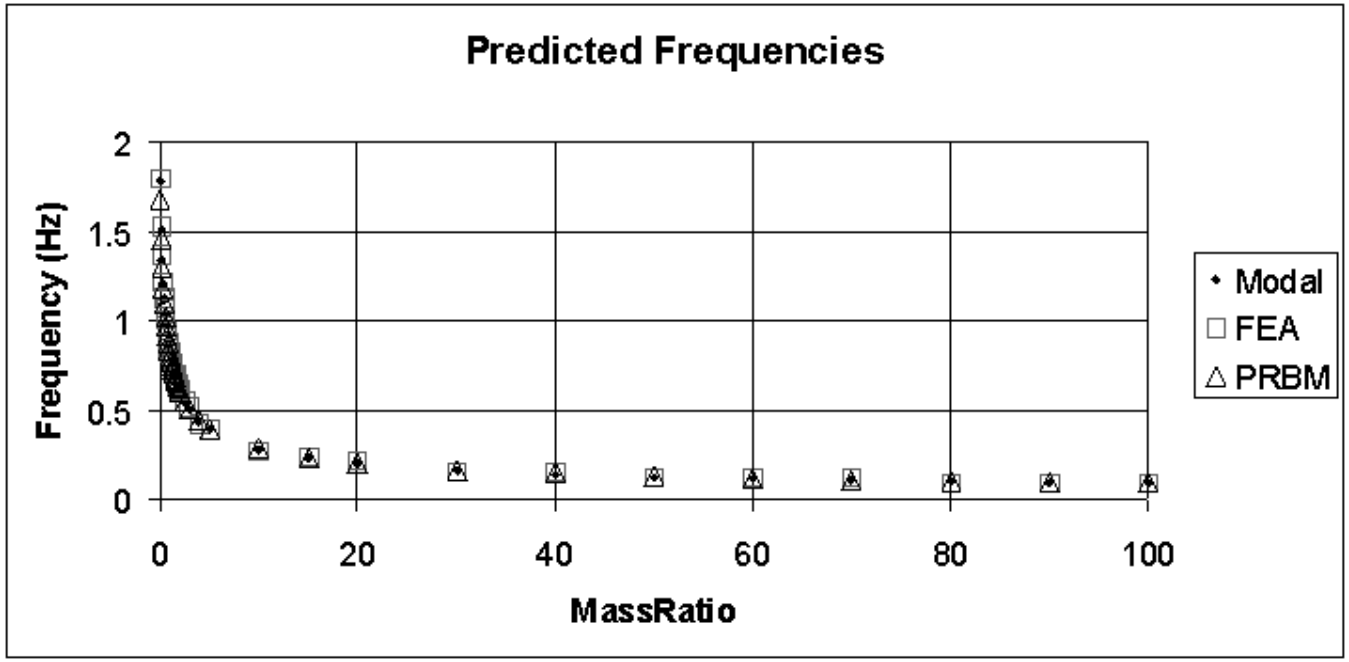

Figure 4.7: This data represents the resonance frequency of a cantilever beam with an increasing point mass.

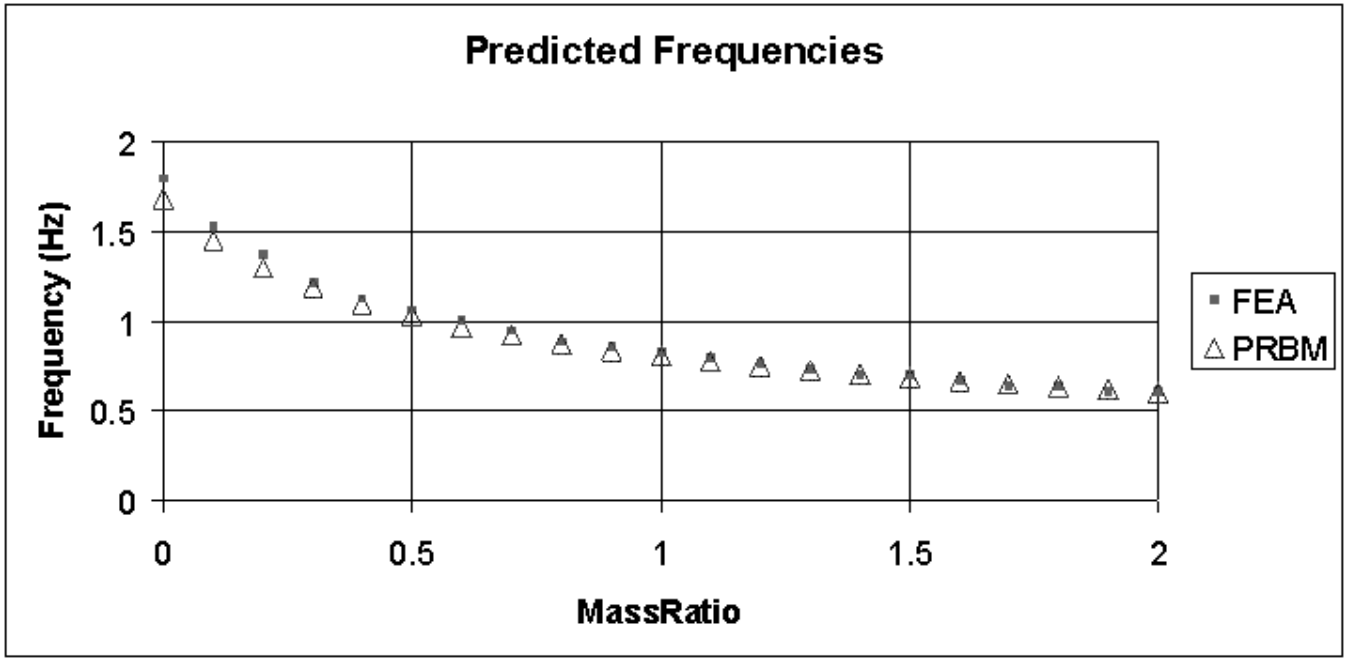

Figure 4.8: Plot of the predicted frequencies for the smaller masses, both FEA and PRBM model.

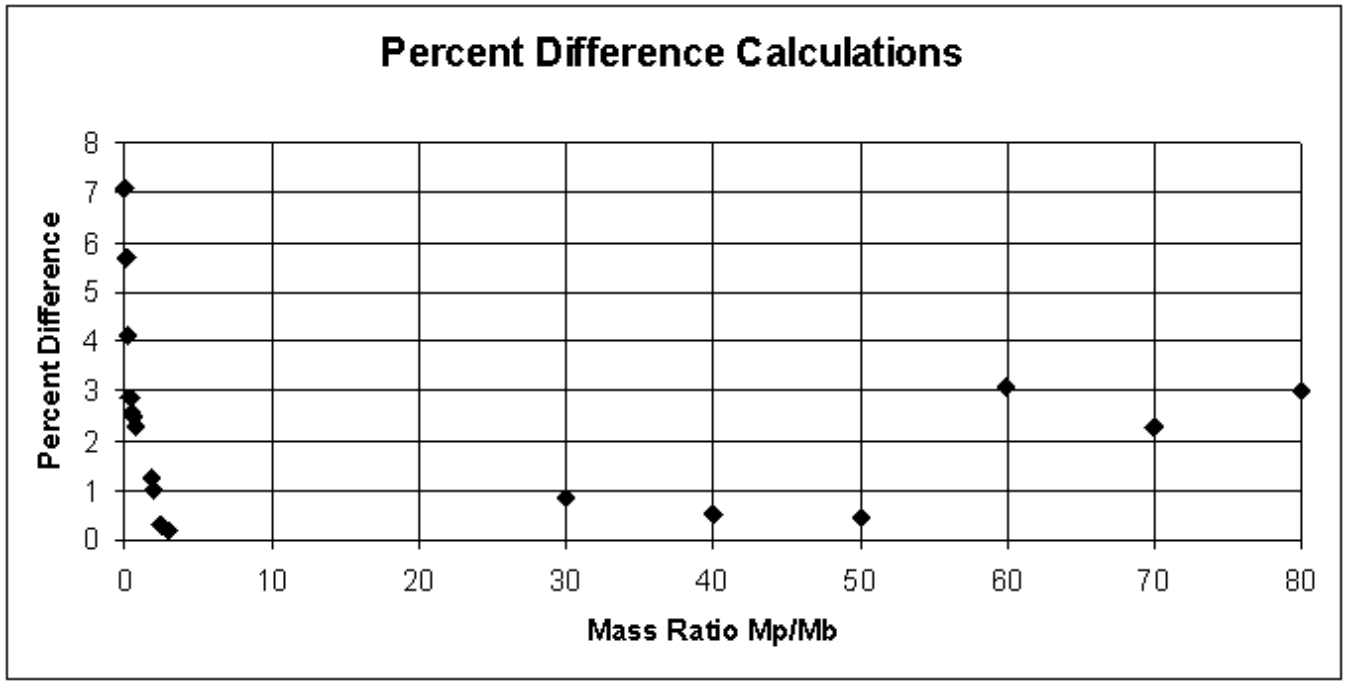

Figure 4.9: Percent difference between the FEA technique and the PRBM technique.

Table 4.2: Resonance Frequency Comparisons Based on End Mass

Mass Ratio	Measured Resonance Frequency (Hz)	Uncertainty
0.000	1.78	$\pm$0.04 (Hz)
0.082	1.58	$\pm$0.04 (Hz)
0.165	1.40	$\pm$0.04 (Hz)
0.247	1.27	$\pm$0.04 (Hz)
0.330	1.15	$\pm$0.10 (Hz)
0.824	0.86	$\pm$0.02 (Hz)
0.989	0.79	$\pm$0.02 (Hz)
1.153	0.74	$\pm$0.02 (Hz)
1.318	0.68	$\pm$0.03 (Hz)
1.483	0.64	$\pm$0.03 (Hz)

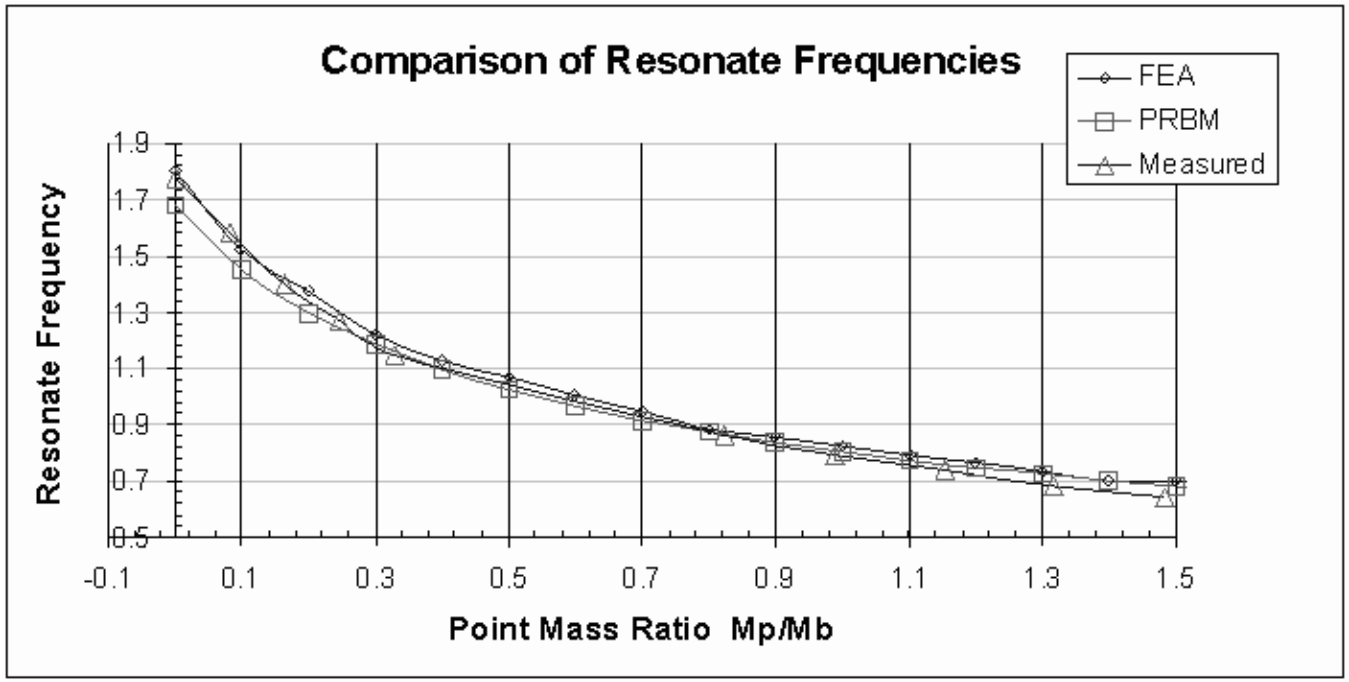

Figure 4.11: The predicted frequencies, from FEA and the PRBM, compared with the measured frequencies.

Table 4.3: Resonance Frequency Comparisons Based on Initial Conditions

Initial Deflection	FEA Resonance Frequency (Hz)	Uncertainty
6.1 cm	0.3967	$\pm$0.015 (Hz)
12.2 cm	0.3967	$\pm$0.015 (Hz)
18.3 cm	0.3967	$\pm$0.0075 (Hz)
24.4 cm	0.3967	$\pm$0.0075 (Hz)
30.5 cm	0.3967	$\pm$0.0075 (Hz)
36.6 cm	0.3967	$\pm$0.0075 (Hz)
42.7 cm	0.3967	$\pm$0.0075 (Hz)
48.8 cm	0.3967	$\pm$0.0075 (Hz)

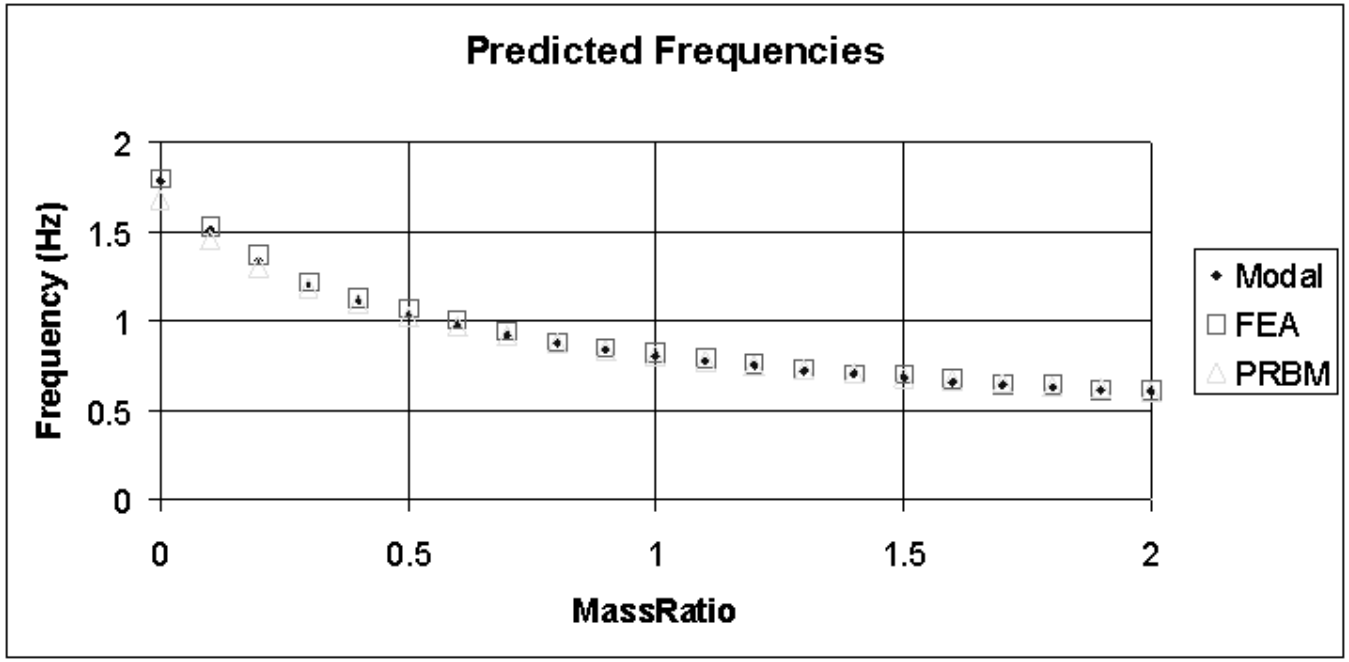

Figure 4.13: Showing the modal frequency along with the prediction from the nonlinear FEA and the PRBM.

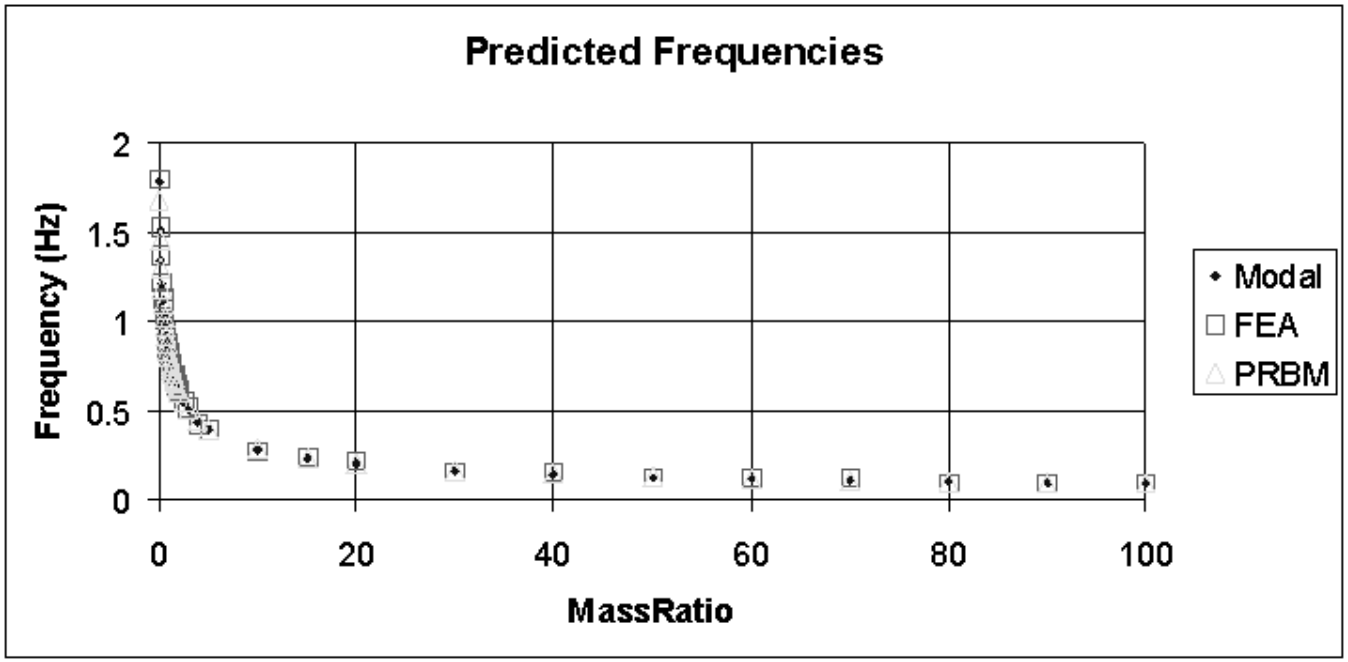

Figure 4.14: Diagram of the various loads on a cantilever beam based on the PRBM.

The results show that the predictions of the FEA model and the predictions of the PRBM both agree, and that the system can be modeled with a linear differential equation. This is a result that would not be expected from a system with the non-linearities that are associated with nonlinear deflection of this magnitude. However, it is exactly what is expected, and required for the PRBM to be considered accurate in predicting the dynamics of compliant mechanisms. Since the PRBM predicts that the behavior is related to a linear ordinary differential equation.

4.7 Summary

In this chapter, several methods of analyzing the dynamics of a flexible segment were discussed. Reasons for choosing FEA for comparison were set forth, and a discussion of the application of the analytical equations of motion for a flexible segment subjected to dynamic loads was presented. From the analytical model, several restrictions were presented for the PRBM under dynamic loading conditions. The restrictions were then discussed in light of applications to various types of mechanisms incorporating fixed-pinned segments, fixed-fixed segments, and small-length flexural pivots.

In order to validate the results that were obtained from FEA, test beams were made and the resonance frequencies were measured. The results showed a good correlation between the values predicted by the PRBM, FEA, and measured data. In addition, it was shown that the modal frequency matched the predictions of PRBM and FEA results, suggesting that the PRBM method is a viable method for predicting the dynamic behavior of flexible segments. Although this result is not one that would be intuitively expected, it is a result that was required for the PRBM to be considered a viable method of predicting the resonance frequencies of compliant mechanisms.

The major contribution of this chapter was to show that the PRBM can be used to predict the dynamic behavior of a flexible segment. Since the PRBM can be used to predict the behavior of a flexible segment, the PRBM should be able to predict the dynamic behavior of mechanisms. The next chapters expand on modeling and using the the PRBM to predict the dynamic behavior of mechanisms.

Chapter 5

Modeling the Dynamics of Compliant Mechanisms using the Pseudo-Rigid-Body Model

There are various methods for modeling the dynamic behavior of mechanisms. Part of the appeal of the Pseudo-Rigid-Body model (PRBM) is that the classical approaches to kinematic and dynamic analysis of mechanisms are still available to the engineer for the design of compliant mechanisms. This chapter will discuss the development of a model for a several compliant mechanisms. Although the models are not new, the provide insight into the methods for examining how a compliant systems behaves. A common method of dynamically modeling a four-bar linkage is through free-body diagrams. This method can be found in various undergraduate texts in great detail. Lagrangian methods for determining the dynamics of these systems are also valuable. These methods can be applied to the systems discussed in this work. It will be assumed that the reader is familiar with all of these methods. Lagrangian methods are reviewed briefly, but details can be found in a variety of texts [45, 46].

The energy in the system[1] is both kinetic (T) and potential (U). The two forms of energy are summed to create a measure of the total energy (E) in the system (with no dissipative losses, such as friction) as

$$T + U = E = constant \tag{5.1}$$

From the conservation of energy, we know that the total differential of energy must be zero

$$dE = d(T + U) = dT + dU = 0. \tag{5.2}$$

[1]This basic argument is presented by [45], pp 207-209

Non-conservative drains (Friction, etc.) can be applied on the right side of the equation if they are required to accurately model the dynamic systems. The potential energy (U) is a function of generalized coordinates (in this case q_i), and the kinetic energy T is a function of both the generalized coordinates and the generalized velocities ($\dot{q}_i$). The derivative of the kinetic energy is

$$dT = \sum_{i=1}^{N} \frac{\partial T}{\partial q_i} dq_i + \sum_{i=1}^{N} \frac{\partial T}{\partial \dot{q}_i} d\dot{q}_i, \tag{5.3}$$

and the derivative of the potential energy is

$$dU = \sum_{i=1}^{N} \frac{\partial U}{\partial q_i} dq_i. \tag{5.4}$$

With some manipulation, it can be shown that:

$$dT = \sum_{i=1}^{N} \left[\frac{d}{dt} \left(\frac{\partial T}{\partial \dot{q}_i} \right) - \frac{\partial T}{\partial q_i} \right] dq_i. \tag{5.5}$$

Combining the derivatives yields:

$$d(T+U) = \sum_{i=1}^{N} \left[\frac{d}{dt} \left(\frac{\partial T}{\partial \dot{q}_i} \right) - \frac{\partial T}{\partial q_i} + \frac{\partial U}{\partial q_i} \right] dq_i = 0. \tag{5.6}$$

Because each of the generalized coordinates is chosen to be independent, the following is true:

$$\frac{d}{dt} \left(\frac{\partial T}{\partial \dot{q}_i} \right) - \frac{\partial T}{\partial q_i} + \frac{\partial U}{\partial q_i} = 0 \qquad i = 1, 2, \cdots N. \tag{5.7}$$

For simplicity, the Lagrangian is defined $\mathcal{L} = (T - U)$. This term is then used to replace the terms for T and U from Equation (5.7) as

$$\frac{d}{dt} \left(\frac{\partial \mathcal{L}}{\partial \dot{q}_i} \right) - \frac{\partial \mathcal{L}}{\partial q_i} = 0 \qquad i = 1, 2, \cdots N. \tag{5.8}$$

The development presented here is a brief summary of the development presented by [45], but it explains how the Lagrangian technique uses the kinetic and potential energies to determine the dynamic behavior of the system. A more detailed derivation could be found in a calculus of variations text [47, 48, 49], or in many classical mechanics texts [33, 46, 50].

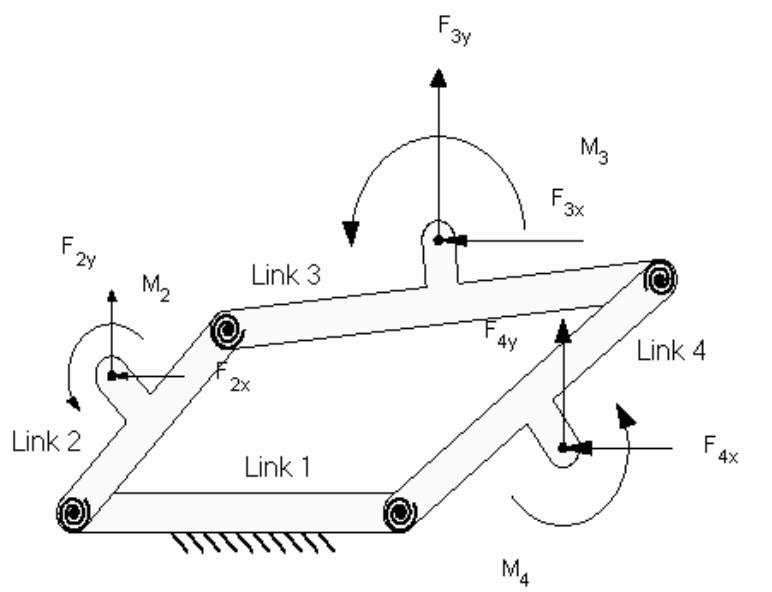

Figure 5.1: The general pseudo-rigid-body four-bar mechanism modeled.

5.1 Model Development

A pseudo-rigid-body four-bar mechanism will be used to model a variety of compliant mechanisms. A general four-bar mechanism is illustrated in Figures 5.1 and 5.2. The motion of each mass depends on the motion of the input. The input angle and generalized coordinate will be the angle of Link 2 (defined in Figure 5.1), θ_2, for each of the mechanisms considered. The mechanism has only one degree of freedom, so only one generalized coordinate and one equation of motion are needed to describe the dynamics of the system. There are a number of ways of determining the kinetic and potential energies in this system. Here, each link is treated as an individual mass with an inertia, and then is combined with all of the others into a coupled dynamic system.

The kinetic and potential energies for Link 2 are not difficult to find, because the center of mass of the first link will always rotate around the first joint. The magnitude of the velocity of the center of mass of Link 2, V_{2cm}, will remain at a constant

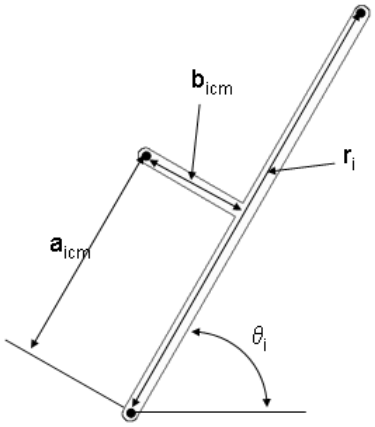

Figure 5.2: Graphical depiction of the terms used to describe the links.

radius ($\sqrt{{a_{2cm}}^2 + {b_{2cm}}^2}$), making the magnitude of the velocity easy to calculate:

$$V_{2cm} = \dot{\theta_2}\sqrt{{a_{2cm}}^2 + {b_{2cm}}^2}. \tag{5.9}$$

Link 3 proves to be more complex, but its center of mass is well defined as

$$x_{3cm} = r_2\cos(\theta_2) + a_{3cm}\cos(\theta_3) - b_{3cm}\sin(\theta_3) \tag{5.10}$$

$$y_{3cm} = r_2\sin(\theta_2) + a_{3cm}\sin(\theta_3) + b_{3cm}\cos(\theta_3). \tag{5.11}$$

The velocities can be found from these equations by taking the derivatives and combining them as vectors. The magnitude of the velocity can be manipulated into the following form:

$$V_{3cm} = \sqrt{\begin{array}{c} {r_2}^2{\dot{\theta}_2}^2 + {a_{3cm}}^2\left(\frac{\partial\theta_3}{\partial\theta_2}\right)^2{\dot{\theta}_2}^2 + b_{3cm}\left(\frac{\partial\theta_3}{\partial\theta_2}\right)^2{\dot{\theta}_2}^2 \\ +2a_{3cm}r_2\left(\frac{\partial\theta_3}{\partial\theta_2}\right){\dot{\theta}_2}^2\cos(\theta_2-\theta_3) + 2b_{3cm}r_2\left(\frac{\partial\theta_3}{\partial\theta_2}\right){\dot{\theta}_2}^2\sin(\theta_2-\theta_3). \end{array}} \tag{5.12}$$

The velocity of the center of mass of Link 4, V_{4cm} can be simplified to:

$$V_{4cm} = \left(\frac{\partial\theta_4}{\partial\theta_2}\dot{\theta_2}\right)\sqrt{{a_{4cm}}^2 + {b_{4cm}}^2}, \tag{5.13}$$

which shows that the center of mass will always rotate about the pin joint that is fixed to ground. The total kinetic energy is:

$$T = \frac{1}{2}m_2{V_{2cm}}^2 + \frac{1}{2}m_3{V_{3cm}}^2 + \frac{1}{2}m_4{V_{4cm}}^2 + \frac{1}{2}I_2\dot{\theta}_2^2 + \frac{1}{2}I_3\dot{\theta}_3^2 + \frac{1}{2}I_4\dot{\theta}_4^2, \tag{5.14}$$

where the velocities are given by the equations above, m_i is the mass of Link i, and I_i is the mass moment of inertia of Link i.

The following terms prove useful in developing the potential energy of the mechanism:

$$\begin{aligned} \psi_1 &= \theta_2 - \theta_{2o} \\ \psi_2 &= (\theta_2 - \theta_{2o}) - (\theta_3 - \theta_{3Ao}) \\ \psi_3 &= (\theta_4 - \theta_{4o}) - (\theta_3 - \theta_{3Bo}) \\ \psi_4 &= \theta_4 - \theta_{4o}. \end{aligned} \tag{5.15}$$

The potential energy from the torsional springs is

$$U = \frac{1}{2}K_1{\psi_1}^2 + \frac{1}{2}K_2{\psi_2}^2 + \frac{1}{2}K_3{\psi_3}^2 + \frac{1}{2}K_4{\psi_4}^2. \tag{5.16}$$

The Lagrangian (L) can be written as

$$\begin{aligned} L = \tfrac{1}{2}m_2{V_{2cm}}^2 + \tfrac{1}{2}m_3{V_{3cm}}^2 + \tfrac{1}{2}m_4{V_{4cm}}^2 + \\ \tfrac{1}{2}I_2\dot{\theta}_2^2 + \tfrac{1}{2}I_3\dot{\theta}_3^2 + \tfrac{1}{2}I_4\dot{\theta}_4^2 - \tfrac{1}{2}K_1{\psi_1}^2 - \tfrac{1}{2}K_2{\psi_2}^2 - \\ \tfrac{1}{2}K_3{\psi_3}^2 - \tfrac{1}{2}K_4{\psi_4}^2. \end{aligned} \tag{5.17}$$

The resulting value is then applied to the Lagrangian equation, which is

$$\frac{d}{dt}\left(\frac{\partial L}{\partial \dot{\theta}_2}\right) - \frac{\partial L}{\partial \theta_2} = -Q_{\theta_2}. \tag{5.18}$$

Because of the large amount of algebra that is required for the development of the resulting dynamic equation, only the final results are presented here. A few definitions that aid in equation simplification are described first. The kinematic coefficients are

$$\frac{\partial \theta_3}{\partial \theta_2} = h_{32} = \frac{r_2 \sin(\theta_4 - \theta_2)}{r_3 \sin(\theta_3 - \theta_4)}, \tag{5.19}$$

$$\frac{\partial \theta_4}{\partial \theta_2} = h_{42} = \frac{r_2 \sin(\theta_3 - \theta_2)}{r_3 \sin(\theta_3 - \theta_4)}; \tag{5.20}$$

The derivatives of the kinematic coefficients with respect to time are

$$\begin{aligned} \dot{h}_{32} = & \frac{r_3 r_2 \sin(\theta_3 - \theta_4)\cos(\theta_4 - \theta_2)(\dot{\theta}_4 - \dot{\theta}_2)}{r_3^2(\sin(\theta_3 - \theta_4))^2} \\ & - \frac{r_2 r_3 sin(\theta_4 - \theta_2)\cos(\theta_3 - \theta_4)(\dot{\theta}_3 - \dot{\theta}_4))}{r_3^2(\sin(\theta_3 - \theta_4))^2} \end{aligned} \tag{5.21}$$

and

$$\begin{aligned} \dot{h}_{42} = & \frac{r_4 r_2 \sin(\theta_3 - \theta_4)\cos(\theta_3 - \theta_2)(\dot{\theta}_3 - \dot{\theta}_2)}{r_4^2(\sin(\theta_3 - \theta_4))^2} \\ & - \frac{r_2 r_4 \sin(\theta_3 - \theta_2)\cos(\theta_3 - \theta_4)(\dot{\theta}_3 - \dot{\theta}_4)}{r_4^2(\sin(\theta_3 - \theta_4))^2}; \end{aligned} \tag{5.22}$$

and the derivatives with respect to θ_2 are

$$\begin{aligned} \frac{\partial h_{32}}{\partial \theta_2} = & \frac{r_3 r_2 \sin(\theta_3 - \theta_4)\cos(\theta_4 - \theta_2)(h_{42} - 1)}{r_3^2(\sin(\theta_3 - \theta_4))^2} \\ & - \frac{r_2 r_3 \sin(\theta_4 - \theta_2)\cos(\theta_3 - \theta_4)(h_{32} - h_{42})}{r_3^2(\sin(\theta_3 - \theta_4))^2} \end{aligned} \tag{5.23}$$

$$\begin{aligned} \frac{\partial h_{42}}{\partial \theta_2} = & \frac{r_4 r_2 \sin(\theta_3 - \theta_4)\cos(\theta_3 - \theta_2)(h_{32} - 1)}{r_4^2(\sin(\theta_3 - \theta_4))^2} \\ & - \frac{r_2 r_4 \sin(\theta_3 - \theta_2)\cos(\theta_3 - \theta_4)(h_{32} - h_{42})}{r_4^2(\sin(\theta_3 - \theta_2))^2}. \end{aligned} \tag{5.24}$$

The derivatives with respect to θ_2 of the velocities of Link 3 and Link 4 are required

$$\begin{aligned} \frac{\partial V_{3cm}}{\partial \theta_2} = & \left[\frac{(a_{3cm}h_{32} + r_2\cos(\theta_2 - \theta_3))\left(a_{3cm}\frac{\partial h_{32}}{\partial \theta_2} - r_2 \sin(\theta_2 - \theta_3)(1 - h_{32})\right)}{\sqrt{a_{3cm}h_{32} + r_2\cos(\theta_2 - \theta_3))^2 + (b_{3cm}h_{32} + r_2\sin(\theta_2 - \theta_3))^2}} \right] \dot{\theta}_2 \\ & + \left[\frac{(b_{3cm}h_{32} + r_2\sin(\theta_2 - \theta_3))\left(b_{3cm}\frac{\partial h_{32}}{\partial \theta_2} + r_2 \cos(\theta_2 - \theta_3)(1 - h_{32})\right)}{\sqrt{a_{3cm}h_{32} + r_2\cos(\theta_2 - \theta_3))^2 + (b_{3cm}h_{32} + r_2\sin(\theta_2 - \theta_3))^2}} \right] \dot{\theta}_2 \end{aligned} \tag{5.25}$$

and

$$\frac{\partial V_{4cm}}{\partial \theta_2} = \dot{\theta}_2 \frac{\partial h_{42}}{\partial \theta_2}\sqrt{a_{4cm}^2 + b_{4cm}^2}. \tag{5.26}$$

With these, it is possible to evaluate the Lagrangian equation (Equation (5.18)). The values of each of the terms are shown below:

$$\begin{gathered}\frac{d}{dt}\left(\frac{\partial L}{\partial \dot{\theta}_2}\right) = m_2\ddot{\theta}_2(a_{2cm}^2 + b_{2cm}^2) + m_4\ddot{\theta}_2 h_{42}^2(a_{4cm}^2 + b_{4cm}^2) \\ +2m_4\dot{\theta}_2\dot{\theta}_{42}(a_{4cm}^2 + b_{4cm}^2) + m_3\ddot{\theta}_2[(a_{3cm}h_{32} + r_2\cos(\theta_2 - \theta_3))^2 + \\ (h_{32}b_{3cm} + r_2\sin(\theta_2 - \theta_3))^2] \\ +2m_3\dot{\theta}_2[(a_{3cm}h_{32} + r_2\cos(\theta_2 - \theta_3))(a_{3cm}\dot{h_{32}} - r_2\sin(\theta_2 - \theta_3)(\dot{\theta}_2 - \dot{\theta}_3)) + \\ (b_{3cm}h_{32} + r_2\sin(\theta_2 - \theta_3))(b_{3cm}h_{32} + r_2\sin(\theta_2 - \theta_3)(\dot{\theta}_2 - \dot{\theta}_3))] \\ +I_2\ddot{\theta}_2 + I_3\ddot{\theta}_2 h_{32}^2 + I_4\ddot{\theta}_2 h_{42}^2 + 2I_3 h_{32}\dot{h_{32}}\dot{\theta}_2 + 2I_4\dot{\theta}_2 h_{42}\dot{h_{42}}\end{gathered} \tag{5.27}$$

and

$$\begin{gathered}\frac{\partial L}{\partial \theta_2} = m_3 V_{3cm}\frac{\partial V_{3cm}}{\partial \theta_2} + m_4 V_{4cm}\frac{\partial V_{4cm}}{\partial \theta_2} + I_3\dot{\theta_2}^2 h_{32}\frac{\partial h_{32}}{\partial \theta_2} + I_4\dot{\theta_2}^2 h_{42}\frac{\partial h_{42}}{\partial \theta_2} \\ -k_1\psi_1 - k_2\psi_2(1 - h_{32}) - k_3\psi_3(h_{42} - h_{32}) - k_4\psi_4 h_{42}.\end{gathered} \tag{5.28}$$

For the case of no damping, $Q_{\theta_2} = 0$, so these two equations can be substituted into Equation (5.18) to obtain the equation of motion of the general PRBM four-bar mechanism.

5.2 Modeling Straight-Line Mechanisms with Heavy Shuttles

Straight-line mechanisms with a heavy shuttle can be modeled in the same manner as the general four-bar mechanism, but the special geometry makes it possible to have a simplified model. The requirement of the heavy shuttle allows the inertias of the flexible segments to be ignored. The basic model is illustrated in Figure 5.3. It will be assumed that the spring will have very little mass in comparison with the mass of the shuttle. This is consistent with the mechanisms for which this model will be used. The mechanisms have only one degree of freedom, and hence one generalized coordinate. In this case, the coordinate will be defined by x. The resulting equation of motion is

$$M_s\ddot{x} + F_d(\dot{x}) + K(x)x = 0, \tag{5.29}$$

where $F_s(x)$ is a nonlinear representation of the force applied from the spring, M_s is the mass of the shuttle, and $F_d(\dot{x})$ is the total damping force on the mechanism. This will allow multiple models to be tested and evaluated. Because the damping

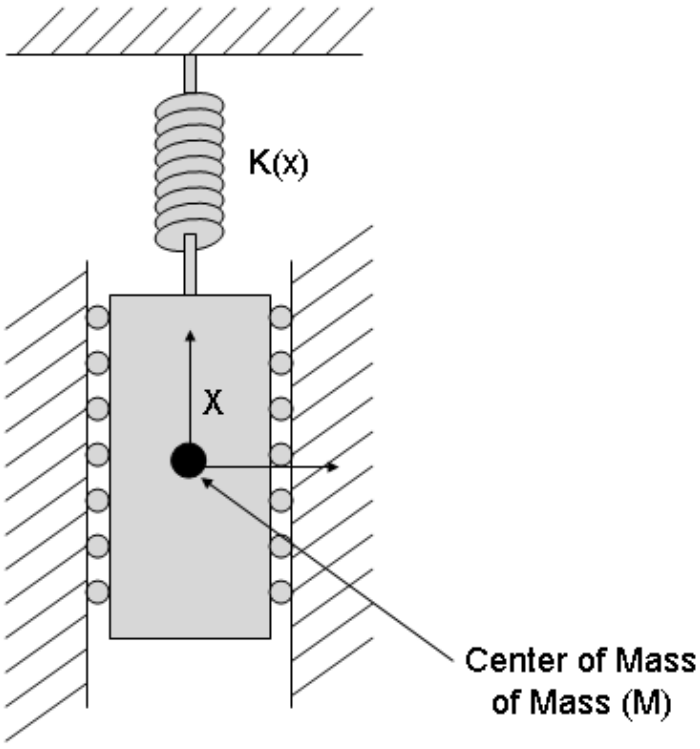

Figure 5.3: The generic model used in the development of the equations of motion for a linear mechanism. Note that the mass of the spring is assumed to be zero, and the shuttle mass will be the dominant mass in the system.

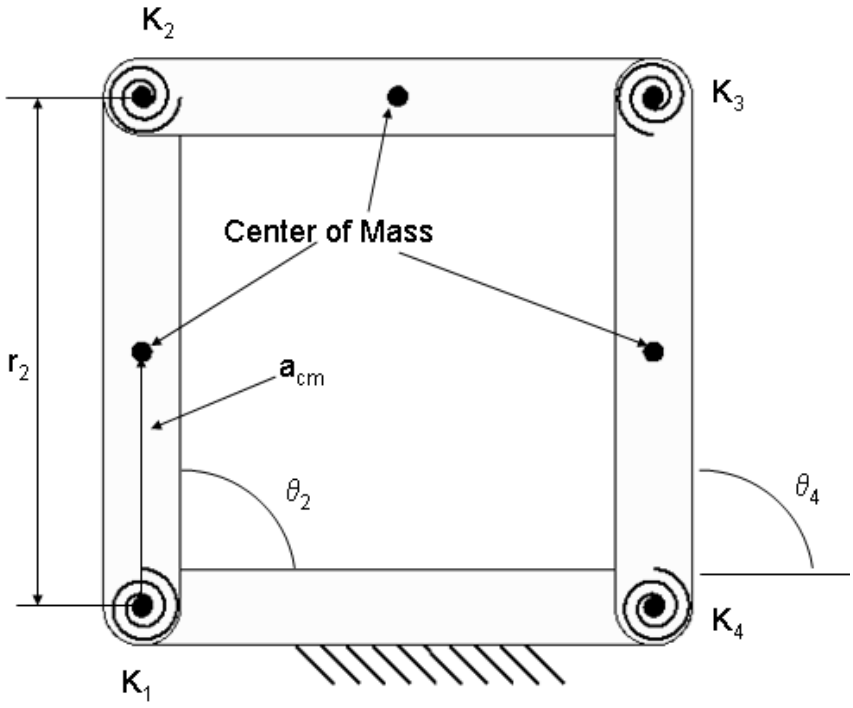

Figure 5.4: The PRBM for a parallel mechanism.

terms are assumed to be negligible for the devices in this work, the equation can be simplified to:

$$M\ddot{x} + K(x)x = 0. \tag{5.30}$$

The equation of motion for this type of mechanism is relatively simple in comparison to the equations of motion of a four-bar mechanism.

5.3 Modeling the Dynamics of Parallel Mechanisms

Lagrangian techniques can also be used to derive the equations of motion for parallel mechanisms, such as the one illustrated in Figure 5.4. The coupler mass will travel in a circular path with a radius the same as the length of the side links. The coupler will not rotate, so the rotational inertia of the coupler can be ignored. The velocities of each of the centers of mass of the PRBM links are listed in Table 5.1. The kinetic energy of the mechanism is defined by

Table 5.1: Link Velocities

Link 1 =	0
Link 2 =	$\frac{1}{2}r_2\dot{\theta}_2$
Link 3 =	$r_2\dot{\theta}_2$
Link 4 =	$\frac{1}{2}r_2\dot{\theta}_2$,

$$T = \frac{1}{2}m_3(r_2\dot{\theta_2})^2 + \frac{1}{2}m_2(\frac{1}{2}r_2\dot{\theta_2})^2 + \frac{1}{2}m_4(\frac{1}{2}r_2\dot{\theta_2})^2, \tag{5.31}$$

where r_2 is the length of the PRBM Link 2 (the segment between the grounded segment and the coupler), and θ_2 is the angle between the grounded segment and the PRBM Link 2. The kinetic energy of each of the two side links can also be found easily, since they rotate around the grounded pin joints. Note that in this case the effects of the rotational inertia must also be included.

The potential energy comes strictly from the torsional springs (ignoring gravitational effects). A deflection of $\theta_2 - \theta_{2o}$ creates a deflection of $\theta_2 - \theta_{2o}$ for each of the torsional springs. The potential energy is

$$U = \frac{1}{2}(K_1 + K_2 + K_3 + K_4)(\theta_2 - \theta_{2o})^2. \tag{5.32}$$

The Lagrangian (L), is

$$L = T - U = \frac{1}{2}m_3(r_2\dot{\theta_2})^2 + \tag{5.33}$$
$$\frac{1}{2}m_2(\frac{1}{2}r_2\dot{\theta_2})^2 + \frac{1}{2}m_4(\frac{1}{2}r_2\dot{\theta_2})^2 + \frac{1}{2}I_2\dot{\theta_2}^2 + \frac{1}{2}I_4\dot{\theta_2}^2$$
$$-\frac{1}{2}(K_1 + K_2 + K_3 + K_4))(\theta_2 - \theta_{2o})^2.$$

Applying Equation (5.18) and rewriting the equation into a compact form gives the equation of motion as

$$((m_3 + \frac{1}{4}(m_2 + m_3))r_2{}^2 + I_2 + I_4)\ddot{\theta}_2 \tag{5.34}$$
$$+(K_1 + K_2 + K_3 + K_4))(\theta_2 - \theta_{2o}) = 0. \tag{5.35}$$

From this equation the resonance frequency of the system is:

$$\omega_n = \sqrt{\frac{K_1 + K_2 + K_3 + K_4}{(m_3 + \frac{m_2+m_4}{4})r_2{}^2 + I_2 + I_4}}. \tag{5.36}$$

Equation (5.36) provides the resonance frequency of each of the parallel mechanisms tested in Chapter 6, when the proper values are substituted into the equation. The specific details of each of the parameters are also discussed in Chapter 6.

5.4 Summary

In this chapter the concept behind the development of the equation of motion of a general PRBM mechanism was presented. The PRBM allowed the development of the dynamics of these mechanisms, based on traditionally accepted mechanism analysis techniques. The ability to use traditional techniques is a significant advantage to the designer, allowing the use of methods that have been proven over time. The next chapter discusses using the PRBM and compares the results to measurements on actual systems.

Chapter 6

Model Comparisons

Chapter 4 focused on individual segments of the Pseudo-Rigid-Body Model (PRBM). This chapter examines the combined effect of the individual segments as components in more complex mechanisms. The various models are compared to either test results or finite element analysis (FEA) results, and in a few cases they are compared to both. This chapter also discusses the specifics of the mechanisms tested, and the resulting comparison to measured/FEA results. The method of testing was chosen based on the best method available for the mechanisms and will be discussed in each section. In this chapter, the mechanisms that are studied are all macro sized devices; the next chapter extends the study to micro mechanisms.

6.1 Parallel Mechanisms

The parallel mechanism is a very commonly used mechanism and has been used in the research of various authors [9, 51, 52]. Because of the frequent use of this mechanism and the ease of reconfiguration, the parallel mechanism was chosen for study in detail. The configurations of the mechanisms chosen to be studied are shown in Figure 6.1. They were selected to provide coverage of the majority of individual segments, as well as combinations of various types of individual segments.

6.1.1 Dynamic Results

Figure 6.1 shows the compliant parallel mechanisms that were used in this study. The mechanism configurations are referred to as Parallel A, Parallel B, Parallel C, and Parallel D, respectively.

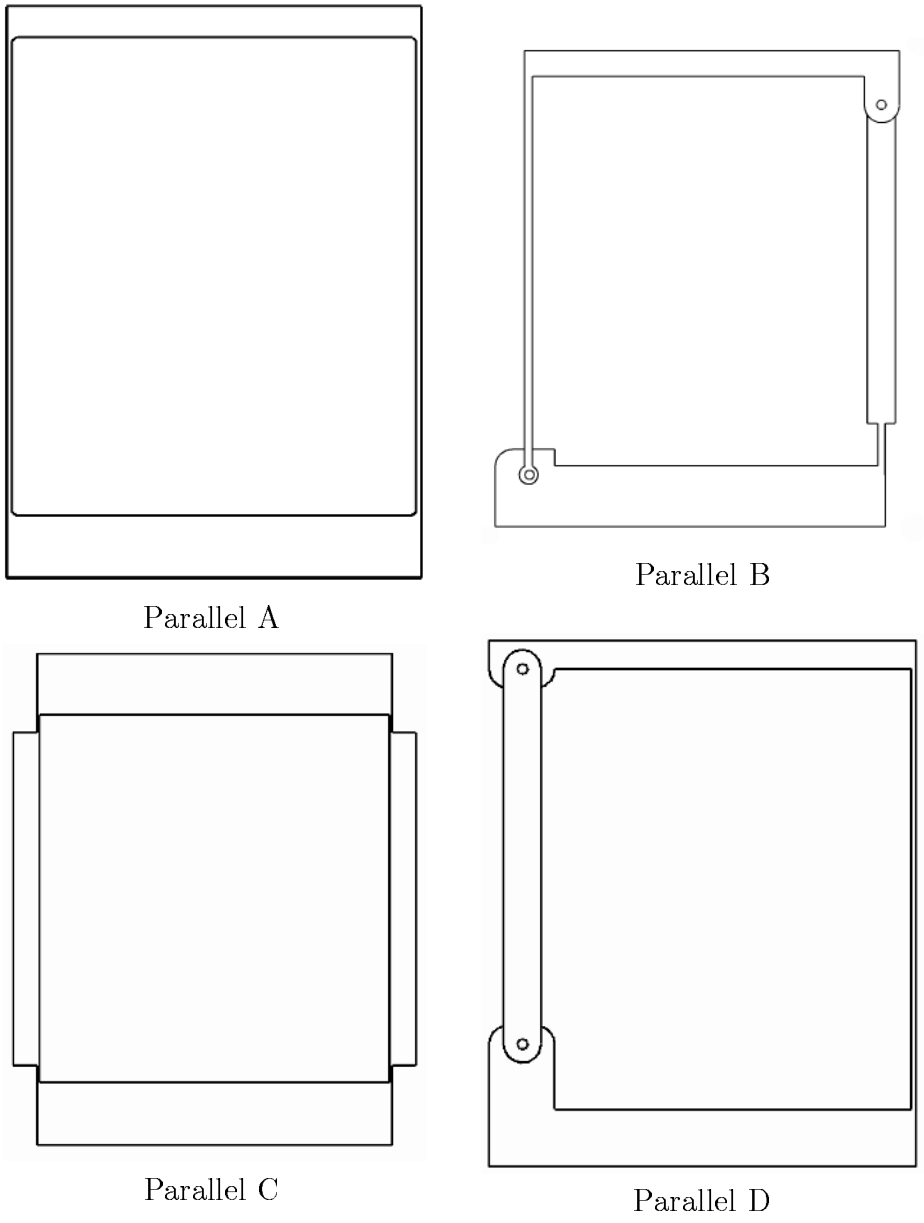

Figure 6.1: Tested configurations of the Compliant Parallel Guiding Mechanism.

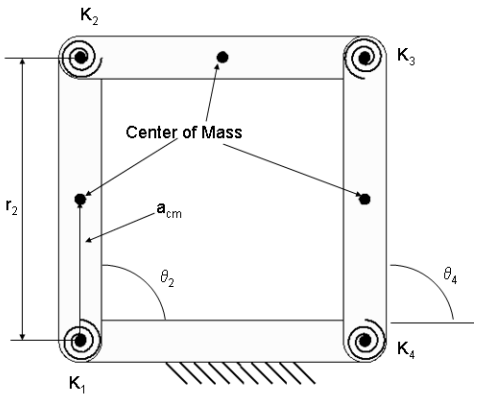

Figure 6.2: A depiction of the PRBM for each of the mechanisms in Figure 6.1.

Each of these compliant parallel guiding mechanisms have a similar PRBM which is illustrated in Figure 6.2. The torsional spring values depend on the mechanism configuration, and the geometry of the flexible segments. The dynamic equations of motion were developed in Section 5.3 and the equation of motion is given by Equation (5.35). Although the individual segments of the mechanisms were changed for all of the models, the dynamic model was similar for all of the parallel mechanisms. The only change between configurations came from the changed values of the spring constants. In the case of the parallel mechanism there are 28 known configurations of viable compliant mechanisms [9]. All of these could be modelled with the same PRBM by changing the related parameters. This allows a large amount of flexibility in behavior without changing the path properties.

With known geometries and the masses, it was possible to predict the first resonance frequency of the parallel mechanisms. Each of the configurations shown in Figure 6.1 was manufactured and tested. The mechanisms were constructed of polypropylene (Young's modulus 1.38×10^9 Pa) and steel (Young's modulus 207×10^9 Pa). Table 6.1 lists the geometry and masses of the mechanisms that were tested (LFS stands for long flexible segment, and SFLP is for small length flexural pivot). The segments are labeled in Figure 6.3.

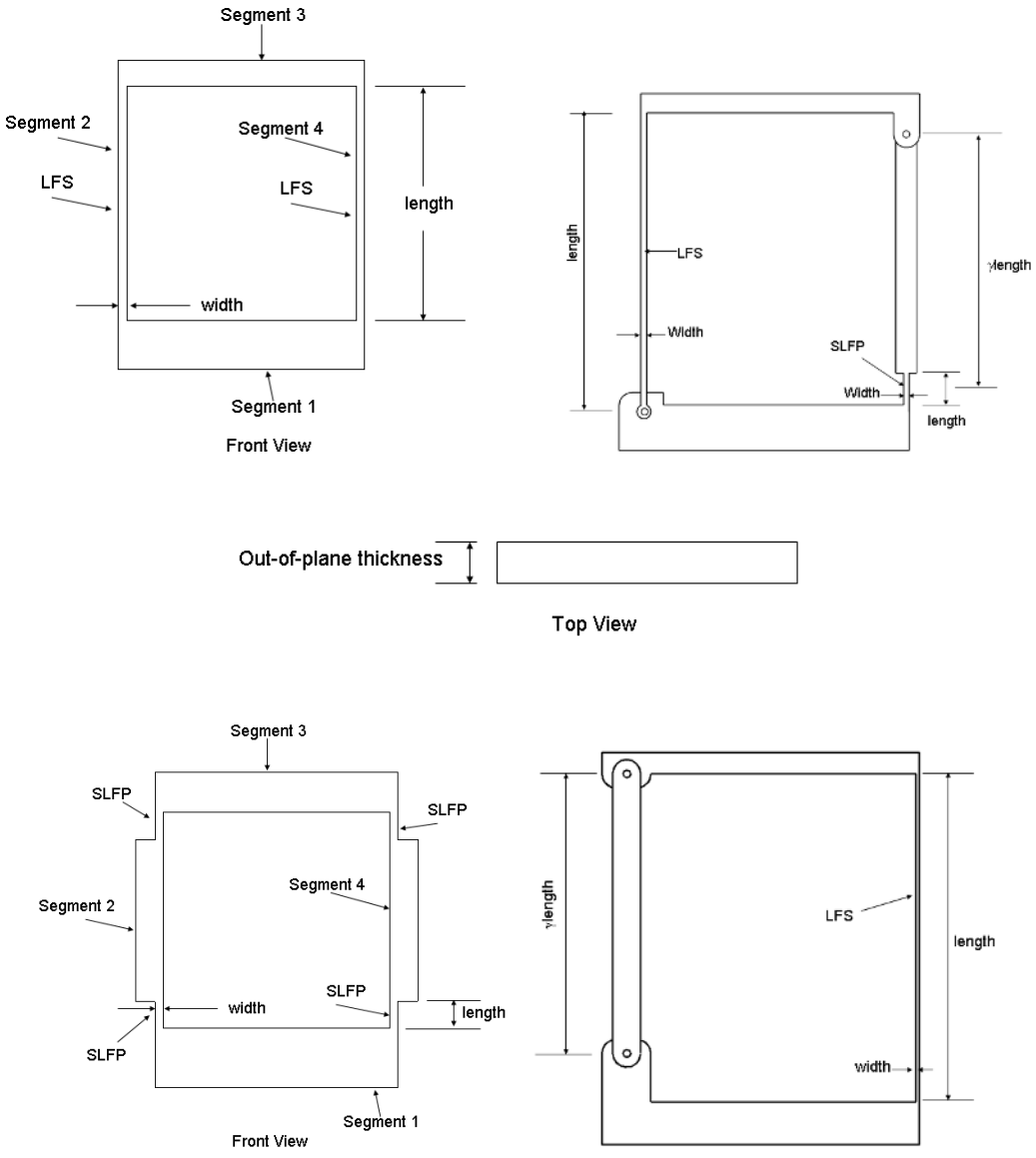

Figure 6.3: A description of the dimensions given in Table 6.1.

Table 6.1: Dimensions of the parallel mechanisms that were built and tested for dynamic response.

	A	B	C	D	A(Steel)
LFS length	118.6 mm	118.6 mm	–	118.6 mm	355.6 mm
LFS width	1.8 mm	2.2 mm	–	1.7 mm	0.89 mm
SLFP length	–	12.6 mm	7.9 mm	–	–
SLFP width	–	2.4 mm	0.86 mm	–	–
Out-of-plane thickness	6.35 mm	6.35 mm	6.35 mm	6.35 mm	31.5mm
Mass of segment 2	–	–	4.0 g	6.48 g	–
Mass of segment 3	11.0 g	11.3 g	12.25 g	11.05 g	375.1 g
Mass of segment 4	–	5.09 g	4.0 g	–	–

This simple model predicts that the mechanisms will respond with an oscillatory motion. Although the model does not include the damping, one would predict a small amount of damping in the actual system. If the damping is small, it should not affect the resonance frequencies of the mechanisms. If, however, the damping is large, then there will be a shift in frequency. Each of the mechanisms was tested five times in order to provide a reliable average resonance frequency. Most of the frequency data came from measuring the output of an accelerometer attached to the coupler of the parallel mechanisms.

The configurations of Parallel A, Parallel A(Strobe), Parallel A(Steel) are all the same type of mechanism. The difference between Parallel A, and Parallel A(Strobe) comes from the method of measuring the natural frequency. In the case of Parallel A, the natural frequency was measured using an accelerometer that added mass to the coupler of the mechanism. The Parallel A(Strobe) did not need any additional mass added for measurement. In the case of Parallel A(Steel) the difference is in both the size and the material properties. The Steel configuration was made from flexible segments made of spring steel. With Aluminium rigid segments. Figure 6.4 shows a photograph of the Parallel A(Steel) Mechanism.

Figure 6.4: Photograph of the Parallel A(Steel) configuration of the mechanism.

6.1.2 Experimental Results

The mechanisms were tested and the damped resonance frequency measured. Results for all of the mechanisms (with the exception of Parallel A(Steel), and Parallel A(Strobe)) were taken for a period of 1.024 seconds, allowing a resolution of 0.98 Hz in the frequency band or a possible error measurement error of ± 0.49 Hz. For Parallel A(Steel), a longer time period could be measured because of the very low damping in the system. For Parallel A(Strobe) the measurement system is different, and required tuning the strobe. Five sets of data were taken and averaged in order to determine the resonance frequency of each of the mechanisms. The parallel mechanisms were mounted to a stationary platform, and deflected to an initial deflection and then released. The resulting oscillatory motion was captured using a standard system for measuring the output of the accelerometer mounted on the coupler of the mechanism. Table 6.2 shows the results of the tests that were conducted. As can be easily seen from Table 6.2, the value of the damping ratio is small. This means that the measured

Table 6.2: Resonance Frequencies for Parallel Mechanisms

Mechanism	Measured Damped Resonance Frequency(Hz)	Modeled Undamped Resonance Frequency(Hz)	Percent error	Approximate Damping Ratio (Based on Measured Data)
Parallel A	14.6	14.2	2.7	0.032
Parallel A (strobe)	18.6	18.8	1.1	0.032
Parallel A (Steel)	3.2	3.0	6.3	0.01
Parallel B	14.7	13.8	6.0	0.057
Parallel C	5.9	5.7	3.4	0.10
Parallel D	8.3	7.6	8.0	0.085

damped resonance frequency of the measured structures will be essentially the same as the undamped resonance frequency in each of the cases. Thus, a direct comparison of the predicted and measured resonance frequencies is justified.

As the results demonstrate, there is less than nine percent error between the measurement and predicted results for these mechanisms. All but one of the mechanisms were constructed with polypropylene (the exception being Parallel A (Steel) where the flexible segments were made out of Steel). Parallel A and Parallel A (Strobe) are exactly the same type of mechanism. Parallel A was measured with an accelerometer placed on the end of the mechanism. The accelerometer had mass, which affected the resonance frequency. Note also that the Parallel A configuration has the smallest value for damping. The majority of the friction in the Parallel A (Steel) configuration was due to air, while the plastic version of that mechanism had some added damping that comes from the properties of the plastic. The Parallel B and D configurations both had pin joints that somewhat increased the damping. Overall, the PRBM was able to predict the resonance frequency of each of the mechanisms.

Parallel A (Steel) was modeled with FEA in order to ensure that the FEA matched the physical predictions. This provides a validation for the FEA model, and shows that the experimental and the FEA are matching. The results of the FEA predicted a resonance frequency of 2.96 Hz, the PRBM predicted 3.0 Hz, and the

Table 6.3: Resonance Frequency Comparisons Hoeken Mechanism

Mechanism	Measured Damped Resonance Frequency(Hz)	Modeled Undamped Resonance Frequency(Hz)	Percent error	Approximate Damping Ratio (Based on Measured Data)
Hoeken A	16.6	16.7	0.6	0.085
Hoeken B	6.7	6.2	7.5	0.124

measured frequency was 3.2 Hz. This is a reasonable margin of error between the three methods.

6.2 Hoeken Straight-Line Mechanism

The Hoeken straight-line mechanism is provided as a second example. The link lengths are given in general form as $r_1 = 2r_2$, $r_3 = 2.5r_2$, $r_4 = 2.5r_2$, and $a = 5r_2$. In this case, $r_2 = 2.7$ cm. An illustration of the PRBM of a Hoeken mechanism is given in Figure 6.5. In order to demonstrate the versatility of the PRBM, the resonance frequency predictions for the Hoeken straight-line mechanism were made using a commercial package made for kinematic analysis of mechanisms (Working Model IID Student edition 4.1). Commercial kinematic software is not designed to be used for compliant mechanisms, however by using the PRBM, the mechanism's path and dynamic behavior can be easily modeled using the previously existing kinematics packages and equations. The resonance frequency of the mechanism was excited and measured using an experimental setup similar to the parallel mechanisms setup.

The Hoeken straight-line mechanisms were constructed of polypropylene (Young's modulus 1.38 x 10^9 Pa), including mechanisms of type Hoeken A and Hoeken B as shown in Figure 6.7. The small-length flexural pivots (SLFP) for Hoeken A each had a length of 0.635 cm, width of 0.13 cm, and an out-of-plane thickness of 0.635 cm as defined in Figure 6.6. The long flexible segments (LFS) for the Hoeken B mechanism each had widths of 0.114 cm and an out-of-plane thickness of 0.635 cm, and their lengths were 3.2 cm for the shorter segment, and 8.1 cm for the longer segment.

Table 6.4: Dimensions Hoeken A

Dimension	Value	Unit
a	0.635	cm
b	8.84	cm
c	9.00	cm
d	1.16	cm
e	2.49	cm
f	2.38	cm
g	0.688	cm
h	19.84	cm
j	1.59	cm
theta	46	degrees

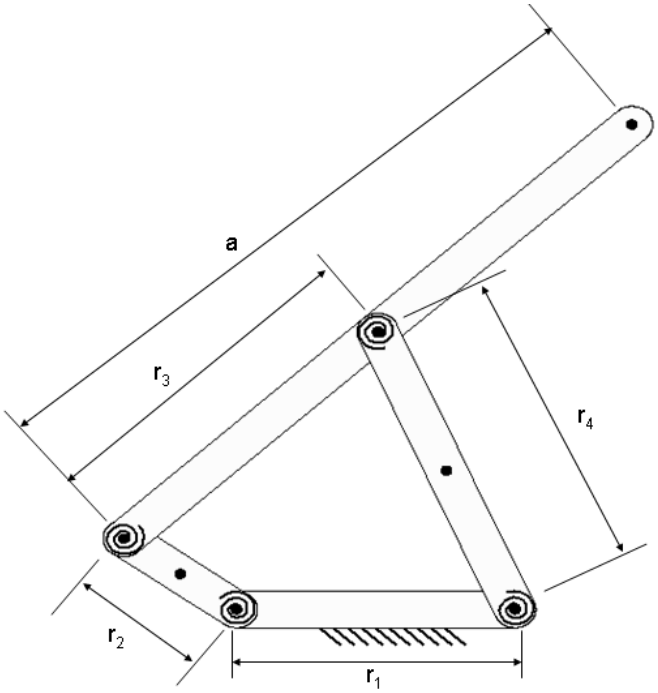

Figure 6.5: A depiction of the PRBM for each of the Hoeken straight line mechanisms.

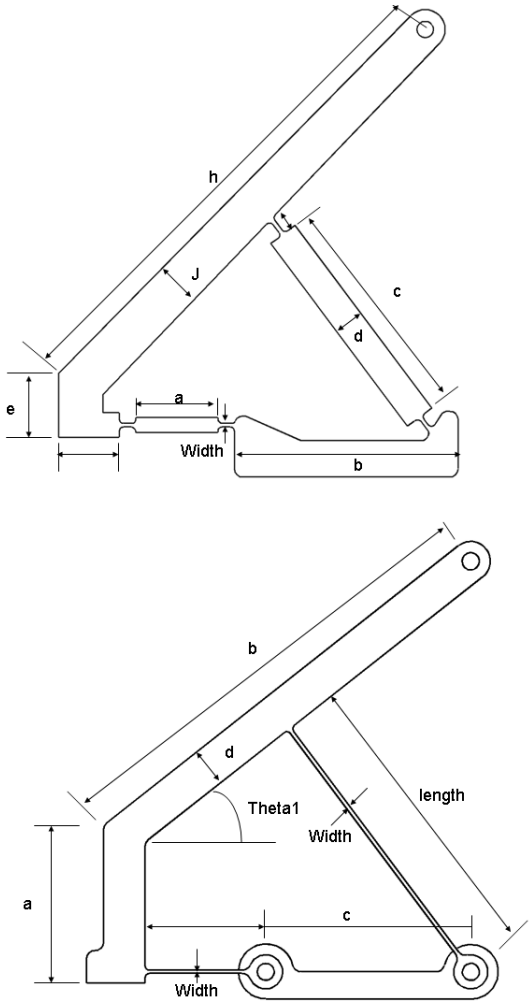

Figure 6.6: A depiction of the PRBM for each of the Hoeken straight line mechanisms.

Table 6.5: Dimensions Hoeken B

Dimension	Value	Unit
a	4.14	cm
b	11.88	cm
c	5.508	cm
d	1.062	cm
theta	40	degrees

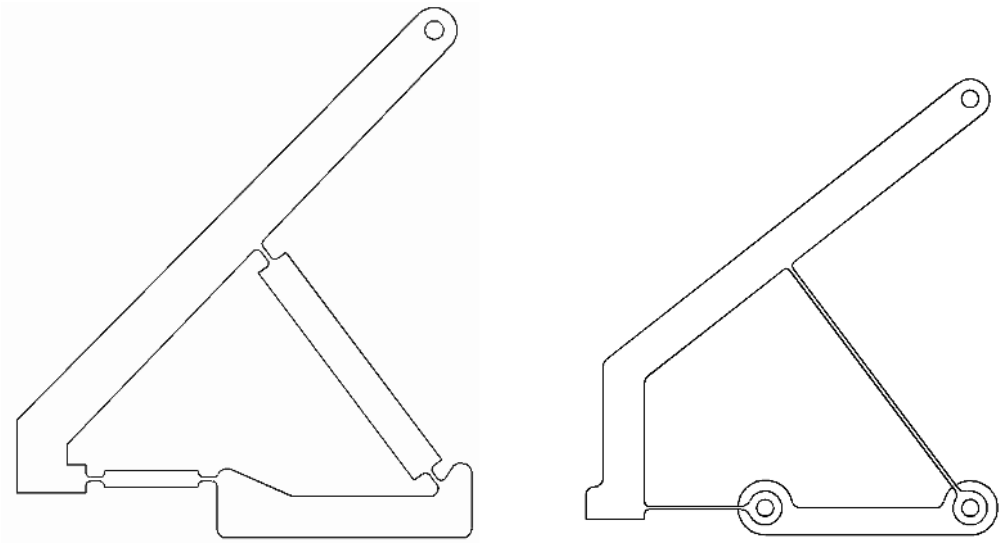

Figure 6.7: A depiction the Hoeken straight line mechanisms tested.

All other dimensions are given in Tables 6.5 and 6.4 with Figure 6.6 illustrating the dimensions. The mechanisms were all measured with the same experimental setup as was used for the parallel mechanisms. The mass of the coupler links are approximately the same at 2 grams, with an accelerometer placed on the tip with a mass of 3 grams. The accelerometer is the dominant mass in the system.

Table 6.3 shows the resonance frequencies that were measured and the predictions. Again the predictions are within 10% of measured resonance frequencies.

6.3 Young Mechanism

Bistable mechanisms have received attention from various researchers [11, 12, 53, 54, 55] over the past few years. Bistable mechanisms are valuable in many low-power situations because power is only required to change the state of the mechanisms, and not to hold the mechanism in either state.

Since a bistable mechanism is often used as a switch, it is important to understand its dynamics in order to know how fast a mechanism can be switched. The switching speed depends on the type of mechanism that was used, how it is actuated,

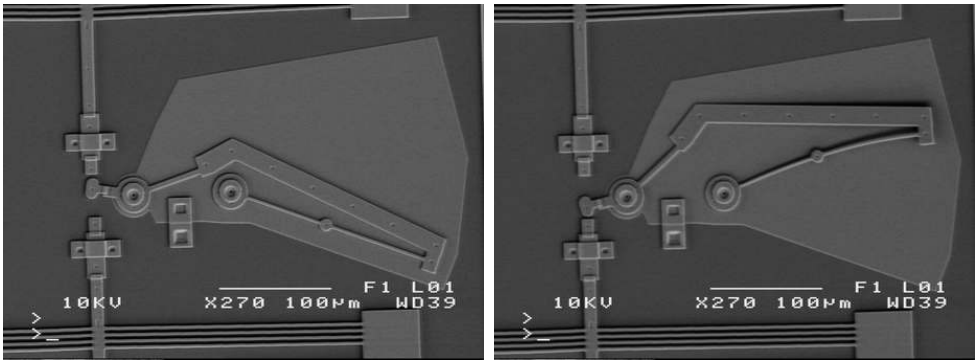

Figure 6.8: Scanning Electron Microscope images of a Young mechanism in both stable positions.

and the design and materials that were used in construction. The goal for this work is not to evaluate every possible mechanism, but to provide a good understanding of how well the PRBM is able to predict the transient response of compliant mechanisms. Development of a modeling technique will increase the ability of the designer to look at the requirements and choose designs that improve the dynamic response. Although much of this work is of interest because of the expanding area of MEMS, there are many reasons for understanding the dynamics of larger devices as well.

The Young mechanism (named because it was developed at Brigham Young University) is a four-bar equivalent mechanism. The Young mechanism is designed in such a way that it has two pin joints to ground and two floating pin joints. The two pin joints to ground remain traditional pin joints, and the two floating pin joints are replaced by flexible segments. Figure 6.8 shows a Scanning Electron Microscope image of the micro version of the Young mechanism in both stable positions, and Figure 6.9 shows a macro version of this same mechanism that was built and tested.

6.3.1 Experimental Setup

Several Young mechanisms were built and tested to determine the response and the behavior of the mechanisms. They were constructed out of polypropylene and tested using a rotary optical encoder. There were five mechanisms created out

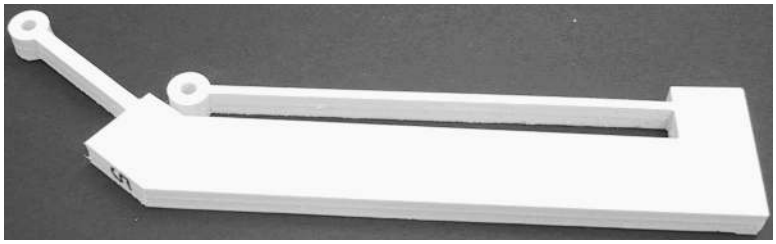

Figure 6.9: Number 5 test specimen for testing the dynamics of macro compliant mechanisms.

of quarter-inch polypropylene, and five out of half-inch polypropylene. They were all machined on the same CNC Machine with the same end mill and the same settings. Table 6.6 lists the geometry and relative masses of the machined test mechanisms. Figure 6.10 shows the mechanism dimensions. The devices were tested in a random order, with the same computer used for all of the tests. Each mechanism was tested five times. Since the software was not designed to sample at a given frequency, the results were sampled as fast as the computer could sample. The data sets were then digitally re-sampled and the results were broken up into two portions. Each portion corresponded to a stable position of the mechanism. The data sets were then taken through a Fast-Fourier-Transform (FFT) in order to determine the frequency of oscillation about the stable position. Figure 6.9 is a photograph of one of the Young mechanisms used in the study.

6.3.2 Results

Table 6.7 shows the measured resonance frequencies. The manufactured position of the Young mechanism provides an interesting point of comparison (the manufactured positions is shown in Figure 6.8 on the left). Because of the design of the Young mechanism that was used in this test, the mechanism is unable to physically travel past the manufactured position. This is simply due to the link lengths that have been specified by the design of the mechanism. The effects can also be seen in the measured dynamic response such as is shown in Figure 6.11 (first stable equilibrium

Table 6.6: Young Mechanism Specifications

Parameter	Value	Unit
Radius of Gyration (Coupler)	7.567	cm
Mass (Link 2, half-inch)	0.45	grams
Mass (Coupler, half-inch)	10.5	grams
Mass (Link 4, half-inch)	0.71	grams
Mass (Link 2, quarter-inch)	0.22	grams
Mass (Coupler, quarter-inch)	5.25	grams
Mass (Link 4, quarter-inch)	0.36	grams
Spring Constant (Link 2, half-inch)	122.9e6	dyne× cm
Spring Constant (Link 4, half-inch)	79.42e6	dyne× cm
Spring Constant (Link 2, quarter-inch)	61.45e6	dyne× cm
Spring Constant (Link 4, quarter-inch)	39.71e6	dyne× cm
Link Length 1	7.62	cm
Link Length 2	5.53	cm
Link Length 3	18.84	cm
Link Length 4	16.07	cm
Flexible Segment Length 2 (LFS)	6.525	cm
Flexible Segment Length 4 (LFS)	18.96	cm
Flexible Segment Width 2	0.594	cm
Flexible Segment Width 4	0.324	cm
Out-of-Plane Thickness, half-inch	1.27	cm
Out-of-Plane Thickness, quarter-inch	0.64	cm
Young's Modulus	$1.38\ x\ 10^9$	Pa

Table 6.7: Young Mechanism Resonance Frequencies about Stable Positions

Size	Measured Damped Resonance Frequency(Hz)	Upper Limit (95%)	Lower Limit (95%)
Quarter-inch (Stable Position 1)	8.41	8.51	8.32
Quarter-inch (Stable Position 2)	8.49	8.57	8.41
Half-inch (Stable Position 1)	8.93	9.0	8.86
Half-inch (Stable Position 2)	9.01	9.08	8.94

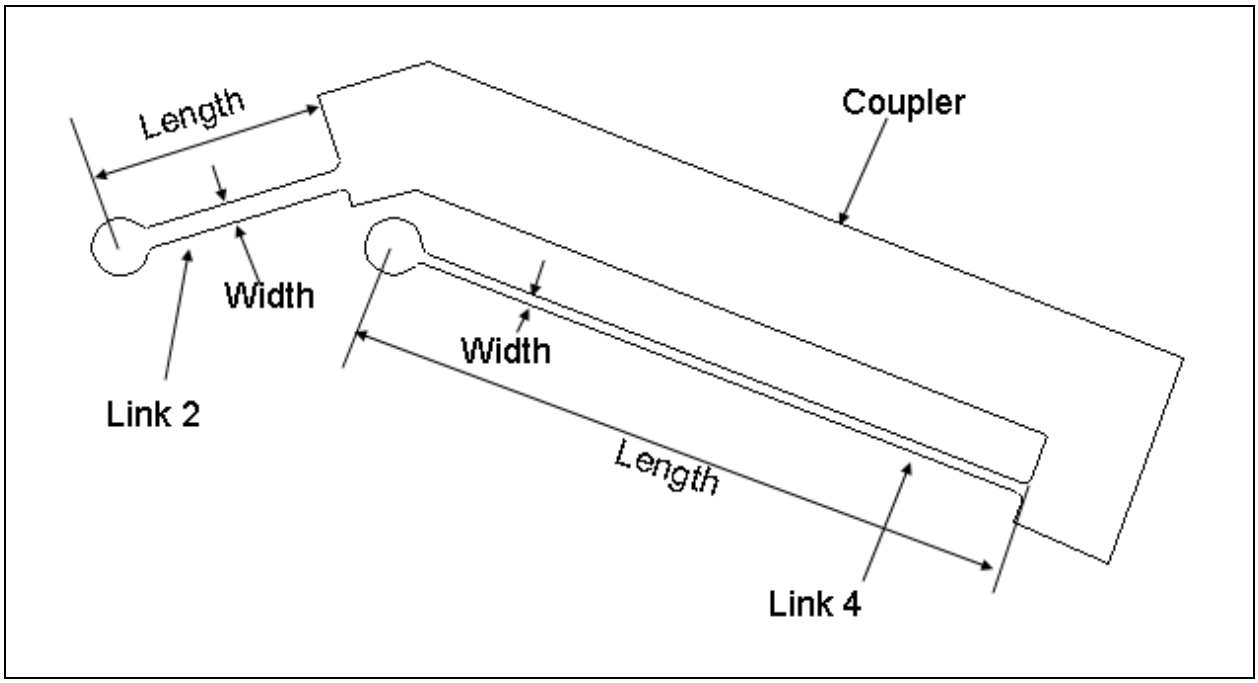

Figure 6.10: Graphical description of the young mechanism dimensions.

position) and Figure 6.12 (second stable equilibrium position). Note that the lower portion of the dynamic response is not symmetric about the manufactured position. Although the flexible system is able to travel beyond the manufactured position, the general behavior of the mechanism is different outside of the viable range for the four-bar mechanism.

Several sets of the frequency plots resulting from the FFT of the measured data are shown in Figures 6.13-6.15. Each of the figures represent data from a different test run, and a different test mechanism. They are referred to respectively as set A,B, and C. They show a sampling of the results from the mechanisms that were tested. They each show the peak that is produced from the resonance frequency of the mechanism.

In order to continue modelling this mechanism as a traditional four-bar, the momentum must be transferred into the axial stiffness of the rigid links in the four-bar model. The Young mechanism provides a good example of an implied constraint on

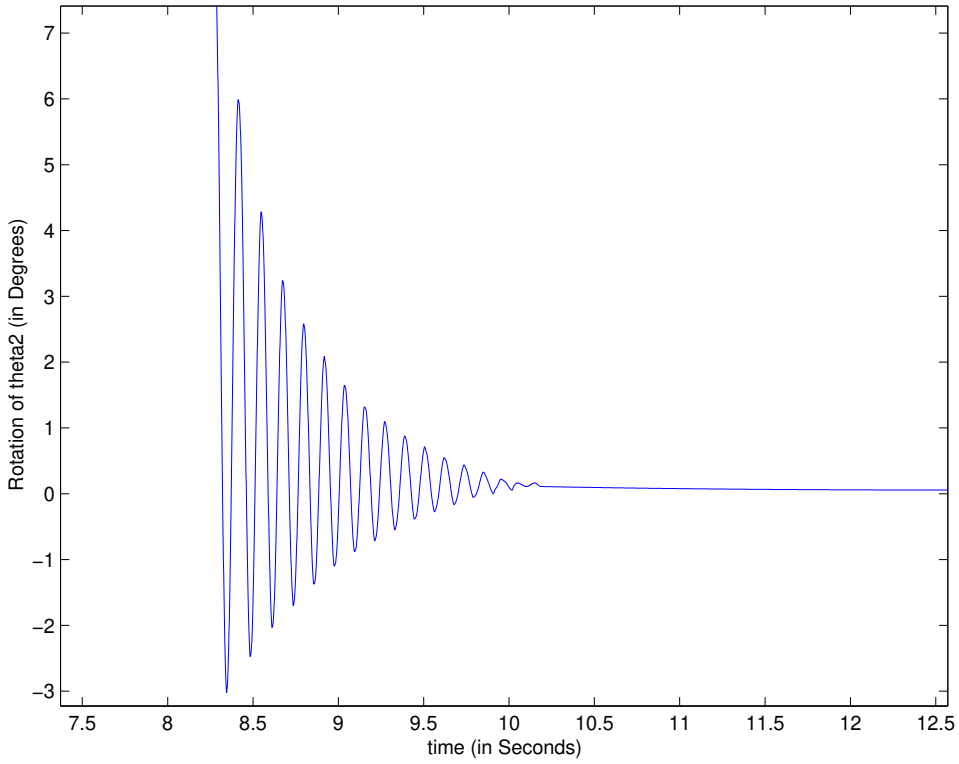

Figure 6.11: The measured transient response of the Young mechanism around the manufactured stable position.

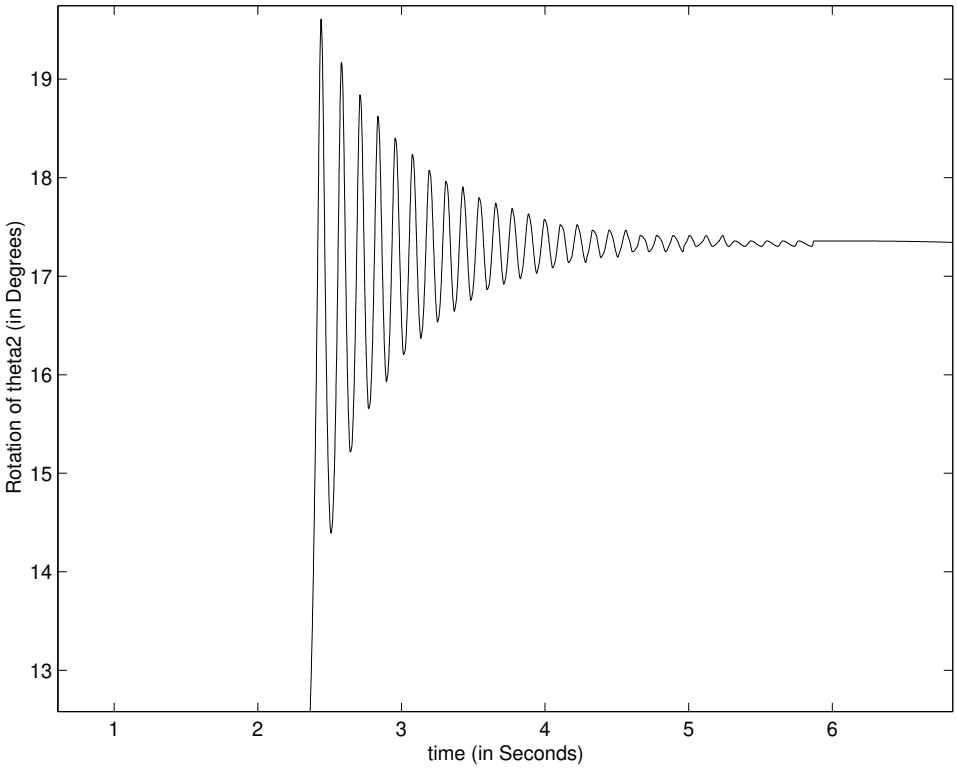

Figure 6.12: The measured transient response of the young mechanism around the second stable position.

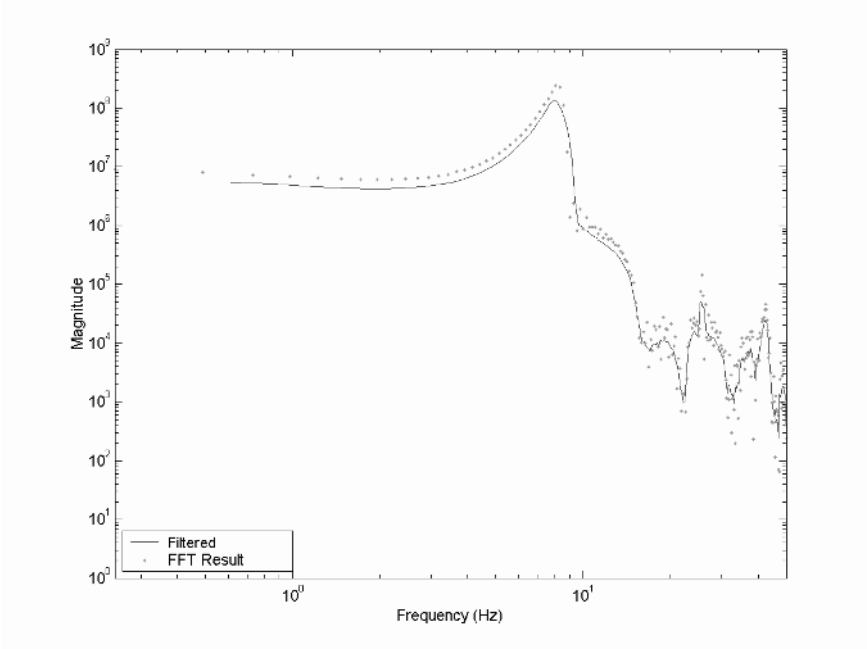

Figure 6.13: Plot showing the resulting frequency plot from the FFT of set A of the measured data from the Young mechanisms.

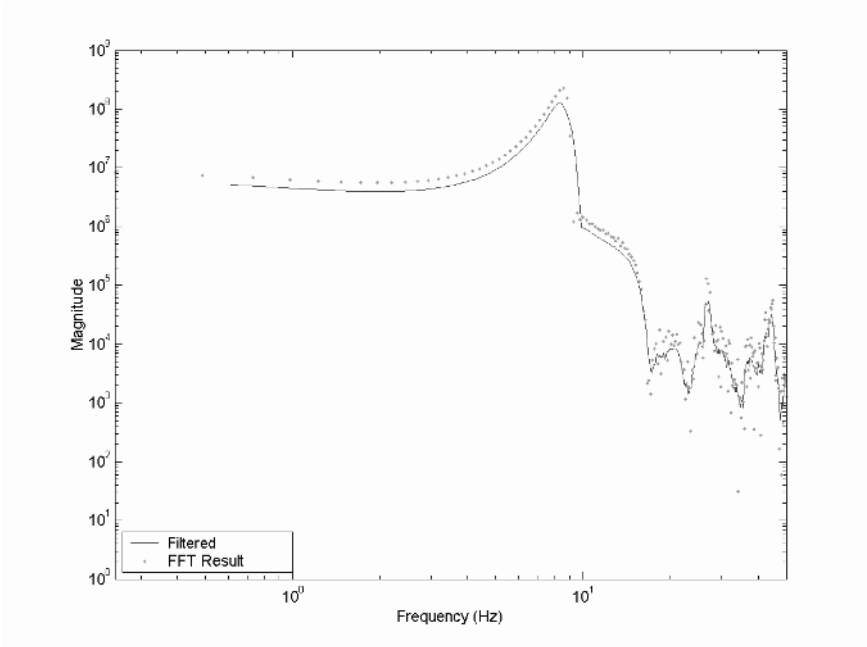

Figure 6.14: Plot showing the resulting frequency plot from the FFT of set B of the measured data from the Young mechanisms.

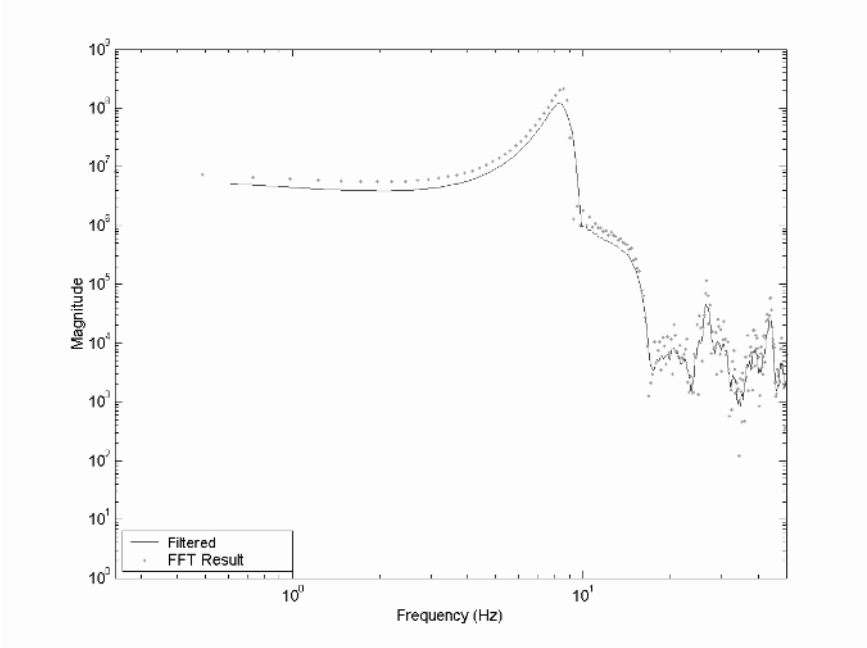

Figure 6.15: Plot showing the resulting frequency plot from the FFT of set C of the measured data from the Young mechanisms.

the ability of the PRBM to predict the dynamic behavior of compliant mechanisms, that is the model must be valid over the entire range of motion to accurately describe the path and dynamics of the system. This mechanism also shows that the behavior around a linkage discontinuity is not exactly the same as the behavior would be if the mechanisms were completely rigid. The result is suggests that discontinuous points should be avoided. By defining the potential energy around the useful areas of the mechanism, and by increasing the value of the potential energy just beyond the end of the travel of the mechanism, the resonance frequencies can be examined, and compared to the PRBM. The exact model used is given in Appendix B.2. The potential energy and the modified potential energy are shown in Figures 6.16 and 6.17. The only difference is that the potential energy is defined at the lower values of the angle. With the a sharp increase in potential energy starting just prior to the undefined location, this will have a mild influence on the dynamic behavior; however, it represents a good approximation of the physical constraints in the system.

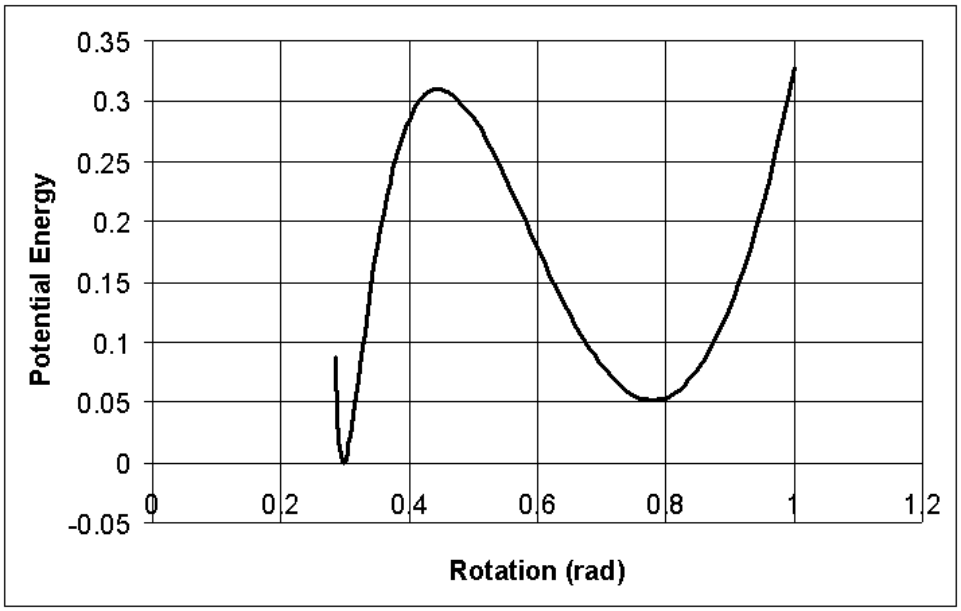

Figure 6.16: Unmodified Potential Energy.

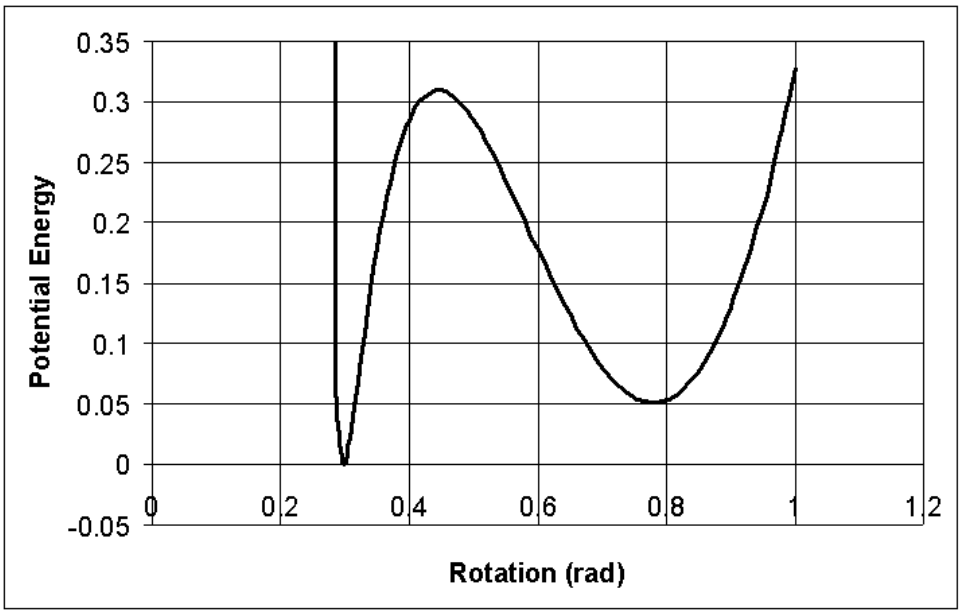

Figure 6.17: Modified Potential Energy

The PRBM of the Young mechanism is strongly influenced by the initial conditions of the mechanism. There are two reasons for this dependence. The first is related to the geometry that is used in the mechanism. Figure 6.18 shows the nonlinear behavior of θ_3 and θ_4 with respect to the change in θ_2. The figure also suggests that there will be more significant effects around the manufactured position of the mechanism than around the second stable position. This is due to the large change in the derivative of θ_3 and θ_4 with respect to θ_2. At first the derivative is very large, and then it gradually decreases as the mechanism moves further. Because the angles change in a nonlinear fashion, the equations of motion that result are nonlinear. According to Figure 6.18, the effects around the second stable position should not be as dominate as the effects around the manufactured position. This can be seen in Table 6.8. The results that are tabulated are based on the model that was presented in Chapter 5 in Section 5.1. The model is the generalized model for the dynamic behavior of a four-bar mechanism. The factors that affect this particular model (r_1, r_2, r_3, K_1, K_2, etc.) were adjusted to match the characteristics of the Young mechanism as described in this section. The complete mathematical model that was used is included in the Appendix (Section B.2).

The second effect that causes the initial conditions to play a significant role in the dynamic behavior comes from the combination of the rotations (discussed previously) and the large coupler inertia. The parallel mechanisms do not allow for rotation of the coupler. The Young mechanism, however, depends on rotation of the coupler as part of its motion. For the Young mechanisms tested, the large link has a significant rotational inertia, and must rotate during motion. Neither of these problems caused difficulties for the PRBM. They did define a range of resonance frequencies where the mechanisms would resonance depending on the initial conditions. The results are contained in Table 6.8. The span of results clearly covers the measured data. The PRBM can predict the first modal frequency of the mechanism.

In order to compare equivalent systems, the Young mechanism was modeled using FEA. Again, as with previous models, beam elements were used to define the the mechanism. Both PRBM and FEA models were given a similar initial condition of

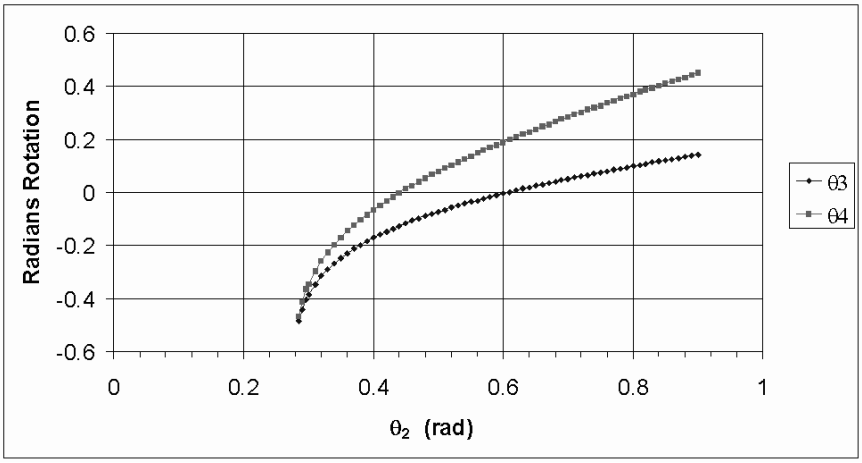

Figure 6.18: A comparison of the relative change in the rotational angles of the large inertia, and the input angles. The graphic shows why the mechanism exhibits nonlinear behavior.

Table 6.8: Young Mechanism Resonance Frequencies about the Manufactured Stable Position as Predicted by the PRBM

initial $\Delta\theta_2$ from the Stable Position (rad)	PRBM Resonance Frequency(Hz)	Resolution
0.053	14.9	$\pm$0.25
0.12	9.1	$\pm$0.25

Table 6.9: Young Mechanism Resonance Frequencies about the Second Stable Position as Predicted by the PRBM

initial $\Delta\theta_2$ from the Stable Position (rad)	PRBM Resonance Frequency(Hz)	Resolution
0.327	5.0	$\pm$0.25
0.277	7.9	$\pm$0.25
0.227	9.1	$\pm$0.25
0.177	9.8	$\pm$0.25
0.127	10.25	$\pm$0.25
0.077	10.8	$\pm$0.25
0.027	10.8	$\pm$0.25

$\Delta\theta_2 = 0.11$ and the resulting resonance frequencies were obtained and are contained in Table 6.10. The results the FEA prediction and the PRBM prediction are within ten percent of each other.

Table 6.10: Young Mechanism Resonance Frequencies about the First Stable Equilibrium Position

FEA Resonance Frequency(Hz)	PRBM Resonance Frequency(Hz)	Percent Difference
8.42 $\pm$0.167	9.05 $\pm$0.25	7.5 percent

6.3.3 Fixed-Fixed Flexible Segments

The cross-axis flexural pivot provides a good example of a mechanism that could not be easily modeled without the use of the fixed-fixed model developed in

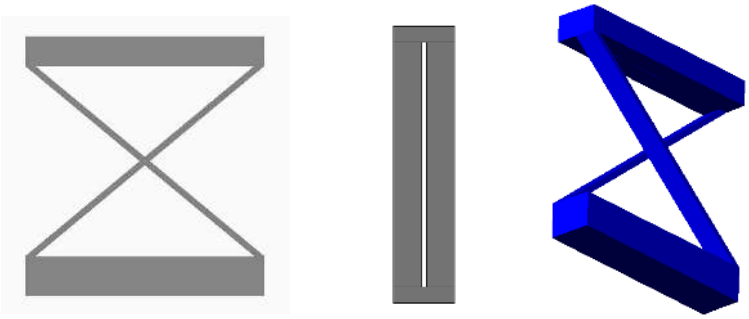

a) Front View b) Side View c) Isometric View

Figure 6.19: Representation of a cross axis flexural pivot. The a) frontal, b) side, and c) isometric views are included.

Table 6.11: Flexible Beam Geometry and Material Properties

Property	Value	Unit	Value	Unit
Modulus of Elasticity	$30x10^6$	psi	206.8	GPa
density-beam	0.28	lb/in^3	7.8	g/cm^3
out-of-plane thickness (everything)	1.25	in	3.18	cm
width (flexible segments)	0.03125	in	0.0794	cm
Poisons Ratio	0.3	-	0.3	-
flexible segment length	33.9	in	86.2	cm

previous chapters. An illustration of the cross-axis flexural pivot is shown in Figure 6.19. This section discusses a cross-axis flexural pivot design with varying masses. Finite element analysis (FEA) was performed using the same beam elements as in the previous models. Table 6.11 lists the specific dimensions and material properties of the various models analyzed. The PRBM of the cross-axis flexural pivot is shown in Figure 6.20. The coupler size and mass were varied, but all of the other parameters listed in Table 6.11 were identical across the models. The width and length terms are shown in Figure 6.21. The height of the rigid segment was changed based on the flexible segment. The height was changed between twice as much and twenty times as much as the width of the flexible segments. The mechanism was then deflected in steps to an x deflection of 16 inches (40.64 cm), and released. The models were

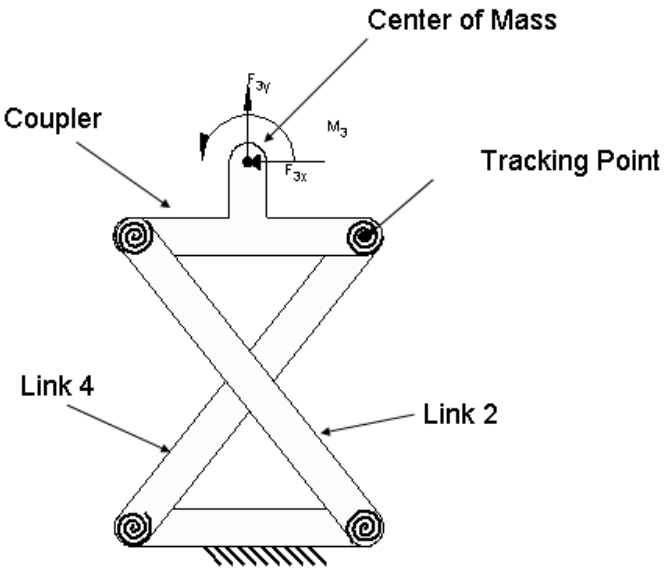

Figure 6.20: Figure showing the PRBM dimensions of the cross axis flexural pivot.

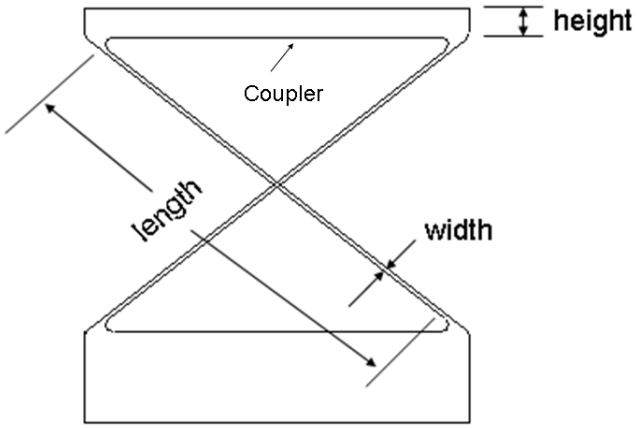

Figure 6.21: Figure showing the dimensions of the cross axis flexural pivot.

run for a period of twenty seconds and the results were obtained by taking an FFT, as was done with the other FEA models. The resulting frequencies listed in Table 6.12 were compared with the frequencies that resulted from the fixed-fixed PRBM. The initial angle of the link in the PRBM was rotated -64.2 degrees (-1.21 radians) rotation to provide the same deflection as was used in the FEA model.

The results are based on the model that was presented in Chapter 5 in Section 5.1 (the generalized model for the dynamic behavior of a four-bar mechanism). The factors that affect this particular model ($r_1,\ r_2,\ r_3, K_1,\ K_2,$ etc.) were adjusted to match the characteristics of the cross-axis flexural pivot as described in this section. The complete mathematical model is similar to the one presented for the Young mechanism, (Appendix Section B.2).

The relative mass number, ρ_m, is the equivalent mass of the of the upper beam. A relative mass number of 2 means that the mass of the beam is twice the mass of a steel beam with the same length as the coupler (in this case 24 inches, or 60.96 cm). Giving a mass of 0.373 lbm or 0.169 kg for a beam of $\rho_m = 2$. The first coupler has a mass equivalent to the sum of the masses of both the flexible segments. The results are not as accurate as the results obtained from previous models. The results shown in Table 6.12 have the trend that would be expected from varying the mass of the coupler. As the mass of the coupler is increased the accuracy of the model also increases, for the reasons presented earlier. The larger masses tend to have a better performance because they create loading conditions that are better simulated by the PRBM. The FEA data is less accurate at the largest masses due to a decrease in accuracy of the FFT, because the FEA model was only simulated for a 20-second period of time.

6.3.4 Modal Frequency of the Cross-Axis Flexural Pivot

The determining factor for how well a compliant mechanism will compare to the modal frequency is determined by the extent of the nonlinearities associated with the PRBM. If properly designed, the cross-axis flexural pivot is not very nonlinear. In this case the model is nonlinear, but due to the design, the path of the mass has a

nearly circular motion. The modal frequencies should therefore be a good prediction of both the PRBM, and nonlinear FEA results. Table 6.13 shows the tabulated modal data with the previous results. In this case it is obvious that the modal frequency is again the same as the frequency that was predicted by both the nonlinear FEA, and the PRBM. In this case, the nonlinearities in the system are not significant.

At this point it is important to ask what advantages the PRBM modeling technique provides over a modal frequency analysis. The modal frequency in most cases does provide an accurate result. The PRBM model gives a great deal more information than is provided by the modal frequency analysis. For the mechanisms that have been discussed in this work, the frequency of oscillation is used as a common parameter to compare the various models, and to show the ability of the models to predict that aspect of the dynamic behavior. The PRBM does, however, provide several additional information about the motion of the mechanism. In the case of the cross-axis flexural pivot, the behavior over time is produced, such as shown by Figure 6.22, where the FEA solution is compared to the PRBM solution. Note that the behavior is very similar. The PRBM allows for a completed deflection path of the mechanisms over time, where the modal frequency analysis will only provide a frequency of vibration, and small deflection results.

In addition the coupler angles are known from the PRBM model and shown with the other angles over time in Figure 6.23. This behavior is not available through a simple modal analysis. The rotation of the coupler can be analyzed and the deflection path of a system can be found. The rotation of the coupler in Figure 6.23 is θ_3. The PRBM allows the deflections, forces (and stresses), and path of the mechanism to be determined for a mechanism that is subjected to a large deflection. A modal frequency analysis cannot provide the same level of information.

6.4 Summary

In this chapter, several compliant mechanisms that fit within the scope of the PRBM were examined and the results compared to FEA and physical testing. The wide range of mechanisms that were tested allowed for each type of PRBM

Table 6.12: Cross-Axis Flexural Pivot Resonance Frequencies

Relative mass ρ_m	FEA Resonance Frequency(Hz)	PRBM Resonance Frequency(Hz)	Percent Difference
3	0.55	0.6	9
4	0.49	0.53	8.2
8	0.37	0.39	5.4
10	0.34	0.35	2.9
15	0.27	0.29	7.4
20	0.23	0.25	8.7

Table 6.13: Cross-Axis Flexural Pivot Resonance and Modal Frequencies

Relative mass ρ_m	FEA Resonance Frequency(Hz)	PRBM Resonance Frequency(Hz)	Modal Frequency
3	0.55	0.60	0.53
4	0.49	0.53	0.47
8	0.37	0.39	0.35
10	0.34	0.35	0.32
15	0.27	0.29	0.26
20	0.23	0.25	0.23

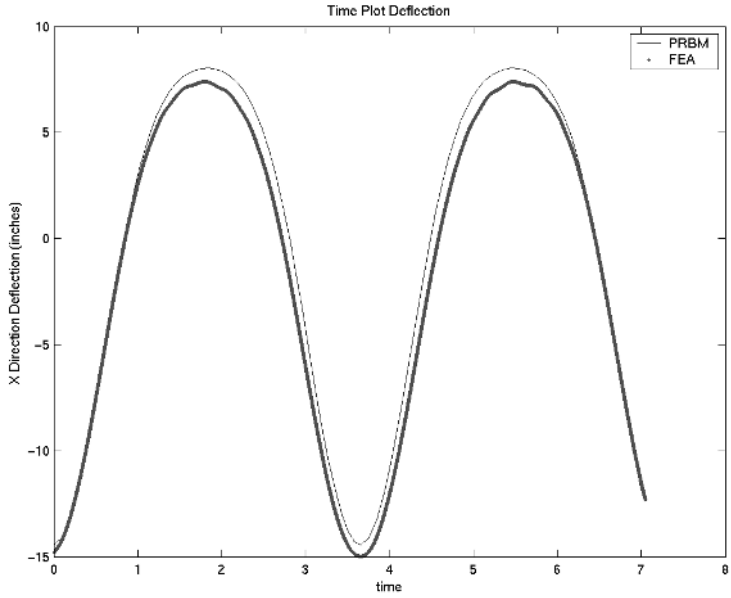

Figure 6.22: PRBM prediction of the path of the tracking point.

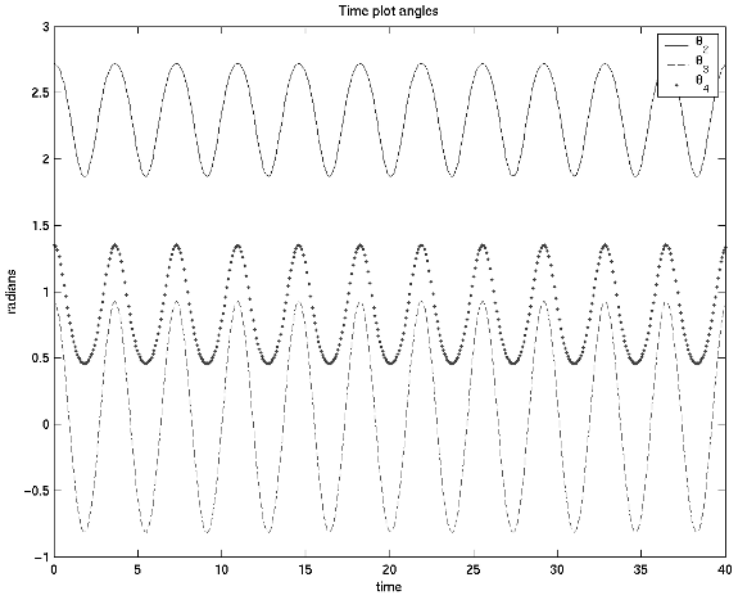

Figure 6.23: PRBM prediction of the rotations of the various links. θ_3 is the rotation of the coupler.

segment (discussed in Chapter 4) to be evaluated. In several cases, combinations of the differing segments were tested, which showed some of the versatility of the techniques. It is important to note that the dynamic behavior for all of the parallel mechanisms could be determined with a single dynamic model, allowing the designer to change joint types without the need for the development of a new model. In the case of the parallel mechanism, this allows twenty-eight [9] configurations of the mechanism to be modeled without significant changes in the dynamic model or the path of the mechanism.

The contributions that were made in this chapter come from demonstrating the use of the PRBM to exam the dynamic behavior of several compliant mechanisms. The predictions of the PRBM have been compared with alternative analytical methods and experimental results. This chapter suggests that the PRBM is a viable representation of the physical system, for use in compliant mechanism design.

Chapter 7

Micro Mechanisms

7.1 Important Effects of Scaling

One of the most appealing reasons to study micro mechanisms is the extreme change in the dynamic behavior that can come from the size change. Most engineers are aware of the effects of scaling in engineering systems. Quite often these effects can be significant and can provide problems with scaled prototypes. This section discusses the effects of significant reductions in the linear dimensions of compliant mechanisms.

Most of the dominant effects of scaling can be examined by using a very simple system, such as micro parallel mechanism. The parallel mechanism is one of the most frequently used micro mechanisms because of its simple design. It can also be made in a single layer, and thus can be produced at many fabrication facilities. A graphic depicting a generic folded beam structure which uses the parallel mechanism is shown in Figure 7.1 along with a parallel mechanism. The parallel mechanism makes a very useful example because it is easily produced, and the dynamic behavior has been discussed previously in this work.

All of the results depend on the changes that occur in the mass. If some general properties, lengths, and thicknesses are defined, then the mass of each section can be calculated. The specifications are shown in Figure 7.2. Note that all dimensions are given in terms of the variable L. The value of the coupler mass can be calculated as

$$M = (\frac{\rho L^3}{1000}). \tag{7.1}$$

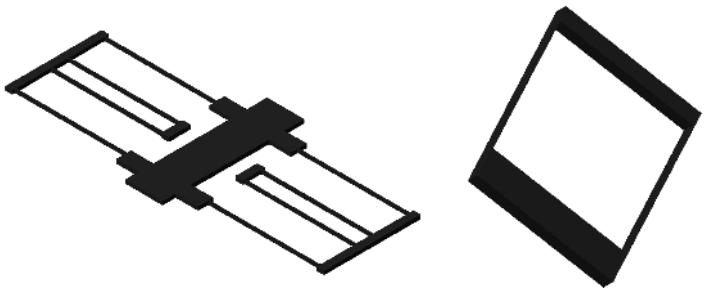

Figure 7.1: An isometric view of a folded beam structure which is a combination of several parallel mechanisms (Left), and a parallel mechanism (right).

The values of the masses for the flexible segments can also be calculated as

$$M_f = \frac{\rho L^3}{10000}\rho. \tag{7.2}$$

The value of the mass is directly proportional to the cube of the length. The interesting developments come from identifying the other parameters that are involved in the dynamic behavior, and then relating them back to the mass.

The spring constant for a fixed-guided mechanism is $K = \frac{2\gamma K_\Theta EI}{L}$ [13], where K is the torsional spring constant, γ is the characteristic radius factor, K_Θ is the stiffness coefficient, E is the Modulus of Elasticity, I is the area moment of inertia, and L is the length of the flexible segment. Using the relationships shown in Figure 7.2, the following equation can be derived for the value of the torsional spring stiffness:

$$K = \frac{2\gamma K_\Theta E \frac{L}{100} \times (\frac{L}{100})^3}{12L} = \frac{\gamma K_\Theta E L^3}{600,000,000} \tag{7.3}$$

The Pseudo-Rigid-Body Model(PRBM) of this mechanism has one degree of freedom and the dynamic equation of motion is

$$M(\gamma L)^2\ddot{\Theta} + 4K\Theta = 0, \tag{7.4}$$

where M is the mass of the shuttle, L is the length defined in Figure 7.2, Θ is the PRBM angle, and K is the torsional spring constant for a single fixed-guided segment. This is the same as Equation (5.35) except that the mass of the flexible segments was set to zero and, since the stiffness of each torsional spring is the same, they were also

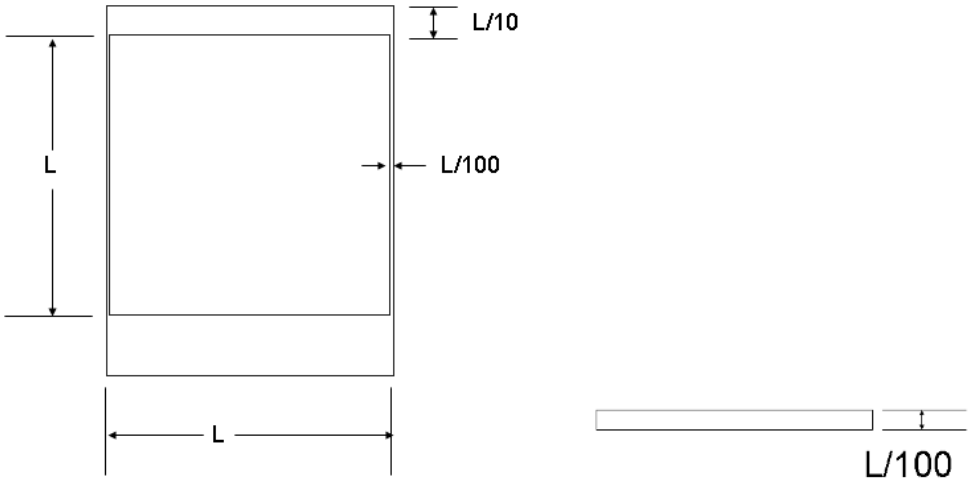

Figure 7.2: A top view and front view of a parallel mechanism with basic size relationships.

lumped into a single parameter K with a factor of 4 to account for the four springs. The natural frequency is $\omega_n = \sqrt{\frac{4K}{M(\gamma L)^2}}$. Substituting the values previously defined for K and M the value of the frequency yields

$$\omega_n = \frac{1}{L}\sqrt{\frac{K_\Theta E}{150,000\rho\gamma}} = \frac{C}{L}, \tag{7.5}$$

where C is constant if the material is not changed. The equation shows that as the length is decreased the resonance frequency of the system increases proportionally. The resonance frequency for a nonlinear dynamic equation of motion would have a similar change in resonance frequency. This effect is due to the quadratic increase in the ratio of the spring constants to the mass contained in the system.

The important concepts of dynamics of compliant mechanisms that has been discussed, is that the stiffness to mass ratio will increase as the size decreases. This implies that the spring forces will tend to have a large impact on the systems, and in turn will dominate the behavior of the mechanism. This is important as actuators are introduced into the systems, since it suggests that the actuator can be sized based on the springs and that the mass of the mechanism will typically not play a significant role.

7.2 Micro Cantilever Beams

The previous section illustrated the behavior of micro mechanisms, but these effects have been demonstrated in an actual physical system. Hosaka et al. [56] presents measurements of the dynamic behavior of a cantilever beam. The cantilever beam was scaled in the same fashion as the mechanism presented earlier, in that each linear dimension of the beam was scaled proportional to the length of the beam.

Although the majority of the research presented in this dissertation is compared to finite element analysis (FEA), the results of the cantilever beams were compared to measurements published in [56]. The authors discuss energy dissipation modes in mechanical systems, and present plots of two cantilever beams. The authors do not attempt to model the dynamic behavior of the beams since their focus is on the dissipation effects in the system. The results that they provide show resonance frequencies of 750 Hz and 750,000 Hz for beam lengths of 10^{-2} m and 10^{-5} m respectively. The height and width were defined by the length of the beam. The width was the length of the beam divided by 10 and the height was the length of the beam divided by 100. The beam was constructed of bulk permalloy, with material properties defined as density $\rho_b = 8600\frac{\text{kg}}{\text{m}^3}$ and $E = 186$ GPa. Using these dimensions and material properties the resonance frequency predicted by the PRBM can be easily calculated. The PRBM predictions were obtained using the same dynamic model that was presented earlier in this work, and were calculated as 710 Hz and 710,000 Hz. Note that they are related linearly with respect to the length as was predicted from the results discussed in the previous section. The predictions of the PRBM are about five percent lower than the measured results in [56]. The predictions from the FEA result in frequencies of 763 ± 25 Hz and $763,000 \pm 25,000$ Hz. The measured data is between the FEA prediction and the PRBM prediction, exactly as was the case for the macro beams.

Although this section did not add any new research, the discussion has shown that the predictions of both FEA and PRBM models are matching results that have measured on the micro scale. This provides additional confidence in using both FEA, and the PRBM to model micro mechanisms.

Table 7.1: Comparisons of Resonance Frequencies for Parallel Mechanism

Length (micron)	PRBM Resonance Frequency Prediction(Hz)	FEA Resonance Frequency Prediction(Hz)	Percent Difference
350	18,017	16,800 (80% deflection)	7.2
3,500	1,801.7	1,680 (80% deflection)	7.2
35,000	180.17	168 (80% deflection)	7.2
350	18,017	17,000 (50% deflection)	6.0
3,500	1,801.7	1,700 (50% deflection)	6.0
35,000	180.17	170 (50% deflection)	6.0

7.3 Micro Compliant Parallel Mechanism Dynamic Response

This section will take the parallel mechanism that was presented in Section 7.1 and compare the PRBM results with FEA results for various lengths. The dimensions given in Figure 7.2 were used for both the PRBM and FEA. Three lengths were compared in order to show the change in frequency that is caused by a decrease in the size of the mechanism. The deflection is based on the length of the flexible segments. Two levels of deflection were examined: 80% and 50% deflection. An 80% deflection means that the coupler was deflected horizontally by 80% percent of the length, or for 50%, the coupler was deflected by half of the length. The lengths that were chosen and the predicted resonance frequencies are listed in Table 7.1. The properties used for the model were that of polysilicon (Young Modulus 179×10^9 Pa and Density 2,330 Kg/m^3). The FEA model was based on beam elements, as were the previous models.

As expected, the FEA and the PRBM are within less than ten percent of each other. The PRBM calculations are based on the equations that were presented

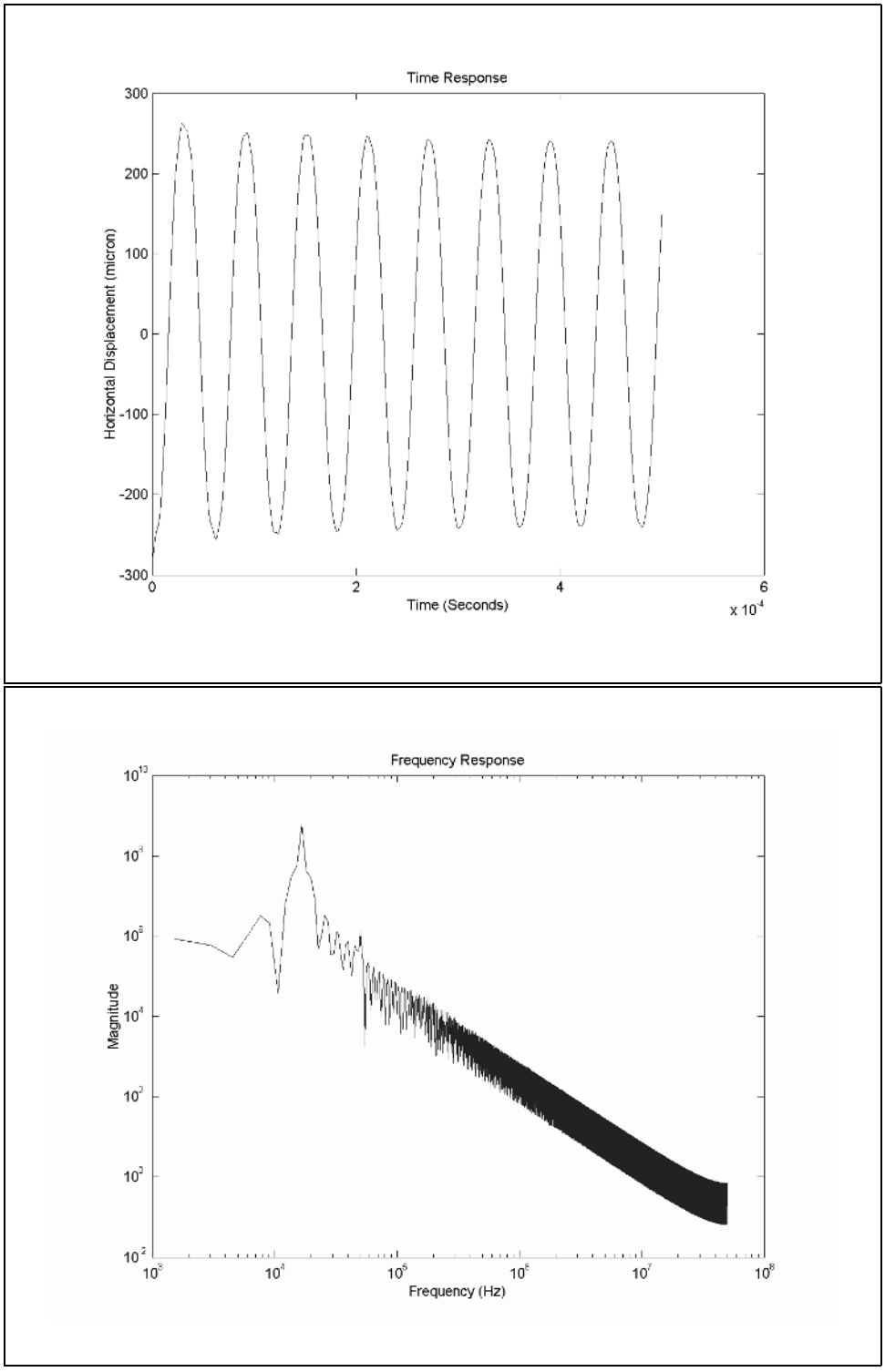

Figure 7.3: Resulting plots (350 micron leg lengths, 80% deflection) for the time characteristics of the horizontal displacement, and the resulting frequency response.

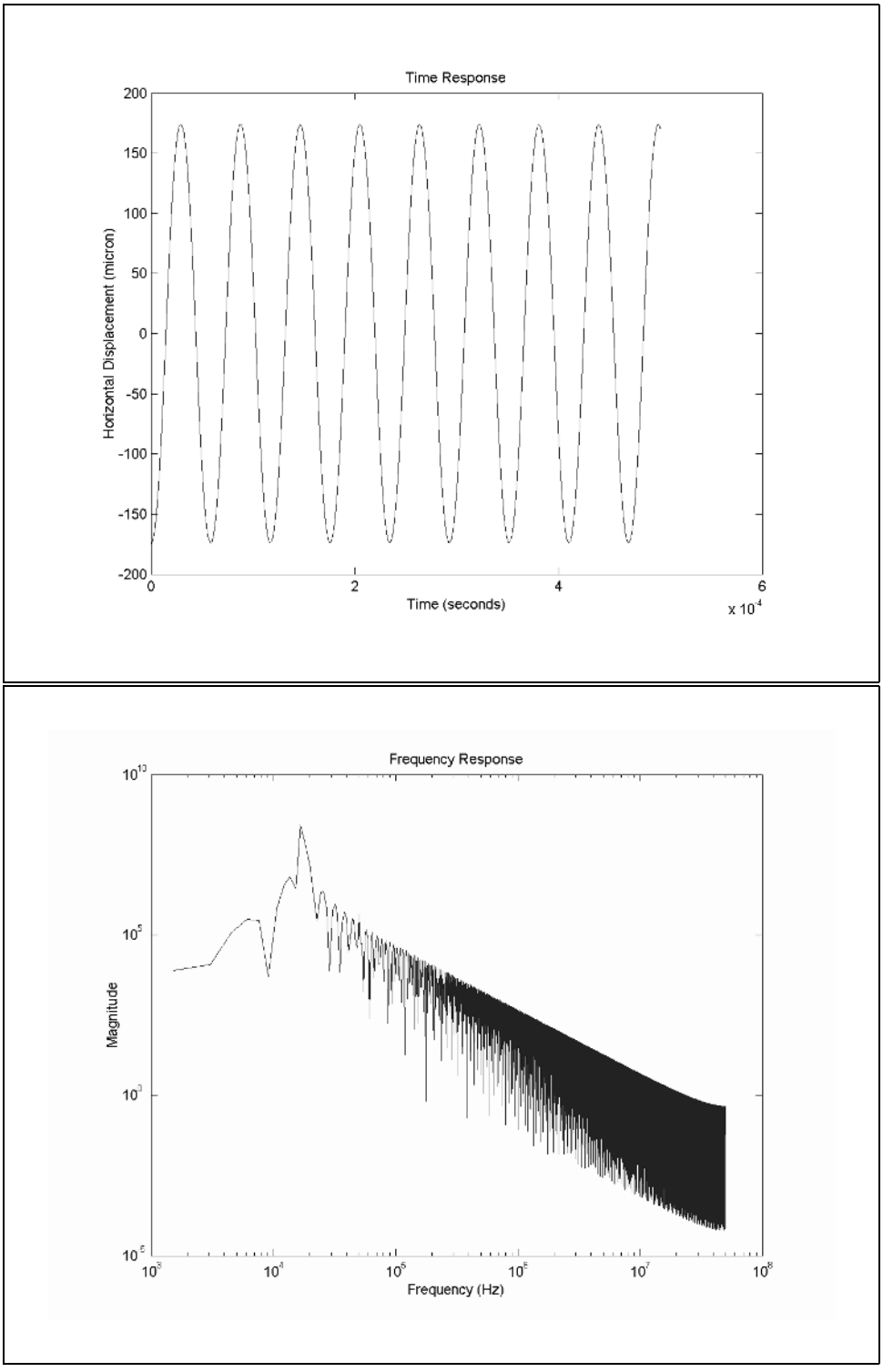

Figure 7.4: Resulting plots (350 micron leg lengths, 50% deflection) for the time characteristics of the horizontal displacement, and the resulting frequency response (FFT).

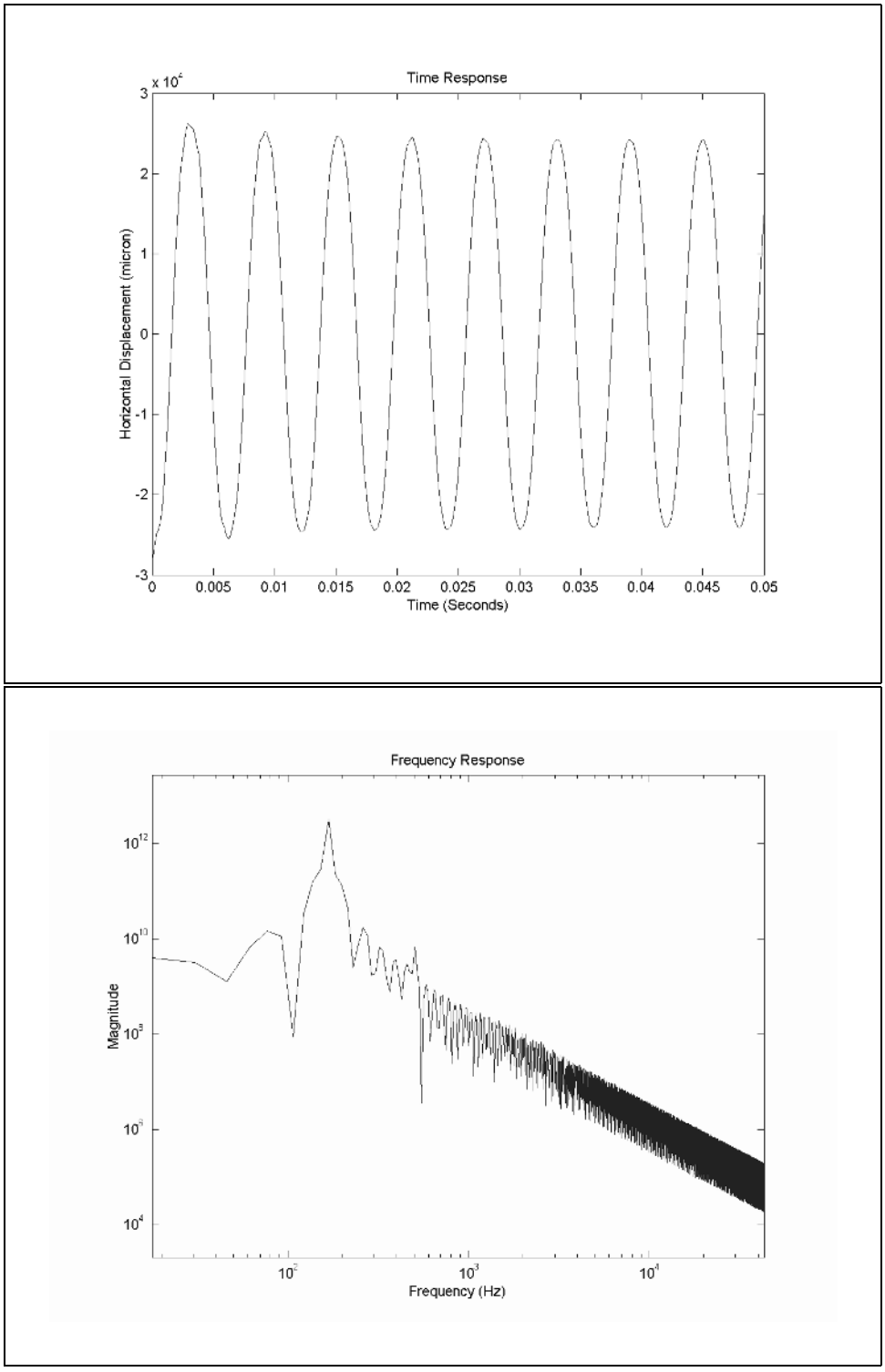

Figure 7.5: Resulting plots (35,000 micron leg lengths, 80% deflection) for the time characteristics of the horizontal displacement, and the resulting frequency response.

earlier, and the FEA result is based on the horizontal displacement over time of the end of the coupler. Plots representing the time response and the FFTs of the data are provided in Figures 7.3-7.5.

7.3.1 Modal Frequency Behavior

The modal behavior of the parallel mechanism is worth examining. The PRBM that was given for the dynamic response of the parallel mechanism Equation (5.35) is linear. This would suggest that the nonlinear FEA and the modal analysis should be very similar. Table 7.2 shows all three methods of calculating the dynamic response of the mechanisms (PRBM, FEA, Modal). There are several interesting points to note, the first is that the nonlinear FEA prediction varies between the two deflections. Although in both cases the resonance frequency is near the modal frequency of the mechanism. The PRBM predicts that the system will behave with a linear differential equation, which in turn predict that the resonance frequency of the system should remain the same regardless of the amount of initial deflection. In the beams that were examined earlier (Section 4.6), the difference, was not as significant as they have been in the parallel mechanism. This would be expected since the fixed-guided beam is essentially a combination of two cantilever beams. As the number of approximations increases, the variation from the FEA result would be expected to increase.

7.4 Folded Beam Structure

The folded beam structure shown in Figure 7.6 is an interesting mechanism to examine. Note that this mechanism is comprised of multiple parallel mechanisms. The combination of parallel mechanisms makes an interesting example of what happens as mechanisms become more complex. The basic model for the folded beam structure was presented in Section 5.2. Note that the model is nonlinear, suggesting that the frequency of the mechanism will not change based on the initial conditions.

The results that compare the parallel mechanisms FEA results with the PRBM, are listed in Table 7.1. The parallel mechanism resonance frequency is over predicted by the PRBM by six to seven percent. Since the folded beam structure combines

Table 7.2: Comparisons of Resonance Frequencies for Parallel Mechanism

Length (micron)	PRBM Resonance Frequency Prediction(Hz)	FEA Resonance Frequency Prediction(Hz)	Modal Frequency
350	18,000	16,800 (80% deflection)	17000
3,500	1,800	1,680 (80% deflection)	1700
35,000	180	168 (80% deflection)	170
350	18,000	17,000 (50% deflection)	17000
3,500	1,800	1,700 (50% deflection)	1700
35,000	180	170 (50% deflection)	170

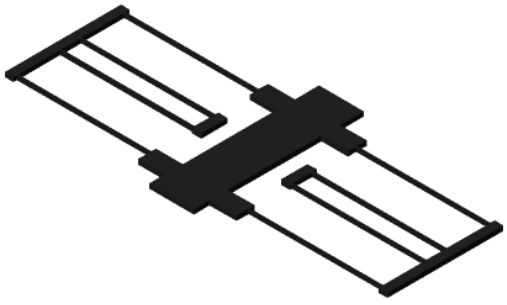

Figure 7.6: An isometric view of a folded beam structure.

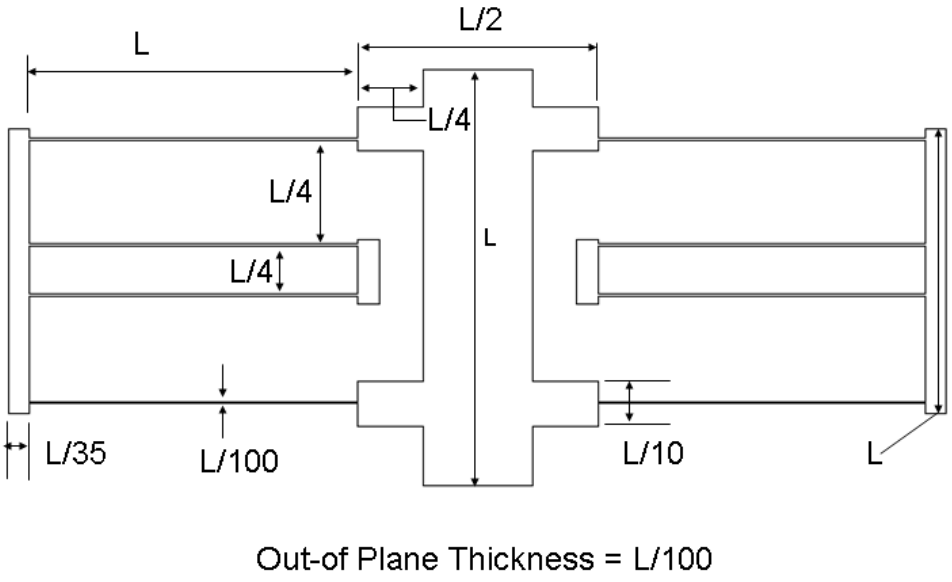

Figure 7.7: Mechanical dimensions of the folded beam structure.

two springs in series, one would expect that the overall system response would have a larger percent difference. If the predictions are correct, the percent difference should be between 12 and 14 percent. Table 7.3 shows the results of a comparison between the FEA results and the PRBM results for a parallel mechanism. The properties used for the model were that of polysilicon (Young Modulus 179×10^9 Pa, and Density 2,330 Kg/m^3). The model was again based on beam elements, as have been the previous models.

The results suggests that as the number of combined compliant segments is increased, that the percent difference between the results that are obtained through FEA and the results obtained through the PRBM will increase. This suggests that as mechanisms become more complex, the difficulties in predicting the system using the PRBM increases. This result is expected in any type of modeling where an approximate model is used for multiple subcomponents of the complete system.

Table 7.3: Predicted resonance frequencies from the PRBM and FEA for folded beam mechanisms. Small deflection theory yields a result of 10,200 Hz as the resonance frequency

LFS Length (μm)	PRBM Resonance Frequency Prediction(Hz)	FEA Resonance Frequency Prediction(Hz)	Percent Difference
350	–	9,044 (Modal Frequency)	–
350	10,400 $\pm$50	9,160 $\pm$300 (35 micron deflection)	13.5
350	10,400 $\pm$50	9,160 $\pm$300 (50 micron deflection)	13.5
350	10,400 $\pm$50	9,160 $\pm$300 (100 micron deflection)	13.5

7.5 Compliant Roberts Straight Line Mechanism

The Compliant Roberts straight-line mechanism uses the fixed-fixed PRBM that was presented earlier in this work. The basic mechanism is shown in Figure 7.8.

Table 7.4: Dimensions Roberts Straight-Line Mechanism

Dimension	Value	Unit
length	1,059	μm
width	9	μm
a	370	μm
b	852	μm
c	1,959	μm
angle of flexible segment	$\frac{\pi}{3}$	radians
Density	2,330	Kg/m^3
Young's Modulus	179×10^9	Pa

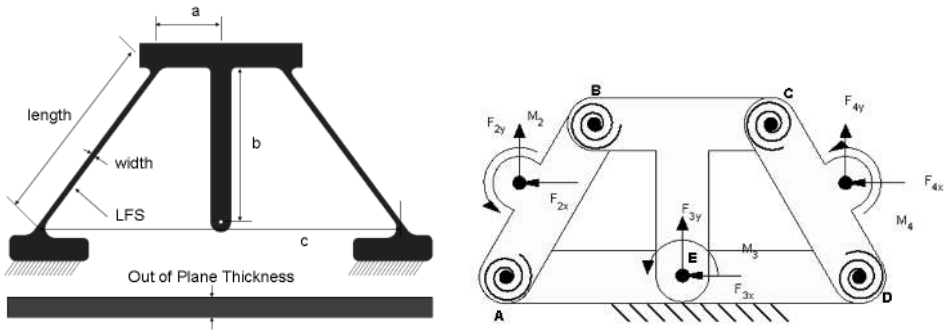

Figure 7.8: Compliant Roberts Straight-Line mechanism with PRBM Model.

The Roberts straight line mechanism is defined by the following constraint [13]:

$$AB = BE = CE = DC, \text{ and } AD = 2BC \tag{7.6}$$

The geometry for the compliant version is designed so that the PRBM matches the rigid-body Roberts straight-line mechanism. The example mechanism had flexible link lengths of 1,059 μm. The resonance frequency predicted by FEA was 6,100 $\pm$ 350 Hz. The PRBM predicts a resonance frequency of 5,750 Hz. The resulting percent difference between FEA and the PRBM is 9.8%. The properties used for the model were that of polysilicon (Young's Modulus 179x10^9 Pa, and Density 2,330 Kg/m^3). The PRBM of the mechanism was rotated through a change of rotation of 2.7 radians and the FEA deflected point E (of Figure 7.8 on the PRBM) 675 μm. The model was again based on beam elements, as have been the previous models.

The PRBM for this mechanism was again the generalized model that was presented in Section 5.1. The only parameters that need to be added are the values of the torsional springs. These values can be found based on the work presented in Chapter 3. The first objective is to determine the maximum amount of rotation of the coupler, and the deflection that is associated with that rotation. Both of these parameters can be found from the path curve of the mechanism. In this case the max deflection (y_{def}) is shown in Figure 7.10. The deflection that is perpendicular

to the beam is the value that is needed for the equations. In this case the change in values of the x-deflection yields a $y_{def} = 320$ μm. The maximum deflection and the rotation can then be applied to Equation (3.9). The maximum rotation can also be found from a standard path analysis of the mechanism. The rotation of the coupler, which in this case is the rotation of the end of the beam is shown in Figure 7.11. In this case the maximum rotation is 0.47 radians. The length of the beam was given previously as 1,059 μm. Θ_{Max} can then be determined from

$$\Theta_{Max} = \frac{0.6\theta_E L}{y_{def}} = -0.79 \tag{7.7}$$

Using Figure 3.6 the values of $K_{\Theta A}$ and $K_{\Theta E}$ can be determined. For this problem $K_{\Theta A} = 3.4$ and $K_{\Theta E} = 1.45$ for a load ratio (n) of -0.2 are used. These are then used as torsional stiffness coefficients in the determination of the torsion spring constants. The complete Matlab model for this mechanism is shown in Appendix B.3.

Since this particular mechanism has been shown in some detail, and since it uses a modeling technique that is presented in this work, it is useful to compare the FEA predicted deflections with the PRBM predicted deflections. The results of the FEA for the deflection in the x direction were presented in Figure 7.9. The y deflection that was predicted is shown in Figure 7.12. The corresponding prediction of the PRBM are shown in Figures 7.13 and 7.14. The x-deflection paths both match and exhibit the same general behavior. The y deflection is not quite as clean, partially due to some rounding that is inherent to the FEA code, but the PRBM and the FEA both predict some deflection in the y direction. This demonstrates the usefulness of the modeling technique presented in Chapter 3 for designing a mechanism for a specified output path. The rotations of each of the angles in the PRBM are also shown in Figure 7.15.

It is also important to note that the FEA-predicted modal analysis for this mechanism is 5,400 Hz, which is very similar to the PRBM prediction of the same system, although the full nonlinear FEA analysis predicts a higher resonance frequency. The models produce roughly the same results. Although the modal frequency does

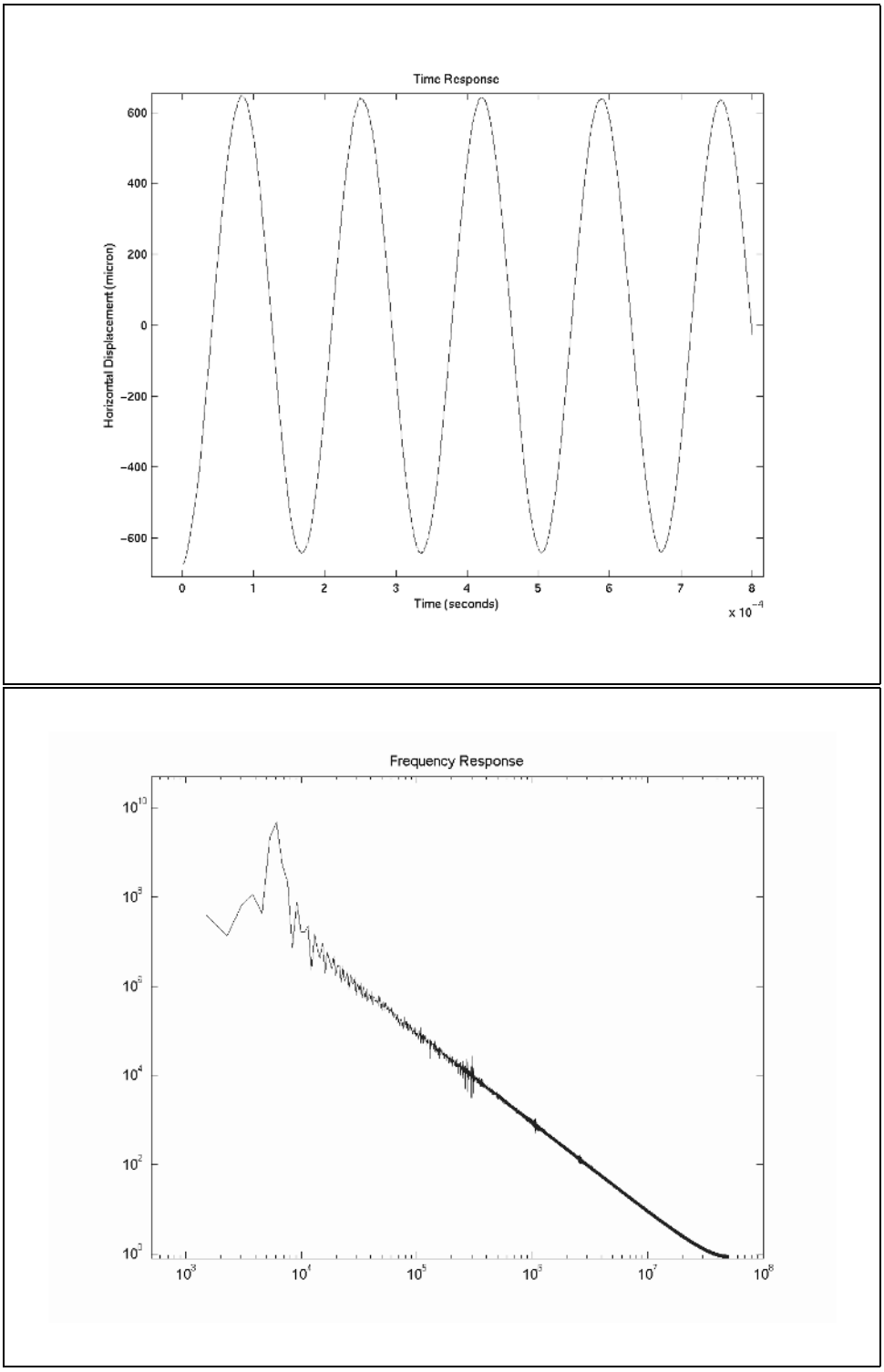

Figure 7.9: Resulting plots (900 micron equivalent leg lengths, 675 micron deflection) for the time characteristics of the horizontal displacement, and the resulting frequency response.

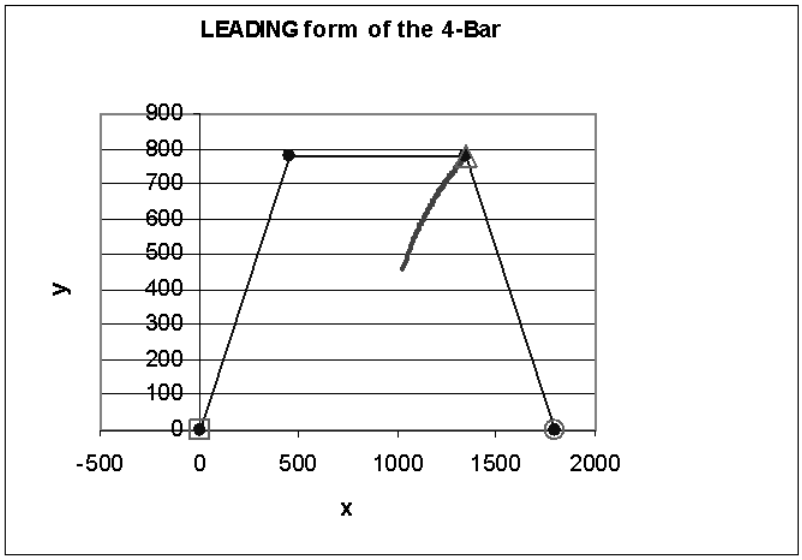

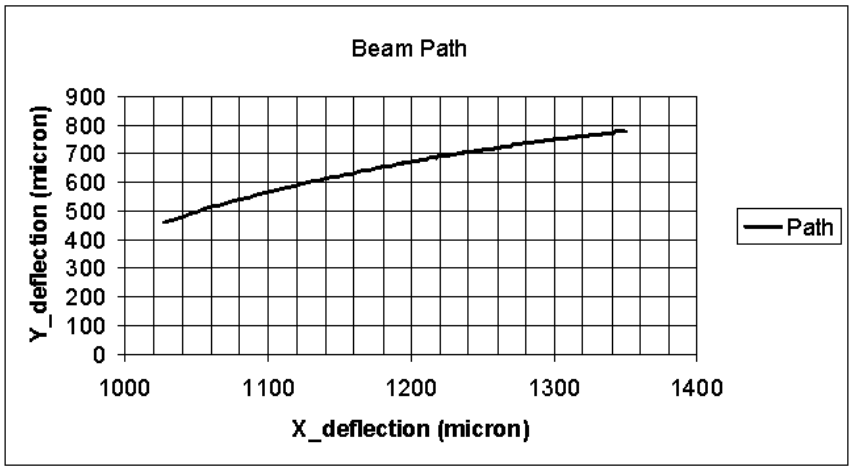

Figure 7.10: Approximate beam deflection of a cantilever beam in a compliant Roberts straight-line mechanism.

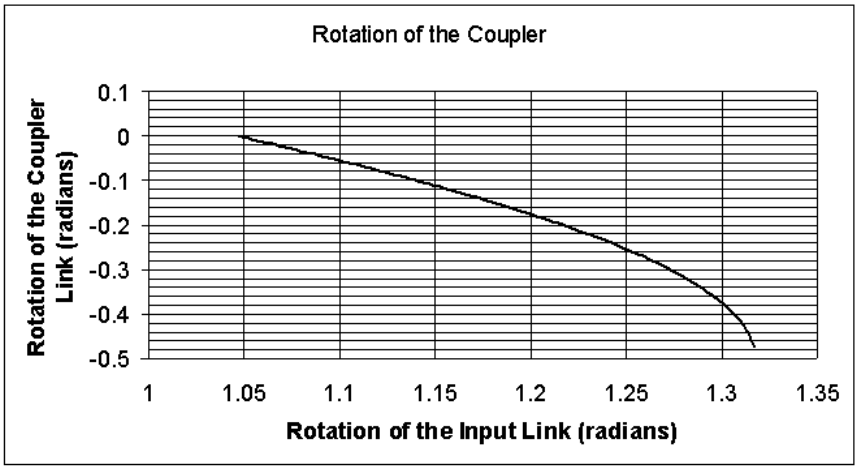

Figure 7.11: Rotation of the coupler in a Roberts straight-line mechanism.

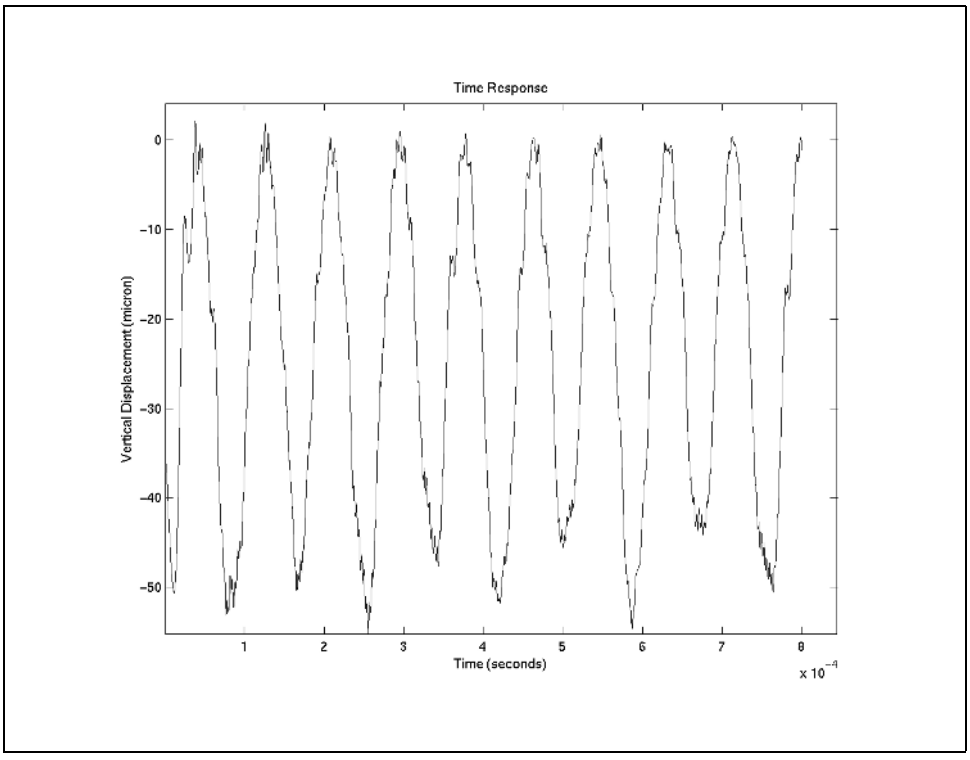

Figure 7.12: FEA prediction of the y deflection.

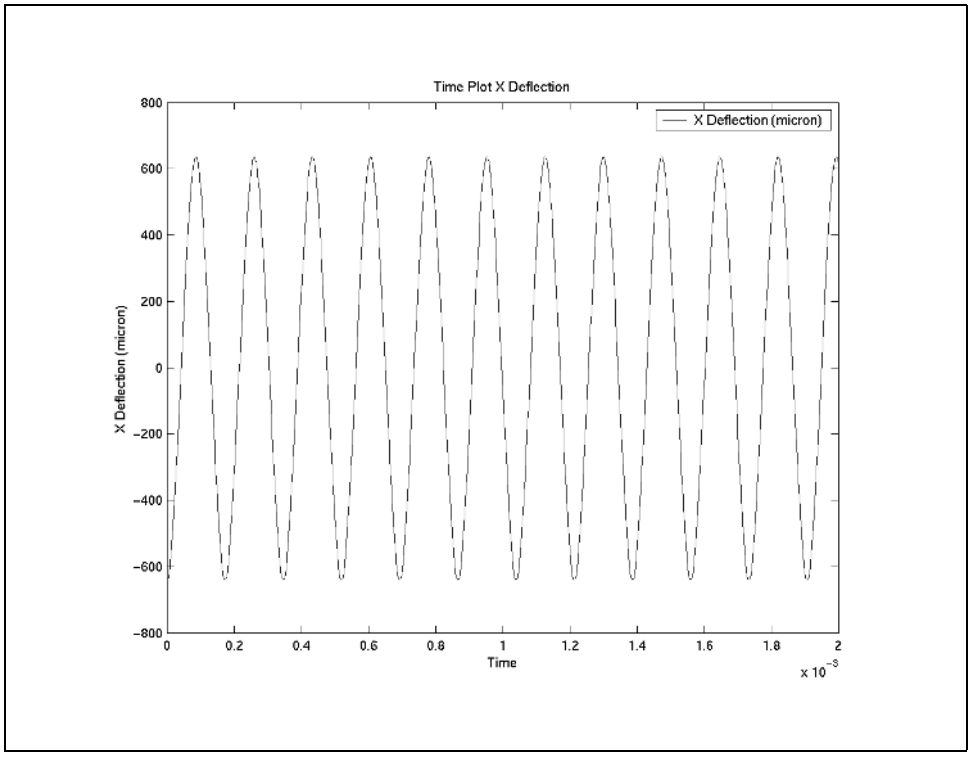

Figure 7.13: PRBM dynamic response of the x direction deflection.

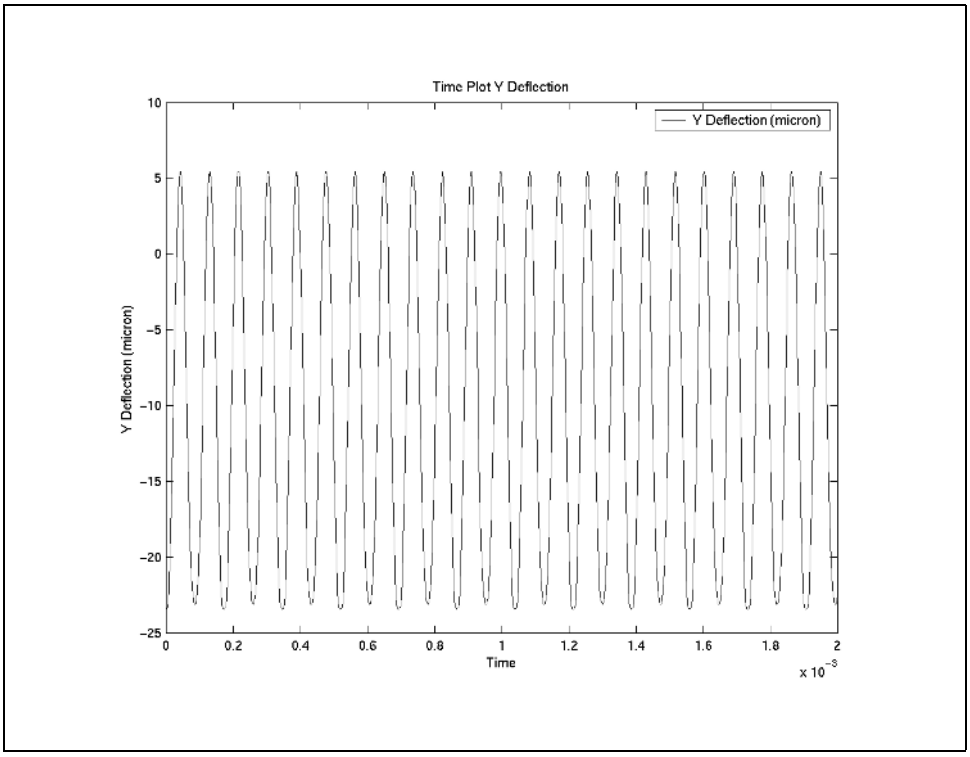

Figure 7.14: PRBM dynamic response of the y direction deflection.

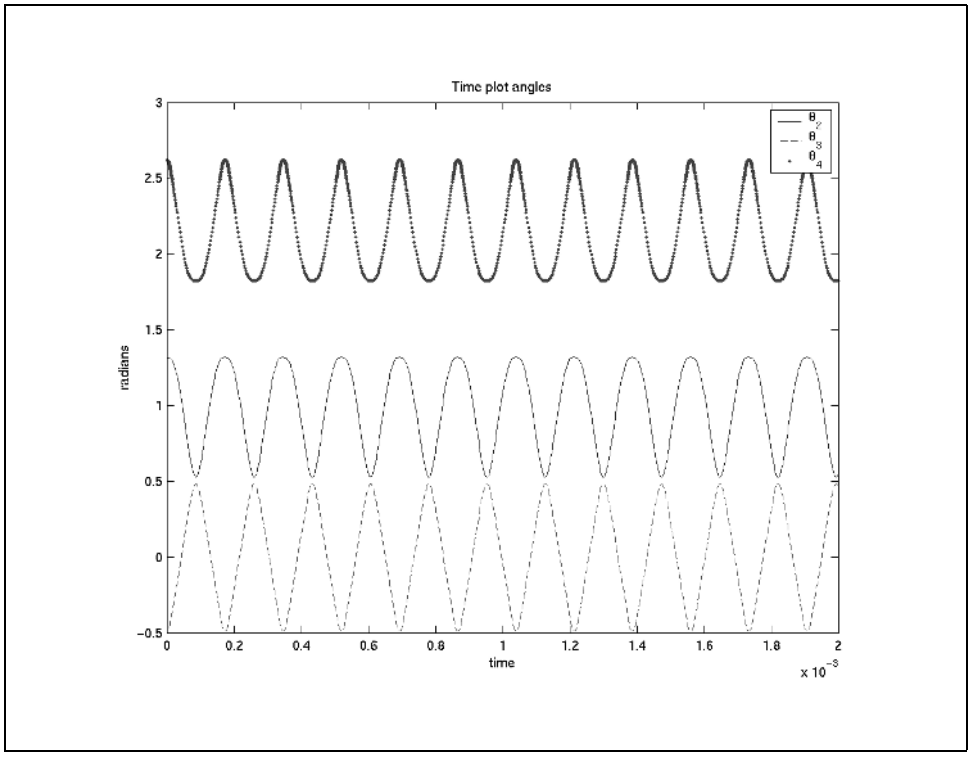

Figure 7.15: PRBM dynamic response showing the response of the angles in the PRBM model.

do an excellent job of predicting the resonance frequency, the modal analysis is not able to predict the paths of the mechanisms as were shown in Figures 7.13 and 7.14.

7.6 Summary

This section has explored details specific to modeling micro compliant mechanisms. The work examined a micro cantilever beam, and discussed the effects that scaling of the beam would have on the dynamic characteristics of the beam. Several micro beams were simulated using the PRBM and then compared with FEA and experimental results that have been published by other authors. The results correlated well with the data that was obtained from the macro testing of cantilever beams. The section then concluded with a discussion of micro mechanisms, where several mechanisms were examined and compared with FEA results. The mechanisms again showed that the PRBM technique is a good representation of the first resonance frequency of the system. The folded beam structure showed that as the mechanisms become more complex, the predictions of the resonance frequencies and dynamic responses of the system will tend to degrade.

The major contribution of this section was to show that the PRBM can be used to predict the dynamic behavior of micro compliant beams and mechanisms. It was also shown in this chapter that as the mechanisms grow more complex, the predictions of the PRBM begin to degrade.

Chapter 8

Conclusions and Recommendations

This work examined several details of the Pseudo-Rigid-Body Modeling (PRBM) technique. It specifically considered the development of a modeling method for cantilever beams with force and moment loads applied to the end. An examination of the ability of the PRBM to predict the dynamic characteristics of both cantilever beams and compliant mechanisms was also discussed in detail. The PRBM was then compared with experimental data, as well as finite element analysis (FEA). Each of the contributions that was made to the theory of compliant mechanisms is presented in the next section.

8.1 Contributions of This Work

8.1.1 Force and Moment Loads (Fixed-Fixed Flexible Segments)

The development of a PRBM for a segment that is subject to force and moment loads has allowed new developments and configurations of mechanisms. The cross-axis flexural pivot mechanism with fixed-fixed segments is a one of many systems that are difficult to model without the use of the modeling technique presented in this research. Additionally, the cross-axis flexural pivot can be better understood through the use of this model. The method will continue to enable additional mechanisms to be designed and the behavior to be predicted.

8.1.2 Dynamic Behavior of the PRBM

The ability of the PRBM to predict the dynamic behavior of compliant mechanisms allows the designer more flexibility in design. One example is the parallel mechanism, which has 28 configurations of compliant systems that will mimic the behavior of the rigid link parallel mechanism. This allows a variety of first modal behaviors to be exhibited and predicted by a single PRBM. This leads to the development of simpler models to be used with control schemes, as well as the determination of resonance modes. The models conform to accepted theory in traditional mechanism design and analysis. Thus, the designer can use traditional mechanism design theory for more complex and unique compliant mechanisms, and allows the use of commercially available mechanism analysis software.

8.1.3 Micro Compliant Mechanisms

The research discussed the ability of the PRBM to predict the resonance frequencies of mechanisms and cantilever beams at the micro scale. The modeling techniques that have applied at the macro scale are shown to also apply at the micro scale. The predictions of the PRBM are compared with either predictions from FEA and/or measured results.

In addition to the application of the PRBM on the micro scale, a discussion is presented that shows the trends that should be expected as compliant mechanisms are reduced in size. It was shown through study of parallel mechanism that as the size decreases, the expected resonance frequency should increase linearly. In addition, the effects of the area-based damping terms will also increase in a linear manner, if all other system parameters remain constant. This allows the designer to devise better mechanisms by anticipating problems that can come from scaling the system down in size.

8.2 Future Directions of This Work

This research has opened the possibilities of further study. Three possible ideas are presented here.

8.2.1 Dynamic-Based Design of Compliant Mechanisms

The ability of the PRBM to be used in the dynamic analysis of mechanisms opens the possibility of the same model being used to predict the behavior of a significant number of configurations of any given mechanism. This essentially gives the designer a larger set of configurations from which they are able to produce different dynamic responses by changing the type of flexible joints contained in the mechanism. The joint types can be changed without having to adjust the path through which the mechanism travels. The flexibility leads to the question of dynamic response. How does the desired dynamic response influence the criteria for the design of the mechanism? Could rules be developed that will discuss the possibilities and options that are available to the designer for a given desired dynamic response? An example would be developing a mechanism for an approximate path and the desired dynamic behavior. The task of the designer is to then take the system, and optimize between the desired path and the dynamic response, while minimizing the stresses. Currently, there are no set rules to define the relationships without defining the entire model. The ability to adapt designs to fit the dynamic constraints based on a simple set of rules would allow the designer more flexibility and greater accuracy in fitting the desired response.

8.2.2 Model Prediction Based on the Dynamic Response

In some cases, the model that appropriately fits a compliant mechanism is not always apparent from just looking at the mechanism. In many ways, the dynamic characteristics can help determine some important modeling parameters. For example, consider a system with a stiff spring and two soft springs, and assume that the two soft springs change their behavior if the system is operated above 10 Hz. The stiff spring is stiff enough that a frequency below 20 Hz does not produce sufficient inertial forces to deflect the spring. A simple example of a system that would produce this type of result is a set of two parallel mechanisms shown in Figure 8.1. The dynamic model for this system would be a two degree of freedom model of the system. It consists of two independent PRBM's that are coupled at the intersection point. A

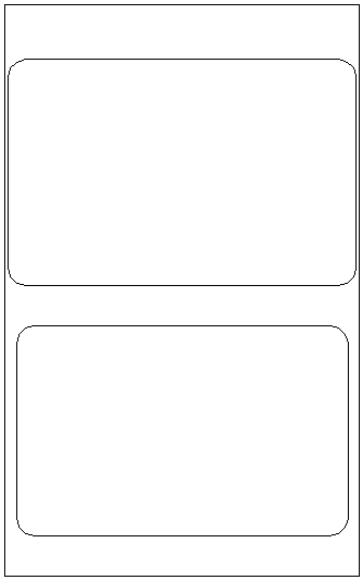

Figure 8.1: A system that has two perceived degrees of freedom, and one practical degree of freedom.

two degree of freedom model would be a good model for the system. However, is a two degree of freedom model excessive? Could the dynamic trends of this system be adequately captured by a single degree of freedom system?

A cantilever beam will have a first, second, third, etc., modal frequency. Each change in modal frequency will change the method for modeling the system accurately. The hypothesis would then be that the number of degrees of freedom in a PRBM would correspond to the number of modal frequencies below the second modal frequency of the structural member with the lowest modal frequency. For the system above, the second modal frequency of the upper portion of the system would be modeled, and the second modal frequency would be determined. If the second modal frequency of the upper beams is less than the first modal frequency of the lower portion of the system, then the lower portion of the system can be ignored, and only the upper portion would be required to model the system. The foundation in this theory is that the PRBM model will fail as the second modal frequency of any member is exceeded. It will provide some insight in answering the question of how

thin a rigid member could be before the deflection of the rigid body needs to be taken into account.

8.2.3 Mechanical Energy Harvesting

If the mechanical systems can harvest or draw power from surroundings or a generated source, then they have potential of becoming amplifiers, or something very similar to a transistor. This is an important mechanism which is slowing the development of complete systems that have the capability to perform complex tasks in a micro mechanism array. In some cases, a complete satellite could be placed on a single chip. Other sophisticated mechanisms could also be developed to solve a variety of safety and security issues. This would be accomplished by a study of mechanical energy harvesting. It would involve a clear understanding of mechanical systems on the macro scale that are moved by changes in the environment.

The research would be divided into two focus areas. The first would be a study of systems that utilize mechanical energy harvesting. Understanding how and why these systems work will be a significant key to developing a method for combining these systems. Also important in this portion of the research would be the categorizing of systems defining clear input and outputs of various systems, and creating ways in which they can interact.

The second phase of the research would be to take the macro examples and several other mechanical systems, and combine them on the micro scale. The energy to move the system would then come from the environment, or from a source of mechanical power.

8.3 Summary

This research discussed how the PRBM can be used by a designer in developing dynamic models for compliant mechanisms. The results also suggest that the PRBM provides a reasonable model for determining the dynamic response of compliant mechanisms. The work has suggested areas of focus where the PRBM technique are accurate, and areas where the predictions are not as accurate. Several of the

significant factors that affect the ability of the PRBM to determine the dynamic characteristics were presented, with the various models that show the importance of the changes in the behavior. In addition to the contributions of this research, several areas of future research were presented. Each of these areas of future research build upon the research that was presented, and are areas where significant research can still be performed.

Bibliography

[1] S. Vogel, "Better Bent than Broken," *Discover*, pp. 62–67, May 1995.

[2] S. Vogel, *Cats' Paws and Catipults: Mechanical Worlds of Nature and People.* New York and London: W. W. Norton and Company, first ed., 1998.

[3] L. L. Howell and A. Midha, "A Method for the Design of Compliant Mechanisms with Small-Length Flexural Pivots," *Journal of Mechanical Design*, vol. 116, no. 1, pp. 280–290, 1994.

[4] G. K. Ananthasuresh, S. Kota, and N. Kikuuchi, "Strategies for Systematic Synthesis of Compliant MEMS," *Proceedings of the 1994 ASME Winter Annual Meeting, Symposium on MEMS: Dynamics Systems and Control*, vol. DSC-Vol 55-2, pp. 93–96, 1994.

[5] G. K. Ananthasuresh and S. Kota, "Designing Compliant Mechanisms," *Mechanical Engineering*, vol. 117, no. 11, pp. 93–96, 1995.

[6] M. I. Frecker, S. Kota, and N. Kikuchi, "Use of Penalty Function in Topological Synthesis and Optimization of Strain Energy Density of Compliant Mechanisms," *Proceedings of the 1997 ASME Design Engineering Technical Conferences*, 1997, DETC97/DAC-3760.

[7] O. Sigmund, "On the Design of Compliant Mechanisms Using Topology Optimization," *Mechanics of Structures and Machines*, vol. 25, no. 4, pp. 495–526, 1997.

[8] C. B. W. Pedersen, T. Buhl, and O. Sigmund, "Topology Synthesis of Large-Displacement Compliant Mechanisms," *Procdeedings of the 1999 ASME Design Engineering Technical Conferences*, 1999, DETC99/DAC-8554.

[9] J. M. Derderian, L. L. Howell, M. D. Murphy, S. M. Lyon, and S. D. Pack, "Compliant Parallel-Guiding Mechanisms," *Proceedings of the 1996 ASME Design Engineering Technical Conference*, 1996, 96-DETC/MECH-1208.

[10] A. J. Millar, L. L. Howell, and J. N. Leonard, "Design and Evaluation of Compliant Constant-Force Mechanisms," *Preceedings of the 1996 ASME Mechanisms Conference*, 1996, 96-DETC/MECH-1209.

[11] P. G. Opdahl, "Modeling and Analysis of Compliant Bi-stable Mechanisms Using the Pseudo-Rigid-Body Model," Master's thesis, Brigham Young University, December 1996.

[12] B. D. Jensen, "Identification of Macro- and Micro- Compliant Mechanism Configurations Resulting in Bistable Behavior," Master's thesis, Brigham Young University, August 1998.

[13] L. L. Howell, *Compliant Mechanisms*. John Wiley and Sons, 2001.

[14] L. L. Howell, "The Design and Analysis of Large-Deflection Members in Compliant Mechanisms," Master's thesis, Purdue, August 1991.

[15] L. L. Howell and A. Midha, "Parametric Deflection Approximations for End-Loaded, Large-Deflection Beams in Compliant Mechanisms," *Journal of Mechanical Design*, vol. 117, no. 1, pp. 156–165, 1995.

[16] L. L. Howell and A. Midha, "Parametric Deflection Approximations for Initially Curved, Large-Deflection Beams in Compliant Mechanisms," *Proceedings of the 1996 ASME Design Engineering Technical Conferences*, 1996, DETC96/Mech-1215.

[17] K. E. Bisshopp and D. C. Drucker, "Large Deflection of Cantilever Beams," *Quarterly of Applied Mathematics*, vol. 3, no. 3, pp. 272–275, 1945.

[18] R. Frisch-Fay, *Flexible Bars*. Washington D. C.: Butterworth, 1962.

[19] K. Mattiasson, "Numerical Results from Large Deflection Beam and Frame Problems Analyzed by Means of Elliptic Integrals," *International Journal for Numerical Methods in Engineering*, vol. 17, pp. 145–153, 1981.

[20] B. A. Coulter and R. E. Miller, "Numerical Analysis of a Generalized Plane Elastica with Non-linear Material Behavior," *International Journal for Numerical Methods in Engineering*, vol. 26, pp. 617–630, 1988.

[21] T. C. Hill and A. Midha, "A Graphical User-Driven Newton-Raphson Techniquefor Use in the Analysis and Design of Compliant Mechanisms," *Journal of Mechanical Design*, vol. 112, no. 1, pp. 123–130, 1990.

[22] H. B. Harrison, "Post-buckling Analysis of Non-Uniform Elastic Columns," *International Journal for Numerical Methods in Engineering*, vol. 7, pp. 195–210, 1973.

[23] I. Her, A. Midha, and B. A. Salamon, "A Methodology for Compliant Mechanisms Design, Part II: Shooting Method and Application," *Proceedings of the 18^{th} ASME Design Automation Conference*, vol. 44-2, pp. 39–45, 1992.

[24] B. T. Edwards, "Functionally Binary Pinned-Pinned Segments," Master's thesis, Brigham Young University, December 1996.

[25] A. Saxena and S. N. Kramer, "A Simple and Accurate Method for Determining Large Deflections in Compliant Mechanisms Subjected to End forces and Moments," *Journal of Mechanical Design*, vol. 120, no. 3, pp. 392–400, 1998.

[26] L. W. Tsai, C. Kimball, D. DeVoe, and J. Maloney, "Modeling and Batch Fabrication of Spatial Micro Manipulators," in *Proceedings of the 2000 ASME Design Engineering Technical Conferences*, September 2000 , DETC2000/Mech-14116.

[27] H. D. Eckhardt, *Kinematic Design of Machines and Mechanisms.* McGraw-Hill, 1998.

[28] R. Talman, *Geometric Mechanics.* John Wiley and Sons, Inc., 2000.

[29] C. T. F. Ross, *Dynamics of Mechanical Systems.* Chichester, PO20 6QL England: Horwood Publishing Chichester, 1997.

[30] G. F. Franklin, J. D. Powell, and A. Emami-Naeini, *Feedback Control of Dynamic Systems.* Addison-Wesley Publishing Company, Inc., third ed., June 1994.

[31] J. M. T. Thompson and H. B. Stewart, *Nonlinear Dynamics and Chaos.* John Wiley snd Sons, 1986.

[32] M. Cartmell, *Introduction to linear, Parametric and Nolinear Vibrations.* Chapman and Hall, 1990.

[33] A. A. Shabana, *Dynamics of Multibody Systems.* Cambridge University Press, second ed., 1998.

[34] A. A. Shabana, *Vibration of Discrete and Continuous Systems.* Springer, second ed., 1997.

[35] R. L. Huston, *Multibody Dynamics.* Butterworth-Heinemann, Stoneha, MA, 1990.

[36] E. V. Zakhariev, "Nonlinear Dynamics of Rigid Flexible Multibody Systems," in *Proceedings of DETC'99*, September 1999 , DETC99/VIB-8248.

[37] Koichi Honke and Yoshio Inoue and Eiko Hirooka and Naoki Sugano, "A Study on the Simulation of Flexible Link Mechanics Based on FEM," in *Proceedings of DETC'97*, September 1999, DETC97VIB4210.

[38] N. T., S. N., and R. S., "A survey of Finite Elemennts Methods Application for the Dynamic Analysis of Robot Manipulators," in *Modeling, Simulation & Control*, vol. 27, pp. 23–34, May 1990.

[39] A. Banerjee and S. Nagarajan, "Efficient Simulation of Large Overall Motion of Beams Undergoing Large Deflection," in *Multibody System Dynamics*, vol. 1, 1997.

[40] C. Boyle, L. Howell, S. Magleby, and M. Evans, "Dynamic Modeling of Compliant Constant-Force Compression Mechanisms," *Mechanism and Machine Theory, in press.*

[41] A. Midha, M. Murphy, and L. Howell, "Compliant Constant-Force Mechanisms and Devices Formed Therin," United States Patent No. 5,649,454, 1995.

[42] M. Evans and L. Howell, "Constant-Force End-Effector Mechanism," *Proceedings of the IASTED International Conference, Robotics and Applications*, pp. 250–256, Oct. 28-30.

[43] C. L. Boyle, "A Closed-Form Dynamic Model of the Compliant Constant-Force Mechanism Using the Pseudo-Rigid-Body Model," Master's thesis, Brigham Young University, August 2001.

[44] J. E. Marsden, A. J. Tromba, and A. Weinstein, *Basic Multivarialbe Calculus.* 175 Fifth Avenue, New York, NY 10010, USA: Springer-Verlag New York, Inc., 1993.

[45] W. T. Thomson and M. D. Dahleh, *Theory of Vibration with Applications.* Upper Saddle River, New Jersey 07458: Prentice Hall, fifth ed., 1998.

[46] H. Glodstein, *Classical Mechanics.* Addison-Wesley, first ed., 1980.

[47] J. Jost and X. Li-jost, *Calculus of Variations.* Cambridge, UK: Cambridge University Press, first ed., 1998.

[48] N. I. Akhiezer, *The Calculus of variations.* New York and London: Blaisdell Publishing Company, first ed., 1962. Translated from the Russian by Aline H. Frink.

[49] M. J. Forray, *Variational Calculus in Science and Engineering.* New York and London and San Francisco and Toronto and Sydney: McGraw-Hill, first ed., 1968.

[50] M. Tabor, *Chaos And Integrability in Nonlinear Dynamics.* New York and Chichester and Brisbane and Toronto and Singapore: John Wiley & Sons, first ed., 1989.

[51] F. D. Bona and S. Zelenika, "Characterization of High Precision Parallel Spring Translators," *International Progress in Precision Engineering*, pp. 761–772, 1993.

[52] F. D. Bona, M. G. Munteanu, and S. Zelenika, "Non-Linear Analysis of Parallel Spring Systems," *Proceedings of the 2-nd National Conference on Boundary and Finite Element*, pp. 8–17, 1993.

[53] H. Matoba, T. Ishikawa, C. Kim, and R. Muller, "A Bistable Snapping Microactuator," *Proceedings of the IEEE Micro Electro Mechanical Systems*, pp. 45–50, Jan 25-28 1994, Oiso, Japan.

[54] M. Saif, "On a Tunable Bistable MEMS – Theory and Experiment," *Journal of Microelectromechanical Systems*, vol. 9, no. 2, pp. 157–170, 2000.

[55] Y.-J. Yang and C.-J. Kim, "Dynamics of a Bistable Snapping Microactuator," *Proceedings of SPIE*, vol. 2443, pp. 754–762., 1995.

[56] H. Hosaka, K. ITAO, and S. Kuroda, "Evaluation of Energy Dissipation Mechanisms in Vibrational Microactuators," *Proceedings of the IEEE Micro Electro Mechanical Systems*, pp. 193–198, 1994.

Appendix

Appendix A

Supplementary Beam Models

A.1 Modeling the Deflected Shape of a Compliant Segment

This section presents a model for Predicting the deflected shape of a long flexible compliant segment based on a technique derived from the Pseudo-Rigid-Body model (PRBM). The deflected shape of a compliant beam is of interest for several reasons. Possibly the most significant of those is to visualize what is happening with the beam. This allows the designer to avoid collision of the flexible members with other portions of the mechanisms. Most research to this point has focused on the end point of the beam, and the orientation and final position of a beam for a given load. The location of the end of the beam is naturally the most important part of the path of the beam, but additional information is also valuable in design.

The modeling technique is simple and it starts out with a PRBM model of the end location of the beam. The PRBM results in the end location of the beam, as well as the rotation of the end of the cantilever beam [13]. Figures A.1, and A.2 show the cantilever beam, and the PRBM that is associated with a cantilever beam. The end angle of the beam is given by $\theta_E = c_\Theta \Theta$ [13]. The end location of the beam is given by $a = (1-\gamma)L + \gamma L\cos(\Theta)$, and $b = \gamma L \sin(\Theta)$ [13]. That completely defines the end location of the beam. If the beam is split at point A (Figure A.1), then the loading conditions on the shorter beam are still the same, but rotated, as shown in Figure A.3. If this beam is then rotated, it to has an identical PRBM to the previous beam, with a different length.

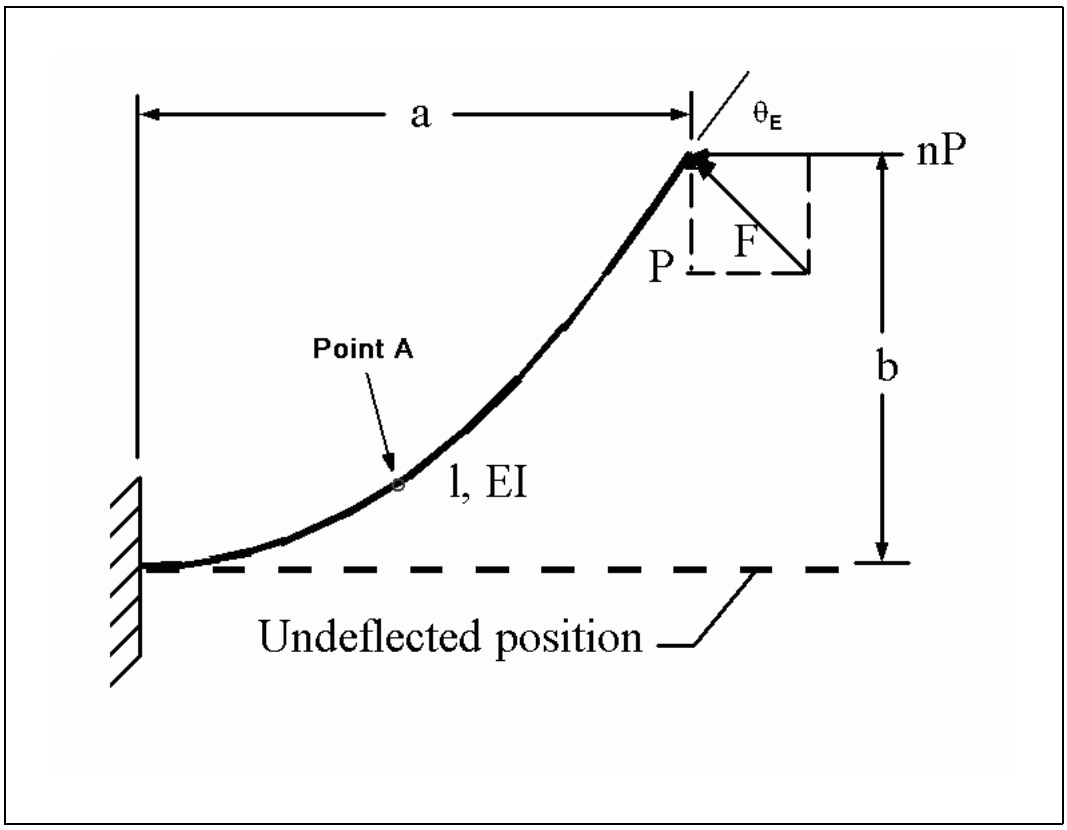

Figure A.1: A deflected cantilever beam, showing the various properties of the beam and the loading conditions.

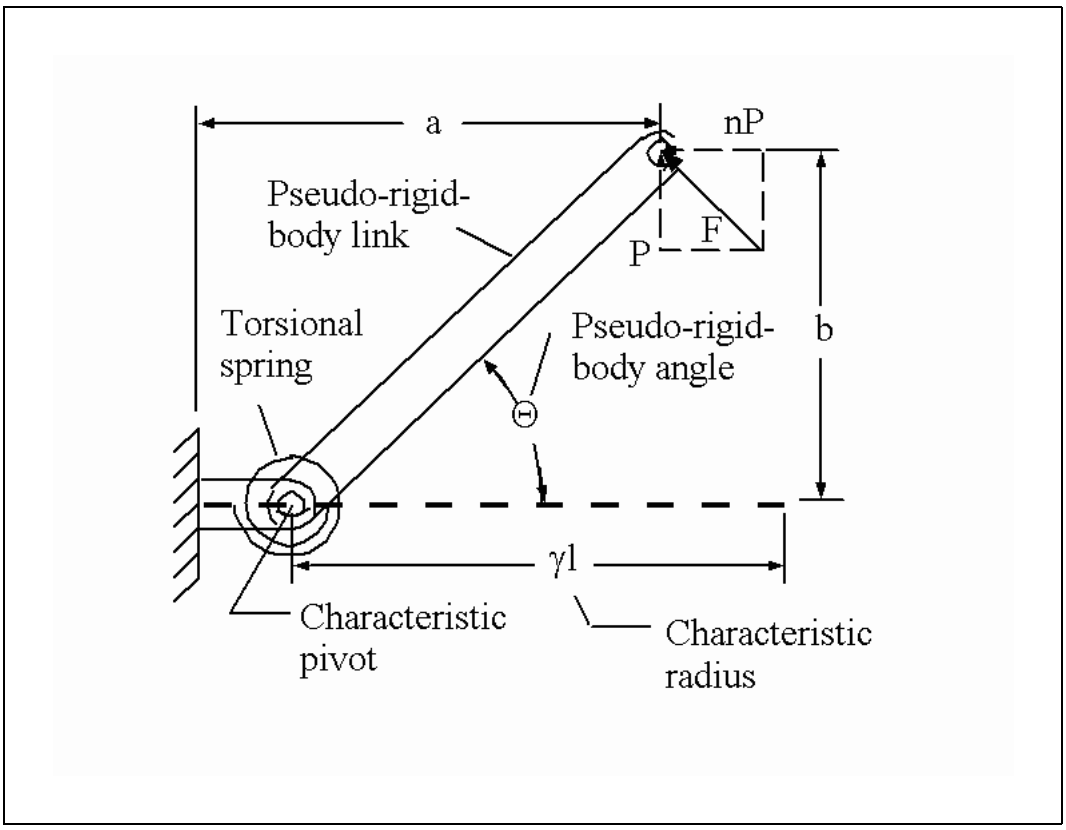

Figure A.2: The Pseudo-Rigid-Body model of a cantilever beam with graphical representations of the various components.

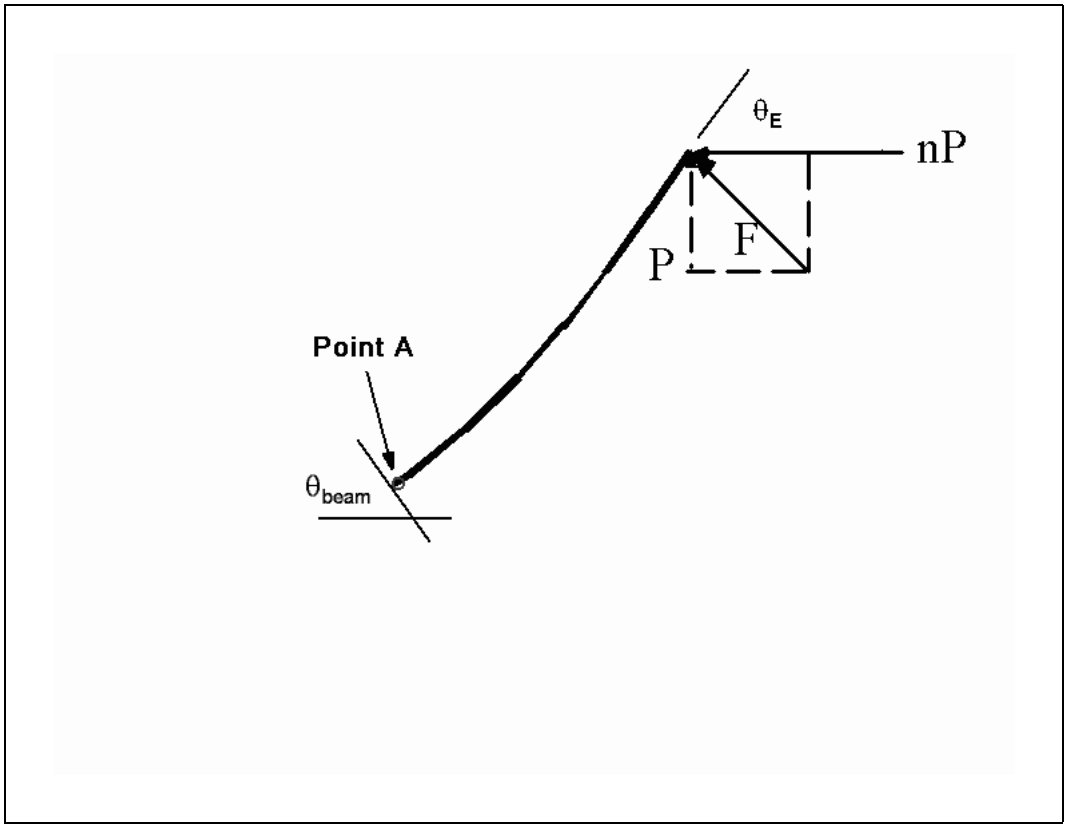

Figure A.3: A deflected cantilever beam cut at a center location in the beam.

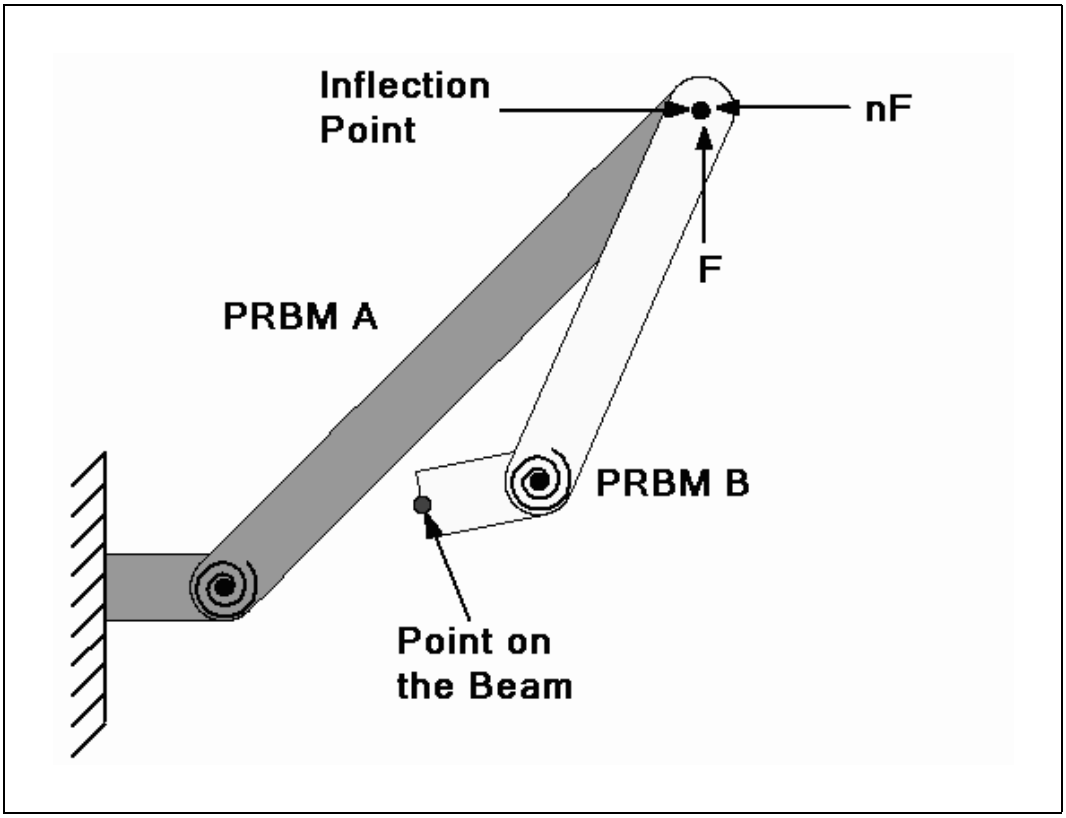

Figure A.4: A graphical depiction of combining two cantilever beams to find a central location on the beam.

This suggests that the position and loads that are associated with point A (Figure A.1) can be found if the two models are combined. Figure A.4 shows the result of combining the models. Note that they have been combined at the inflection point. They are combined at the inflection point because all of the properties of both beams are know at that location. This combination of models allows the forces, moments, and position of any location on the cantilever beam to be found. The process for combining the PRBM models is discussed in more detail in the following paragraphs.

The modeled path of a beam is shown in Figure A.5. The basic idea behind the model is that the length of the beam is unimportant. Since the Pseudo-Rigid-Body model (PRBM) will work for any beam length, having the same load with a different length beam will cause the moment to change at the base of the beam. Since the

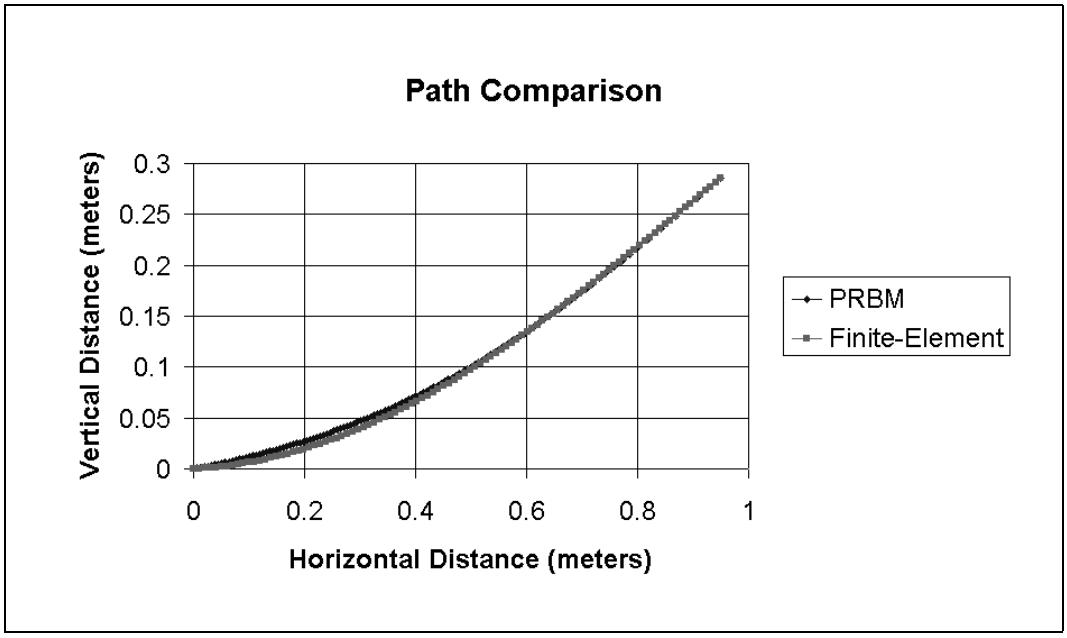

Figure A.5: The path of the beam as represented by the PRBM modeling technique.

curvature of the beam is known at the end of the beam, two PRBM models can be tied at that point each with a different length, and different loading conditions. This is demonstrated in Figure A.4 with two PRBM models coming from the end location of the beam. The curvature of the beam at the end of the beam is given by

$$\theta_E = C_\Theta \Theta. \tag{A.1}$$

All of the PRBM's must have the same final angle at the tip of the beam where no curvature exists. This is because all of the models share that location. Essentially the beams all have the same end location and rotation. Each model is then extended back at different lengths. The base of each of the models then becomes the location of the beam at the given length of the second PRBM. As the length of the second model is then varied, each location on the beam can be calculated.

Obviously Equation (A.1) is not the only equation required to define the path. The following force equations are needed for each of the PRBM's:

$$K_A\Theta_A = F\gamma_A l_A \cos(\Theta_A) + nF\gamma_A l_A \sin(\Theta_A), \tag{A.2}$$

and

$$K_B\Theta_B = F\gamma_B l_B \cos(\Theta_B + \beta) + nF\gamma_B l_B \sin(\Theta_B + \beta). \tag{A.3}$$

Dividing the two equations by each other yields

$$\frac{K_A\Theta_A}{K_B\Theta_B} = \frac{\gamma_A l_A \cos(\Theta_A) + n\gamma_A l_A \sin(\Theta_A)}{\gamma_B l_B \cos(\Theta_B + \beta) + n\gamma_B l_B \sin(\Theta_B + \beta)}. \tag{A.4}$$

With some manipulation this can be further simplified to

$$\frac{l_B^2}{l_A^2} = \frac{K_{\Theta A}\Theta_A(\cos(\Theta_A) + n\sin(\Theta_A))}{K_{\Theta B}\Theta_B(\cos(\Theta_B + \beta) + n\sin(\Theta_B + \beta))}. \tag{A.5}$$

where

$$\beta = (c_A - 1)\Theta_A - (c_B - 1)\Theta_B. \tag{A.6}$$

which comes from matching the end angles of both PRBM models. Finally the rotation of point A can be determined by:

$$\Theta_{beam} = c_A\Theta_A - c_B\Theta_B, \tag{A.7}$$

With these equations it is possible to track any point on the beam. Figure A.5 shows the results of a PRBM for determining the path, and an FEA approach under the same loading conditions. It is important to mention that the process will require solving a nonlinear equation if the lengths are chosen as the variable that is changed. However, if the angle is chosen, then the equations become simple and very easy to manipulate. A second point of interest is what happens to the equations if the lengths are the same. Note that in this case, the right side of the equation also becomes one, and the equations match exactly as expected.

A.2 Modified Chain Algorithm

The modified chain algorithm is a method of decoupling the geometry of a flexible segment from the material properties. This is similar to the PRBM, and a strong mathematical basis for allowing a PRBM to be used. The modified chain

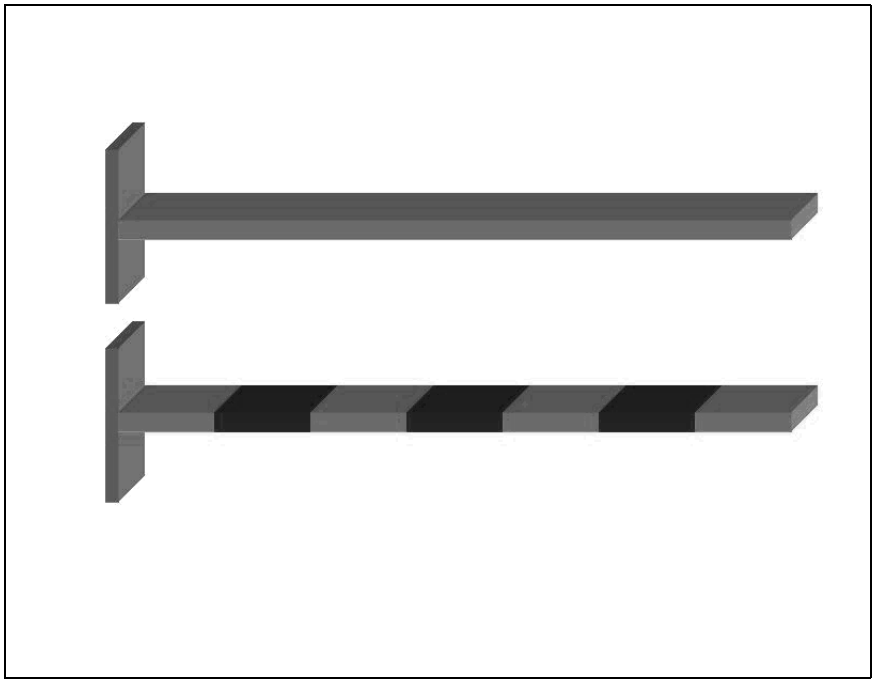

Figure A.6: Beam elements for the modified chain algorithm.

algorithm is based on small-deflection theory, similar to finite element analysis (FEA). First the flexible segment is broken up into a set number of smaller segments, as is shown in Figure A.6. Since the beam is broken up into small segments, using small deflection theory on each of the segments is reasonable. The accuracy would naturally improve as the size of the beam elements is reduced. Assuming that the beam is supplied with both a vertical force and a horizontal force results in equations A.8 - A.11 for any beam element[1]. Since only the tangential force will cause a deflection for these elements.

$$\theta_{F_i} = \frac{F_{T_i} {L_i}^2}{2EI}, \tag{A.8}$$

where F_{T_i} is the tangential load applied to the small segment; E is the modulus of elasticity; I is the moment of inertia, and L_i is the length of the element.

[1]As denoted by the subscript i

The deflection of the first element can also be determined and is given in Equation (A.9)

$$\delta_{F_i} = \frac{F_{T_i} {L_i}^3}{3EI}, \tag{A.9}$$

where δ_{F_i} is the deflection of the beam element. The next two equations describe deflection and rotation of the beam based on the applied moment M_i.

$$\theta_{M_i} = \frac{M_i L_i}{EI} \tag{A.10}$$

$$\delta_{M_i} = \frac{M_i {L_i}^2}{2EI} \tag{A.11}$$

Since the segments are undergoing small deflections, superposition can be used to find the total deflection for each of the individual segment. There are multiple methods of using these equations to determine the deflection of a long segment. However, all of these equations depend upon both the modulus of elasticity, and the area moment of inertia. Since it is desired to have a more general solution to this equation, a strategy for eliminating both of these terms in the equations was developed. upon examination of the to beam elements one at a time, it is not too difficult to see how to eliminate some of these undesired terms. Using the i^{th} and the $i+1^{th}$ beam segments and looking at the ratio of deflection between the two segments due to the force yields.

$$\frac{\delta_{F_{T_i}}}{\delta_{F_{T_{i+1}}}} = \frac{\frac{F_{T_i} {L_i}^3}{3EI}}{\frac{F_{T_{i+1}} {L_{i+1}}^3}{3EI}} \tag{A.12}$$

The same definition for the forces and moments as was used in Figure 2.4 and shown again here for convenience as Figure A.7. The tangential force that is applied to the each beam segment can be defined by

$$F_{T_i} = P\sqrt{cos^2(\psi_i) + n^2 sin^2(\psi_i)}. \tag{A.13}$$

Substituting this result into Equation (A.12) results[2] in

$$\frac{\delta_{F_{T_i}}}{\delta_{F_{T_{i+1}}}} = \frac{\sqrt{cos^2(\psi_i) + n^2 sin^2(\psi_i)}}{\sqrt{cos^2(\psi_{i+1}) + n^2 sin^2(\psi_{i+1})}}. \tag{A.14}$$

[2]Note that it is possible to continue this derivation, assuming that the lengths of the beam segments change throughout the beam. However for simplicity the segment lengths will be assumed to remain constant for the remainder of the discussion.

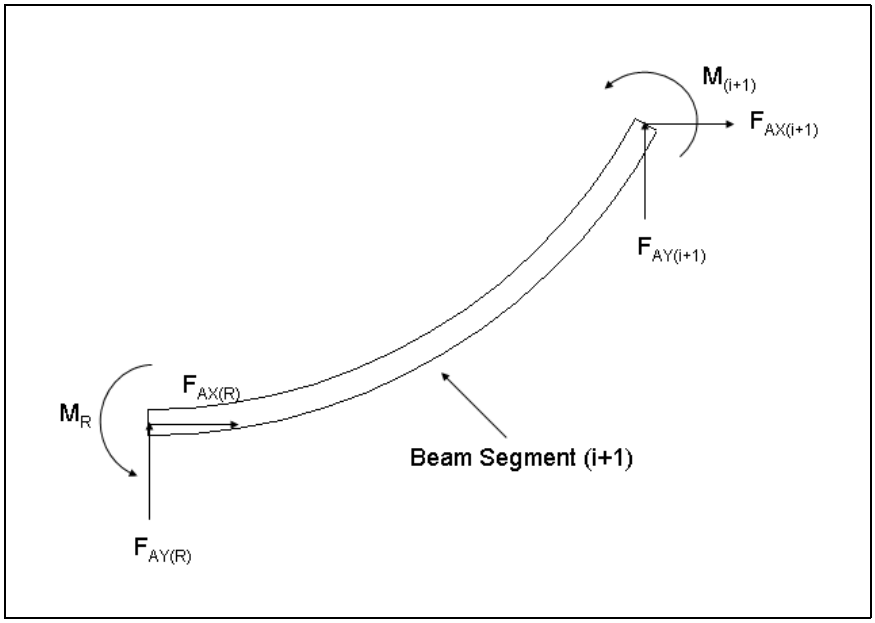

Figure A.7: A beam element (i+1) with applied end-force and moment loads.

Equation (A.14) shows that the only value required for determining the change in the rotation between any two segments is the value of n, and the value of the two angles (ψ_i and ψ_{i+1}) which define the orientation of each of the beam segments. Note that this factor is very nearly one for really small segment lengths. There are other similar ratios that allow for the complete elimination of the modulus of elasticity, and the moment of inertia of the beam. These are not discussed here in detail, however it should be apparent from the resulting equations presented here.

$$\frac{\theta_{F_{T_i}}}{\theta_{F_{T_{i+1}}}} = \frac{\sqrt{cos^2(\psi_i) + n^2 sin^2(\psi_i)}}{\sqrt{cos^2(\psi_{i+1}) + n^2 sin^2(\psi_{i+1})}} \tag{A.15}$$

$$\frac{\delta_{F_{T_i}}}{\theta_{F_{T_i}}} = \frac{2L}{3} \tag{A.16}$$

$$\frac{\delta_{M_i}}{\theta_{M_i}} = \frac{L}{2} \tag{A.17}$$

$$\theta_{M_{i+1}} = \theta_{M_i} - 2\sqrt{\frac{cos^2(\psi_{i+1}) + n^2 sin^2(\psi_{i+1})}{cos^2(\psi_i) + n^2 sin^2(\psi_i)}}\ \theta_{F_{T_i}} \tag{A.18}$$

$$\psi_{i+1} = \psi_i \ + \ \theta_{F_{T_i}} \ + \ \theta_{M_i} \tag{A.19}$$

With these equations the entire path of the beam can be determined from the length, the rotation of the end of the beam, the y-deflection and the ratio of the vertical and horizontal forces. The material properties and the geometry are not significant in determining the deflection path of the mechanism. Again the most powerful portion of this method is not from the use of the method, but from the mathematical validation that a model could be created that is independent of material, and cross section and is still capable of predicting the deflection of the beam.

Figure A.8 shows the results of applying the algorithm, as compared with the other techniques that have been presented. Please note that the modified chain algorithm and the element based solution both require iteration in order to solve the system of equations. This accounts for the slight variations between the two methods. If both were solved with greater precision, they would be identical. The advantage that comes from the modified chain algorithm is that the path of the beam and the deflection are no longer dependent upon the material properties. They can be solved without choosing the material. This work also shows a mathematical justification of the PRBM's ability to predict the path of a deflected segment without the required knowledge of material properties.

A.3 Application to curved Beams

The Bernoulli-Euler equation says the curvature of the beam depends on the moment applied to the beam at any given point, the relationship can be applied in reverse. Because the curvature of the beam is known, the force and moment that are required to get that curvature can be determined. Since the most useful curvature is usually the simplest case, the circular curvature is the most common in beams in part because it is easily modeled. The moment that is required is easily mapped back to a radius as

$$\frac{d\theta}{ds} = \frac{M}{EI} = \frac{1}{R} \tag{A.20}$$

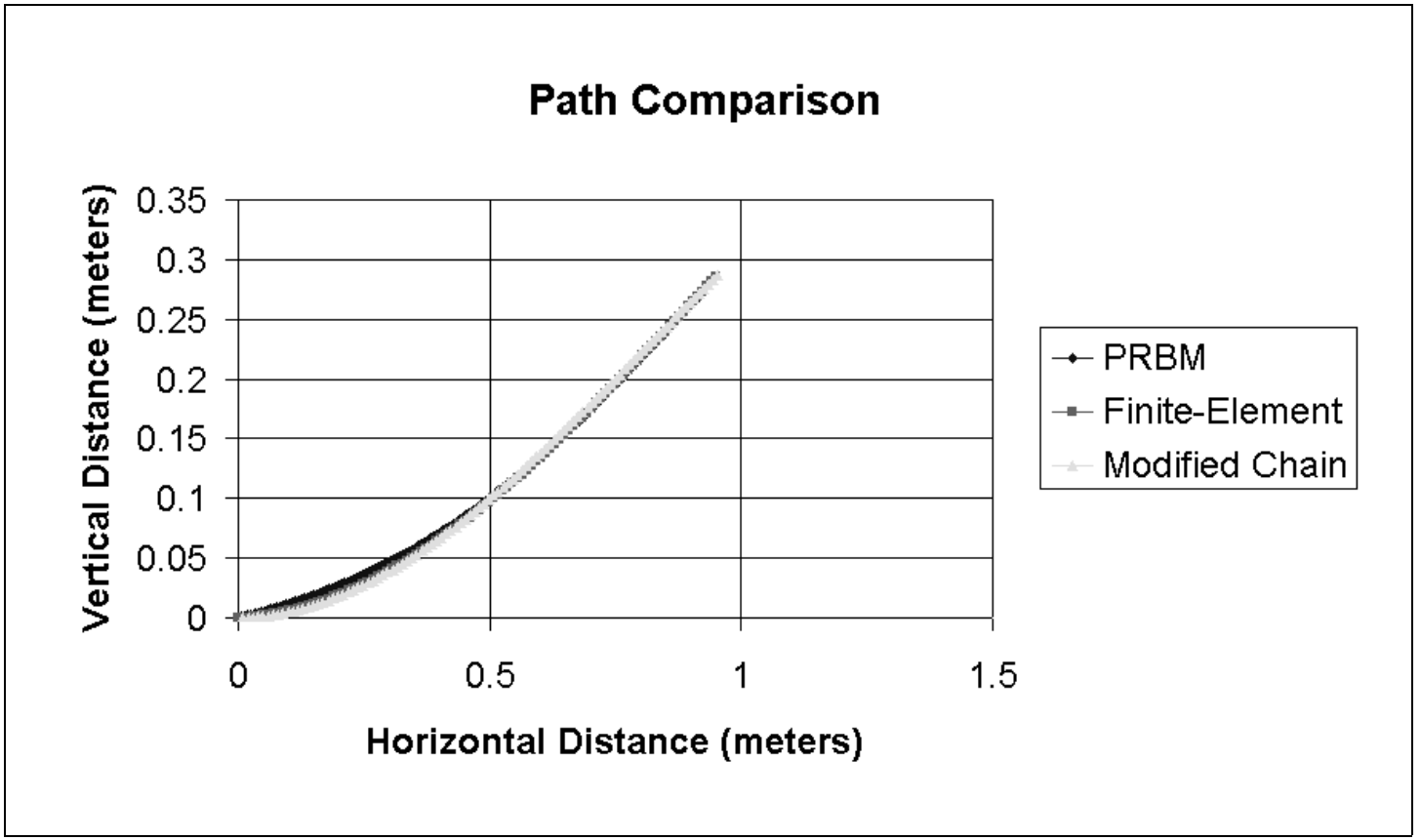

Figure A.8: A comparison of an element based solution, PRBM solution, and a modified chain algorithm solution.

Since the moment and radius of curvature of a circular beam are so readily interchangeable, the transformation between a curved beam and a beam with a moment load is simple. The path for the end of a moment loaded beam will have the same deflection path for the endpoint as a beam with a radius that satisfies Equation (A.20) The only difference is the amount of stress that is present in the beam.

Appendix B

Matlab Files

This section contains a sampling of the Matlab batch files that were used to model the compliant systems. The Matlab code is specific to the model for which it is presented. Many of them contain files that are called by the main file. All of the files from each section must be used for the complete model to work.

B.1 Micro Folded Beam PRBM

Main.m

```
clear all;
close all;
options = odeset('RelTol', 1e-4,'AbsTol',1e-6);
Length = 350; %micron
timinc = 0.0001;
TSPAN = 0:timinc:10.0;
[t,y] = ode45('micro',[TSPAN],[0,(0.035722/2)]);
%figure(1)
%plot(t,y(:,1))
figure(2)
plot(t,y(:,2))
figure(1)
i = 1;
n = 0;
yt = y(:,2);
```

```
ny = 2*0.85*Length*sin(y(:,2));
plot(t,ny)
temp = size(yt);
temp = temp(1);
while n < temp
      i = i + 1;
      n = 2^i;
end
Y = fft(yt,n);
Pyy = Y.*conj(Y)/n;
f = 1/timinc*(0:(n/2-1))/n;
Pyyh = Pyy(1:n/2);
[ Value,index] = max(Pyyh);
Frequency = f(index)
figure(3)
plot(f,Pyy(1:n/2))
FStep = f(10)-f(9)
```

micro.m

```
function xdot = micro(t,x)
Length = 35000;
E = 176e6;
rho1 = 2.330e-12;
gam = 0.85;
ktheta = 2.65;
K = 2*gam*ktheta*E*Length^ 3/1200000000;
Mass = 3*rho1*Length^ 3/1000;
xdot(1) = -16*K*x(2)/(4*gam*gam*Mass*Length*Length*cos(x(2)));
xdot(2) = x(1);
xdot = xdot';
```

B.2 Generic Four-bar Dynamic Model Applied to the Young Mechanism

main.m

```
clear;
time = 2.0; %Run time of the system.
theta_o = 0.75; % This is the angle where the mechanism starts from.
options = odeset('RelTol', 1e-4 ,'AbsTol',[ 1e-8 1e-8] );
[ t,x] = ode45('dynamics',[0.0 time],[theta_o 0.00],options);
%ode45('dynamics',[ 0.0 time] ,[theta_o 0.00],options);
load Data.txt;
for i = 1:size(x(:,1))

        Output = gstress(x(i,1), Data);

        Stress1(i) = Output(1);

        Stress2(i) = Output(2);

        Stress3(i) = Output(3);

        Stress4(i) = Output(4);

        theta_3(i) = Output(5);

        theta_4(i) = Output(6);
end
st1 = Data(18)*ones(size(x(:,1)));
st2 = Data(19)*ones(size(x(:,1)));
st3 = Data(20)*ones(size(x(:,1)));
st4 = Data(21)*ones(size(x(:,1)));
figure(1);
plot(t,x(:,1),t,theta_3,'-',t,theta_4,'.');
title('Time plot angles');
xlabel('time');
ylabel('radians');
```

```
legend('theta_2','theta_3','theta_4');
figure(2);
plot(t,x(:,2));
title('Time plot theta_{2d}');
xlabel('time');
ylabel('radians/second');
figure(3);
plot(t,Stress1,t,st1,'.',t,-st1,'.');
title('Time Plot Stress Joint 1');
xlabel('Time');
ylabel('Stress');
legend('Stress Value','Frac U B','Frac L B');
figure(4);
plot(t,Stress2,t,st2,'.',t,-st2,'.');
title('Time Plot Stress Joint 2');
xlabel('Time');
ylabel('Stress');
legend('Stress Value','Frac U B','Frac L B');
figure(5);
plot(t,Stress3,t,st3,'.',t,-st3,'.');
title('Time Plot Stress Joint 3');
xlabel('Time');
ylabel('Stress');
legend('Stress Value','Frac U B','Frac L B');
figure(6);
plot(t,Stress4,t,st4,'.',t,-st4,'.');
title('Time Plot Stress Joint 4');
xlabel('Time');
ylabel('Stress');
legend('Stress Value','Frac U B','Frac L B');
```

dynamics.m

```
function xdot = vdpol(t,x)
theta_2 = x(1);
theta_2d = x(2);
Write = 0;
if( t < 0.000000001 )

      Write = 1;
end
%Stresses
xdot = [ theta_2d; theta_2dd(theta_2,theta_2d, Write)] ;
```

theta_2dd.m

```
function output = theta_pre(theta_2,theta_2d, Write);
b = 0.000002; %a form of damping
%theta_2o is the angle at which the mechanism is at rest
theta_2o = 0.296705973;
%These are limiters for the possible range of motion
%typically these should not be canged
limita = 2*pi;
limitb = -2*pi;
%Adjustments for the masses
%This progam assumes that it is given the mas at the center of mass
m_2 = 0.00445414;
m_3 = 0.105;%Kg
m_4 = 0.00706346;
%Rotational Inertia should be around the center of mass
I_2 = 1.6e-6;
I_3 = 6.0586e-4;
I_4 = 2.118e-5;
%Used to avoid devison by Zero
```

```
Z = 0.0000000001;
%Thicknesses (meters) Out of Plane
t_1 = 0.0127;
t_2 = 0.0127;
t_3 = 0.0127;
t_4 = 0.0127;
%Height of the sements (meters)
h_1 = 0;
h_2 = 0.005;
h_3 = 0.003;
h_4 = 0;
%Area Inertia (meters^ 4)
AI_1 = (t_1*h_1^ 3)/12;
AI_2 = (t_2*h_2^ 3)/12;
AI_3 = (t_3*h_3^ 3)/12;
AI_4 = (t_4*h_4^ 3)/12;
% Flexible segment lengths (meters) If Zero use Z
L_1 = Z;
L_2 = 0.06525;
L_3 = 0.18974;
L_4 = Z;
%Modulas of Elasticity (Pascals)
E_1 = 1378950000;
E_2 = 1378950000;
E_3 = 1378950000;
E_4 = 1378950000;
%Yield Stress (Pascals)
st1 = 31000000;
st2 = 31000000;
st3 = 31000000;
```

```
st4 = 31000000;
%Link Lengths Set link length on two, and the multiple for each of the others
r_2 = 0.05546471; %meters
c_1 = 1.37797;
c_3 = 3.40836;
c_4 = 2.90775;
%Locations for the ceters of mass
%assumes that these are taken from the first joint on the link
%link 2
a_2cm = r_2/2;
b_2cm = 0.00;
%Link 3
a_3cm = .13102082;
b_3cm = 0.02461006;
%Link 4
a_4cm = c_4*r_2/2;
b_4cm = 0.00;
%Stiffness
%SLFP K = E*I/length
%Fixed pinned K = gam*Ktheta*E_i*AI_i/L_i
%Fixed Guided K = 2*gam*Ktheta*E_i*AI_i/L_i
gam = 0.85;
Ktheta = 2.65;
%spring constants calculated using PRBM technique.
k_1 = 0;
k_2 = 0;
k_3 = 0;
k_4 = 0;
if( L_1 > Z)
```

```
        k_1 = E_1*AI_1/L_1;
end
if( L_2 > Z)

        k_2 = gam*Ktheta*E_2*AI_2/L_2;
end
if( L_3 > Z)

        k_3 = gam*Ktheta*E_2*AI_2/L_2;
end
if( L_4 > Z)

        k_4 = E_4*AI_4/L_4;
end
k_1 = 0;
k_2 = 0;
k_3 = 0;
k_4 = 0;
%Nothing below this line should ever be changed!!!!!!!!!!!
%These parameters are for use in the computations
zero = 0.000000001;
flag = 0.0;
%Link Lengths
r_3 = c_3*r_2;
r_4 = c_4*r_2;
r_1 = c_1*r_2;
if (Write)
```

```
        save Data.txt theta_2o AI_1 AI_2 AI_3 AI_4 r_1 r_2 r_3 r_4 k_1 k_2 k_3 k_4 t_1
        t_2 t_3 t_4 st1 st2 st3 st4 -ASCII

end
%Four bar model is built into angles.
temp = angles(r_1,r_2,r_3,r_4,theta_2o);
%theta_2o = temp(1);
theta_3o = temp(2);
theta_4o = temp(3);
%Four bar model is built into angles
temp = angles(r_1,r_2,r_3,r_4,theta_2);
%theta_2 = temp(2);
theta_3 = temp(2);
theta_4 = temp(3);
%Calculates the deflection from steady state conditions
psi_1 = theta_2-theta_2o;
psi_2 = theta_2-theta_2o -(theta_3-theta_3o);
psi_3 = theta_4-theta_4o -(theta_3-theta_3o);
psi_4 = theta_4-theta_4o;
%This is simply a chech to see if the following equation are going to work.
sin34 = sin(theta_3-theta_4);
if(abs(sin34) < zero)


        sin34 = zero;

        flag = flag+1

end;
%Calculates the kinematic coefficients
h32 = (r_2*sin(theta_4-theta_2))/(r_3*sin34);
h42 = (r_2*sin(theta_3-theta_2))/(r_4*sin34);
%Calculates the derivative of the kinematic coefficients
```

h32da = r_3*r_2*sin(theta_3-theta_4)*cos(theta_4-theta_2)*(theta_2d*h42-theta_2d);

h32db = -r_2*r_3*sin(theta_4-theta_2)*cos(theta_3-theta_4)*(theta_2d*h32-theta_2d*h42);

h32d = (h32da+h32db)/(r_3*(sin34))^ 2;

h42da = r_4*r_2*sin(theta_3-theta_4)*cos(theta_3-theta_2)*(theta_2d*h32-theta_2d);

h42db = -r_2*r_4*sin(theta_3-theta_2)*cos(theta_3-theta_4)*(theta_2d*h32-theta_2d*h42);

h42d = (h42da+h42db)/(r_4*(sin34))^ 2;

%The rest of this is the dynamic equations of motion

ph32a = r_3*r_2*sin(theta_3-theta_4)*cos(theta_4-theta_2)*(h42-1.00);

ph32b = -r_2*r_3*sin(theta_4-theta_2)*cos(theta_3-theta_4)*(h32-h42);

ph32 = (ph32a+ph32b)/(r_3*(sin34))^ 2;

ph42a = r_4*r_2*sin(theta_3-theta_4)*cos(theta_3-theta_2)*(h32-1.00);

ph42b = -r_2*r_4*sin(theta_3-theta_2)*cos(theta_3-theta_4)*(h32-h42);

ph42 = (ph32a+ph32b)/(r_3*(sin34))^ 2;

v_3cm = theta_2d*sqrt((a_3cm*h32+r_2*cos(theta_2-theta_3))^ 2+(b_3cm*h32+r_2*sin(theta_2-theta_3))$\hat{2}$);

a1 = (a_3cm*h32+r_2*cos(theta_2-theta_3))*(a_3cm*ph32-r_2*sin(theta_2-theta_3)*(1-h32));

a2 = (b_3cm*h32+r_2*sin(theta_2-theta_3))*(b_3cm*ph32+r_2*cos(theta_2-theta_3)*(1-h32));

a3 = (a_3cm*h32+r_2*cos(theta_2-theta_3))^ 2+(b_3cm*h32+r_2*sin(theta_2-theta_3))$\hat{2}$;

if(abs(a3) < zero)

    a3 = zero;

    flag = flag+1

end;

pv_3cm = (a1+a2)*theta_2d/(sqrt(a3));

v_4cm = theta_2d*h42*sqrt(a_4cm^ 2+b_4cm$\hat{2}$);

pv_4cm = theta_2d*ph42*sqrt(a_4cm^ 2+b_4cm$\hat{2}$);

temp1 = m_2*(a_2cm^ 2+b_2cm$\hat{2}$)+ m_4*h42$\hat{2}$*(a_4cm$\hat{2}$+b_4cm$\hat{2}$);

```
temp2 = 2*m_4*theta_2d*h42d*(a_4cm^ 2+b_4cm2̂);
temp3 = m_3*((a_3cm*h32+r_2*cos(theta_2-theta_3))^ 2+(b_3cm*h32+r_2*sin(theta_2-
theta_3))2̂);
at1 = (a_3cm*h32+r_2*cos(theta_2-theta_3))*(a_3cm*h32d-r_2*sin(theta_2-theta_3)*(theta_2d-
theta_2d*h32));
at2 = (b_3cm*h32+r_2*sin(theta_2-theta_3))*(b_3cm*h32d+r_2*cos(theta_2-theta_3)*(theta_2d-
theta_2d*h32));
temp4 = 2*m_3*theta_2d*(at1+at2);
temp5 = I_2+I_3*h32^ 2+I_4*h422̂;
temp6 = 2*I_3*h32d*theta_2d+2*I_4*theta_2d*h42d;
temp7 = m_3*v_3cm*pv_3cm+m_4*v_4cm*pv_4cm+I_3*theta_2d^ 2*h32*ph32+I_4*theta_2d2̂*h
temp8 = -potential_d(theta_2);
temp9 = temp2+temp4+temp6-temp7-temp8 + b*theta_2d;
den = (temp1+temp3+temp5);
if(abs(den) < zero)


    den = zero;

    flag = flag+1

end
theta_2dd = -temp9/den;
output = [ theta_2dd] ;
```

angles.m

```
function output = angles(r_1, r_2, r_3, r_4, theta_2a )
load Young_old.txt
theta2 = Young_old(:,1);
theta3 = Young_old(:,2);
theta4 = Young_old(:,3);
theta_3a = interp1(theta2,theta3,theta_2a,'spline');
```

```
theta_4a = interp1(theta2,theta4,theta_2a,'spline');
output = [ theta_2a, theta_3a, theta_4a] ;
```

potential_d.m

```
function output = potential_d( theta_2a )
load Potential_data.txt
theta2 = Potential_data(:,1);
p_d = Potential_data(:,2);
Potential = interp1(theta2,p_d,theta_2a,'spline');
output = [ Potential] ;
```

B.3 Generic Four-bar Dynamic Model Applied to the Roberts Straight Line Mechanism

main.m

```
clear;
time = 0.002; %Run time of the system.
theta_o = 1.317; % This is the angle where the mechanism starts from.
options = odeset('RelTol', 1e-4,'AbsTol',1e-6);
timinc = 0.000001;
TSPAN = 0:timinc:time;
options = odeset('RelTol', 1e-5,'AbsTol',[ 1e-4 1e-4] );
[ t,x] = ode45('dynamics',[0.0 time],[theta_o 0.00],options);
%ode45('dynamics',[ 0.0 time] ,[theta_o 0.00],options);
load Data.txt;
yt = x(:,1);
for i = 1:size(x(:,1))
    Output = gstress(x(i,1), Data);

    Stress1(i) = Output(1);
```

```
        Stress2(i) = Output(2);

        Stress3(i) = Output(3);

        Stress4(i) = Output(4);

        theta_3(i) = Output(5);

        theta_4(i) = Output(6);

end
r_2 = 900;
for j = 1:size(x(:,1))


        xp(j) = r_2*cos(x(j,1))+r_2/2*cos(theta_3(j))+(r_2/sqrt(2)+r_2*(1-.85)/.85*sin(pi/3))*sin

        yp(j) = r_2*sin(x(j,1))+r_2/2*sin(theta_3(j))-(r_2/sqrt(2)+r_2*(1-.85)/.85*sin(pi/3))*cos(t

end
xp = xp - 900;
st1 = Data(18)*ones(size(x(:,1)));
st2 = Data(19)*ones(size(x(:,1)));
st3 = Data(20)*ones(size(x(:,1)));
st4 = Data(21)*ones(size(x(:,1)));
figure(1);
plot(t,x(:,1),t,theta_3,'--',t,theta_4,'.');
title('Time plot angles');
xlabel('time');
ylabel('radians');
legend('\ theta_2','\ theta_3','\ theta_4');
figure(2);
plot(t,x(:,2));
title('Time plot theta_{2d}');
xlabel('time');
```

```
ylabel('radians/second');
figure(3);
plot(t,Stress1,t,st1,'.',t,-st1,'.');
title('Time Plot Stress Joint 1');
xlabel('Time');
ylabel('Stress');
legend('Stress Value','Frac U B','Frac L B');
figure(4);
plot(t,Stress2,t,st2,'.',t,-st2,'.');
title('Time Plot Stress Joint 2');
xlabel('Time');
ylabel('Stress');
legend('Stress Value','Frac U B','Frac L B');
figure(5);
plot(t,Stress3,t,st3,'.',t,-st3,'.');
title('Time Plot Stress Joint 3');
xlabel('Time');
ylabel('Stress');
legend('Stress Value','Frac U B','Frac L B');
figure(6);
plot(t,Stress4,t,st4,'.',t,-st4,'.');
title('Time Plot Stress Joint 4');
xlabel('Time');
ylabel('Stress');
legend('Stress Value','Frac U B','Frac L B');
figure(7)
plot(t,xp);
title('Time Plot X Deflection');
xlabel('Time');
ylabel('X Deflection (micron)');
```

```
legend('X Deflection (micron)');
figure(8)
plot(t,yp);
title('Time Plot Y Deflection');
xlabel('Time');
ylabel('Y Deflection (micron)');
legend('Y Deflection (micron)');
i = 1;
n = 0;
temp = size(yt);
temp = temp(1);
while n < temp


    i = i + 1;

    n = 2^ i;

end
Y = fft(yt,n);
Pyy = Y.*conj(Y)/n;
f = 1/timinc*(0:(n/2-1))/n;
Pyyh = Pyy(1:n/2);
[ Value,index] = max(Pyyh);
Frequency = f(index)
figure(9)
plot(f,Pyy(1:n/2))
FStep = f(10)-f(9)
```

dynamics.m

```
function xdot = vdpol(t,x)
theta_2 = x(1);
theta_2d = x(2);
Write = 0;
if( t < 0.000000001 )


    Write = 1;

end
%Stresses
xdot = [ theta_2d; theta_2dd(theta_2,theta_2d, Write)] ;
```

theta_2dd.m

```
function output = theta_pre(theta_2,theta_2d, Write);
b = 2e-30; %a form of damping
%theta_2o is the angle at which the mechanism is at rest
theta_2o = pi/3;
flag = 0;
flag2 = 0;
flag3 = 0;
%These are limiters for the possible range of motion
%typically these should not be canged
limita = 2*pi;
limitb = -2*pi;
%Adjustments for the masses
%This progam assumes that it is given the mas at the center of mass
m_2 = 0;%1.98e-10;
m_3 = 3.54e-9;%Kg
m_4 = 0;%1.98e-10;
%Rotational Inertia should be around the center of mass
```

I_2 = 0;

I_3 = 8.51e-18;

I_4 = 0;

%Used to avoid devison by Zero

Z = 1e-25;

zero = 1e-25;

%Area Inertia (meters^ 4)

AI_1 = 6.37875e-22;

AI_2 = 6.37875e-22;

AI_3 = 6.37875e-22;

AI_4 = 6.37875e-22;

%Thicknesses (meters)

t_1 = 9e-6;

t_2 = 9e-6;

t_3 = 9e-6;

t_4 = 9e-6;

% Flexible segment lengths (meters) If Zero use Z

L_1 = 900e-6/.85;

L_2 = 900e-6/.85;

L_3 = 900e-6/.85;

L_4 = 900e-6/.85;

%Modulas of Elasticity (Pascals)

E_1 = 176e9;

E_2 = 176e9;

E_3 = 176e9;

E_4 = 176e9;

%Yield Stress (Pascals)

st1 = 137895000;

st2 = 137895000;

st3 = 137895000;

```
st4 = 137895000;
%Link Lengths Set link length on two, and the multiple for each of the others
r_2 = 900e-6; %meters
c_1 = 2;
c_3 = 1;
c_4 = 1;
%Locations for the ceters of mass
%assumes that these are taken from the first joint on the link
%link 2
a_2cm = r_2/2;
b_2cm = 0.00;
%Link 3
a_3cm = (c_3*r_2)/2.00;
b_3cm = -140e-6;
%Link 4
a_4cm = c_4*r_2/2;
b_4cm = 0.00;
%Stiffness
%SLFP K = E*I/length
%Fixed pinned K = gam*Ktheta*E*I/length
%Fixed Guided K = 2*gam*Ktheta*E*I/length
%spring constants calculated using PRBM technique.
k_1 = 0;
k_2 = 0;
k_3 = 0;
k_4 = 0;
```

```
if( L_1 > Z)
    k_1 = 2*0.85*3.4*E_1*AI_1/L_1;
end
if( L_2 > Z)
    k_2 = 2*0.85*1.45*E_2*AI_2/L_2;
end
if( L_3 > Z)
    k_3 = 2*0.85*1.45*E_3*AI_3/L_3;
end
if( L_4 > Z)
    k_4 = 2*0.85*3.4*E_4*AI_4/L_4;
end
%Nothing below this line should ever be changed!!!!!!!!!!!
%With the exception of the fixed-fixed model,
%These parameters are for use in the computations
%Link Lengths
r_3 = c_3*r_2;
r_4 = c_4*r_2;
r_1 = c_1*r_2;
if (Write)
    save Data.txt theta_2o AI_1 AI_2 AI_3 AI_4 r_1 r_2 r_3 r_4 k_1 k_2 k_3 k_4 t_1
    t_2 t_3 t_4 st1 st2 st3 st4 -ASCII
```

```
end
%Four bar model is built into angles.
temp = angles(r_1,r_2,r_3,r_4,theta_2o);
%theta_2o = temp(1);
theta_3o = temp(2);
theta_4o = temp(3);
%Four bar model is built into angles
temp = angles(r_1,r_2,r_3,r_4,theta_2);
%theta_2 = temp(2);
theta_3 = temp(2);
theta_4 = temp(3);
%Calculates the deflection from steady state conditions
psi_1 = theta_2-theta_2o;
psi_2 = theta_2-theta_2o - (theta_3-theta_3o);
psi_3 = theta_4-theta_4o - (theta_3-theta_3o);
psi_4 = theta_4-theta_4o;
psi_3m = -(theta_3-theta_3o);
psi_2m = -(theta_3-theta_3o);
%This is simply a chech to see if the following equation are going to work.
sin34 = sin(theta_3-theta_4);
if(abs(sin34) < zero)


    sin34 = zero;

    flag = flag+1

end;
%Calculates the kinematic coefficients
h32 = (r_2*sin(theta_4-theta_2))/(r_3*sin34);
h42 = (r_2*sin(theta_3-theta_2))/(r_4*sin34);
%Calculates the derivative of the kinematic coefficients
```

```
h32da = r_3*r_2*sin(theta_3-theta_4)*cos(theta_4-theta_2)*(theta_2d*h42-theta_2d);
h32db = -r_2*r_3*sin(theta_4-theta_2)*cos(theta_3-theta_4)*(theta_2d*h32-theta_2d*h42);
h32d = (h32da+h32db)/(r_3*(sin34))^ 2;
h42da = r_4*r_2*sin(theta_3-theta_4)*cos(theta_3-theta_2)*(theta_2d*h32-theta_2d);
h42db = -r_2*r_4*sin(theta_3-theta_2)*cos(theta_3-theta_4)*(theta_2d*h32-theta_2d*h42);
h42d = (h42da+h42db)/(r_4*(sin34))^ 2;
%The rest of this is the dynamic equations of motion
ph32a = r_3*r_2*sin(theta_3-theta_4)*cos(theta_4-theta_2)*(h42-1.00);
ph32b = -r_2*r_3*sin(theta_4-theta_2)*cos(theta_3-theta_4)*(h32-h42);
ph32 = (ph32a+ph32b)/(r_3*(sin34))^ 2;
ph42a = r_4*r_2*sin(theta_3-theta_4)*cos(theta_3-theta_2)*(h32-1.00);
ph42b = -r_2*r_4*sin(theta_3-theta_2)*cos(theta_3-theta_4)*(h32-h42);
ph42 = (ph32a+ph32b)/(r_3*(sin34))^ 2;
v_3cm = theta_2d*sqrt((a_3cm*h32+r_2*cos(theta_2-theta_3))^ 2+(b_3cm*h32+r_2*sin(theta_2-
theta_3))2^);
a1 = (a_3cm*h32+r_2*cos(theta_2-theta_3))*(a_3cm*ph32-r_2*sin(theta_2-theta_3)*(1-
h32));
a2 = (b_3cm*h32+r_2*sin(theta_2-theta_3))*(b_3cm*ph32+r_2*cos(theta_2-theta_3)*(1-
h32));
a3 = (a_3cm*h32+r_2*cos(theta_2-theta_3))^ 2+(b_3cm*h32+r_2*sin(theta_2-theta_3))2^;
if( abs(a3) < zero)


      a3 = zero;

      flag2 = flag2+1

end;
pv_3cm = (a1+a2)*theta_2d/(sqrt(a3));
v_4cm = theta_2d*h42*sqrt(a_4cm^ 2+b_4cm2^);
pv_4cm = theta_2d*ph42*sqrt(a_4cm^ 2+b_4cm2^);
temp1 = m_2*(a_2cm^ 2+b_2cm2^)+ m_4*h422^*(a_4cm2^+b_4cm2^);
```

```
temp2 = 2*m_4*theta_2d*h42d*(a_4cm^ 2+b_4cm2̂);
temp3 = m_3*((a_3cm*h32+r_2*cos(theta_2-theta_3))^ 2+(b_3cm*h32+r_2*sin(theta_2-
theta_3))2̂);
at1 = (a_3cm*h32+r_2*cos(theta_2-theta_3))*(a_3cm*h32d-r_2*sin(theta_2-theta_3)*(theta_2d-
theta_2d*h32));
at2 = (b_3cm*h32+r_2*sin(theta_2-theta_3))*(b_3cm*h32d+r_2*cos(theta_2-theta_3)*(theta_2d-
theta_2d*h32));
temp4 = 2*m_3*theta_2d*(at1+at2);
temp5 = I_2+I_3*h32^ 2+I_4*h42̂2;
temp6 = 2*I_3*h32d*theta_2d+2*I_4*theta_2d*h42d;
temp7 = m_3*v_3cm*pv_3cm+m_4*v_4cm*pv_4cm+I_3*theta_2d^ 2*h32*ph32+I_4*theta_2d2̂*h42*ph4
%The following line is only for the modified model for fixed-fixed flexible segments
temp8 = (-2*k_1*psi_1+k_2*psi_2m*(h32)-2*k_4*psi_4*h42+k_3*psi_3m*(h32));
temp9 = temp2+temp4+temp6-temp7-temp8 + b*theta_2d;
den = (temp1+temp3+temp5);
if(abs(den) < zero)

      den = zero;

      flag3 = flag3+1
end
theta_2dd = -temp9/den;
output = [ theta_2dd] ;
```

angles.m

```
function output = angles(r_1, r_2, r_3, r_4, theta_2 )
load rob900.txt
theta2 = rob900(:,1);
theta3 = rob900(:,2);
theta4 = rob900(:,3);
theta_3 = interp1(theta2,theta3,theta_2,'spline');
theta_4 = interp1(theta2,theta4,theta_2,'spline');
```

```
%differ = theta_2 - theta_4
output = [ theta_2, theta_3, theta_4] ;
```

B.4 Generic Four-bar Dynamic Model Applied to the Cross-Axis Flexural Pivot

main.m

```
clear all;
time = 40.00; %Run time of the system.
theta_o = pi*3/4+.413; % This is the angle where the mechanism starts from.
options = odeset('RelTol', 1e-5 ,'AbsTol',[ 1e-4 1e-4] );
[ t,x] = ode45('dynamics',[0.0 time],[theta_o 0.00],options);
%ode45('dynamics',[ 0.0 time] ,[theta_o 0.00],options);
load Data.txt;
for i = 1:size(x(:,1))


    Output = gstress(x(i,1), Data);

    Stress1(i) = Output(1);

    Stress2(i) = Output(2);

    Stress3(i) = Output(3);

    Stress4(i) = Output(4);

    theta_3(i) = Output(5);

    theta_4(i) = Output(6);

end
theta_2 = x(:,1);
st1 = Data(18)*ones(size(x(:,1)));
```

```
st2 = Data(19)*ones(size(x(:,1)));
st3 = Data(20)*ones(size(x(:,1)));
st4 = Data(21)*ones(size(x(:,1)));
figure(1);
plot(t,x(:,1),t,theta_3,'-',t,theta_4,'.');
title('Time plot angles');
xlabel('time');
ylabel('radians');
legend('\ theta_2','\ theta_3','\ theta_4');
figure(2);
plot(t,x(:,2));
title('Time plot theta_{2d}');
xlabel('time');
ylabel('radians/second');
if 0
        figure(3);
        plot(t,Stress1,t,st1,'.',t,-st1,'.');
        title('Time Plot Stress Joint 1');
        xlabel('Time');
        ylabel('Stress');
        legend('Stress Value','Frac U B','Frac L B');
        figure(4);
        plot(t,Stress2,t,st2,'.',t,-st2,'.');
        title('Time Plot Stress Joint 2');
        xlabel('Time');
```

```
        ylabel('Stress');

        legend('Stress Value','Frac U B','Frac L B');

        figure(5);

        plot(t,Stress3,t,st3,'.',t,-st3,'.');

        title('Time Plot Stress Joint 3');

        xlabel('Time');

        ylabel('Stress');

        legend('Stress Value','Frac U B','Frac L B');

        figure(6);

        plot(t,Stress4,t,st4,'.',t,-st4,'.');

        title('Time Plot Stress Joint 4');

        xlabel('Time');

        ylabel('Stress');

        legend('Stress Value','Frac U B','Frac L B');
end
temp = angles(1,2,3,4,pi/4);
theta2_o = temp(1);
theta3_o = temp(2);
theta4_o = temp(3);
b3 = 1.798;
figure(7)
x1 = 28.85*cos(theta_2')+(20.4+1.798)*cos(theta_3)-b3*sin(theta_3);
y1 = 28.85*sin(theta_2')+(20.4+1.798)*sin(theta_3)+b3*cos(theta_3);
plot(x1,y1)
figure(8)
```

```
plot(t,x1)
figure(9)
plot(t,y1)
```

dynamics.m

```
function xdot = vdpol(t,x)
theta_2 = x(1);
theta_2d = x(2);
Write = 0;
if( t < 0.000000001 )

    Write = 1;

end
%Stresses
xdot = [ theta_2d; theta_2dd(theta_2,theta_2d, Write)] ;
```

theta_2dd.m

```
function output = theta_pre(theta_2,theta_2d, Write);
b = 0.0000002; %a form of damping
%theta_2o is the angle at which the mechanism is at rest
theta_2o = 3*pi/4;
%These are limiters for the possible range of motion
%typically these should not be canged
limita = 2*pi;
limitb = -2*pi;
%Adjustments for the masses
%This progam assumes that it is given the mas at the center of mass
m_2 = 0.169;
m_3 = 4*0.119+0.0254;%Kg
m_4 = 0.169;
```

%Rotational Inertia should be around the center of mass

I_2 = m_2*(0.7328)^ 2/12;

I_3 = m_3*(0.6096)^ 2/12;

I_4 = m_4*(0.7328)^ 2/12;

%Used to avoid devison by Zero

Z = 0.0000000001;

%Area Inertia (meters^ 4)

AI_1 = 1.323164e-12;

AI_2 = 1.323164e-12;

AI_3 = 1.323164e-12;

AI_4 = 1.323164e-12;

%Thicknesses (meters)

t_1 = 0.00079375;

t_2 = 0.00079375;

t_3 = 0.00079375;

t_4 = 0.00079375;

% Flexible segment lengths (meters) If Zero use Z

L_1 = 0.8621;

L_2 = 0.8621;

L_3 = 0.8621;

L_4 = 0.8621;

%Modulas of Elasticity (Pascals)

E_1 = 206800000000;

E_2 = 206800000000;

E_3 = 206800000000;

E_4 = 206800000000;

%Yield Stress (Pascals)

st1 = 137895000;

st2 = 137895000;

st3 = 137895000;

```
st4 = 137895000;
%Link Lengths Set link length on two, and the multiple for each of the others
r_2 = 0.73279; %meters
c_1 = -.7071;
c_3 = .7071;
c_4 = 1;
%Locations for the ceters of mass
%assumes that these are taken from the first joint on the link
%link 2
a_2cm = 0.00;
b_2cm = 0.00;
%Link 3
a_3cm = (c_3*r_2)/2.00;
b_3cm = 0.065;
%Link 4
a_4cm = 0.00;
b_4cm = 0.00;
%Stiffness
%SLFP K = E*I/length
%Fixed pinned K = gam*Ktheta*E*I/length
%Fixed Guided K = 2*gam*Ktheta*E*I/length
%spring constants calculated using PRBM technique.
k_1 = 0;
k_2 = 0;
k_3 = 0;
k_4 = 0;
if( L_1 > Z)
    k_1 = 2*0.85*1.75*E_1*AI_1/L_1;
    %k_1 = 2*0.85*2.65*E_1*AI_1/L_1;
```

```
end
if( L_2 > Z)

    k_2 = 2*0.85*1.25*E_2*AI_2/L_2;

    %k_2 = 2*0.85*0*E_2*AI_2/L_2;

end
if( L_3 > Z)

    k_3 = 2*0.85*1.25*E_3*AI_3/L_3;

    %k_3 = 2*0.85*0*E_3*AI_3/L_3;

end
if( L_4 > Z)

    k_4 = 2*0.85*1.75*E_4*AI_4/L_4;

    %k_4 = 2*0.85*2.65*E_4*AI_4/L_4;

end
%Nothing below this line should ever be changed!!!!!!!!!!!
%With the exception of the fixed-fixed model,
%These parameters are for use in the computations
zero = 0.000000001;
flag = 0.0;
%Link Lengths
r_3 = c_3*r_2;
r_4 = c_4*r_2;
r_1 = c_1*r_2;
if (Write)
```

```
    save Data.txt theta_2o AI_1 AI_2 AI_3 AI_4 r_1 r_2 r_3 r_4 k_1 k_2 k_3 k_4 t_1
    t_2 t_3 t_4 st1 st2 st3 st4 -ASCII

end
%Four bar model is built into angles.
temp = angles(r_1,r_2,r_3,r_4,theta_2o);
%theta_2o = temp(1);
theta_3o = temp(2);
theta_4o = temp(3);
%Four bar model is built into angles
temp = angles(r_1,r_2,r_3,r_4,theta_2);
%theta_2 = temp(2);
theta_3 = temp(2);
theta_4 = temp(3);
%figure(12)
%plot(theta_2,theta_4,'x')
%hold on
%plot(theta_2,theta_3,'o')
%Calculates the deflection from steady state conditions
psi_1 = theta_2-theta_2o;
psi_2 = theta_2-theta_2o - (theta_3-theta_3o);
psi_3 = theta_4-theta_4o - (theta_3-theta_3o);
psi_4 = theta_4-theta_4o;
psi_3m = -(theta_3-theta_3o);
psi_2m = -(theta_3-theta_3o);
%This is simply a chech to see if the following equation are going to work.
sin34 = sin(theta_3-theta_4);
if(abs(sin34) < zero)

    sin34 = zero;

    flag = flag+1
```

```
end;
%Calculates the kinematic coefficients
h32 = (r_2*sin(theta_4-theta_2))/(r_3*sin34);
h42 = (r_2*sin(theta_3-theta_2))/(r_4*sin34);
%Calculates the derivative of the kinematic coefficients
h32da = r_3*r_2*sin(theta_3-theta_4)*cos(theta_4-theta_2)*(theta_2d*h42-theta_2d);
h32db = -r_2*r_3*sin(theta_4-theta_2)*cos(theta_3-theta_4)*(theta_2d*h32-theta_2d*h42);
h32d = (h32da+h32db)/(r_3*(sin34))^ 2;
h42da = r_4*r_2*sin(theta_3-theta_4)*cos(theta_3-theta_2)*(theta_2d*h32-theta_2d);
h42db = -r_2*r_4*sin(theta_3-theta_2)*cos(theta_3-theta_4)*(theta_2d*h32-theta_2d*h42);
h42d = (h42da+h42db)/(r_4*(sin34))^ 2;
%The rest of this is the dynamic equations of motion
ph32a = r_3*r_2*sin(theta_3-theta_4)*cos(theta_4-theta_2)*(h42-1.00);
ph32b = -r_2*r_3*sin(theta_4-theta_2)*cos(theta_3-theta_4)*(h32-h42);
ph32 = (ph32a+ph32b)/(r_3*(sin34))^ 2;
ph42a = r_4*r_2*sin(theta_3-theta_4)*cos(theta_3-theta_2)*(h32-1.00);
ph42b = -r_2*r_4*sin(theta_3-theta_2)*cos(theta_3-theta_4)*(h32-h42);
ph42 = (ph32a+ph32b)/(r_3*(sin34))^ 2;
v_3cm = theta_2d*sqrt((a_3cm*h32+r_2*cos(theta_2-theta_3))^ 2+(b_3cm*h32+r_2*sin(theta_2-
theta_3))^2);
a1 = (a_3cm*h32+r_2*cos(theta_2-theta_3))*(a_3cm*ph32-r_2*sin(theta_2-theta_3)*(1-
h32));
a2 = (b_3cm*h32+r_2*sin(theta_2-theta_3))*(b_3cm*ph32+r_2*cos(theta_2-theta_3)*(1-
h32));
a3 = (a_3cm*h32+r_2*cos(theta_2-theta_3))^ 2+(b_3cm*h32+r_2*sin(theta_2-theta_3))^2;
if( abs(a3) < zero)

    a3 = zero;

    flag = flag+1
```

```
end;
pv_3cm = (a1+a2)*theta_2d/(sqrt(a3));
v_4cm = theta_2d*h42*sqrt(a_4cm^ 2+b_4cm2^);
pv_4cm = theta_2d*ph42*sqrt(a_4cm^ 2+b_4cm2^);
temp1 = m_2*(a_2cm^ 2+b_2cm2^)+ m_4*h422^*(a_4cm2^+b_4cm2^);
temp2 = 2*m_4*theta_2d*h42d*(a_4cm^ 2+b_4cm2^);
temp3 = m_3*((a_3cm*h32+r_2*cos(theta_2-theta_3))^ 2+(b_3cm*h32+r_2*sin(theta_2-
theta_3))2^);
at1 = (a_3cm*h32+r_2*cos(theta_2-theta_3))*(a_3cm*h32d-r_2*sin(theta_2-theta_3)*(theta_2d-
theta_2d*h32));
at2 = (b_3cm*h32+r_2*sin(theta_2-theta_3))*(b_3cm*h32d+r_2*cos(theta_2-theta_3)*(theta_2d-
theta_2d*h32));
temp4 = 2*m_3*theta_2d*(at1+at2);
temp5 = I_2+I_3*h32^ 2+I_4*h422^;
temp6 = 2*I_3*h32d*theta_2d+2*I_4*theta_2d*h42d;
temp7 = m_3*v_3cm*pv_3cm+m_4*v_4cm*pv_4cm+I_3*theta_2d^ 2*h32*ph32+I_4*theta_2d2^*h42*ph4
%The following line is only for the modified model for fixed-fixed flexible segments
%This is the derivative with respect to theta2 of the potential energy
temp8 = -(2*k_1*psi_1+k_2*psi_2m*(h32)+2*k_4*psi_4*h42-k_3*psi_3m*(h32));
%temp8 = -k_1*psi_1-k_2*psi_2*(1-h32)-k_3*psi_3*(h42-h32)-k_4*psi_4*h42;
temp9 = temp2+temp4+temp6-temp7-temp8 + b*theta_2d;
den = (temp1+temp3+temp5);
if(abs(den) < zero)

      den = zero;


      flag = flag+1
end
theta_2dd = -temp9/den;
output = [ theta_2dd] ;
```

angles.m

```
function output = angles(r_1, r_2, r_3, r_4, theta_2 )
load cross28_85x24.txt
theta2 = cross28_85x24(:,1);
theta3 = cross28_85x24(:,2);
theta4 = cross28_85x24(:,3);
theta_3 = interp1(theta2,theta3,theta_2,'spline');
theta_4 = interp1(theta2,theta4,theta_2,'spline');
%differ = theta_2 - theta_4
output = [ theta_2, theta_3, theta_4] ;
```

B.5 Young Mechanism Data Analysis File

Data_Anal2.m

```
clear all
pp = 11;
qq = 5;
temp_hold = abs('.');
Temp_char = num2str(pp);
Temp_char2 = num2str(qq);
Temp_name = cellstr([ 'Thick', Temp_char] );
Temp_name = strcat(Temp_name, '_');
Temp_name = strcat(Temp_name, Temp_char2);
file_name = cellstr([ temp_hold,'txt'] );
fname = strcat(Temp_name , file_name)
load(char(fname));
temp = eval(char(Temp_name));
deltaT = (0.001);
theta2 = temp(:,2);
time = temp(:,1);
```

```
order = 6;
temp = size(theta2);
temp = temp(1);
tend = time(end);
tvec = 0:deltaT:tend;
k = 1
for i = 2:temp

        if theta2(i) ~= theta2(i-1)

                thetap(k) = theta2(i);

                timep(k) = time(i);

                k = k + 1;

        end
end
y_data = (interp1(timep,thetap,tvec,'cubic'))';
temp = size(y_data);
temp = temp(1);
[ b,a] = butter(order,.2);
y_data2 = 0;
y_data2(1:(order+1)) = zeros(1,(order+1));
i = order+1;
y_data2 = filtfilt(b,a,y_data);
filter_finished = 1
y_data2(1:2*order) = zeros(2*order,1);
y_data2((temp-(2*order-1)):temp) = zeros(1,2*order);
y_datadf = diff(y_data2)/0.001;
y_datadu = diff(y_data)/0.001;
y_datadf(1:200*order) = zeros(1,200*order);
y_datadf((temp-(100*order-1)):temp) = zeros(1,100*order);
y_datadu(1:200*order) = zeros(1,200*order);
```

```
y_datadu((temp-(100*order-1)):temp) = zeros(1,(100*order));
figure(1)
plot(time(1:temp), y_datadf,'r')
hold on
plot(time(1:temp), y_datadu,'b')
hold off
k = 1;
p = 1;
i = 101;
while i < temp - 1400

    if abs(y_datadf(i)) > 1000
        y_dataduc(p,1:2500) = y_datadu(i-99:i+2400)';

        y_datadfc(p,1:2500) = y_datadf(i-99:i+2400)';

        k = k + 2500;

        i = i + 2000;

        p = p + 1
    else
        i = i + 1;
    end
end
for kp = 1:(p-1)

    kp

    temp1 = size(y_datadfc(kp,:))

    if temp1(1) > temp1(2)
        temp1 = temp1(1);
    else
        temp1 = temp1(2);
    end

    n = 0;

    while 2^ n < temp1
        n = n + 1;
```

```
end

Data_pt = 2^ n

Y = fft(y_dataduc(kp,:), Data_pt);

Pyy = Y.*conj(Y) / Data_pt;

deltaT = (0.001);

tempb = size(Pyy);

if tempb(1) > tempb(2)
      tempb = tempb(1);
else
      tempb = tempb(2);
end

deltaT = (0.001);

f1 = 1/deltaT*(0:((Data_pt)/2 - 1))/Data_pt;

Step = 5;

for i = (Step+1):tempb

      Pyy2(i-Step) = 0;

      for k = 1:Step

            Pyy2(i-Step) = Pyy2(i-Step) + Pyy(i-k)*exp((Step+1-k)/Step)/exp(1);

      end

      Pyy2(i-Step) = Pyy2(i-Step)/Step;
end

deltaT = (0.001);

f = 1/deltaT*((Step)/2:((Data_pt)/2 - 1))/Data_pt;

figure(3)

semilogy(f,Pyy2(1:((Data_pt - Step)/2)),'r',f1,Pyy(1:((Data_pt)/2)),'g.')
```

```
xlabel('Frequency (Hz)')

ylabel('Magnitude')

axis([ 0 50 1 1000000000] );

difference = 10;

h = difference;

[ Y,I] = max(Pyy2(1:Data_pt/2));

Temp_data = Pyy2(I:Data_pt/2);

[ Y2,I2] = max(Temp_data);

I3 = I2;

ave3 =-.01;

if I < difference + 1
      I = difference + 1
end

ave2 = mean(Pyy2((I-difference/2):(I+difference/2)));

while (ave3 - ave2) < 0.001
      ave2 = ave3;

      h = h + 1;

      [ Y3,I3] = max(Temp_data(h:end));

      I3 = I3 + h;

      ave3 = mean(Temp_data((h-difference/2):(h+difference/2)));
end

freq1(kp) = f(I)

freq2(kp) = f(I3+I)

Temp_name2 = strcat(Temp_name, 'fig');
```

```
fn = Temp_name2;

figure(3)

print( 3, '-depsc2', char(fn))

figure(3)

print( 3, '-dpng', char(fn))

figure(3)

print( 3, '-dtiff', char(fn))

[ Y,I] = max(Pyy(1:Data_pt/2));

Temp_data = Pyy(I:Data_pt/2);

[ Y2,I2] = max(Temp_data);

I3 = I2;

ave3 =-.01;

if I < difference + 1
      I = difference + 1
end

ave2 = mean(Pyy2((I-difference/2):(I+difference/2)));

while (ave3 - ave2) < 0.001
      ave2 = ave3;

      h = h + 1;

      [ Y3,I3] = max(Temp_data(h:end));

      I3 = I3 + h;

      ave3 = mean(Temp_data((h-difference/2):(h+difference/2)));
end

freq1a(kp) = f(I)
```

```
        freq2a(kp) = f(I3+I)

        if 0
            Y = fft(y_dataduc, Data_pt);

            Pyy = Y.*conj(Y) / Data_pt;

            deltaT = (0.001);


            deltaT = (0.001);

            f1 = 1/deltaT*(0:((Data_pt)/2 - 1))/Data_pt;

            for i = (Step+1):tempb

                Pyy2(i-Step) = 0;

                for k = 1:Step

                end Pyy2(i-Step) = Pyy2(i-Step) + Pyy(i-k);

            end Pyy2(i-Step) = Pyy2(i-Step)/Step;

            deltaT = (0.001);

            f = 1/deltaT*((Step)/2:((Data_pt)/2 - 1))/Data_pt;

            figure(4)

            semilogy(f,Pyy2(1:((Data_pt - Step)/2)),'r',f1,Pyy(1:((Data_pt)/2)),'g.')

            xlabel('Frequency (Hz)')

            ylabel('Magnitude')

            axis([ 10 70 1 1000000000] )

            pause(0.01)
        end
end
```

Appendix C

ANSYS Batch Files

This section contains a sample of the Ansys code that was generated for the finite element analysis that is contained in this thesis. For brevity not all of the batch files were included in this section, but a large sampling of the files are shown. Each file is specific to the model for which it is presented.

C.1 Micro Beam Models

```
/BATCH
/config, nres, 1000000
mod = 186e6 !g/(micron * s)
den1 = 8.600e-12!g/micron^ 3
len1 = 10e3!micron
b1 = len1/10!micron
h1 = len1/100!micron
area1 = b1*h1
Ndiv1 = 40
iner1 = b1*h1*h1*h1/12
/prep7
ET,1,BEAM3
R,1,Area1,iner1,h1, , ,,
NLGEOM, on
MP,EX,1,mod
MP,PRXY,1,0.3
```

MP,dens,1,den1

k,1,0,0

k,2,len1,0

l,1,2,ndiv1

mat, 1

latt,1,1,1,

lmesh,1

dk,1,all,0

FINISH

/solu

antype,trans

trnopt,full

outres,,all

timint, off

nsubst, 11

dk,2,uy,0.025*len1

time, 0.001

lswrite

timint, off

dk,2,uy,0.05*len1

time, 0.002

lswrite

timint, off

dk,2,uy,0.15*len1

time, 0.003

lswrite

timint, off

dk,2,uy,0.25*len1

time, 0.004

lswrite

timint, off

dk,2,uy,0.35*len1

time, 0.005

lswrite

timint, off

dk,2,uy,0.45*len1

time, 0.006

lswrite

timint, off

dk,2,uy,0.55*len1

time, 0.007

lswrite

timint, off

dk,2,uy,0.65*len1

time, 0.008

lswrite

timint, off

dk,2,uy,0.75*len1

time, 0.0085

lswrite

timint, off

dk,2,uy,0.75*len1

time, 0.01

lswrite

time, 0.01

dkdele,2,all

timint,on

deltim, 0.0000001

time, 0.02

lswrite

lssolve,1,11

fini

/post26

nsol, 2, Ndiv1 + ndiv2, U, Y, Y_def

nsol, 3, Ndiv1 + ndiv2, U, X, X_def

prvar, X_def, Y_def

plvar, x_def, y_def

C.2 Micro Roberts Straight Line Mechanism Model

/BATCH

/config, nres, 5000000

mod = 176e6

den1 = 2.330e-12 !g/micron^ 3

den2 = 2.330e-12 !g/micron^ 3

den3 = 2.330e-12 !g/micron^ 3

len1 = 900.0 !micron

Gamma = 0.85

angle = 60/180*3.14159265359

offset = 0 !micron

b1 = len1/85.71 !micron

b2 = len1/85.71 !micron

h1 = len1/100 !micron

h2 = len1/10 !micron

area1 = b1*h1

area2 = b2*h2

ndiv1 = 60

ndiv2 = 30

ndiv3 = 20

iner1 = b1*h1*h1*h1/12

```
iner2 = b2*h2*h2*h2/12
/prep7
ET,1,BEAM3
R,1,area1,iner1,h1, , ,,
NLGEOM, on
MP,EX,1,mod
MP,PRXY,1,0.3
MP,dens,1,den1
k,1,0,0
k,2,len1/Gamma*cos(angle),len1/Gamma*sin(angle)
k,3,len1/Gamma*cos(angle)+len1*(1-(1-Gamma)*cos(angle)),len1/Gamma*sin(angle)
k,4,2*len1/Gamma*cos(angle)+len1*(1-(1-Gamma)*cos(angle)),0
k,5,len1/Gamma*cos(angle)+len1/2*(1-(1-Gamma)*cos(angle)), len1/2*((1-Gamma)*sin(angle)
k,7,len1/Gamma*cos(angle)+len1/2*(1-(1-Gamma)*cos(angle)), len1/Gamma*sin(angle)
l,1,2,ndiv1
l,3,4,ndiv1
l,2,7,ndiv3
l,7,3,ndiv3
l,7,5,ndiv3
latt,1,1,1,
!mesh flexible segments
lmesh,1
lmesh,2
R,2,area2,iner2,h2, , , ,
NLGEOM, on
cnvtol,U,,0.000001,,0.01
cnvtol,F,,0.000001,,0.01
MP,EX,2,mod
MP,PRXY,2,0.3
MP,dens,2,den2
```

```
latt,2,2,1,
lmesh,3
lmesh,4
lmesh,5
ksel,s,kp,,5
nslk,s
*get,ndiv1,node,0,num,max
nsel,all
ksel,all
dk,1,all,0
dk,4,all,0

FINISH
/solu
antype,trans
trnopt,full
outres,,all
timint, off
nsubst, 11
dk,5,ux,-0.1*len1
time, 0.001
lswrite
timint, off
dk,5,ux,-0.15*len1
time, 0.002
lswrite
timint, off
dk,5,ux,-0.20*len1
time, 0.003
lswrite
```

timint, off

dk,5,ux,-0.25*len1

time, 0.004

lswrite

timint, off

dk,5,ux,-.30*len1

time, 0.005

lswrite

timint, off

dk,5,ux,-.35*len1

time, 0.006

lswrite

timint, off

dk,5,ux,-.4*len1

time, 0.007

lswrite

timint, off

dk,5,ux,-.45*len1

time, 0.008

lswrite

timint, off

dk,5,ux,-.55*len1

time, 0.0085

lswrite

timint, off

dk,5,ux,-.55*len1

time, 0.01

lswrite

dkdele,5,all

timint,on

deltim, 0.00000001

time, 0.0108

lswrite

lssolve,1,11

fini

/post26

nsol, 2, Ndiv1, U, Y, Y_def

nsol, 3, Ndiv1, U, X, X_def

nsol, 4, Ndiv1, ROT, Z, Z_rot

prvar, X_def, Y_def, Z_rot

plvar, X_def, Y_def, Z_rot

C.3 Large Parallel Mechanism Model

/BATCH

/config, nres, 1000000

mod = 30e6

LoadF = 47.0*0.00

den1 = 0.28/386.4

den2 = 0.11502/386.4

len1 = 14.5

len2 = .5

len3 = 11.5

b1 = 1.25

b2 = 1.25

h1 = 0.03125

h2 = 0.5

area1 = b1*h1

area2 = b2*h2

ndiv1 = 40

```
ndiv2 = 20.0
iner1 = b1*h1*h1*h1/12
iner2 = b2*h2*h2*h2/12
/prep7
ET,1,BEAM3
R,1,area1,iner1,h1, , ,,
NLGEOM, on
MP,EX,1,mod
MP,PRXY,1,0.3
MP,dens,1,den1
!Define the geometry
k,1,0,0
k,2,len1,0
k,3,0,len3
k,4,len1,len3
l,1,2,ndiv1
l,3,4,ndiv1
l,2,4,ndiv2
latt,1,1,1,
lmesh,1
lmesh,2
R,2,area2,iner2,h2, , , ,
NLGEOM, on
MP,EX,2,mod
MP,PRXY,2,0.3
MP,dens,2,den2
latt,2,2,1,
lmesh,3
dk,1,all,0
dk,3,all,0
```

```
FINISH
/solu
antype,trans
trnopt,full
outres,,all
timint, off
nsubst, 11
dk,2,uy,-0.1
time, 0.001
lswrite
timint, off
dk,2,uy,-0.5
time, 0.002
lswrite
timint, off
dk,2,uy,-0.5
time, 0.003
lswrite
timint, off
dk,2,uy,-1.0
time, 0.004
lswrite
timint, off
dk,2,uy,-1.0
time, 0.005
lswrite
timint, off
dk,2,uy,-1.0
time, 0.006
lswrite
```

timint, off

dk,2,uy,-1.5

time, 0.007

lswrite

timint, off

dk,2,uy,-1.50

time, 0.008

lswrite

timint, off

dk,2,uy,-1.50

time, 0.0085

lswrite

timint, off

dk,2,uy,-1.50

time, 0.0095

lswrite

time, 0.01

dkdele,2,all

timint,on

deltim, 0.0005

time, 40.001

lswrite

lssolve,1,11

fini

/post26

nsol, 2, Ndiv1, U, Y, Y_def

nsol, 3, Ndiv1, U, X, X_def

prvar, X_def, Y_def

plvar, x_def, y_def

C.4 Large Young Mechanism Model

/BATCH

/nerr,10000000

/config, nres, 1000000

mod = 200e3

density = 0.0326952 !Lb/in^ 3

gc = 32.174

ut = 12.0

gc = gc*ut

den1 = density/gc !Lbf-sec^ 2/in$\hat{4}$

den2 = density/gc !Lbf-sec^ 2/in$\hat{4}$

den3 = density/gc !Lbf-sec^ 2/in$\hat{4}$

len1 = 3.0090

len2 = 2.44814

len3 = 0.75110

len4 = 9.99845

len5 = -2.67701

b1 = 0.5

b2 = 0.5

b3 = 0.5

h1 = 0.2338

h2 = 0.1275

h3 = 0.856

area1 = b1*h1

area2 = b2*h2

area3 = b3*h3

Ndiv1 = 30.0

Ndiv2 = 40.0

Ndiv3 = 20.0

iner1 = b1*h1*h1*h1/12

iner2 = b2*h2*h2*h2/12

iner3 = b3*h3*h3*h3/12

/prep7

ET,1,BEAM3

R,1,Area1,iner1,h1, , ,,

NLGEOM, on

MP,EX,1,mod

MP,PRXY,1,0.24

MP,dens,1,den1

k,2,0,0

k,3,len1,0

k,5,len2, len3

k,6, len4, len5

l,2,5,Ndiv1

l,3,6,Ndiv2

l,5,6,Ndiv3

mat, 1

latt,1,1,1,

lmesh,1

mat, 2

R,2,area2,iner2,h2, , , ,

MP,EX,2,mod

MP,PRXY,2,0.3

MP,dens,2,den2

latt,2,2,1,

lmesh,2

mat, 2

R,3,area3,iner3,h3, , , ,

MP,EX,3,mod

MP,PRXY,3,0.3

MP,dens,3,den3

latt,3,3,1,

lmesh,3

dk,2,ux,0

dk,2,uy,0

dk,3,ux,0

dk,3,uy,0

FINISH

/solu

antype,trans

trnopt,full

outres,all,all

timint, off

nsubst, 11

dk,6,uy,0.5

time, 0.001

lswrite

timint, off

dk,6,uy,0.5

time, 0.002

lswrite

timint, off

dk,6,uy,1.0

time, 0.003

lswrite

timint, off

dk,6,uy,1.5

time, 0.004

lswrite

timint, off

dk,6,uy,2.0

time, 0.005

lswrite

timint, off

dk,6,uy,2.5

time, 0.006

lswrite

timint, off

dk,6,uy,3.0

time, 0.007

lswrite

timint, off

dk,6,uy,3.5

time, 0.008

lswrite

timint, off

dk,6,uy,2.0

time, 0.0085

lswrite

timint, off

dk,6,uy,2.0

time, 0.0095

lswrite

time, 0.01

dkdele,6,all

timint,on

deltim, 0.005

time, 3.01

lswrite

lssolve,1,11

fini

/post26

nsol, 2, Ndiv1 + ndiv2, U, Y, Y_def

nsol, 3, Ndiv1 + ndiv2, U, X, X_def

prvar, X_def, Y_def

plvar, x_def, y_def

C.5 Micro Parallel Mechanism Model

/BATCH

/config, nres, 5000000

mod = 176e6

pi = acos(-1)

den1 = 2.330e-12 !g/micron^ 3

den2 = 2.330e-12 !g/micron^ 3

len1 = 350 !micron

a1 = -0.1*len1

a2 = -0.2*len1

a3 = -0.3*len1

a4 = -0.45*len1

a5 = -0.6*len1

a6 = -0.65*len1

a7 = -0.7*len1

a8 = -0.75*len1

a9 = -0.8*len1

a10 = -0.8*len1

b1 = len1/100

b2 = len1/100

h1 = len1/100

h2 = len1/10

area1 = b1*h1

area2 = b2*h2

Ndiv1 = 40

Ndiv3 = 20

iner1 = b1*h1*h1*h1/12

iner2 = b2*h2*h2*h2/12

ksel,s,kp,,2

nslk,s

*get,ndiv2,node,0,num,max

nsel,all

ksel,all

/prep7

ET,1,BEAM3

R,1,Area1,iner1,h1, , ,,

NLGEOM, on

MP,EX,1,mod

MP,PRXY,1,0.3

MP,dens,1,den1

k,1,0,0

k,2,len1,0

k,3,len1,len1

k,4,0,len1

l,1,2,ndiv1

l,2,3,ndiv3

l,3,4,ndiv1

mat, 1

latt,1,1,1,

lmesh,1

lmesh,3

mat, 2

R,2,area2,iner2,h2, , , ,

MP,EX,2,mod

MP,PRXY,2,0.3

MP,dens,2,den2

latt,2,2,1,

lmesh,2

dk,1,all,0

dk,4,all,0

FINISH

/solu

antype,trans

trnopt,full

outres,,all

timint, off

nsubst, 11

dk,2,uy,a1

time, 0.001

lswrite

timint, off

dk,2,uy,a2

time, 0.002

lswrite

timint, off

dk,2,uy,a3

time, 0.003

lswrite

timint, off

dk,2,uy,a4

time, 0.004

lswrite

timint, off

dk,2,uy,a5

time, 0.005

lswrite

timint, off

dk,2,uy,a6

time, 0.006

lswrite

timint, off

dk,2,uy,a7

time, 0.007

lswrite

timint, off

dk,2,uy,a8

time, 0.008

lswrite

timint, off

dk,2,uy,a9

time, 0.0085

lswrite

timint, off

dk,2,uy,a10

time, 0.01

lswrite

dkdele,2,all

timint,on

deltim, 0.00000001

time, 0.0105

lswrite

lssolve,1,11

fini

/post26

nsol, 2, 2, U, Y, Y_def

nsol, 3, 2, U, X, X_def

prvar, X_def, Y_def

plvar, x_def, y_def

C.6 Micro Folded Beam Structure Model

/BATCH

/config, nres, 5000000

mod = 176e6

pi = acos(-1)

den1 = 2.330e-12 !g/micron^ 3

den2 = 2.330e-22 !g/micron^ 3

den3 = 2.330e-12 !g/micron^ 3

len1 = 350 !micron

len2 = len1/3.5

len3 = len1/4

len4 = len1/2

a1 = -0.1*len2

a2 = -0.15*len2

a3 = -0.2*len2

a4 = -0.35*len2

a5 = -0.4*len2

a6 = -0.65*len2

a7 = -0.7*len2

a8 = -0.85*len2

a9 = -1.0*len2

a10 = -1.0*len2

b1 = len1/100

b2 = len1/100

b3 = len1/100

b4 = len1/100

h1 = len1/100

h2 = len1/35

h3 = len1/10

h4 = len1/4

area1 = b1*h1

area2 = b2*h2

area3 = b3*h3

area4 = b4*h4

Ndiv1 = 40

ndiv2 = 10

Ndiv3 = 20

iner1 = b1*h1*h1*h1/12

iner2 = b2*h2*h2*h2/12

iner3 = b3*h3*h3*h3/12

iner4 = b4*h4*h4*h4/12

/prep7

ET,1,BEAM3

R,1,Area1,iner1,h1, , ,,

NLGEOM, on

MP,EX,1,mod

MP,PRXY,1,0.3

MP,dens,1,den1

k,1,0,0

k,2,0,len1

k,3,len3,0

k,4,-len3,0

k,5,len3,len1

k,6,-len3,len1

k,7,len3,3*len3

k,8,len3,len3

k,9,-len3,3*len3

k,10,-len3,len3

k,11,len3+len1,len1

k,12,len3+len1,3*len3

k,13,len3+len1,len3

k,14,len3+len1,0

k,15,-len3-len1,len1

k,16,-len1-len3,3*len3

k,17,-len1-len3,len3

k,18,-len1-len3,0

l,1,2,ndiv3

l,1,3,ndiv3

l,1,4,ndiv3

l,2,5,ndiv3

l,2,6,ndiv3

l,5,11,ndiv1

l,7,12,ndiv1

l,8,13,ndiv1

l,3,14,ndiv1

l,4,18,ndiv1

l,10,17,ndiv1

l,9,16,ndiv1

l,6,15,ndiv1

l,11,12,ndiv3

l,12,13,ndiv3

l,13,14,ndiv3

l,15,16,ndiv3

l,16,17,ndiv3

l,17,18,ndiv3

mat, 1

latt,1,1,1,

lmesh,6

lmesh,7

lmesh,8

lmesh,9

lmesh,10

lmesh,11

lmesh,12

lmesh,13

mat, 2

R,2,area2,iner2,h2, , , ,

MP,EX,2,mod

MP,PRXY,2,0.3

MP,dens,2,den2

latt,2,2,1,

lmesh,14

lmesh,15

lmesh,16

lmesh,17

lmesh,18

lmesh,19

mat, 3

R,3,area3,iner3,h3, , , ,

MP, EX,3,mod

MP,PRXY,3,0.3

MP,dens,3,den3

latt,3,3,1,

lmesh,2

lmesh,3

lmesh,4

lmesh,5

mat,4

R,4,area4,iner4,h4,,,,

MP,EX,4,mod

MP,PRXY,4,0.3

MP,dens,4,den3

latt,4,4,1,

lmesh,1

dk,7,all,0

dk,8,all,0

dk,9,all,0

dk,10,all,0

ksel,s,kp,,2

nslk,s

*get,ndiv1,node,0,num,max

nsel,all

ksel,all

FINISH

/solu

antype,trans

trnopt,full

outres,,all

timint, off

nsubst, 11

dk,2,uy,a1

time, 0.001

lswrite

timint, off

dk,2,uy,a2

time, 0.002

lswrite

timint, off

dk,2,uy,a3

time, 0.003

lswrite

timint, off

dk,2,uy,a4

time, 0.004

lswrite

timint, off

dk,2,uy,a5

time, 0.005

lswrite

timint, off

dk,2,uy,a6

time, 0.006

lswrite

timint, off

dk,2,uy,a7

time, 0.007

lswrite

timint, off

dk,2,uy,a8

time, 0.008

lswrite

timint, off

dk,2,uy,a9

time, 0.0085

lswrite

timint, off

dk,2,uy,a10

time, 0.01

lswrite

dkdele,2,all

timint,on

deltim, 0.0000001

time, 0.0112

lswrite

lssolve,1,11

fini

/post26

nsol, 2, ndiv1, U, Y, Y_def

nsol, 3, ndiv1, U, X, X_def

prvar, X_def, Y_def

plvar, x_def, y_def

C.7 Beam Model

/BATCH

/config, nres, 1000000

mod = 30e6

LoadF = 47.0*10.00

gc = 32.174

ut = 12.0

gc = gc*ut

den1 = 0.28/gc !Slugs/in^ 3

```
den2 = LoadF*0.28/gc + 0.28/gc!Slugs/in^ 3
len1 = 23.5
len2 = .5
b1 = 1.25
b2 = 1.25
h1 = 0.03125
h2 = 0.03125
area1 = b1*h1
area2 = b2*h2
Ndiv1 = 30
ndiv2 = 2.0
iner1 = b1*h1*h1*h1/12
iner2 = b2*h2*h2*h2/12
/prep7
ET,1,BEAM3
R,1,Area1,iner1,h1, , ,,
NLGEOM, on
MP,EX,1,mod
MP,PRXY,1,0.3
MP,dens,1,den1
k,1,0,0
k,2,len1,0
k,3,len1+len2
l,1,2,ndiv1
l,2,3,ndiv2
mat, 1
latt,1,1,1,
lmesh,1
mat, 2
R,2,area2,iner2,h2, , , ,
```

MP,EX,2,mod

MP,PRXY,2,0.3

MP,dens,2,den2

latt,2,2,1,

lmesh,2

dk,1,all,0

FINISH

/solu

antype,trans

trnopt,full

outres,,all

timint, off

nsubst, 11

dk,3,uy,4.0

time, 0.001

lswrite

timint, off

dk,3,uy,6.0

time, 0.002

lswrite

timint, off

dk,3,uy,8.0

time, 0.003

lswrite

timint, off

dk,3,uy,10.0

time, 0.004

lswrite

timint, off

dk,3,uy,12.0

time, 0.005

lswrite

timint, off

dk,3,uy,14.0

time, 0.006

lswrite

timint, off

dk,3,uy,16.0

time, 0.007

lswrite

timint, off

dk,3,uy,17.0

time, 0.008

lswrite

timint, off

dk,3,uy,18.0

time, 0.0085

lswrite

timint, off

dk,3,uy,18.0

time, 0.0095

lswrite

time, 0.01

dkdele,3,all

timint,on

deltim, 0.0005

time, 80.01

lswrite

lssolve,1,11

fini

/post26

nsol, 2, Ndiv1 + ndiv2, U, Y, Y_def

nsol, 3, Ndiv1 + ndiv2, U, X, X_def

prvar, X_def, Y_def

plvar, x_def, y_def